Mechanistic analysis of the Zika virus translation-replication switch

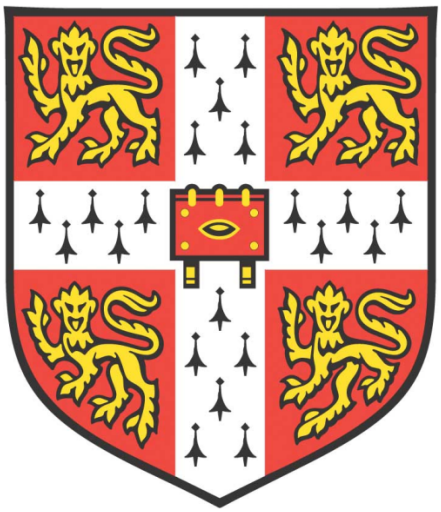

Thomas James Sanford

Robinson College

May 2019

This dissertation is submitted for the degree of Doctor of Philosophy

Declaration

This dissertation is the result of my own work and includes nothing which is the outcome of work done in collaboration except as declared in the Preface and specified in the text.

It is not substantially the same as any that I have submitted, or, is being concurrently submitted for a degree or diploma or other qualification at the University of Cambridge or any other University or similar institution except as declared in the Preface and specified in the text. I further state that no substantial part of my dissertation has already been submitted, or, is being concurrently submitted for any such degree, diploma or other qualification at the University of Cambridge or any other University or similar institution except as declared in the Preface and specified in the text.

It does not exceed the prescribed word limit for the relevant Degree Committee.

Abstract

Title: Mechanistic analysis of the Zika virus translation-replication switch

Author: Thomas James Sanford

The genomes of positive-sense RNA viruses are required for both translation and replication during infection. These two processes are antagonistic in nature, each requiring the RNA template in opposite directions. Thus, the balance between these processes during infection must be tightly regulated. Zika virus (ZIKV) is a capped, positive-sense RNA virus of the *Flavivirus* genus, which contains several notable human pathogens including Dengue virus (DENV) and Japanese encephalitis virus. Infection with ZIKV has been linked to congenital microcephaly as well as Guillain-Barré syndrome in infected adults. During infection, flavivirus replication is known to require genome circularisation, mediated by long-range RNA-RNA interactions between *cis*-acting elements at the 5′ and 3′ ends of the genome. This facilitates the translocation of the viral polymerase NS5 from its site of recruitment at the 5′ end of the genome to the 3′ end in order to begin negative-strand RNA synthesis. However, it is unknown how the switch from genome translation to genome replication during flavivirus infection is regulated. The work presented for this thesis uses an *in vitro* reconstitution approach to study translation initiation on ZIKV, in which purified components of the translational machinery are added to the RNA and 48S complex formation upon initiating codons assayed using toeprinting. This technique allows the examination of both recruitment and scanning of the 40S ribosomal subunit, as well as the influence of RNA secondary structure on this process. It is shown that ZIKV translation is cap-dependent using the canonical set of initiation factors and that, under these conditions, recruitment of the viral polymerase to the 5′ proximal stem-loop specifically inhibits translation initiation. Furthermore, circularisation of ZIKV and DENV genomes abrogates viral translation initiation through inhibition of ribosome scanning, subsequently re-directing the ribosome towards upstream near-cognate initiation codons. Conversely, the linear form of the viral genome, which predominates during infection, is shown to be translation-competent. This thesis therefore proposes a model by which the viral polymerase and dynamic viral genome conformations together prime a genome for replication by ensuring ribosome clearance, thus allowing replication to occur unimpeded.

Acknowledgements

First and foremost, I would like to thank my PhD supervisor Trevor Sweeney for everything he has done over the last few years. I really cannot thank him enough for taking me on as a student and for all of the guidance, support, assistance and patience he has given me. I have really enjoyed my time working with him, no doubt because of his humour and enthusiasm, and I am sad it is coming to an end.

I would also like to thank the members of the Sweeney lab for creating a fantastic work environment. Harriet has been an endless source of support and kindness since the start and I will deeply miss our cups of tea together. I am extremely grateful for the help she has given me with designing some of the figures in this thesis and for experimental discussions. In addition, Skye, Renata, Ted and Xin have been a pleasure to work with during my time in the lab. I'd especially like to thank Ted for performing the experiment in Appendix B and for providing translation-competent Vero cell lysate.

I'd also like to thank my mentor Ian Brierley for useful discussions and experimental ideas, as well as the entire Division of Virology. The Labs on Level 5 are an extremely special place to work and I will look back on my time as a PhD student extremely fondly.

Thanks also to the Wellcome Trust and the Infection, Immunity and Inflammation program at Cambridge for enabling me to undertake this PhD.

Finally, this journey has not been without its ups and downs so I'd like to thank my family for reminding me of what is truly important and for their steadfast belief that I could do this. Joachim has been my anchor throughout all of this, and I am forever in his debt.

Contents

List of figures

List of tables

List of appendices

Abbreviations

4E-BP	eIF4E binding protein
3' SL	3' stem-loop
ABC	ATP-binding cassette
ADE	Antibody-dependent enhancement
Ago	Argonaute protein
AS	Ammonium sulphate
ASO	Antisense oligonucleotide
AUF1	AU-rich element RNA-binding protein 1
BHK	Baby hamster kidney
C	Capsid
cHP	C coding region hairpin
CITE	Cap-independent translation elements
CrPV	Cricket paralysis virus
Cryo-EM	Cryo-electron microscopy
CS	Cyclisation sequence
DAR	Downstream of AUG region
DB	Dumbbell
DCS-PK	Downstream of 5' CS pseudoknot
DEAE	Diethylaminoethyl
DENV	Dengue virus
E	Envelope
E. coli	*Escherichia coli*
eIF	Eukaryotic initiation factor
eIF4Gm	eIF4G, middle fragment ($eIF4G_{736-1115}$)
EMCV	Encephalomyocarditis virus
EMSA	Electrophoretic mobility shift assay
Fluc	Firefly luciferase
FPLC	Fast protein liquid chromatography
GAP	GTPase activating protein
GEF	Guanine nucleotide exchange factor
HCV	Hepatitis C virus
icDNA	Infectious cDNA
IFIT	Interferon-induced proteins with tetratricopeptide repeats

IRES	Internal ribosome entry site
ISFV	Insect-specific flavivirus
ITAF	IRES *trans*-acting factors
JEV	Japanese encephalitis virus
M	Membrane
m^6A	N^6-methyladenosine
MBFV	Mosquito-borne flavivirus
miRNA	MicroRNA
Mnk	Mitogen-activated protein kinase-interacting kinase
MTase	Methyltransferase
mTOR	Mammalian target of rapamycin
NKFV	No-known-vector flavivirus
Nluc	Nanoluciferase
NMIA	N-methylisatoic anhydride
P-PMOs	Peptide-conjugated phosphorodiamidate morpholino oligomers
PABP	Poly(A)-binding protein
PAGE	Polyacrylamide gel electrophoresis
PCBP2	Poly(C)-binding protein 2
PERK	PKR-like endoplasmic reticulum kinase
PKR	Protein kinase R
PV	Poliovirus
prM	Precursor of membrane
PTB	Polypyrimidine tract-binding protein
RdRp	RNA-dependent RNA polymerase
RRL	Rabbit reticulocyte lysate
RSW	Ribosomal salt wash
RT	Reverse transcriptase
SCR	Scrambled oligonucleotide
sfRNA	Subgenomic flavivirus RNAs
SHAPE	Selective 2′-hydroxyl acylation analysed by primer extension
sHP	Small hairpin
SLA	Stem-loop A
SLB	Stem-loop B
SRP	Signal recognition particle
SSL	Side stem-loop

SV	Sindbis virus
TBE	Tris-Borate-EDTA
TBFV	Tick-borne flavivirus
TL	Top loop
UAR	Upstream of AUG region
UFS	5′-UAR-flanking stem
uORF	Upstream open reading frame
UTR	Untranslated region
vATPase	Vacuolar ATPase
WNV	West Nile virus
xrRNA	Exonuclease-resistant RNA
YFV	Yellow fever virus
ZIKV	Zika virus

1 Introduction

Viruses are obligate intracellular parasites that are responsible for a wide range of human and animal diseases. While the majority of positive-sense RNA viruses (whose viral genomes are functional mRNAs) express their own polymerase proteins to replicate their genome, these viruses are still dependent upon interaction with additional host factors to complete their lifecycle (Ahlquist *et al*, 2003). In particular, viruses are completely dependent upon co-option of the host protein synthesis machinery to translate their genome (Walsh & Mohr, 2011).

Translation is the fundamental process by which mRNA is decoded to produce functional proteins and is a key step in the regulation of gene expression. This process is mediated by ribosomes across all kingdoms of life, which in eukaryotes consist of two subunits; the large 60S subunit and the small 40S subunit, both of which are made up of ribosomal proteins and ribosomal RNA. The universally conserved core of the ribosome is responsible for both peptide bond formation and mRNA decoding (Schmeing & Ramakrishnan, 2009). A mRNA-binding cleft exists between the head and body of the small ribosomal subunit which also contains three binding sites for tRNA; the A site which binds incoming aminoacyl-tRNA, the P site which holds the peptidyl-tRNA linked to the nascent polypeptide chain and the E site where deacylated P site tRNA is ejected following peptide bond formation (Ramakrishnan, 2002). Recent crystal structures of yeast ribosomes (Ben-Shem *et al*, 2010, 2011) and cryo-electron microscopy (cryo-EM) structures of human ribosomes (Khatter *et al*, 2015) have revealed a wealth of information about these highly complex molecular machines in eukaryotes.

Translation consists of three main stages; initiation, elongation and termination. Of these, initiation is considered to be the stage at which most regulation is exerted and involves decoding of an AUG start codon on mRNA by a specialised methionyl tRNA (Met-$tRNA_i^{Met}$) (Sonenberg & Hinnebusch, 2009). In eukaryotes, start codon recognition occurs predominantly through a scanning mechanism, during which ribosomal preinitiation complexes are loaded onto mRNA at the 5' end and subsequently scan through the 5' untranslated region (UTR) for a cognate AUG codon (or more rarely a near-cognate non-AUG initiation codon). This process is highly coordinated, requiring no less than nine eukaryotic initiation factors (eIFs; Table 1.1), many of which including eIF2 (eIF2α, eIF2β and eIF2γ) and eIF3 (eIF3a-m) consisting of multiple subunits (Jackson *et al*, 2010).

Table 1.1 Eukaryotic initiation factors

Adapted from Jackson *et al*, 2010. The core initiation factors are underlined while auxiliary factors are not. There are three paralogues of eIF4A (eIF4AI – III), with the homologues eIF4AI and eIF4AII possessing functionally similar roles in initiation. Two paralogues of eIF4G exist (eIF4GI and eIF4GII) which show some selectivity to certain mRNAs (Jackson *et al*, 2010).

Name	Number of subunits and size (kDa)	Function
eIF2	3 (36.1, 38.4 and 51.1)	Forms the eIF2-GTP-Met-tRNA$_i^{Met}$ ternary complex thus recruits Met-tRNA$_i^{Met}$ to the ribosome
eIF3	13 (800 total)	Interacts with 40S, eIF1, eIF4G and eIF5 to stimulate ternary complex binding to 40S, attachment and scanning of the 43S complex as well as 40S/60S recycling
eIF1	1 (12.7)	Ensures the fidelity of and promotes scanning, stimulates ternary complex binding to 40S and prevents premature eIF5-induced hydrolysis of eIF2-GTP
eIF1A	1 (16.5)	Cooperates with eIF1 in scanning and initiation codon selection and stimulates ternary complex binding to 40S
eIF4E	1 (24.5)	Binds to the 5' cap structure of mRNA
eIF4A	1 (46.1)	DEAD-box and ATP-dependent RNA helicase
eIF4G	1 (175.5)	Interacts with eIF4E, eIF4A, eIF3, PABP and mRNA in addition to enhancing eIF4A helicase activity
eIF4F	3 (246.1 total)	Comprised of eIF4E, eIF4A and eIF4G; unwinds the 5' terminal region of mRNA and promotes 43S attachment and scanning
eIF4B	1 (69.3)	RNA-binding protein that enhances eIF4A helicase activity
eIF4H	1 (27.4)	RNA-binding protein that enhances eIF4A helicase activity and is homologous to a fragment of eIF4B
eIF5	1 (49.2)	GTPase activating protein that triggers hydrolysis of eIF2-GTP upon start codon recognition
eIF5B	1 (138.9)	Ribosome-dependent GTPase that mediates 40S and 60S ribosomal subunit joining
eIF2B	5 (33.7, 39.0, 50.2, 59.7 and 80.3)	Guanine nucleotide exchange factor that promotes GDP-GTP exchange on eIF2
DHX29	1 (155.3)	DExH-box helicase that binds directly to 40S facilitating scanning on mRNAs with highly structured 5' UTRs and start codon recognition
PABP	1 (70.7)	Binds to the 3' poly(A) tail of mRNA and eIF4G to enhance binding of eIF4F to the 5' cap structure

1.1 Canonical translation initiation

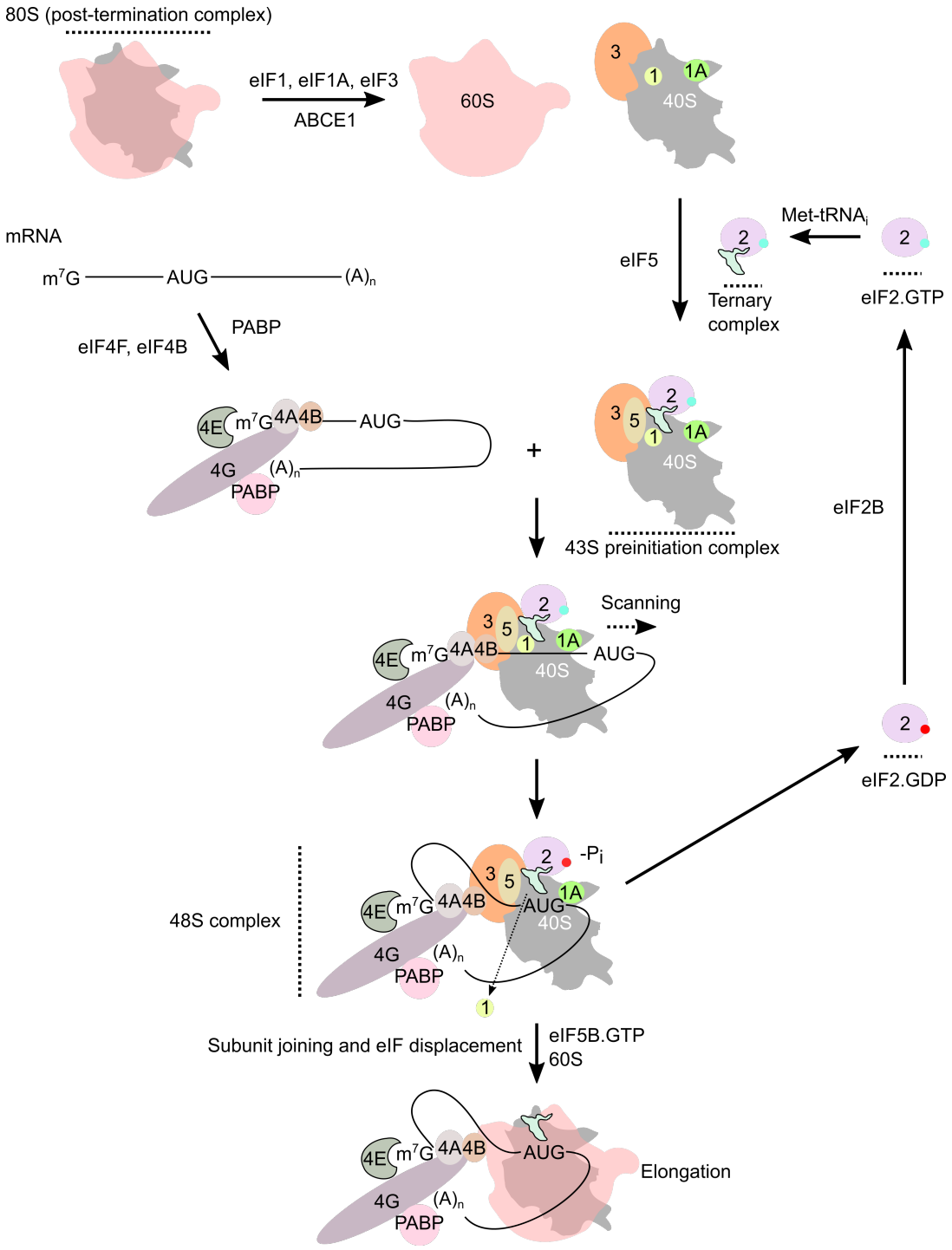

Figure 1.1 Schematic of eukaryotic translation initiation

Post-termination complexes are initially recycled to yield separate 60S and 40S subunits. Following formation of a 43S preinitiation complex and unwinding of the 5' terminal end of mRNA by eIF4F, eIF4B and PABP, 43S complexes are attached and scan down the mRNA for an initiation codon in good sequence context. Initiation codon recognition leads to the formation of a "closed complex", displacement of eIF1 and hydrolysis of eIF2-GTP by eIF5. Subunit joining and initiation factor release is subsequently mediated by hydrolysis of eIF5B-GTP. eIF2-GDP is recycled to eIF2-GTP by eIF2B. GTP is represented as a blue ball whereas GDP is represented as a red ball (Jackson *et al*, 2010; Hinnebusch & Lorsch, 2012).

1.1.1 43S complex formation

An overview of canonical translation initiation is shown in Figure 1.1. As translation is a cyclical process, initiation begins with the recycling of the 40S small ribosomal subunit from release factor eRF1-containing post-termination 80S ribosomal complexes (Jackson *et al*, 2010). This is achieved due to the activities of the ATP-binding cassette (ABC) family member ABCE1 in conjunction with eIF3, eIF1 and eIF1A. Together, these proteins split the post-termination ribosomal complex to form a free 60S subunit and a mRNA- and deacylated tRNA-bound 40S subunit, whose subsequent release is mediated by eIF1 and the eIF3j subunit of eIF3 (Pisarev *et al*, 2007a, 2010). The 40S-eIF1-eIF1A-eIF3 complex is subsequently joined by the ternary complex comprised of eIF2, Met-tRNA$_i^{Met}$ and GTP to form a 43S preinitiation complex. Formation of this complex prevents re-association of the 40S ribosomal subunit with free 60S subunit (Kolupaeva *et al*, 2005). Recent cryo-EM structures have shown that eIF3 forms a five-lobed structure at the back of the 40S ribosomal subunit, while the ternary complex is positioned close to the P site at the ribosomal subunit interface (Hashem *et al*, 2013a; des Georges *et al*, 2015). eIF1 and eIF1A bind as monomers and reside at the P site (Lomakin *et al*, 2003; Rabl *et al*, 2011) and A site (Yu *et al*, 2009), respectively. Cryo-EM structures of yeast 40S ribosomal subunits bound to eIF1 and eIF1A has illustrated that binding induces opening of the mRNA entry channel (Passmore *et al*, 2007).

1.1.2 Attachment of 43S preinitiation complexes to mRNA

Cellular mRNAs typically possess a 5' cap1 structure (m^{7}GpppNm; where Nm denotes any nucleotide with 2′-O methylation) as well as a 3' poly(A) tail (Sonenberg & Hinnebusch, 2009). While 43S preinitiation complexes alone are sufficient to attach to model RNAs containing unstructured 5' UTRs (Pestova & Kolupaeva, 2002), cellular mRNAs typically possess sufficient RNA secondary structure for 43S complex loading to additionally require the cooperative actions of eIF4F and eIF4B or eIF4H. These factors act to unwind the 5' cap-proximal secondary structure in order to generate a ssRNA landing pad upon which the 43S preinitiation complex can load, thus activating the mRNA (Jackson *et al*, 2010).

eIF4F is a protein complex consisting of the cap-binding protein eIF4E, the helicase eIF4A and the scaffold protein eIF4G which binds eIF4E, eIF4A, eIF3 and poly(A)-binding protein (PABP) (Jackson *et al*, 2010). Numerous structural studies (reviewed in Von Der Haar *et al*, 2004) have illustrated that eIF4E binding to the 5' cap structure depends on the stacking of two tryptophan residues with the methylated guanylate moiety of the cap structure. Unlike yeast

eIF4G (Gross *et al*, 2003), mammalian eIF4G does not increase the affinity of eIF4E for the cap structure (Slepenkov *et al*, 2008) but instead stimulates this interaction by directly binding to mRNA and increasing the local concentration of eIF4E around the cap (Yanagiya *et al*, 2009). eIF4A is a DEAD-box helicase consisting of two RecA-like domains that have been proposed to alternate between "open" and "closed" conformations, with its ATP-binding site at the domain interface (Andersen *et al*, 2006). The helicase activity of eIF4A is enhanced by its association with eIF4G (Schutz *et al*, 2008; Oberer *et al*, 2005) and by eIF4B or eIF4H (Rogers *et al*, 2001; García-García *et al*, 2015; Sun *et al*, 2012), homologous proteins that both possess RNA recognition motifs. While unclear, it has been proposed that eIF4B/eIF4H-mediated eIF4A helicase enhancement occurs as a result of ssRNA binding, thus preventing mRNA re-annealing (Marintchev *et al*, 2009). The interaction between eIF4G and PABP bound to the 3' poly(A) tail forms a "closed-loop structure", thought to stimulate the attachment of the 43S preinitiation complex to the mRNA (Hinnebusch & Lorsch, 2012).

It is important to note however that the mechanism by which the eIF4E-bound capped mRNA enters the mRNA-binding channel on the 40S ribosomal subunit during 43S preinitiation complex attachment remains unclear (Jackson *et al*, 2010). Sterically, it would be difficult for eIF4E-bound mRNA to "thread" through the mRNA-binding channel, requiring separation of the two, and an alternative model was proposed whereby the mRNA "slots" into the binding channel downstream of the cap structure. However, in this model the initiator tRNA would be unable to inspect certain nucleotides immediately downstream of the cap. Both models are illustrated in Figure 1.2. A recent study using an *in vitro* reconstitution approach on model RNAs has illustrated that the very 5' terminal nucleotides are inspected following 43S complex attachment providing support for the "threading model" (Kumar *et al*, 2016b), although further structural analysis is required to confirm these findings.

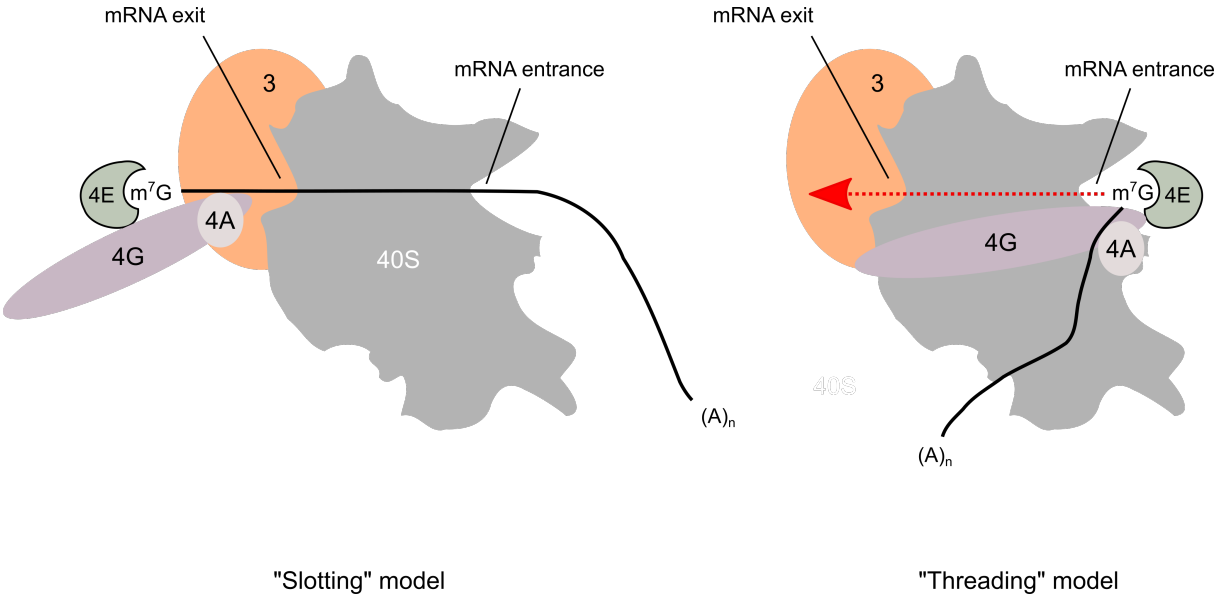

Figure 1.2 Hypothetical models of eIF4F-mediated ribosomal attachment to mRNA

According to the "slotting" model (left), eIF4E resides close to the mRNA exit channel on the 40S subunit. 40S subunits are recruited to an internal region of the mRNA which "slots" directly into the mRNA-binding channel without disruption of the eIF4E-cap interaction, preventing 5' terminal nucleotides from being inspected by Met-tRNA$_i^{Met}$. eIF4F is positioned at the lagging end of the scanning preinitiation complex. In the "threading model" (right), eIF4E is located close to the mRNA entrance channel. Disruption of the eIF4E-cap interaction is required to permit the 'threading" of mRNA directly into the mRNA-binding channel on the 40S subunit (indicated by a red line), thus allowing Met-tRNA$_i^{Met}$ to inspect 5' terminal nucleotides. eIF4F is positioned at the leading edge of the scanning preinitiation complex. For simplicity, only eIF4F, eIF3 and the 40S subunit are shown.

1.1.3 Ribosome scanning of mRNA 5' UTRs

After attachment, 43S preinitiation complexes scan down the mRNA towards the initiating AUG codon. Scanning consists of two related processes; resolution of mRNA secondary structure and ribosomal movement along it (Jackson *et al*, 2010). Scanning is an intrinsic property of 43S preinitiation complexes along unstructured model RNAs without factors required for RNA unwinding, in a process that is dependent upon the scanning-competent conformation of the 40S ribosomal subunit induced by eIF1 and eIF1A (Pestova & Kolupaeva, 2002; Passmore *et al*, 2007). It has been well characterised that stable RNA secondary structure can act as an impediment to ribosome scanning (Kozak, 1991; Babendure *et al*, 2006) and efficient resolution of only weak RNA secondary structures requires ATP, eIF4A, eIF4B and eIF4F (Pestova & Kolupaeva, 2002). The more stable the RNA structure, the higher the dependence on eIF4A and ATP (Svitkin *et al*, 2001; Jackson, 1991). However, the precise positioning of eIF4A within the scanning complex is unknown. Studies have suggested that eIF4A might contact the RNA upstream of the scanning preinitiation complex, unwinding

mRNA structure before entry into the mRNA-binding channel (Kumar *et al*, 2016b; Marintchev *et al*, 2009). An alternative model is that eIF4A and eIF4B work together to act exclusively as a clamp behind the scanning ribosomal complex, preventing 3'-5' backsliding and imposing unidirectionality (Spirin, 2009). A study examining the selection of two AUG codons in close proximity has suggested that ribosome scanning involves backwards "fluttering" of about 15 nt, with net movement in the 5'-3' direction (Matsuda & Dreher, 2006).

Studies performed in a reconstitution system for translation initiation have illustrated that, in addition to eIF4A, the DExH-box helicase DHX29 is required for translation initiation on RNAs containing highly structured 5' UTRs (Pisareva *et al*, 2008). DHX29 directly interacts with 40S subunits through a unique N-terminal region and NTP hydrolysis by its two RecA domains is essential for its role in initiation (Dhote *et al*, 2012). Knockdown of DHX29 *in vivo* reduces polysome assembly and impairs cancer cell proliferation (Parsyan *et al*, 2009). A cryo-EM structure of DHX29 bound to the 43S preinitiation complex has illustrated that DHX29 resides at helix H16 of the 40S ribosomal subunit near the mRNA-binding cleft and contacts eIF3 (Hashem *et al*, 2013a). It is unclear whether DHX29 unwinds mRNA secondary structure directly or instead indirectly facilitates scanning by inducing conformational changes within the 40S subunit. A recent study using a crosslinking approach in an *in vitro* system has shown that DHX29 addition does not affect the mRNA path into the 40S entry channel and moreover the helicase only weakly interacts with the mRNA in this region (Pisareva & Pisarev, 2016a). This suggests that DHX29, by contacting eIF3, facilitates higher processivity by remodelling the scanning ribosomal complex and not by direct mRNA unwinding. The yeast DEAD-box helicase protein Ded1 has also been implicated in scanning (Chuang *et al*, 1997), especially on long 5' UTRs (Berthelot *et al*, 2004), although the involvement of mammalian homologue DDX3 is less well defined (Abaeva *et al*, 2011; Jackson *et al*, 2010).

1.1.4 Initiation codon recognition

Scanning 43S complexes possess a discriminatory mechanism to promote recognition of the correct initiation codon. This codon is typically the first AUG codon present in good Kozak sequence context (GCC(A/G)CCAUGG), with a purine at the -3 position and G at the +4 position (where A within AUG is designated +1; Kozak, 1991). eIF1 plays a key role in the fidelity of selection, whose presence prevents recognition of near-cognate codons and AUGs present in poor sequence context, as well as triggering disassembly of complexes formed upon cap-proximal AUG codons (Pestova *et al*, 1998a; Pestova & Kolupaeva, 2002; Pisarev *et al*,

2006). eIF1A is known to act synergistically with eIF1 (Pestova *et al*, 1998a) and the two together are responsible for maintaining the scanning-competent conformation of the small ribosomal subunit (Passmore *et al*, 2007). In the current model, establishment of correct codon-anticodon base-pairing by Met-tRNA$_i^{Met}$ within the ribosomal P site is thought to require a conformational change to a scanning-incompetent form, antagonised by eIF1 (Jackson *et al*, 2010). Once this base-pairing has been established, the eIF1A-40S interaction is tightened (Maag *et al*, 2006) and eIF1 is displaced from the preinitiation complex (Unbehaun *et al*, 2004b; Lomakin *et al*, 2003; Maag *et al*, 2005). Consistent with this, mutations in yeast eIF1 that accelerate eIF1 disassociation from the 43S preinitiation complex *in vitro* trigger an increase in selection of UUG codons *in vivo*, highlighting the importance of eIF1 departure in the fidelity of initiation codon selection (Cheung et al, 2007). It is thought that the eIF2α subunit of eIF2 interacts with the purine at the -3 position, antagonising disassembly of the 43S preinitiation complex by eIF1 and facilitating start codon selection (Pisarev et al, 2006).

DHX29 has also been proposed to play a role in the fidelity of start codon selection. Using a reconstitution system for translation initiation, it was shown that DHX29 promotes linear scanning by ensuring that mRNA enters the binding channel on the 40S subunit in a single-stranded form, thus preventing "bypass" of stem-loop structures (Abaeva *et al*, 2011). Furthermore, DHX29 addition promotes recognition of AUG codons but not near-cognate CUG codons in a manner dependent upon its interaction with eIF1A, most likely through conformational modulation of the scanning ribosomal complex (Pisareva & Pisarev, 2016b). As two subunits of eIF3 (eIF3a and eIF3c) also interact with eIF1 and eIF1A, eIF3 may additionally influence initiation codon selection (Querol-Audi *et al*, 2013). Upon start codon recognition and establishment of correct codon-anticodon base-pairing, the scanning 43S complex forms a 48S complex at the initiating codon.

1.1.5 Commitment and 60S ribosomal subunit joining

The commitment step which commits the assembled 48S complex to 60S ribosomal subunit joining is mediated by eIF5, an eIF2-specific GTPase activating protein (GAP) (Jackson *et al*, 2010). eIF5 interacts with the eIF2 subunit eIF2β and induces the GTPase activity of eIF2γ, potentially by acting as a classical GAP by providing an arginine finger (Paulin *et al*, 2001). GTP hydrolysis leads to partial dissociation of eIF2 from the preinitiation complex by reducing its affinity for Met-tRNA$_i^{Met}$ (Pisarev *et al*, 2006; Kapp & Lorsch, 2004). Premature hydrolysis and subsequent Pi release is prevented by eIF1 (Unbehaun *et al*, 2004b; Algire *et al*, 2005), which departs from the preinitiation complex upon establishment of correct codon-anticodon

base-pairing (Maag *et al*, 2005). A recent cryo-EM structure of the yeast preinitiation complex has suggested that the N-terminal domain of eIF5 contacts the site vacated by eIF1 on the 40S subunit (Llácer *et al*, 2018). eIF5 also possesses GDP dissociation inhibitor activity independent of its GAP activity and thus negatively regulates the recycling of eIF2-GDP by the guanine nucleotide exchange factor (GEF) eIF2B to reform eIF2-GTP (Jennings & Pavitt, 2010).

The joining of the 60S ribosomal subunit and subsequent departure of eIFs is mediated by eIF5B, a ribosome-dependent GTPase (Unbehaun *et al*, 2004b; Pestova *et al*, 2000). 60S joining requires GTP-bound eIF5B but is independent of GTP hydrolysis. GTPase activity is triggered by the interaction of eIF5B with the C-terminal tail of eIF1A (Olsen *et al*, 2003; Marintchev *et al*, 2003; Acker *et al*, 2006) which accelerates the release of eIF1A and eIF5B from the 80S ribosomal complex (Pestova *et al*, 2000; Shin *et al*, 2002; Acker *et al*, 2009). At this point productive protein synthesis can begin. Some factors such as eIF3 may remain transiently associated with the elongating ribosome, which could permit rescanning and reinitiation following translation of a short upstream open reading frame (uORF) (Jackson *et al*, 2010; Pöyry *et al*, 2004).

1.1.6 Control

Mechanisms that regulate translation initiation fall broadly into one of two categories; those that directly impact eIFs and thus impact all scanning-dependent initiation events or those that impact certain mRNAs specifically (Jackson et al, 2010). A well-established example of the former is phosphorylation of the eIF2α subunit of eIF2 on serine-51 by one of four mammalian kinases including protein kinase R (PKR), whose activation by dsRNA is important in cellular antiviral responses, and PKR-like endoplasmic reticulum kinase (PERK), which is activated by ER stress as part of the unfolded protein response in the ER lumen (reviewed in Proud, 2005). Phosphorylation of eIF2α triggers sequestration of the GEF eIF2B by eIF2α-GDP, thus preventing recycling of eIF2-GDP to eIF2-GTP and inhibiting ternary complex formation. While this typically downregulates translation of most cellular transcripts, certain transcripts are preferentially upregulated. A well-characterised example is ATF4, the mRNA of which possesses two uORFs. Under conditions of reduced ternary complex, reinitiation at the second inhibitory uORF following translation of the first is reduced, thus permitting increased translation of the downstream main ORF (Vattem & Wek, 2004).

eIF4F is also affected by phosphorylation both directly and indirectly. Hypo-phosphorylation of eIF4E-binding proteins (4E-BP1-3 in mammals) leads to sequestration of eIF4E from its interaction with eIF4G thus abrogating cap-dependent translation initiation, whereas phosphorylation of 4E-BPs by the kinase mammalian target of rapamycin (mTOR) releases this inhibition (Ma & Blenis, 2009). Direct phosphorylation of eIF4E is mediated by mitogen-activated protein kinase-interacting kinase (Mnk) 1/2 at serine-209, leading to translational upregulation of certain classes of mRNAs involved in cell proliferation, interferon production and inflammation through a poorly characterised mechanism (Furic et al, 2010; Herdy et al, 2012; Ueda et al, 2004; Waskiewicz et al, 1997).

Translational regulation of specific mRNAs can occur through a variety of different mechanisms but often involves the recognition and binding of an RNA-binding protein to appropriate accessible sequences located either at the 5' or 3' UTR of the mRNA (Jackson et al, 2010; Gebauer & Hentze, 2004). A well characterised example is binding of the iron regulatory proteins to a specific stem-loop motif within the 5' UTR of the ferritin mRNAs, which block eIF4F-dependent recruitment of the 43S preinitiation complex under conditions of iron depletion (Gray & Hentze, 1994; Muckenthaler et al, 1998). Most protein-binding regulatory motifs are found within the 3' UTR of mRNAs and are typically involved with the formation of an inhibitory “closed loop” to spatially occlude the recruitment of eIF4F to the 5' cap structure, highlighting the importance of interactions between the 5' and 3' ends of mRNA in translation regulation. An example of such a loop is found during vertebrate oocyte maturation on mRNAs containing uridine-rich cytoplasmic polyadenylation elements within their 3' UTRs. This motif is bound by the cytoplasmic-polyadenylation-element-binding protein, which interacts with a protein possessing an eIF4E-binding domain known as Maskin, in turn disrupting the eIF4E-eIF4G interaction thus decreasing translation initiation (Stebbins-Boaz *et al*, 1999).

The 3' UTRs of mRNAs are also targeted by microRNAs (miRNAs), typically 21 to 25 nt in length, that base-pair imperfectly with specific RNA sequences in complex with Argonaute proteins (Ago1-4 in humans) (Jackson *et al*, 2010). While initially it was unclear whether miRNAs hindered translation or enhanced degradation of target mRNAs, the current model is that both occur sequentially, with translational inhibition preceding mRNA degradation (Djuranovic *et al*, 2012; Bazzini *et al*, 2012; Meijer *et al*, 2013). The mechanism of translational inhibition is unclear, but has been proposed to involve eIF4AII (Meijer *et al*, 2013), one of two mammalian homologues of eIF4A that are not functionally identical (Galicia-Vázquez *et al*, 2012) and differentially regulated during cellular differentiation (Galicia-Vázquez *et al*, 2014).

It is becoming increasingly apparent that modifications to ribosomal RNA and nonessential ribosomal proteins also impart regulation upon translation initiation and mRNA selection (Kwan & Thompson, 2019). This challenges the paradigm that ribosomes are merely the protein synthesis machinery and opens up new avenues of translational control to investigate. For example, the ribosomal protein RPL38 helps to selectively facilitate the translation of *Hox* mRNAs that are important in mammalian development (Kondrashov *et al*, 2011; Xue *et al*, 2015).

1.2 Noncanonical mechanisms of translation initiation

Cap-dependent translation is typically downregulated under conditions of cellular stress (Wek, 2018) or during some viral infections (Stern-Ginossar *et al*, 2018). As a result, cellular or viral proteins that are required to adapt or survive are synthesised via noncanonical mechanisms of translation initiation. These mechanisms vary with regards to eIF requirement, whether scanning or 5' cap recognition are used and the cellular conditions in which they occur. Detailed knowledge of these mechanisms have lagged behind our understanding of canonical translation initiation largely due to a lack of genetic and biochemical systems, as many of these mechanisms function only in mammals and not yeast (Kwan & Thompson, 2019).

1.2.1 IRES-mediated

An internal ribosome entry site (IRES) is a complex RNA secondary structure that facilitates the direct recruitment of ribosomes and eIFs internally in a 5'- and cap-independent manner. These diverse structures are often used by viruses during infection to ensure translation of their own genomes at the expense of the host genome under conditions of translational suppression (Jackson *et al*, 2010; Walsh & Mohr, 2011; Lozano & Martínez-Salas, 2015). Viral IRESs are classified based on their structure, eIF requirement and mechanism of initiation (Kwan & Thompson, 2019). Examples of different types of IRES are shown in Table 1.2.

Table 1.2 IRES classification

Adapted from Kwan & Thompson, 2018. Type I-V refer to picornaviral IRES subtypes. Many IRESs also require cellular IRES *trans*-acting factors (ITAFs) for activity. eIF4Gm ($eIF4G_{736-1115}$), middle fragment of eIF4G; PV, poliovirus; EMCV, encephalomyocarditis virus; HAV, hepatitis A virus; HCV, hepatitis C virus; CrPV, cricket paralysis virus; HIV, human immunodeficiency virus; SIV, simian immunodeficiency virus; FIV, feline immunodeficiency virus.

Name	eIF requirement	Examples	Notable features
Type I	eIF2, eIF3, eIF4A, eIF4Gm	PV, enterovirus 71, bovine enterovirus, coxsackievirus B3, human rhinovirus 2	Ribosomal scanning from site of recruitment
Type II	eIF2, eIF3, eIF4A, eIF4B, eIF4Gm	EMCV, foot-and-mouth disease virus, Theiler's murine encephalomyelitis virus	Initiates translation directly from site of recruitment
Type III	eIF2, eIF3	Avian encephalomyelitis virus, porcine teschovirus 1, simian picornavirus 9	
Type IV	eIF2, eIF3, eIF4A, eIF4B, eIF4E, eIF4G	HAV	eIF4E requirement but not cap-binding
Type V	eIF2, eIF3, eIF4A, eIF4B, eIF4Gm	Aichivirus	Absolutely dependent on DHX29
HCV-like	eIF2, eIF3	HCV, classical swine fever virus	Can bind directly to the 40S subunit
Dicistrovirus	None	CrPV, *Drosophila* C virus, influenza A virus, *Plautia stali* intestine virus	Initiates in the absence of eIFs
Retrovirus	eIF4A, eIF4G, eIF5A	HIV-1, SIV, FIV, human T-cell leukaemia virus 1	
Herpesvirus	eIF4F	Kaposi sarcoma herpesvirus, Marek's disease virus	

The first to be identified were the IRESs from the *Picornaviridae* family members poliovirus (PV) (Pelletier & Sonenberg, 1988) and encephalomyocarditis virus (EMCV) (Jang *et al*, 1988), both ~450 nt long which exemplify Type I and Type II IRESs, respectively. Subsequent reconstitution experiments have shown that both require all but eIF4E and the N-terminal domain of eIF4G (in which the eIF4E-binding site is located) of the canonical set of translation initiation factors (Pestova *et al*, 1996a, 1996b). Both types of IRES rely on the specific recruitment of eIF4G to a domain adjacent to a Yn-Xm-AUG motif (pyrimidine tract-spacer-AUG) within the IRES structure (Kolupaeva *et al*, 2003; de Breyne *et al*, 2009). This interaction allows these IRESs to retain activity in virus-infected cells when eIF4G has been cleaved by viral proteases, thus "shutting off" host cell translation (Gradi *et al*, 1998). Both IRES types also require additional cellular factors termed IRES *trans*-acting factors (ITAFs) for efficient

activity, namely polypyrimidine tract-binding protein (PTB) (Pilipenko *et al*, 2000) in the case of EMCV and poly(C)-binding protein 2 (PCBP2) in PV (Sweeney *et al*, 2014).

Hepatitis C virus (HCV), a member of the family *Flaviviridae* and the genus *Hepacivirus*, contains a 341 nt IRES (Hellen, 2009). Biochemical reconstitution experiments have revealed that the 40S ribosomal subunit, Met-tRNA$_i^{Met}$ and eIF2 are sufficient for 48S complex formation in the absence of other factors in a scanning-independent manner, with eIF3 stabilising this complex and playing a role in 60S subunit joining along with eIF5 and eIF5B (Reynolds *et al*, 1996; Pestova *et al*, 1998b; Locker *et al*, 2007). As such, the HCV IRES functionally replaces the activity of the eIF4F complex in translation initiation. Under conditions of cellular stress, the IRES also facilitates an eIF2-independent mode of initiation (Pestova *et al*, 2008). The HCV IRES can directly interact with both eIF3 and the 40S ribosomal subunit (Pestova *et al*, 1998b) and recent high resolution cryo-EM structures have provided mechanistic insights into these interactions (Hashem *et al*, 2013b; Quade *et al*, 2015; Yamamoto *et al*, 2015).

The most elegant form of viral IRES is exemplified by the *Dicistroviridae* family member cricket paralysis virus (CrPV), which possesses a ~200 nt sequence that directly positions the non-AUG initiation codon of the IRES within the A site of the 40S ribosomal subunit in the absence of Met-tRNA$_i^{Met}$ and eIFs (Sasaki & Nakashima, 2002; Pestova & Hellen, 2003; Schüler *et al*, 2006). Interestingly, both the CrPV (Spahn *et al*, 2004) and HCV (Spahn *et al*, 2001) IRESs induce conformational changes in the 40S ribosomal subunit, similar to the conformational changes induced by binding of eIF1 and eIF1A within the 43S preinitiation complex (Passmore *et al*, 2007). This illustrates that mRNA structure alone is capable of mediating ribosome recruitment and manipulation.

1.2.2 Cap-independent translation elements

Cap-independent translation elements (CITEs) are responsible for the translation of plant viruses of the families *Tombusviridae* and *Luteoviridae* whose RNAs lack 5' cap structures and poly(A) tails (Kwan & Thompson, 2019). These elements are typically found within the 3' UTR and recruit the 40S ribosomal subunit by directly interacting with the eIF4F complex, with long-range RNA-RNA interactions bridging the 5' and 3' UTRs to facilitate loading and subsequent scanning at the 5' end. CITEs vary dramatically in sequence and structure and to date seven different classes have been described (Miras *et al*, 2017). A well characterised CITE is found

within barley yellow dwarf virus RNA, which binds predominately to eIF4G within the eIF4F complex (Treder *et al*, 2008; Sharma *et al*, 2015). This element contains a 17 nt conserved sequence (GGAUCCUGGGAAACAGG) involved in the formation of a stem-loop structure required for this recruitment.

1.2.3 N^6-methyladenosine

Methylation of adenine residues within mRNA to generate N^6-methyladenosine (m^6A) is the most common form of mRNA posttranscriptional modification and has been linked to mRNA turnover and translational efficiency (reviewed in Peer *et al*, 2018). A recent study has found that these modifications within the 5' UTR can mediate cap-independent translation initiation through direct interaction with eIF3 in a manner requiring a free 5' end (Meyer *et al*, 2015). By mapping m^6A modifications under different cellular conditions, it has been shown that m^6A modifications are enriched within the 5' UTRs of nascent mRNAs following heat shock, suggesting that this mechanism could act to ensure translation of stress response factors under conditions of cellular stress (Meyer *et al*, 2015; Zhou *et al*, 2015). Further research is required to investigate the mechanism and regulation of m^6A-mediated initiation.

1.2.4 eIF2D

eIF2D (also known as Ligatin) is a protein that was identified through its ability to deliver Met-$tRNA_i^{Met}$ to 40S ribosomal subunits in the absence of GTP (Dmitriev *et al*, 2010) and separately through its ability to release deacylated tRNA and mRNA from recycled 40S subunits (Skabkin *et al*, 2010). In a reconstitution system, eIF2D can replace eIF2 in mediating translation initiation on several mRNAs including the 26S subgenomic RNA of Sindbis virus (SV) (Skabkin *et al*, 2010), thus potentially explaining how translation of this RNA continues during infection despite translational shutoff induced by eIF2α phosphorylation (McInerney *et al*, 2005; Ventoso *et al*, 2006). However, this mechanism has been poorly characterised and is thought to depend on direct recruitment of the 40S ribosomal subunit to the initiating AUG codon of SV 26S mRNA, rather than scanning (Skabkin *et al*, 2010). In comparison to eIF2-GTP which binds Met-$tRNA_i^{Met}$ and delivers it to the 40S subunit (Jackson *et al*, 2010), the interaction of eIF2D with Met-$tRNA_i^{Met}$ is 40S-dependent and thus it has been proposed that eIF2D acts to anchor initiator tRNA to the small ribosomal subunit (Skabkin *et al*, 2010; Weisser *et al*, 2017). Cryo-EM and crystal structures of 40S ribosomal subunits bound to eIF2D or MCT-1/DENR (related proteins which are homologous to the N- and C-terminal regions of eIF2D, respectively) have illustrated that eIF2D occupies the equivalent position as eIF1, as

well as partially overlapping binding sites for eIF2, eIF5, eIF5B and eIF3 (Lomakin *et al*, 2017; Weisser *et al*, 2017). It is likely therefore that eIF2D acts at multiple stages during translation initiation.

1.2.5 eIF3d

Using an immunoprecipitation approach, it was shown that eIF3 binds directly to a large number of cellular mRNAs linked to cell proliferation including *c-JUN* and either mediates translational activation or repression through binding to different RNA secondary structures (Lee *et al*, 2015). A follow-up study has illustrated that a subunit of eIF3, eIF3d, possesses cap-binding activity and thus permits eIF4E-independent translation of *c-JUN* (Lee *et al*, 2016). eIF3d exhibits structural homology to DXO proteins, a family of 5' cap endonucleases (Chang *et al*, 2012; Jiao *et al*, 2013), with an additional insertion termed the "RNA gate" thought to prevent promiscuous cap binding through allosteric interactions with other eIF3 subunits (Lee *et al*, 2016). Furthermore, *c-JUN* mRNA contains a *cis*-acting element that blocks eIF4F-dependent ribosome recruitment, ensuring that translation only occurs through this eIF4E-independent mechanism (Lee *et al*, 2016). It remains to be determined how widespread eIF3d-specific translation initiation is and whether it is exploited by viruses during infection to escape regulation by 4E-BPs.

1.2.6 Ribosomal shunting

Some notable exceptions to the linear mode of scanning performed by the 43S preinitiation complex during translation initiation have been identified. For example, scanning complexes upon late adenovirus mRNAs have been shown to undergo ribosome shunting under the conditions of reduced eIF4E phosphorylation, in which the ribosomes are recruited to the mRNA in a 5' end-dependent manner before subsequently bypassing large sections of mRNA including stable secondary structures inhibitory to translation (Yueh & Schneider, 1996). Evidence for this mechanism comes from the fact that translation from an additional AUG codon inserted within the bypassed region on shunt-competent adenovirus reporter RNAs transfected into 293 cells is not seen during late adenovirus infection or following heat shock, both of which inhibit eIF4E phosphorylation. Instead, translation only initiates from the downstream authentic AUG codon. Comparatively, in uninfected cells products from both the introduced and authentic AUG codons are observed, suggesting that under normal physiological conditions both linear scanning and shunting occur (Yueh & Schneider, 1996). The shunting mechanism is dependent upon a 200 nt tripartite leader sequence, which is

complimentary to the 18S rRNA 3' hairpin of the 40S ribosomal subunit, and is promoted by interaction of the adenovirus 100k protein with eIF4G (Yueh & Schneider, 2000, 1996; Xi *et al*, 2005). As ribosome shunting on cauliflower mosaic virus requires translation of a short uORF, it has been speculated that shunting may represent a special form of reinitiation (Pooggin *et al*, 1998; Ryabova & Hohn, 2000). Many questions still remain about precisely how such complexes are reinitiated following shunting and the eIFs required for this process.

Taking all of the evidence into consideration then, the study of translation is ultimately still in its infancy. While many of the key factors and regulatory mechanisms controlling canonical translation initiation have been identified, key details regarding the topology of the scanning complex as well as the involvement of additional factors such as nonessential ribosomal proteins are still ill-defined. Additionally, it is becoming increasingly apparent that translation initiation can occur through a variety of noncanonical mechanisms, many of which have so far have been poorly characterised both in terms of mechanistic detail and in terms of prevalence. As obligate intracellular parasites that manipulate the host cell translation machinery, viruses have provided an invaluable tool to probe many of these different mechanisms. Looking to the future, the major challenge lies in determining the relative contribution of these initiation mechanisms to overall gene expression in different physiological states, such as during cancer progression or early in mammalian development.

1.3 Flavivirus classification and disease

The genus *Flavivirus* of the family *Flaviviridae* consists of more than 70 positive-sense RNA viruses, many of which are human pathogens including Dengue virus (DENV), made up of four closely related but antigenically distinct serotypes (1-4), and Zika virus (ZIKV). Other notable members include West Nile virus (WNV), yellow fever virus (YFV) and Japanese encephalitis virus (JEV). These viruses are typically arthropod-borne (and are thus classified as arboviruses) and have been traditionally assigned based on their arthropod vectors into one of three clusters; mosquito-borne (MBFVs), tick-borne (TBFVs) and no-known-vector (NKFVs) flaviviruses (Kuno *et al*, 1998; Cook & Holmes, 2006). While the MBFVs and the TBFVs can replicate in both vertebrates and arthropods, NKFVs have typically only been isolated from vertebrates and are bat- or rodent-associated (Blitvich & Firth, 2017). More recently, a fourth cluster has been identified referred to as insect-specific flaviviruses (ISFVs), members of which can only replicate in insect cells and not mammalian cells (Kuno, 2007; Cook *et al*, 2012).

The MBFVs (hence referred to as flaviviruses) can be further subdivided into Old World viruses linked to *Aedes* species mosquito transmission that cause haemorrhagic fever symptoms such as DENV and YFV or Old and New World viruses linked to *Culex* species mosquito transmission that cause encephalitis disease symptoms such as JEV and WNV (Huang *et al*, 2014). The emergence and persistence of these viruses is likely linked to the expanding habitat ranges of their insect vectors (Liang *et al*, 2015), as well as globalisation and poor environmental sanitation within densely populated urban areas (Imperato, 2016). While efforts to control vector-mediated transmission have been made (Benelli & Mehlhorn, 2016), ethical issues surrounding the use of transgenic mosquitoes (Resnik, 2014) and chemical resistance (Liu, 2015) have provided obstacles.

ZIKV infection is mainly linked to *Aedes* species mosquito transmission, although in contrast to other pathogenic flaviviruses ZIKV can also spread horizontally from person to person through sexual contact or vertically from mother to foetus (Petersen *et al*, 2016). While distinct African and Asian lineages exist, differing less than 5 % at the amino acid level (Haddow *et al*, 2012), neutralisation studies suggest that ZIKV exists as a single serotype (Dowd *et al*, 2016). ZIKV infection is usually asymptomatic but common symptoms include rash, arthritis or arthralgia, conjunctivitis, myalgia, headache and retro-orbital pain (Petersen *et al*, 2016). During the recent epidemic in Brazil (2015-2016), a striking increase in congenital microcephaly cases was observed and a case-control study has found an increased risk of microcephaly associated with ZIKV infection (de Araújo *et al*, 2016, 2018). Findings from this study have been supported by evidence showing that ZIKV genetic material can be detected within the amniotic fluid surrounding an infected foetus (Calvet *et al*, 2016) and from foetal brain tissue (Mlakar *et al*, 2016; Driggers *et al*, 2016). Furthermore, it has been shown in numerous *in vivo* and *in vitro* models that ZIKV infection disrupts neurodevelopment (Cugola *et al*, 2016; Miner *et al*, 2016; Qian *et al*, 2016; Tang *et al*, 2016; Adams Waldorf *et al*, 2016). ZIKV infection has also been linked to other severe neurological diseases including the autoimmune disease Guillain-Barré syndrome in infected adults (Cao-Lormeau *et al*, 2016).

To date, there is no approved vaccine or specific antiviral against ZIKV infection and prescribed treatment is palliative. Numerous attempts have been made to screen FDA-approved drugs for antiviral activity generating hits such as the anthelminthic niclosamide, the antimicrobial daptomycin and the antibiotic azithromycin (Xu *et al*, 2016; Barrows *et al*, 2016; Retallack *et al*, 2016), although their efficacy is limited. A better understanding of how flaviviruses such as

ZIKV co-opt the host cell machinery during infection could lead to new therapeutic targets being identified, whether they be viral or cellular in origin.

1.4 Flavivirus genome organisation

The flaviviral genome consists of a positive-sense single-stranded RNA of ~11 kb in size. The genome possesses a cap1 structure (m^7GpppAmp) at its 5' end (Ray et al, 2006; Zhou et al, 2007; Saeedi & Geiss, 2013) but lacks the 3' poly(A) tail (Wengler & Wengler, 1981) that is characteristic of cellular mRNAs. The genome consists of a single ORF flanked by 5' and 3' UTRs of ~100 nt and 400-700 nt, respectively (Rice et al, 1985). The ORF is expressed as a single polyprotein that is co- and post-translationally cleaved to yield 10 different mature proteins (Rice et al, 1985; Nowak et al, 1989; Bera et al, 2007). A schematic of flavivirus genome organisation is shown in Figure 1.3.

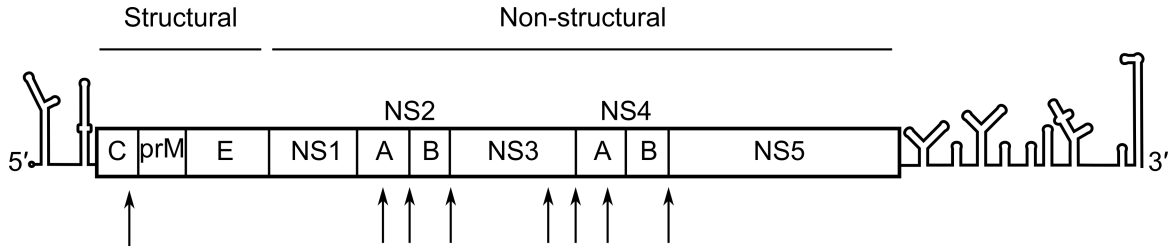

Figure 1.3 Schematic of flavivirus genome organisation

The structural proteins consist of capsid (C), precursor of membrane (prM) and envelope (E) proteins. The non-structural (NS) proteins possess numerous activities. Broadly, NS1 functions in negative-strand synthesis and protection from cell compliment, NS2A/B and NS4A/B are involved with replication complex assembly at the ER, NS2B-NS3 function as a protease and NS5 possesses RNA-dependent RNA polymerase and capping activity. The genome is translated as a single polyprotein before cleavage by NS2B-NS3 (cleavage sites are indicated by arrows) and other cellular proteases. The viral 2K peptide is entirely membrane-inserted and formed from protease cleavage between NS4A and NS4B (Fernández-Sanlés *et al*, 2017; Barrows *et al*, 2018).

1.5 The flavivirus lifecycle

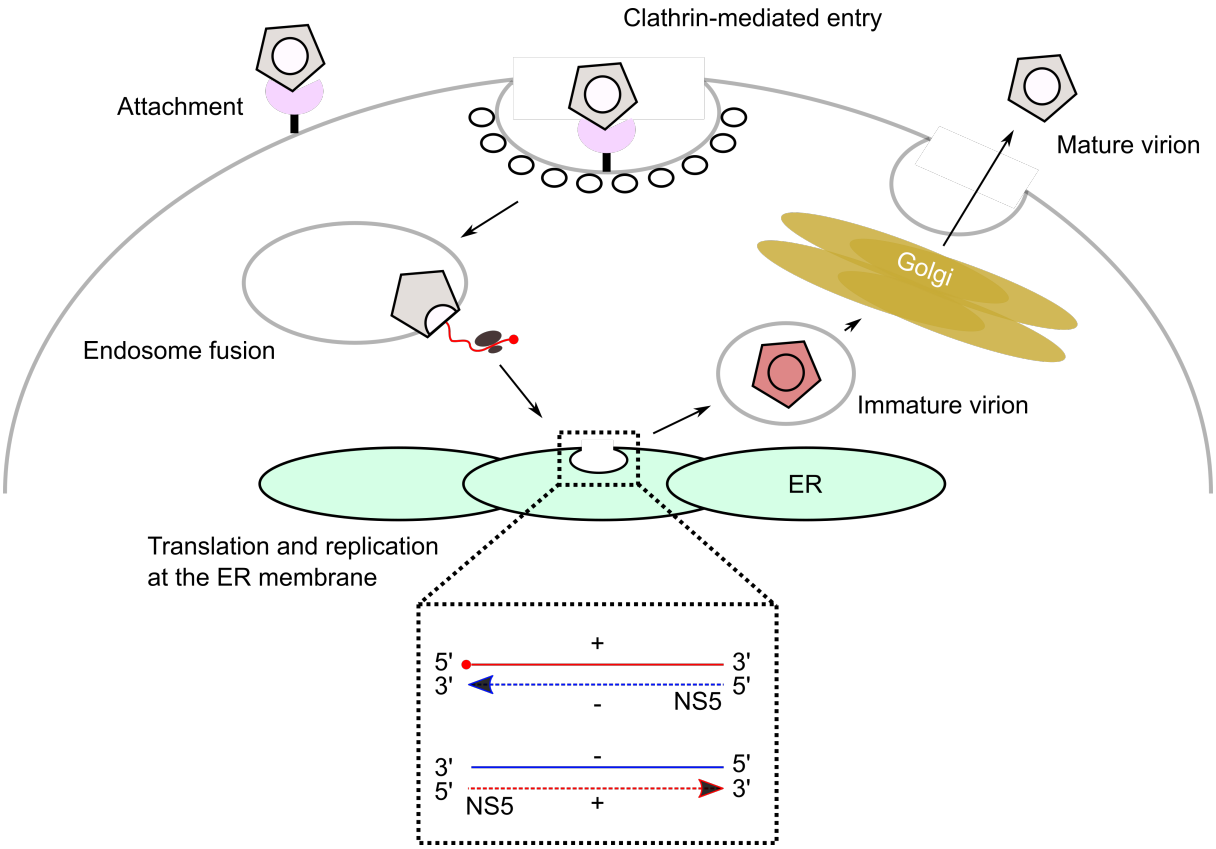

Figure 1.4 Schematic of the flavivirus lifecycle

Attachment occurs through a variety of different receptors and co-receptors. Entry is clathrin-mediated and genome release into the cytosol depends upon the low pH environment of the endosome. Engagement of the genome by the translation machinery results in ER-localisation and subsequent translation. Genome replication takes place within ER-derived replication complexes. Virion assembly takes place at the ER membrane and virion maturation occurs within the Golgi network driven by changes in pH (Fernández-Sanlés *et al*, 2017; Barrows *et al*, 2018). Positive-sense RNA is in red whereas negative-sense is in blue.

1.5.1 Virion structure and attachment

Cryo-EM has shown that mature flavivirus virions are structurally well conserved (typically 50 nm in diameter) and consist of an icosahedral shell containing 180 copies each of the envelope (E) glycoprotein with the membrane (M) protein or precursor membrane (prM) protein anchored in a lipid membrane (Sirohi *et al*, 2016; Kuhn *et al*, 2002; Zhang *et al*, 2013; Mukhopadhyay *et al*, 2003; Kostyuchenko *et al*, 2016). Little is known about the structure of the interior, presumed to contain a single viral genome complexed with several hundred copies of the capsid (C) protein (Garcia-Blanco *et al*, 2016).

Cell attachment is mediated by the viral E protein, the structure of which differs around glycosylation sites at the virion exterior between flaviviruses (Sirohi *et al*, 2016; Kostyuchenko

et al, 2016). It is likely that flaviviruses require multiple different low affinity receptors and co-receptors that define pathogenesis and tissue tropism, potentially explaining the broad range of disease manifestations seen in infected patients (Cruz-Oliveira *et al*, 2015). Several have been characterised for DENV and include the mannose receptor on macrophages (Miller *et al*, 2008) and the dendritic cell-specific ICAM3 grabbing nonintegrin on immature dendritic cells (Pokidysheva *et al*, 2006). Receptors for ZIKV have been less well-characterised, although several studies have proposed that the receptor tyrosine kinase Axl acts as a major entry receptor for ZIKV in neural stem cells (Hamel *et al*, 2015; Savidis *et al*, 2016; Nowakowski *et al*, 2016).

It has been well-established that secondary infection by a different DENV serotype is associated with severe dengue disease in a phenomenon termed antibody-dependent enhancement (ADE) (Guzman *et al*, 2013; Halstead & O'Rourke, 1977). An explanation for this observation is that heterotypic antibodies produced against the first DENV serotype recognise and bind to the heterologous serotype but instead of mediating virus neutralisation, facilitate internalisation of antibody-bound virions within FcγR-expressing cells (Guzman *et al*, 2013; Murphy & Whitehead, 2011). This provides an additional uptake mechanism for infectious DENV into typically non-permissive cell types. While it was initially hypothesised that ADE of ZIKV in response to a primary DENV infection may provide a mechanism for crossing the placental barrier, recent *in vivo* studies have suggested that a pre-existing DENV infection does not pre-dispose rhesus macaques or human patients to ZIKV infection (McCracken *et al*, 2017; Pantoja *et al*, 2017; Terzian *et al*, 2017).

1.5.2 Entry

Clathrin-mediated endocytosis is thought to be the primary mechanism by which flavivirus virions enter both mammalian and mosquito cells (Chu & Ng, 2004; van der Schaar *et al*, 2008; Acosta *et al*, 2008; Mosso *et al*, 2008). Single particle tracking of DENV virions in African green monkey kidney cells illustrates that virions are initially delivered into early Rab5-labelled endosomes that subsequently mature into Rab7-positive late endosomes, from within which membrane fusion occurs (van der Schaar *et al*, 2008). This membrane fusion is thought to depend on the actions of the cellular vacuolar ATPase (vATPase), a multi-subunit protein that actively pumps protons into the endosome thus lowering pH (Forgac, 2007). Ingestion of the vATPase inhibitor bafilomycin or depletion of vATPase subunits was found to reduce DENV titres *in vivo* during infection of mosquitos (Kang *et al*, 2014). Additionally, the FDA-approved drug chloroquine that inhibits endosome acidification has been shown to impair ZIKV

infectivity and vertical transmission within mouse models of infection, suggesting that targeting viral entry may represent a potential therapeutic target (Shiryaev *et al*, 2017; Li *et al*, 2017).

Evidence from structural studies has suggested that flaviviral entry from within the late endosome relies upon pH-dependent trimerization of the E protein thus exposing a fusion peptide (Modis *et al*, 2004; Mukhopadhyay *et al*, 2005). This ultimately results in the fusion of the viral and endosomal membranes thus depositing the viral RNA in complex with viral C protein into the cytosol. The mechanism of genome release from this complex is unclear, but it has been linked to C protein ubiquitination (Byk *et al*, 2016) and ribosome elongation (Garcia-Blanco *et al*, 2016).

1.5.3 Viral translation

Translation of the flavivirus genome during infection is thought to initiate through a cap- and eIF4E-dependent mechanism, as the viral genome encodes the activities required for addition of a 5' cap1 structure including N-7 and 2′-O methylation (Ray *et al*, 2006; Egloff *et al*, 2002; Issur *et al*, 2009; Bartelma & Padmanabhan, 2002; Wengler & Wengler, 1993). A mRNA cap structure is illustrated in Figure 1.5. It has been shown that addition of an N-7 methylated cap greatly enhances translation of a luciferase-containing WNV replicon (Ray *et al*, 2006) and a firefly luciferase (Fluc) reporter flanked by the UTRs of DENV (Chiu *et al*, 2005) following transfection into baby hamster kidney (BHK) or Vero cells, respectively. Furthermore, mutational analysis of WNV infectious clones has shown that virally-encoded cap N-7 methylation activity is essential for viral replication (Zhou *et al*, 2007; Dong *et al*, 2008a). Comparatively, 2′-O methylation of the cap-proximal nucleotide (distinguishing a “self” cap1 structure from a “non-self” cap0 structure) is not essential for viral replication but instead has been proposed to prevent recognition from the interferon-induced proteins with tetratricopeptide repeats (IFIT) family of RNA-binding proteins, as IFIT1 can attenuate 2′-O methyltransferase-deficient ZIKV and WNV (Daffis *et al*, 2010; Johnson *et al*, 2018). As IFIT1 has been shown to inhibit cap-dependent translation initiation by outcompeting eIF4F for binding to the cap0 structure (Kumar *et al*, 2014), taken together, these data suggest that a cap-dependent mechanism of translation initiation plays an important role during flavivirus infection.

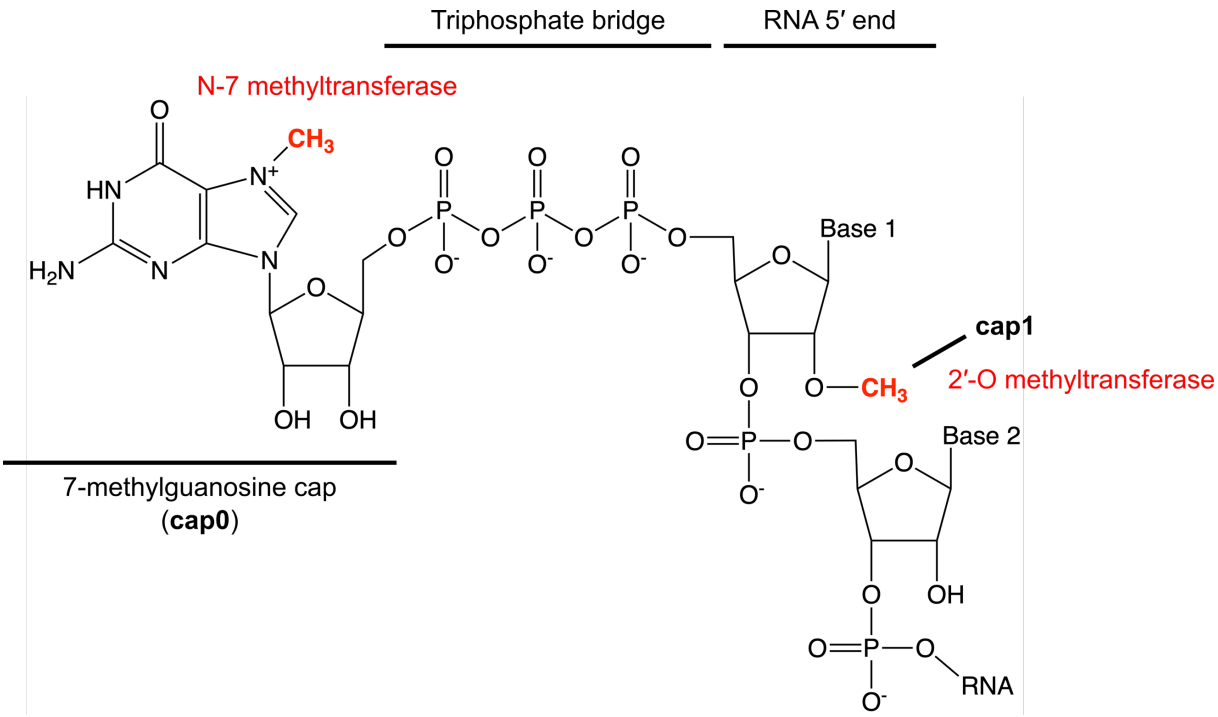

Figure 1.5 The 5′ cap structure

The cap structure is attached to the 5′ end of mRNA via a 5′-5′ triphosphate bridge. Indicated in red are the methyl groups (and corresponding enzymatic activities) whose addition is catalysed by NS5 (Ray *et al*, 2006; Egloff *et al*, 2002). 2′-O methylation of the cap-proximal nucleotide is found in higher eukaryotes and distinguishes a cap1 from a cap0 structure (Kumar *et al*, 2014).

However, a recent study has shown using polysome profiling of infected human hepatoma Huh7 cells that DENV (all serotypes), ZIKV and WNV infection all induce host cell translational repression at the initiation stage and suppress stress granule formation (Roth *et al*, 2017). This translational repression occurs independently of characterised pathways of inhibition, namely phosphorylation of eIF2α or eIF4E sequestration by 4E-BP1. Furthermore, DENV infection was found to phosphorylate eIF4E through Mnk1, and while eIF4E phosphorylation was not responsible for host cell translational suppression or DENV replication, active Mnk1 signalling was found to enhance infectious DENV particle production (Roth *et al*, 2017). As such, the mechanism that allows translation of flaviviral genomes under these conditions at the expense of cellular mRNAs is unclear.

One hypothesis is that flaviviruses can switch from a cap-dependent mechanism of translation initiation to a cap-independent mechanism under certain cellular conditions. DENV titres are unaffected when infected Vero or BHK cells are treated with drugs that result in the sequestration of eIF4E by 4E-BP1 or are depleted of eIF4E by siRNA (Edgil *et al*, 2006). Furthermore, efficient translation of an ApppN-capped (thus abolishing the interaction with eIF4E in comparison to m^7GpppN-capped) Fluc reporter flanked by the DENV UTRs in BHK

cells only occurs under conditions of eIF4E sequestration, in a manner dependent upon both viral UTRs. This is consistent with the switch to a cap-independent mechanism only occurring under conditions of limited eIF4E availability. In agreement with this, transfection of ApppN-capped full-length DENV RNA into BHK cells only leads to productive infection (typically 20-30 % of the m^7GpppN-capped equivalent) under pharmacological inhibition of eIF4E availability (Edgil *et al*, 2006).

While this cap-independent mechanism of flaviviral translation initiation is proposed to be non-IRES mediated (Edgil *et al*, 2006), a recent study has demonstrated that short nucleotide sequences within the 5' UTRs of DENV (96 nt) and ZIKV (107 nt) function as IRESs in mammalian BHK cells (Song *et al*, 2019). The cellular conditions in which such a mechanism might operate during infection remains to be determined and the identity of the cellular proteins responsible for this activity are completely unknown. It is likely that cap-dependent and cap-independent (both non IRES and IRES-mediated) mechanisms are important at different stages of the flaviviral lifecycle, the hierarchy of which has implications for targeting translation initiation as a therapeutic strategy. Interestingly, it has also been shown that ribosomal proteins such as RPL18 and RPLP1/2 are required for flavivirus infectivity (Cervantes-Salazar *et al*, 2015; Campos *et al*, 2017), providing an additional level of complexity.

Translation of the flaviviral genome yields a polyprotein. Expression of the C protein within the viral polyprotein is likely to localise the positive-sense RNA genome to the ER membrane following transmembrane domain recognition by the signal recognition particle (SRP) (Garcia-Blanco *et al*, 2016). Subsequent translation is thought to occur in association with ER membranes and a recent study has shown, by combining cell fractionation and ribosome profiling, that positive and negative-strand DENV RNA is highly partitioned within the ER during infection (Reid *et al*, 2018). Polyprotein processing is thought to be mediated by a variety of cellular and viral factors (reviewed in Barrows *et al*, 2018) including the viral protease NS2B-NS3 (Erbel *et al*, 2006; Chambers *et al*, 1990; Falgout *et al*, 1991). Subsequent expression and membrane integration of NS4A/B within the ER likely induces membrane rearrangements to facilitate the establishment of viral replication complexes (Miller *et al*, 2007; Roosendaal *et al*, 2006), which are visible by electron tomography in infected cells (Welsch *et al*, 2009; Cortese *et al*, 2017). The importance of this close ER association has been reaffirmed by genome-wide CRISPR studies illustrating that DENV replication is impaired when host cell factors linked to signal recognition or ER processing are knocked out (Zhang *et al*, 2016; Marceau *et al*, 2016; Savidis *et al*, 2016).

1.5.4 Genome replication

The viral polymerase NS5 and the viral helicase NS3 form the core of the viral replication complex as between them they possess all of the catalytic activities required for genome replication and addition of a 5′ cap structure. NS5 possesses an N-terminal methyltransferase (MTase) domain containing three activities required for cap synthesis (guanylyltransferase, guanine-N7-methyltransferase and nucleoside-2′-O-methyltransferase) and a C-terminal RNA-dependent RNA polymerase (RdRp) domain capable of *de novo* RNA synthesis (Issur *et al*, 2009; Ackermann & Padmanabhan, 2001; Egloff *et al*, 2002; Ray *et al*, 2006). NS3 has serine protease activity facilitated by an N-terminal domain in conjunction with its cofactor NS2B and a C-terminal domain possessing helicase, nucleoside triphosphatase and 5′ RNA triphosphatase activity (Bollati *et al*, 2010). This core complex is tethered to the ER membrane during viral replication due to the interaction of NS3 with its membrane bound cofactor NS2B (Yu *et al*, 2013). Other viral components of the replication complex include the ER lumen-localised NS1 protein and the membrane-associated NS2A, NS2B, 2K and NS4B proteins (Lindenbach & Rice, 1999; MacKenzie *et al*, 1998; Miller *et al*, 2006). Localisation of replication intermediates within a membrane-derived replication complex is likely to prevent recognition by innate immune sensors early in infection (Suthar *et al*, 2013; Hoenen *et al*, 2007).

Detailed biochemical analysis has shown that circularisation of the viral genome through long-range RNA-RNA interactions is necessary for viral replication, with the cap-proximal stem-loop at the 5′ end acting as a promoter for the initiation of negative-strand synthesis (see section 1.6**)** (Filomatori *et al*, 2006; Lodeiro *et al*, 2009; Dong *et al*, 2008b; Filomatori *et al*, 2011). Subsequent replication occurs in a semi-conservative fashion leading to the formation of a dsRNA intermediate (Wengler *et al*, 1978). Very little is known about positive-strand synthesis, but it is likely independent of genome circularisation and thus a single dsRNA intermediate could act as a template to generate many positive-sense RNA genomes. As synthesis of a new positive-strand begins, the currently bound genome would be displaced and undergo further rounds of translation-replication or be packaged into virions (Garcia-Blanco *et al*, 2016).

Capping of the nascent positive-strand RNA is thought to occur simultaneously with synthesis, but little is known about how these two processes are coordinated. The cap1 structure is formed in a three-step process. First, the triphosphatase activity of NS3 removes the terminal γ-phosphate from the 5′ pppA structure before addition of GMP mediated by the guanyltransferase activity of NS5 (yielding GpppA) (Issur *et al*, 2009; Bartelma & Padmanabhan, 2002; Wengler & Wengler, 1993). Finally, the MTase activity of NS5

sequentially methylates the cap at the N-7 position and the 2′-O position of the cap-proximal nucleotide using S-adenosylmethionine as a methyl donor, yielding m^7GpppAmp (Ray *et al*, 2006; Egloff *et al*, 2002).

1.5.5 Virion assembly and egress

Flavivirus assembly occurs at the ER membrane. C, prM and E proteins assemble with viral genomes and bud into the ER lumen which has been visualised by cryo-electron tomography in both mammalian and insect cells (Junjhon *et al*, 2014; Welsch *et al*, 2009). Non-structural proteins including NS2A (Xie *et al*, 2014) and NS3 (Patkar & Kuhn, 2008) are thought to play a role in this process, although so far they have been poorly defined. Interestingly, studies using a DNA-based WNV Kunjin replicon system, in which RNA is produced by nuclear transcription and subsequently translated, replicated and packaged, has shown that a link exists between polymerase activity and viral assembly. Viral packaging of replicon RNA containing a mutated NS5 polymerase active site only occurred after *trans*-complementation of wildtype NS5 activity despite the availability of genomes from nuclear transcription, thus demonstrating that active polymerase activity is required for genome packaging (Khromykh *et al*, 2001b).

Flavivirus virions mature as they travel through the Golgi and the *trans*-Golgi network, driven by the acidic pH within these compartments. This results in the loss of the spiky prM-E trimer projections characteristic of immature viral particles (Zhang *et al*, 2003), making prM accessible to cleavage by the furin cellular protease (Stadler *et al*, 1997). This cleavage event and changes in E protein arrangement lead to mature virion production and subsequent exocytosis from the infected cell (Mukhopadhyay *et al*, 2005).

1.6 RNA structures within flavivirus genomes

The majority of studies examining RNA secondary structure within flavivirus genomes have focused upon the terminal regions which contain numerous discrete RNA secondary structures that are essential for viral translation and viral replication (Gebhard *et al*, 2011). These structures were initially predicted bioinformatically (Brinton *et al*, 1986; Brinton & Dispoto, 1988; Rauscher *et al*, 1997; Thurner *et al*, 2004) and are consistent with data obtained from RNA structure probing approaches both *in vitro* and inside cells during viral infection (Dethoff *et al*, 2018; Huber *et al*, 2019; Li *et al*, 2018). It is important to note however that such predictions typically only support the most stable of several possible genome structures, and indeed data from studies examining RNA-RNA pairing interactions within the viral genome

during infection has suggested that alternative conformations can form (Ziv *et al*, 2018; Li *et al*, 2018). Regardless, the predicted structures present within the 5' and 3' terminal regions are highly conserved within the *Flavivirus* genus despite the lack of extensive sequence conservation (Brinton & Dispoto, 1988). With regards to the 5' region, the impact of RNA secondary structures have mostly been examined in DENV and subsequently extrapolated to other flaviviruses (Fernández-Sanlés *et al*, 2017).

1.6.1 Secondary structures within the 5' terminal region

The 5' UTR of flaviviruses is relatively short compared to IRES-containing members of the *Flaviviridae* family and folds into two discrete structures (Figure 1.6). The first is the cap-proximal stem-loop A (SLA), which folds into a conserved Y-shape due to the presence of a side stem-loop (SSL) emanating from the main structural element (Brinton & Dispoto, 1988). Studies have shown that SLA acts as the promoter for the viral polymerase NS5, facilitating its recruitment to the viral genome during infection (Filomatori *et al*, 2006; Lodeiro *et al*, 2009; Iglesias *et al*, 2011; Bujalowski *et al*, 2017). SLA is also required to direct cap formation at the 5' end of nascent positive-strand genomes during RNA synthesis (Dong *et al*, 2007). Highlighting the importance of the NS5-SLA interaction with regards to capping, transfection of a mutant WNV infectious clone containing only weak N-7 methyltransferase activity produced revertant viruses bearing second site mutations within SLA as well as within NS5 (Zhang *et al*, 2008c). As the cap structure is likely required for efficient translation (Chiu *et al*, 2005; Ray *et al*, 2006), SLA therefore represents a key link between the processes of viral translation and viral replication. It has been speculated that NS5 recruitment to SLA during the course of infection could disrupt ribosome loading onto viral genomes, although this has not been experimentally shown (Garcia-Blanco *et al*, 2016; Friedrich *et al*, 2018).

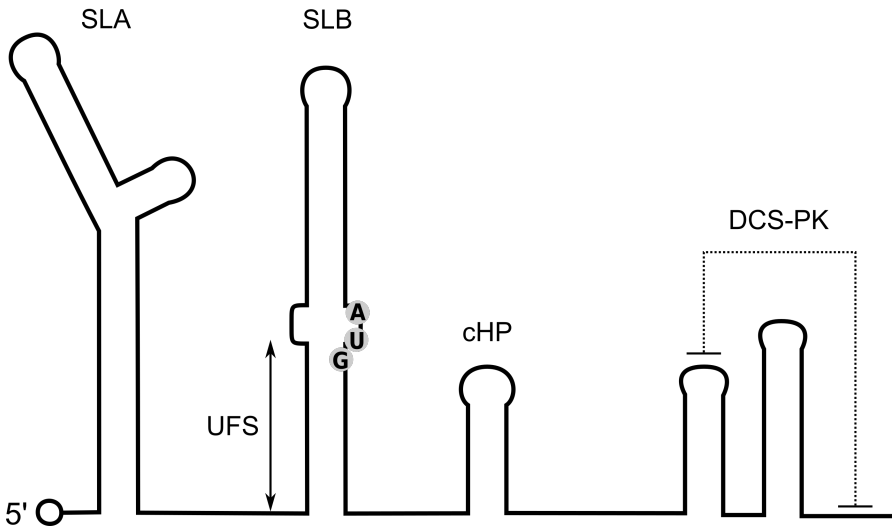

Figure 1.6 Structure of the 5′ terminal region of the flavivirus genome

A schematic illustrating the structure of the 5′ terminal region of the flavivirus genome. The position of the initiating AUG is shown. Pseudoknot interactions are illustrated with a dotted line. The 5′ cap structure is represented as a circle. SLA, stem-loop A; SLB, stem-loop B; cHP, C coding region hairpin; DCS-PK, downstream of 5' CS pseudoknot; UFS, 5′-UAR-flanking stem.

Downstream of SLA in most flaviviruses such as DENV, WNV and ZIKV exists a second smaller stem-loop B (SLB) that is more variable in terms of size and structure than SLA (Brinton & Dispoto, 1988). This stem contains the AUG initiation codon for translation, typically found in poor Kozak sequence context in the majority of MBFVs (Clyde & Harris, 2006; Clyde *et al*, 2008). A U-rich tract separates SLA and SLB in DENV, deletion of which attenuates DENV (Lodeiro *et al*, 2009). A recent study has suggested that this tract actually forms a conserved RNA duplex that effectively extends SLB, termed the 5′-UAR-flanking stem (UFS; Liu *et al*, 2016).

Within the C coding region at the 5' terminal end, the C coding region hairpin (cHP) stem and the downstream of 5' CS pseudoknot (DCS-PK) both play roles in viral replication. The cHP structure has been shown to be required for efficient viral RNA synthesis in both DENV and WNV in a sequence-independent fashion (Clyde *et al*, 2008). Furthermore, this element promotes selection of the poor context translation initiation codon in DENV2 in a manner related to the stability of the cHP stem (Clyde & Harris, 2006). The presence of a stable hairpin ~14 nt downstream of a sub-optimal initiation codon is known to enhance recognition, potentially through slowing of the scanning ribosomal complex during translation initiation (Kozak, 1990). As the cHP stem is typically located 12-16 nt from the initiating AUG in most

MBFVs it likely acts as a conserved translation enhancer (Clyde & Harris, 2006). The dual role of this structure in both viral translation and replication hints at the interplay that occurs between these two processes during infection. Comparatively, the DCS-PK structure enhances viral replication, potentially through regulation of genome cyclisation (Liu *et al*, 2013; de Borba *et al*, 2015).

1.6.2 Secondary structures within the 3' terminal region

The flavivirus 3' UTR can be divided into three domains each containing autonomously folded regions (Figure 1.7). Domain I is the least conserved of the three and is notable for containing two stem-loop structures (SL-I and SL-II) that form pseudoknots (PK1 and PK2) (Kieft *et al*, 2015), although in YFV there is only one (Wang *et al*, 1996). As these structures are capable of stalling the 5'-3' exonuclease XrnI, they have been termed exonuclease-resistant (xr)RNA1 and xrRNA2. xrRNA structures from Murray Valley encephalitis virus and ZIKV have been solved by x-ray crystallography and exhibit complex three-way junction arrangements, providing a mechanistic basis for Xrn1 resistance (Chapman *et al*, 2014; Akiyama *et al*, 2016). These xrRNA structures are linked to the production of short subgenomic flavivirus RNAs (sfRNAs) during infection, which are identical in sequence to the 3' end of the flaviviral genome (Pijlman *et al*, 2008). A variety of functions have been attributed to sfRNAs including host adaptation (Filomatori *et al*, 2017; Villordo *et al*, 2015), innate immune avoidance (Schnettler *et al*, 2013; Schuessler *et al*, 2012; Bidet *et al*, 2014) and modulation of replication (Lin *et al*, 2004).

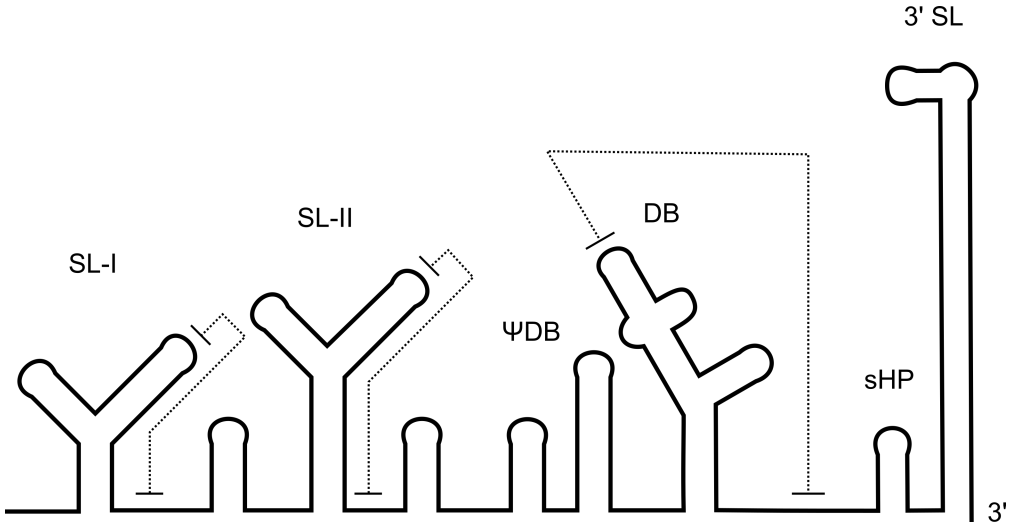

Figure 1.7 Structure of the 3′ terminal region of the flavivirus genome

A schematic illustrating the structure of the 3′ terminal region of the flavivirus genome. DENV and JEV possess two DB structures (not shown here) whereas ZIKV and YFV instead possess a single DB and a pseudo-DB (ψ-DB). Pseudoknot interactions are illustrated with a dotted line. 3' SL, 3' stem-loop; DB, dumbbell; sHP, small hairpin.

Domain II of the 3' UTR contains a conserved structural element known as a dumbbell (DB). Whereas ZIKV and YFV contain a single DB structure, DENV and JEV contain two through duplication (Fernández-Sanlés *et al*, 2017). These DB structures are predicted to form pseudoknots and have been shown by mutation to be important for viral translation and viral replication (Sztuba-Solinska *et al*, 2013; Manzano *et al*, 2011; Men *et al*, 1996; Lo *et al*, 2003; Alvarez *et al*, 2005a), likely through modulation of long-range RNA-RNA interactions (de Borba *et al*, 2015). Furthermore they act as xrRNA structures in certain flaviviral species (Filomatori *et al*, 2017; Kieft *et al*, 2015; Funk *et al*, 2010). A recent study suggests that in DENV these duplicated elements display functional diversification driven by different host-specific requirements as adaptive mutations upon infection of mosquito cells were only observed within DB2 and not DB1 (de Borba *et al*, 2019). A-rich regions around these DB structures in DENV have been shown to act as a binding site for PABP, possibly compensating for the lack of a poly(A) tail at the 3' terminus of the viral genome (Polacek *et al*, 2009b).

Domain III is highly conserved among members of the *Flavivirus* genus and is mainly characterised by the presence of the large 3' stem-loop (3' SL) structure, flanked on the 5' side by a small hairpin (sHP) structure (Barrows *et al*, 2018). The structure of the sHP stem has been shown to be essential for DENV replication (Alvarez *et al*, 2008; Villordo *et al*, 2010), whereas the specific sequence within the loop of the sHP structure is only required for DENV replication in mosquito but not mammalian cells (Villordo & Gamarnik, 2013). The conserved penta-nucleotide sequence at the top of the 3' SL and the stem-loop structure have been shown to be essential for viral replication by mutational analysis (Tilgner *et al*, 2005; Zeng *et al*, 1998; Bredenbeek *et al*, 2003). Comparatively, discrepancies exist regarding the role of the 3' SL in translation. An early study using chimeric CAT reporters containing only the 3' SL of WNV and not the rest of the 3' UTR suggested that the structure acted as a translation inhibitor independently of the 5' UTR in comparison to other viral 3' terminal sequences (Li & Brinton, 2001). A later study using FLuc reporters flanked by the 5' and 3' UTRs of DENV illustrated that the viral 3' UTR could enhance translation largely through the 3' SL structure in a manner independent of the 5' cap and viral 5' UTR (Holden & Harris, 2004). However, a subsequent study using replication-competent DENV replicons has shown that deletion of the entire 3' UTR has little effect on initial viral translation following transfection into BHK or mosquito cells but greatly impacts upon viral replication (Alvarez *et al*, 2005a).

1.6.3 Genome circularisation

Hahn and colleagues initially observed that a conserved 8 nucleotide 5' cyclisation sequence (CS) element present within the N-terminal region of the C coding sequence was complimentary to a sequence at the 3' end of the flavivirus genome (Hahn *et al*, 1987). Further characterisation of this CS element extended the length to 11, 12 and 18 nucleotides for DENV, WNV and YFV, respectively (Alvarez *et al*, 2005b; Corver *et al*, 2003). Mutational studies using infectious clones and replicons has highlighted the requirement for these complementary sequences in viral replication, but not translation, during infection (Alvarez *et al*, 2005a; Lo *et al*, 2003; Khromykh *et al*, 2001a). These studies illustrated that mutations within the 5' or 3' CS element could be rescued by complimentary mutations in the corresponding site that restored base-pairing potential, thus suggesting that sequence complementarity rather than specific nucleotide sequence is important. Later work has illustrated that mismatches within the central portion of the CS site are more tolerated than mutations at the terminal ends, an important consideration when designing live attenuated vaccines through mutation of this element (Basu & Brinton, 2011; Suzuki *et al*, 2008).

Additional regions of sequence complementarity were subsequently identified between the 5' and 3' termini of flaviviral genomes. Similar to the CS element, 5'-3' complementarity of the upstream of AUG region (UAR) sequence was shown to be essential for DENV and WNV replication (Alvarez *et al*, 2008; Zhang *et al*, 2008a). Spontaneous revertant mutations arise that restore sequence complementarity within the 5'-3' UAR elements when this complementarity is abolished by mutation in a DENV infectious clone, illustrating the importance of this interaction (Alvarez *et al*, 2008). Additionally, a similar replication requirement for 5'-3' complementarity exists within the short downstream of AUG region (DAR) (Friebe & Harris, 2010; Friebe *et al*, 2011). These three key regions of long-range RNA-RNA sequence complementarity (CS, UAR and DAR) are thought to be responsible for genome circularisation, in which a “panhandle” structure is formed between the 5' and 3' ends of the flaviviral genome (Figure 1.8). The structure and sequence of the ZIKV genome terminal ends in the linear and circular form are shown in Appendix A.

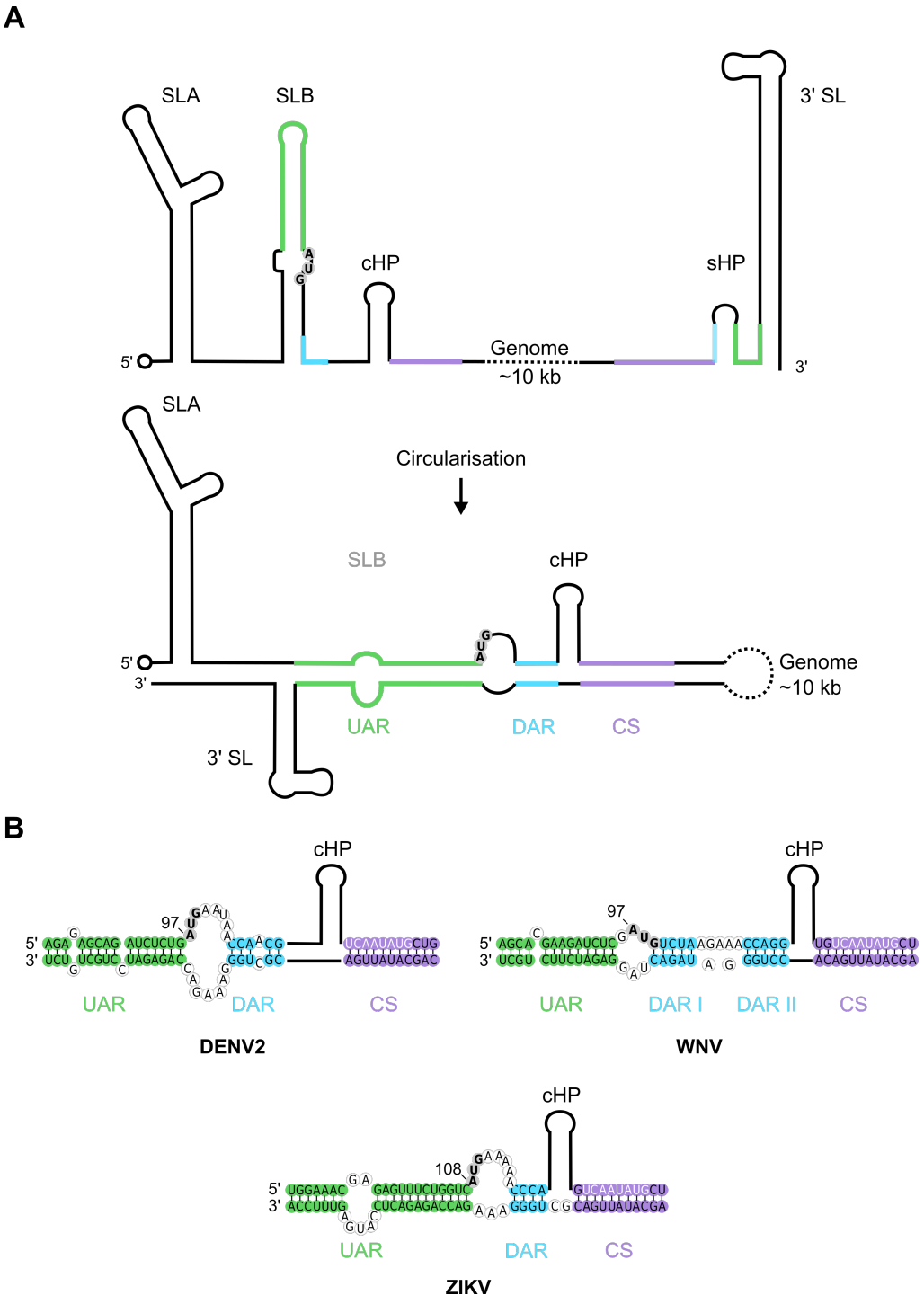

Figure 1.8 Flavivirus genome circularisation is mediated by long-range RNA-RNA interactions

Schematics illustrating **A)** the linear (top) and the circular (bottom) conformations of the flaviviral genome that occur during infection and **B)** the elements important for circularisation from DENV2 (GenBank accession number NC_001474), WNV (GenBank accession number MH170248.1) and ZIKV PE243 strain (Genbank accession number KX197192.1). Sequences corresponding to the UAR, DAR and CS are highlighted in green, blue and purple, respectively. Within the CS, the conserved core element is in white (Hahn *et al*, 1987). In WNV, two DAR motifs have been described (Fernández-Sanlés *et al*, 2017). The initiating AUG is highlighted in bold and the 5′ cap structure is represented as a circle. SLA, stem-loop A; SLB, stem-loop B cHP, C coding region hairpin; sHP, small hairpin; 3' SL, 3' stem-loop.

Direct interaction between isolated 5' and 3' flavivirus genome ends was first visualised by psoralen-UV crosslinking (You *et al*, 2001). A subsequent study utilised electrophoretic mobility shift assays (EMSAs) and showed that interaction between RNA probes corresponding to the 5' and 3' ends of DENV was dependent on sequence complementarity within both the CS and UAR elements (Alvarez *et al*, 2005b). The first evidence that these interactions were capable of circularising the full-length (~11 kb) DENV genome came from atomic force microscopy. In this study, an antisense oligonucleotide of 3.3 kb in length corresponding to the NS4B and NS5 coding region was hybridised to full-length DENV RNA *in vitro* in order to generate an elongated dsRNA segment that enabled interactions between the genomic ends to be readily visualised. Around 25 % of the molecules imaged were found to adopt a circularised conformation (Alvarez *et al*, 2005b). Recent studies have shown that these long-range RNA-RNA interactions can be readily detected in cells during DENV or ZIKV infection by *in cellulo* RNA crosslinking approaches coupled with high-throughput sequencing (Ziv *et al*, 2018; Li *et al*, 2018; Huber *et al*, 2019).

The interactions between a DENV 5' end RNA probe and several mutant 3' end RNA probes containing UAR or CS mutations were analysed in solution by chemical probing, demonstrating that while the 5'-3' CS interaction occurs independently of UAR hybridisation, the 5'-3' UAR interaction is entirely dependent upon CS hybridisation (Polacek *et al*, 2009a). As such, it has been proposed that the 5'-3' CS element first initiates genome circularisation, which is then extended by the formation of the 5'-3' DAR/UAR interactions resulting in the “opening” of the sHP and reorganisation of the 3' SL structure (Friebe & Harris, 2010; Friebe *et al*, 2011). As such, the UAR element has two proposed functions during infection. The first is that it brings the two genomic ends into close proximity. The second is that it mediates structural rearrangement of the 3' SL, thus releasing the very 3' end of the flaviviral genome from sequestration within secondary structure. This facilitates replication of the viral genome by the polymerase NS5, which while initially recruited to SLA at the 5' end of the genome translocates to the 3' end in order to start negative-strand RNA synthesis (Filomatori *et al*, 2006, 2011). This is likely aided by NS5 dimerisation (Klema *et al*, 2016) and interaction of NS5 with the 3′ SL (Hodge *et al*, 2016).

1.6.4 The dynamic genome

The circularisation elements of the flaviviral genome overlap with important local secondary structures found within the viral 5′ and 3′ terminal regions. For instance, the 5′ UAR element is

conformationally locked within SLB by the UFS in the linear form of the viral genome (Liu *et al*, 2016). Within the viral 3′ UTR, the 3′ UAR element locally adopts the sHP structure and the base of the 3′ SL (Villordo *et al*, 2010). Furthermore, the 3′ CS element of DENV is known to lie in a region that forms a pseudoknot with the DB2 structure (Manzano *et al*, 2011; Sztuba-Solinska *et al*, 2013). As such, direct interplay between these competing local and long-range structures influences the degree to which genome circularisation can occur.

Experiments using DENV have illustrated that the balance between the linear and the circular conformations of the viral genome is important during infection (Gebhard *et al*, 2011; Villordo *et al*, 2010). Mutations that stabilise or destabilise competing structures within the 3′ UTR thus favouring the linear or the circular conformation of the viral genome decrease viral replication. Furthermore, spontaneous mutations subsequently arise that restore the equilibrium between the two genomic conformations (Villordo *et al*, 2010). It is likely therefore that many of the mutations described previously within local structures of the 5′ and 3′ terminal regions that impact replication and/or translation alter the thermodynamic stability of local secondary structure, thus disrupting the transition from one genome conformation to another.

Regulation of genome conformation likely occurs predominately through protein binding during the flavivirus lifecycle. Numerous cellular proteins have been identified as binding to the 3′ UTR of DENV including PABP (Polacek *et al*, 2009b), PTB (De Nova-Ocampo *et al*, 2002), translation elongation factor 1α (De Nova-Ocampo *et al*, 2002), La (García-Montalvo *et al*, 2004) and the DEAD-box RNA helicase DDX6 (Ward *et al*, 2011), all of which have been implicated in translation and/or replication. The cellular AU-rich element RNA-binding protein 1 (AUF1) p45 isoform, typically involved in mRNA stability and/or translation, has been shown to facilitate the interaction between 5′ and 3′ cyclisation elements of WNV, DENV and ZIKV through its RNA chaperone and annealing activities. Furthermore, siRNA-mediated knockdown of AUF1 p45 led to a decrease in viral titres during infection, thus illustrating its pro-viral role (Friedrich *et al*, 2014, 2018). Similarly, the host La protein can bind to both the 5′ and 3′ UTRs of JEV and thus may promote genome circularisation (Vashist *et al*, 2011).

Flaviviral proteins have also been implicated in the regulation of genome circularisation. The viral helicase NS3 possesses ATP-independent annealing activity and has been shown to enhance the interaction between isolated DENV 5′ and 3′ terminal region RNA probes (Gebhard *et al*, 2012). Furthermore, the viral polymerase NS5 has been shown to possess weak RNA chaperone activity (Pong *et al*, 2011), highlighting a possible role for the NS5-NS3 protein

complex in this process. Interestingly, the RNA chaperone activity of the WNV C protein has also been shown to facilitate these interactions *in vitro* (Ivanyi-Nagy & Darlix, 2012), potentially to compact the genome in preparation for RNA encapsidation into virions. Consistent with this, recent RNA structure mapping studies have suggested that DENV and ZIKV genomes adopt a circular conformation within the virion (Dethoff *et al*, 2018; Huber *et al*, 2019).

Additional control may come from *trans*-interactions between different RNA species. For instance, the sfRNAs that accumulate during infection possess the 3′ circularisation elements. As a result, these RNAs have the propensity to interact with the 5′ elements of complete genomes thus competing with *cis*-interactions on the same molecule. Such interactions were hypothesised to contribute to the switch from positive-strand to negative-strand RNA synthesis (Lin *et al*, 2004), but experimental data is required to validate this hypothesis. It was recently reported that human miR-21 in complex with an Ago protein interacts with the 5′ CS element of ZIKV and as a result may disrupt circularisation. CRISPR-mediated deletion of *MIR21* or antisense-mediated inhibition of miR-21 was found to reduce genome copies of a ZIKV replicon in human cells, suggesting that this interaction is pro-viral (Ziv *et al*, 2018).

Studies using antisense peptide-conjugated phosphorodiamidate morpholino oligomers (P-PMOs) complimentary to short regions within flavivirus genomes have illustrated that targeting circularisation elements represents a viable therapeutic strategy (Deas *et al*, 2005, 2007; Holden *et al*, 2006; Kinney *et al*, 2005). For example, a P-PMO targeted to the 3′ CS element of WNV was found to effectively reduce viral titre in cell culture by inhibiting replication (Deas *et al*, 2005) and partially protects a mouse from WNV disease with minimal toxicity (Deas *et al*, 2007). However, the therapeutic potential of this strategy is limited by the appearance of resistance mutations. Interestingly, resistance to a P-PMO targeting the 3′ UAR element in WNV can arise through a single mutation within the 3′ UAR, weakening the P-PMO interaction, with a corresponding mutation in the 5′ UAR sequence to maintain 5′-3′ UAR base-pairing (Zhang *et al*, 2008b). Comparatively, a mutation that confers resistance to a P-PMO targeting the 3′ CS element was located outside of the targeted region within the 3′ SL structure (Deas *et al*, 2007). This further highlights the importance of the dynamic nature of flaviviral genomes during infection and the complex interplay that occurs between competing local and long-range structures. A P-PMO targeting the top of the 3′ SL in DENV was found to inhibit both translation and replication of a DENV replicon, indicating that conformational flexibility of the 3′ SL might be important in the regulation of both processes (Holden *et al*, 2006).

1.7 Translation-replication switch in positive-sense RNA viruses

During infection, the genomes of flaviviruses and all positive-sense RNA viruses have three major functions. They have to act as templates for translation to produce the functional proteins required for productive infection. Additionally, these genomes have to act as templates for viral replication, in order to produce nascent genomes. Finally, these nascent genomes must be packaged into progeny virions in order to mediate additional rounds of infection. The balance between these three processes must be tightly regulated to allow efficient viral propagation.

Translation and replication are considered to be antagonistic processes during infection, as each demands the viral genome template in opposite directions (Figure 1.9). The interplay between these two processes has been examined using PV whose translation is IRES-dependent (Pelletier & Sonenberg, 1988). When a luciferase-containing PV replicon is added to a translation-competent cell extract containing an excess of the PV polymerase $3D^{pol}$, RNA synthesis, detected by incorporation of radiolabelled nucleotide into an acid-insoluble fraction, is only observed when ribosomes are first stalled by the drug cycloheximide (Gamarnik & Andino, 1998). Additionally, a series of experiments following synchronous replication of infectious PV RNA in HeLa cell extract has shown that synthesis of full-length negative-strand, but not positive-strand, is enhanced in the presence of puromycin (Barton *et al*, 1999). Puromycin is a polypeptide chain terminator and thus dissociates translating ribosomes from the RNA. Comparatively, drugs like cycloheximide and anisomycin that freeze ribosomes on the RNA were found to inhibit synthesis of full-length negative-strand (Barton *et al*, 1999). These experiments suggest that efficient viral replication only occurs when the genomic template is cleared of translating ribosomes, creating a requirement for a mechanism to prime templates for replication by mediating translation initiation inhibition.

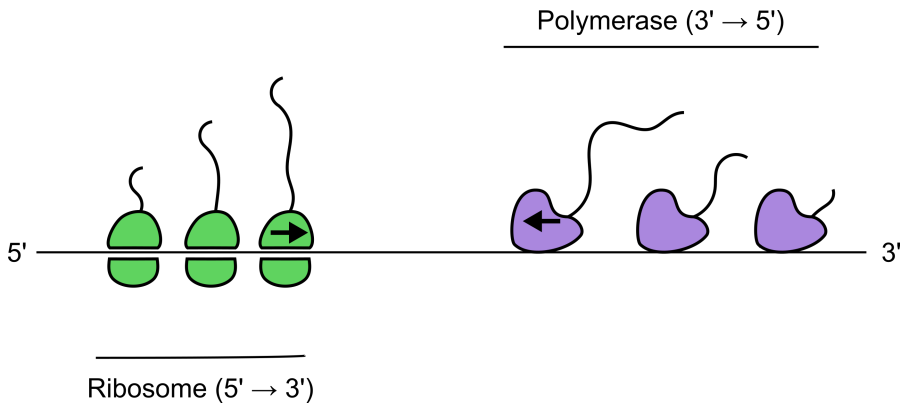

Figure 1.9 Translation and replication both require the genome template of positive-sense RNA viruses

Translation of positive-sense RNA viruses occurs before replication. Ribosomes progress in the 5′-3′ direction, whereas viral polymerases progress in the 3′-5′ direction. Experimental studies on PV have illustrated that viral polymerase is not capable of bypassing translating ribosomes (Gamarnik & Andino, 1998; Barton *et al*, 1999). As such, positive-sense RNA viruses must have a mechanism to regulate these two antagonistic processes.

How and when then is template switching mediated in PV? While it is clear that early in infection, when relatively few genomes are present, the use of each genome template must switch from translation to replication, it was speculated that template usage might be defined late in infection simply by cell compartmentalisation (Caliguiri & Tamm, 1969; Bienz *et al*, 1987; Irurzun *et al*, 1992). However, it has been demonstrated that PV genomes must first be translated to become a suitable template for replication, as mutant PVs containing nonsense mutations within the viral coding sequence could not be rescued *in trans* by co-transfection of a helper genome (Novak & Kirkegaard, 1994). This suggests that a mechanism for template switching is required throughout the viral lifecycle and so compartmentalisation of functionally specialised RNA pools is unlikely to occur. Subsequent studies have shown that template switching in PV is mediated by cleavage of the ITAFs PCBP2 and PTB by a virally encoded protease, thus shutting off translation at defined points in infection, effectively temporally separating translation and replication (Perera *et al*, 2007; Back *et al*, 2002; Chase *et al*, 2014). This acts to ensure that the virally-encoded proteins required for replication are expressed prior to translation inhibition, directly coupling the two processes.

Other mechanisms to temporally separate translation and replication have been described for other positive-sense RNA viruses. For instance, RNA structure probing has shown that a long-range RNA-RNA pseudoknot interaction within the genome of HCV when formed disrupts a stem-loop structure within the viral 3′ UTR implicated in viral replication (Tuplin *et al*, 2012). Furthermore, abrogation of this pseudoknot interaction through mutation of a single nucleotide

was found to reduce translation of HCV reporter RNAs, which could be rescued by introducing a complimentary mutation that restored this long distance interaction, thus suggesting that mutually exclusive RNA interactions could control template usage (Tuplin *et al*, 2015). Additionally, miR-122 has recently been reported to enhance HCV replication but only under conditions of active HCV translation, suggesting that miR-122 might regulate the balance between these two processes (Masaki *et al*, 2015). Using polysome profiling, it was shown that transfection of miR-122 into HCV-infected cells led to a reduction of HCV RNA associated with translating polysomes. Additional experiments illustrated that miR-122 inhibited binding of the ITAF PCBP2 to the HCV genome, thus potentially clearing the viral template of ribosomes for replication, providing a mechanistic basis for these observations (Masaki *et al*, 2015).

1.8 Project aims

Despite the large amount of research that has been performed on flaviviruses, basic fundamental questions regarding their lifecycle still remain. The mechanism of translation initiation used by these viruses to express viral proteins is poorly defined and the eIF requirement is unknown. Furthermore, it is presently unclear how flaviviruses regulate the use of their genomes in the competing processes of translation and replication. Regulation is unlikely to occur simply through compartmentalisation, as throughout DENV infection positive and negative-strand RNA are localised to the ER (Reid *et al*, 2018). A possible mode of regulation could occur through binding of the viral polymerase NS5 to the cap-proximal stem-loop, which could disrupt 43S preinitiation complex loading at the 5′ end therefore clearing the genome of ribosomes prior to replication. Additionally, it has been speculated that transitions between linear and circular genome conformations might provide a mechanism to regulate template usage (Villordo *et al*, 2010), although experimental evidence supporting this hypothesis is lacking.

Using ZIKV as a model flavivirus, the aims of this thesis are therefore: -

- To identify the minimal eIF requirement for efficient 48S complex assembly in a reconstitution system for translation initiation and to investigate scanning of the 5′ UTR.
- To investigate the impact of NS5 recruitment to the cap-proximal structure SLA upon translation initiation.
- To investigate the effect of genome circularisation on translation initiation.

The results of these studies will shed light on a poorly characterised but essential lifecycle switch that occurs during infection of this important class of human pathogen.

2 Materials and Methods

2.1 Plasmids and molecular cloning techniques

Recombinant human eIF expression plasmids have been described previously (Pestova *et al*, 1998a, 1996a; Lomakin *et al*, 2000; Dhote *et al*, 2012; Lomakin *et al*, 2006). cDNA fragments containing the eIF1 and eIF1A coding regions were inserted into pQE31 (Quigen) and pET28 (Novagen) between the BamHI and HindIII sites to yield pQE(His$_6$-eIF1) and pET(His$_6$-eIF1A), respectively (Pestova *et al*, 1998a). pET(His$_6$-eIF4A) and pET(His$_6$-eIF4B) were constructed by cloning multiple cDNA fragments between the 5′ BamHI site and the 3′ NotI (eIF4A) or 3′ AvrII site (eIF4B) of modified pET15b (Novagen) (Pestova *et al*, 1996a). A cDNA fragment corresponding to the coding region of eIF4G$_{736-1115}$ was generated by PCR and inserted between the BamHI and XhoI sites of pET28b (Novagen) to generate pET(His$_6$-eIF4G$_{736-1115}$) (Lomakin *et al*, 2000). The vector for expression of DHX29 containing an N-terminal FLAG and a C-terminal His$_6$-tag was generated by cloning a codon-optimised sequence into pET16b (Novagen) between NcoI and BamHI (Dhote *et al*, 2012). A plasmid encoding both the N-terminal and C-terminal coding regions of methionyl-tRNA synthetase was made by cloning PCR fragments amplified from *Escherichia coli* (*E. coli)* DH5α DNA between the NcoI and XhoI sites of pET28a (Novagen) (Lomakin *et al*, 2006).

Transcription vectors for tRNA$_i^{Met}$ (Pestova & Hellen, 2001), EMCV IRES (Evstafieva *et al*, 1991) and ZIKV^{Fluc} (pUC57-ZIKV-Fluc; Chavali *et al*, 2017) have been described previously. The vector for tRNA$_i^{Met}$ was generated by inserting four synthetic partially overlapping DNA oligomers between the HindIII and BamHI sites of pBR322, and contains the T7 promoter adjacent to the mammalian tRNA$_i^{Met}$ gene with a 3′ BstNI site (Pestova & Hellen, 2001). A plasmid encoding EMCV nt 315 to 1155 downstream of a T7 promoter (pTE1) was generated by inserting a reverse transcribed DNA fragment into the AccI site of pTZ18R (Pharmacia) (Evstafieva *et al*, 1991). pUC57-ZIKV-Fluc was generated by overlap extension PCR of two synthesised cDNA fragments (Integrated DNA Technologies; IDT) corresponding to Fluc flanked by the 5′ and 3′ UTRs of ZIKV PE243 (KX197192.1) with an upstream T7 promoter between the XbaI and HindIII sites of pUC57 (GenScript) (Chavali *et al*, 2017).

Gene fragments containing a 5′ T7 promoter with the first 359 nt of ZIKV PE243 (KX197192.1) with flanking XbaI/HindIII sites (ZIKV$^{5'utr+}$) and the first 329 nt of SV 26S mRNA (MG679380.1) with flanking XhoI/EcoRI sites were synthesised by IDT and cloned into pUC57 (GenScript). SLA mutations in the context of ZIKV$^{5'utr+}$ or ZIKV^{Fluc} were generated by

QuikChange site-directed mutagenesis. ZIKV^{mini} was derived from pUC57-ZIKV-Fluc (Chavali *et al*, 2017) by site-directed mutagenesis, retaining 30 nt each from the 5′ and 3′ ends of the Fluc gene to generate a 60 nt linker between the ZIKV terminal regions. Mutations within the 5′ and 3′ UAR/CS elements in ZIKV^{mini} were generated by site-directed mutagenesis. Gene fragments containing T7 promoter-driven ZIKV^{mini} with mutations in upstream near-cognate codons with flanking XbaI and HindIII sites and wildtype/Δ3′ CS mutant DENV1 (KC692517.1) or DENV4 (FJ196850.1) minigenomes with flanking XbaI and EcoRV sites were synthesised by IDT and cloned into pUC57 (GenScript).

A CopyControl pCC1BAC vector (Epicentre) containing the complete open reading frame of the ZIKV BeH819015 isolate flanked by the 5′ and 3′ UTRs of ZIKV PE243 (KX197192.1; ZIKV^{fl}) and a related plasmid containing an inline duplicate copy of the C protein fused to a nanoluciferase (Nluc) gene and 2A peptide sequence (ZIKV^{Nluc}) were kindly provided by Andres Merits (Mutso *et al*, 2017). The existing SP6 promotor within these ZIKV infectious cDNA (icDNA) plasmids was replaced with a T7 promotor by subcloning a synthetic gene fragment (IDT) between EcoRI and NheI sites. NS5 G_{664}AA and Δ3′ CS mutations were generated by overlap extension PCR to produce a fragment that was inserted between BstBI and PmeI sites. The ZIKV NS5 coding region was subcloned into pET28b (Novagen) between NheI and HindIII sites to generate a bacterial expression construct for NS5^{ZIKV} with an N-terminal His_6-tag.

Restriction enzymes (New England Biolabs, NEB) were used following manufacturer's instructions. Phenol chloroform extraction followed by ethanol precipitation was exclusively used to purify digested ZIKV icDNA plasmids, as these constructs did not bind effectively to spin columns. Ligations were performed using T4 DNA ligase (NEB) following manufacturer's instructions, and in the case of cloning using the ZIKV icDNA plasmids ligations were always performed overnight at 16 °C.

Plasmid stocks were propagated and cloned in either homemade DH5α competent *E. coli* or Turbo competent *E. coli* (high efficiency; NEB) in the case of the ZIKV icDNA plasmids. The Turbo competent *E. coli* lost competency quickly upon storage at -80 °C and when transformed with plasmids containing full-length ZIKV sequences typically produced only small colonies at 37 °C on agar plates containing 12.5 μg/ml chloramphenicol. To obtain plasmid preparations with sufficient yield, multiple colonies were picked and grown in 200 ml of 2xTY liquid media containing 12.5 μg/ml chloramphenicol at 37 °C overnight with shaking. DNA was isolated

using a PureYield plasmid midiprep system (Promega), including the optional endotoxin removal wash.

2.2 *In vitro* transcription

Plasmids were linearised with HindIII (ZIKV$^{5'utr+}$, ZIKV^{Fluc} and ZIKV^{mini}), EcoRI (SV 26S), EcoRV (DENV1/4^{mini} and EMCV IRES), AgeI (ZIKV^{fl} and ZIKV^{Nluc}) or BstNI (tRNA$_i^{Met}$). Unless otherwise indicated, RNAs were transcribed with recombinant T7 polymerase (50 ng/µL) in buffer containing 40 mM HEPES pH 7.5, 32 mM MgOAc, 40 mM DTT, 2 mM spermidine, 10 mM each of ATP, GTP, CTP and UTP, 1.6 U/µL RNaseOUT (Invitrogen) and 2.5 µg linearised transcription plasmid for 2 hrs at 37 °C. Scrambled and targeted antisense RNAs were similarly transcribed from T7 promoter-bearing reverse complement DNA oligos annealed to a T7 promoter-containing forward primer (1 µg of each). Sequences are shown in Table 2.1. DNaseI (40 U / Roche) and 1X incubation buffer were added directly into the transcription reaction with further incubation at 37 °C for 1 hr prior to extraction.

Table 2.1 Antisense oligonucleotides

DNA used as a template for transcription of RNA oligos. The T7 promoter is shown in bold.

ZIKV ASO	AGCATATTGACGCTGGGAAAGACCAGAGACTC**CTATAGTGAGTCGTATTA**
DENV1 ASO	CAGCATATTGACGCTGGGAGAGACCAGAGATCCTGCTGTCT**CTATAGTGAG TCGTATTA**
DENV4 ASO	CAGCATATTGACGCTGGGAAAGACCAGAGATCCTGCTGTCT**CTATAGTGAG TCGTATTA**
SCR	ATGGCAAACCCAGATTGCTATTCCAAACGTCT**CTATAGTGAGTCGTATTA**

ZIKV^{fl} and ZIKV^{Nluc} RNA was isolated by making the total reaction volume up to 300 µl with water before addition of 500 µl TRI reagent (Sigma) and 160 µl chloroform. Following centrifugation (13000 rpm, 10 min, room temperature), the upper aqueous phase (~500 µl) was ethanol precipitated in the presence of 20 ng/µl GlycoBlue (Invitrogen) at -20 °C overnight or -80 °C for 30 min. RNA from all other transcription reactions was extracted with acidic phenol/chloroform prior to ethanol precipitation. Residual nucleotides were removed by running RNA pellets resuspended in water once down an Illustra MicroSpin G-50 column (GE Healthcare). Capped (cap0) RNA was generated post-transcriptionally using the ScriptCap m7G capping system (CellScript) following manufacturer's instructions with 20 U of capping

enzyme at 37 °C for 2 hrs before extraction as described above in the presence of 20 ng/µl GlycoBlue (Invitrogen). RNA pellets resuspended in water were additionally passed down an Illustra MicroSpin G-50 column (GE Healthcare), and experiments involving comparisons between capped and uncapped RNA samples ensured that the RNA had been through an equivalent number of columns. RNA integrity was analysed by agarose gel electrophoresis (Meyers *et al*, 1976) and concentration was determined by measuring absorbance at 260 nm.

The previously reported SP6-driven ZIKV infectious clone (Mutso *et al*, 2017) was transcribed using a SP6 RiboMAX large scale RNA production system (Promega) and subsequently extracted and capped as above.

2.3 Purification of native factors and recombinant proteins

Table 2.2 Composition of buffers used in the purification of native and recombinant proteins

Buffer	Composition
A	20 mM Tris, pH 7.5, 2 mM dithiothreitol (DTT), 4 mM $MgCl_2$, 50 mM KCl
B	20 mM Tris pH 7.5, 2 mM DTT, 4 mM $MgCl_2$, 0.5 M KCl
C	20 mM Tris pH 7.5, 2 mM DTT, 2 mM $MgCl_2$, 100 mM KCl, 0.25 M sucrose
D	20 mM Tris pH 7.5, 2 mM DTT, 0.1 mM EDTA, 10 % glycerol
Q	20 mM Tris, pH 7.5, 2 mM DTT, 0.1 mM EDTA, 5 % glycerol
H	20 mM HEPES, pH 7.5, 2 mM DTT, 0.2 mM EDTA, 5 % glycerol

Native eIF2, eIF3, eIF4F and the 40S ribosomal subunit were purified from rabbit reticulocyte lysate (RRL) (Green Hectares, Illinois) as previously described (Pisarev *et al*, 2007). Briefly, polysomes were precipitated by centrifugation in a Beckman Type 45 Ti rotor (45000 rpm, 7 hrs, 4 °C) in the presence of 0.5 mg/ml Pefabloc (Roche) before resuspension at a final concentration of 150 A_{260}U/ml in Buffer A. A high salt wash was performed by adding KCl (4 M) drop-wise to a final concentration of 0.5 M to remove associated mRNA and proteins. The suspension was centrifuged in a Beckman Type 45 Ti rotor (34500 rpm, 12 hrs, 4 °C) to a yield a pellet from which ribosomal subunits were extracted and a ribosomal salt wash from which eIFs were purified.

The ribosomal pellet was resuspended in Buffer A to a final concentration of 150 A_{260}U/ml. The suspension was incubated on ice for 10 min with 1 mM puromycin (Sigma-Aldrich) to release nascent peptides and then for a further 10 min at 37 °C. A high salt wash was performed by adding KCl (4 M) drop-wise to a final concentration of 0.5 M. 40S and 60S ribosomal subunits were isolated by loading resuspended ribosomal pellets onto a 10-30 % sucrose density gradient in Buffer B. Gradients were centrifuged in a Beckman SW32 Ti rotor (24500 rpm, 14 hrs, 4 °C) and 1 ml fractions were collected. Fractions containing isolated 40S and 60S ribosomal subunits were identified by measuring absorbance at A_{260}, pooled and concentrated in Buffer C before storage at -80 °C.

The ribosomal salt wash was subjected to stepwise ammonium sulphate (AS) precipitation to yield 0-40 %, 40-50 % and 50-70 % AS fractions, sequentially separated by centrifugation in a Beckman JA-25.50 rotor (15000 rpm, 20 min, 4 °C). Pellets were subsequently resuspended in Buffer D + 100 mM KCl. eIF3 and eIF4F were derived from the 0-40 % AS fraction by affinity chromatography using diethylaminoethyl (DEAE) and phosphocellulose (P11) affinity chromatography (Sigma-Aldrich) with elution in Buffer D + 250 mM KCl and Buffer D + 400 mM KCl, respectively. Separation was achieved on 10-30 % sucrose density gradients in Buffer D + 400 mM KCl using a Beckman SW40 Ti rotor (4000 rpm, 23 hrs, 4 °C). 400 µl fractions were collected and absorbance was measured at A_{280} to define fractions containing eIF3 or eIF4F. eIF4F was further purified by immobilized γ-aminophenyl-m^7GTP-(C_{10}-spacer)-agarose (Jena Bioscience) following manufacturer's instructions. eIF2 was derived predominately from the 40-50 % AS fraction (with a small amount from the 0-40 % fraction) by DEAE and P11 affinity chromatography (Sigma-Aldrich) with elution in Buffer D + 250 mM KCl and Buffer D + 800 mM KCl, respectively. Purification of eIF3, eIF4F and eIF2 was completed by fast protein liquid chromatography (FPLC) on a MonoQ 5/50 GL anion exchange column (GE Healthcare) across a 100-500 mM KCl gradient in Buffer Q. eIF3 eluted at ~400 mM KCl, eIF4F eluted at ~340 mM KCl and eIF2 eluted at ~290 mM KCl.

Recombinant eIFs were expressed and purified as previously described (Pisarev *et al*, 2007b). Briefly, recombinant His-tagged eIF1, eIF1A, eIF4A, eIF4B, $eIF4G_{736-1115}$ and methionyl-tRNA synthetase were expressed in E. coli BL21 star (DE3) for 4 hrs at 37 °C following induction with 1 mM IPTG (Sigma-Aldrich). Cells pellets were re-suspended in buffer D + 300 mM KCl with 0.5 mM PMSF (Sigma-Aldrich) and 1 mg/ml lysozyme (Sigma-Aldrich). In the case of eIF4B only, Pefabloc (Sigma-Aldrich) was added to a final concentration of 0.5 mg/ml. Cells were then sonicated (amplitude 10 microns) for 6 x 30 seconds and the lysate clarified

before affinity chromatography on Ni-NTA agarose (Qiagen) following manufacturer's instructions. Purification was completed by FPLC on a MonoQ 5/50 GL anion exchange column (GE Healthcare) or MonoS 5/50 GL cation exchange column (eIF1 and eIF4G$_{736-1115}$ only) column (GE Healthcare) across a 100-500 mM KCl gradient in Buffer Q or Buffer S, respectively. eIF1 eluted at ~250 mM KCl, eIF1A eluted at ~290 mM KCl, eIF4A eluted at ~270 mM KCl, eIF4B eluted at ~360 mM KCl, eIF4G$_{736-1115}$ eluted at ~ 260 mM KCl and methionyl-tRNA synthetase eluted at ~170 mM KCl.

FLAG- and His$_6$-tagged DHX29 was similarly expressed and purified on Ni-NTA agarose (Qiagen) followed by anti-FLAG M2 affinity gel (Sigma-Aldrich) purification following manufacturer's instructions. His-tagged NS5^{ZIKV} was expressed in E. coli Rosetta 2 (DE3) for 20 hrs at 16 °C following induction with 0.4 mM IPTG (Sigma-Aldrich). Purification was achieved on Ni-NTA agarose (Qiagen) as described above before FPLC down a HiLoad 16/600 Superdex 200 pg size exclusion column (GE Healthcare) in Buffer Q + 350 mM KCl. Protein fractions were analysed by SDS-PAGE (Laemmli, 1970). All proteins were stored at -80 °C prior to use.

Native calf liver tRNA (Promega) was purified by FPLC on a Superdex 75 10/300 GL size exclusion column by Dr Trevor Sweeney.

2.4 Aminoacylation of tRNA

In vitro transcribed and native initiator tRNA was charged in a 200 µl reaction containing 30 µg of recombinant methionyl-tRNA synthetase, 40 mM Tris-HCl, pH 7.5, 15 mM $MgCl_2$, 4 mM ATP, 1 mM CTP, 2 µl [^{35}S] methionine (1175 Ci/mmol; PerkinElmer), 75 µM unlabelled methionine, 0.4 U/µl RNAseOUT (Invitrogen) and 50 µg of initiator tRNA. The reaction was incubated at 37 °C for 90 min before the addition of an equal volume of acidic phenol-chloroform. Following centrifugation (13000 rpm, 10 min, room temperature), the aqueous phase was split between four Illustra MicroSpin G-50 columns (GE Healthcare) prior to ethanol precipitation. The degree of methionine incorporation was measured using a Tri-Carb 2800TR liquid scintillation counter (Perkin Elmer).

2.5 Western blotting

Samples were resolved by SDS-PAGE (Laemmli, 1970), transferred to a 0.45 µm nitrocellulose membrane (GVS) using a Trans-Blot SD semi-dry blotter (Bio-Rad) and blocked with 5 %

bovine serum albumin in phosphate-buffered saline (PBS). eIF3d antibody (Proteintech; catalogue number 10219-1-AP) and Goat anti-rabbit IRDye 800CW antibody (Li-Cor) were used for detection using an Odyssey CLx Imaging System (Li-Cor).

2.6 Assembly and analysis of ribosomal complexes

Table 2.3 Primers used for primer extension inhibition assays

All primers were ordered from Eurofins and re-suspended at 1 µg/µl in water.

Target	Sequence
EMCV IRES	TCAATAACTCCTCTGG
ZIKV$^{5'utr+}$/ZIKV^{fl}/ZIKV^{Nluc}	CTTGATTGCCGTGAATCTC
SV 26S	CAGTTGCTGGATTTGAGAAG
ZIKV/DENV minigenomes	CTTACACGGCGATCTTTC

A primer complementary to a sequence ~100 nt downstream of the region of interest on the mRNA transcripts was radiolabelled at the 5′ end with ^{32}P by incubating 0.3 µg of primer and 1 µl [γ-^{32}P] ATP (6000 Ci/mmol; PerkinElmer) with 10 U T4 polynucleotide kinase (3′ phosphatase minus; NEB) and 1X reaction buffer in a final reaction volume of 20 µl at 37 °C for 20 min. The labelled primer was heat inactivated at 75 °C for 5 min prior to use.

48S complexes were assembled as previously described (Sweeney *et al*, 2014). 0.2 pmol RNA was incubated with the indicated eIFs (2 pmol 40S subunit, 4 pmol Met-tRNA$_i^{Met}$, 4 pmol eIF2, 3 pmol eIF3, 10 pmol eIF4A, 5 pmol eIF4B, 2.5 pmol eIF4F, 10 pmol eIF1, 10 pmol eIF1A, 0.4 pmol DHX29, 5 pmol eIF4G$_{736-1115}$) at 37 °C for 10 min in a reaction volume of 20 µl containing Buffer R, which consists of 20 mM Tris, pH 7.5, X mM KCl (where X is the concentration required to make the final KCl concentration = 100 mM), 2.5 mM $MgCl_2$, 2 mM DTT, 0.25 mM spermidine, 32 U RNaseOUT (Invitrogen), 0.4 mM GTP and 2 mM ATP. Hippuristanol in DMSO was kindly provided by Jerry Pelletier (McGill University, Canada) and used where indicated.

Assembled complexes were analysed by primer extension inhibition by the addition of 2.5 U avian myeloblastosis virus RT (AMV-RT; Promega), 15 ng ^{32}P-labelled primer, 8 mM $MgCl_2$ and 0.5 mM dNTPs at 37 °C for 45 min. Following addition of 100 µl of stop solution (12.5 mM EDTA and 0.25 % SDS), cDNA products were phenol/chloroform extracted and ethanol precipitated in the presence of 20 ng/µl GlycoBlue (Invitrogen) before resuspension in

denaturing RNA loading dye (0.05 % bromophenol blue, 0.05 % xylene cyanol, 20 mM EDTA, pH 8.0 and 91 % formamide). Products were resolved on denaturing 7 M urea/6 % polyacrylamide sequencing gels and detected by autoradiography using an FLA 7000 Typhoon scanner (GE Healthcare).

$NS5^{ZIKV}$/RNA complexes (0.2 pmol RNA) or minigenome/small oligo complexes (0.2 pmol minigenome) were formed as described in the protein or RNA EMSA section below, respectively, prior to addition into the 48S assembly reaction unless described otherwise. In the case of 48S complex formation on total RNA from ZIKV-infected Vero cells, RNA from productively infected cells was extracted using TRI-reagent (Sigma-Aldrich) following manufacturer's instructions and 600 ng total RNA at 80000 ZIKV genome copies/ng (quantified by qPCR) was added into the assembly reaction.

2.7 Sequencing

Primer (1 µg) and specific mRNA transcription vector (3 µg) were mixed in 20 µl of water and 2 µl of 2M NaOH added. Following incubation at room temperature for 5 min, the primer-plasmid mix was ethanol precipitated and re-suspended in 8 µl of water. Sequencing reactions were carried out by dideoxy chain termination using a Sequenase version 2.0 DNA sequencing kit (USB) following manufacturer's instructions with 1 µl [α-^{35}S] ATP (1250 Ci/mmol; PerkinElmer). Denaturing RNA loading dye was then added directly to stop the reaction and the sequencing was run alongside the cDNA products from primer extension inhibition on denaturing 7 M urea/6 % polyacrylamide sequencing gels.

2.8 Protein EMSA

In vitro transcribed capped $ZIKV^{5'utr+}$ or $ZIKV^{mini}$ RNA (8.6 pmol) was heated at 75 °C and subsequently snap cooled on ice in the presence of RNA refolding buffer (50 mM Tris, pH 7.5, 100 mM KCl and 5 mM $MgCl_2$). RNA (860 fmol) was subsequently incubated with $NS5^{ZIKV}$ (at a final concentration range of 0 nM to 512 nM) at 30 °C for 15 min in a reaction volume of 10 µl containing Buffer R, 5 µg BSA (Sigma) and 2 µg yeast tRNA (Ambion), unless stated otherwise (the reaction mixtures were preincubated at 30 °C for 5 min prior to RNA inclusion). Following addition of 10x native RNA loading dye (0.05 % bromophenol blue, 0.05 % xylene cyanol FF, 50 % glycerol), reactions were analysed by native PAGE on 5 % polyacrylamide gels containing 5 % glycerol on ice at 4 °C. Gels were run at 100V for 2 hrs ($ZIKV^{5'utr+}$) or 3

hrs ($ZIKV^{mini}$) in 0.5x Tris-Borate-EDTA (TBE) and stained with 1 µg/mL ethidium bromide in 0.5x TBE for 30 min prior to visualisation using a UV transilluminator.

2.9 *In vitro* translations

Translation-competent Vero cell lysate was prepared as previously described (Rakotondrafara & Hentze, 2011) by Dr Ted Fajardo. 12.5 µl translation reactions contained Vero cell lysate (40 %, v/v), 1.6 mM HEPES, pH 7.5, 2 mM creatine phosphate, 0.01 µg/µl creatine kinase, 0.01 mM spermidine, 40 µM amino acids, 2.5 mM ATP, 1 mM GTP, 120 mM KOAc, 2 mM MgOAc, 2 mM DTT and 0.8 U RNaseOUT. $ZIKV^{Fluc}$ RNA (0.2 pmol) or $NS5^{ZIKV}/ZIKV^{Fluc}$ RNA complexes, prepared as described in the protein EMSA section with the highest concentration of $NS5^{ZIKV}$ used, were added to the translation reaction and incubated at 30 °C for 90 min. Reactions were terminated by addition of 50 µl 1x passive lysis buffer (Promega). Fluc activity was measured by GloMax (Promega).

2.10 RNA transfection

Vero cells were cultured in maintenance media consisting of Dulbecco's modified Eagles Medium (DMEM; Sigma) supplemented with 10 % fetal calf serum, 2 mM L-glutamine, penicillin (100 SI units/ml) and streptomycin (100 µg/ml) at 37 °C with 5 % CO_2. Capped, *in vitro* transcribed $ZIKV^{fl}$ or $ZIKV^{Nluc}$ RNA (5 µg) was electroporated into 3 x 10^6 Vero cells suspended in 100 µl of OptiMEM I reduced-serum medium (Life Technologies) using a NEPA21 electroporator (Nepagene) using conditions recommended by the manufacturer (Table 2.4). Cells were recovered in maintenance media at 37 °C for 5 min before being seeded sub-confluently in 24 well plates (for the precise number of cells seeded see the relevant figure legend). Maintenance media was replaced 6 hrs post-electroporation and subsequently every 48 hrs. Samples were harvested for luciferase assays and qPCR analysis at the indicated time points by washing cells 3 times with PBS before addition of 250 µl 1x passive lysis buffer (Promega) at room temperature with shaking.

Table 2.4 The NEPA21 electroporator settings used to electroporate ZIKV^{fl} and ZIKV^{Nluc} into Vero cells

Poring pulse						Transfer pulse					
V	Length (ms)	Interval (ms)	No.	Decay Rate (%)	Polarity	V	Length (ms)	Interval (ms)	No.	Decay rate (%)	Polarity
125	5	50	2	10	+	20	50	50	5	40	+/-

Samples post-lysis were split in half to measure Nluc activity and ZIKV genome copy number separately. Nluc was measured using the Nano-Glo luciferase assay system (Promega) and normalised to protein concentration, determined by BCA assay (Pierce). Total RNA was extracted by adding 250 µl TRI Reagent (Sigma) and 75 µl choroform to 115 µl lysed sample. Following centrifugation (12000 xg, 15 min, 4 °C), the upper layer aqueous layer (~175 µl) was precipitated with an equal volume of isopropanol in the presence of 25 ng/µl GlycoBlue (Invitrogen) at room temperature for 5 min. Following centrifugation (12000 xg, 10 min, 4 °C), the pellet was washed twice with 75 % ice cold ethanol to remove contaminating phenol and salts. Pellets were resuspended in water and RNA was quantified by measuring absorbance at 260 nm. qPCR analysis was performed using a Genesig Standard Zika virus quantification kit and PrecisionPlus One-Step 2x RT-qPCR reagent (Primer Design) on a StepOnePlus real-time PCR system (Applied Biosystems). Per reaction, 0.3 µl primer/probe mix, 5 µl of 2x RT-qPCR reagent and 4.7 µl sample were used ensuring that the total amount of RNA in each reaction was less than 500 ng. Cycling parameters consisted of an RT step (50 °C, 30 min), an initial denaturation step (95 °C, 5 min) and then 45 cycles of amplification (95 °C, 15 sec; 60 °C extension, 1 min) without ROX normalisation.

2.11 SHAPE analysis

RNA (50 nM) was incubated in the presence or absence of 10 mM NMIA (ThermoFisher) in 10 µl of buffer containing 30 mM Tris pH 7.5, 100 mM KCl and 2.5 mM $MgCl_2$ for 45 min at 37 °C. RNA was phenol/chloroform extracted and ethanol precipitated. Modified bases were detected by inhibition of primer extension using 2.5 U AMV-RT in the presence of ^{32}P-labelled primer and 0.5 mM dNTPs. Primers were the same ones used for analysis of assembled ribosomal complexes (Table 2.3). cDNA products were phenol/chloroform extracted and ethanol precipitated in the presence of 20 ng/µl GlycoBlue (Invitrogen) prior to resuspension in denaturing RNA loading dye and subsequent resolution on denaturing 7 M urea/6 % polyacrylamide sequencing gels. Products were detected by autoradiography using an FLA

7000 Typhoon scanner (GE Healthcare) and quantified using ImageQuant TL software (GE Healthcare). Band intensities from sample lanes not treated with NMIA were subtracted from those treated with NMIA to obtain relative SHAPE changes. Data from three experiments was combined, analysed and standard deviations were calculated in GraphPad Prism (Wilkinson *et al*, 2006).

2.12 RNA EMSA

In vitro transcribed wildtype and mutant minigenome RNAs (0.5 pmol) were analysed on a native 4.5 % polyacrylamide gel on ice at 4 °C without prior refolding. Antisense or scrambled RNA oligos (2.4 pmol) were annealed to minigenome RNAs (1.2 pmol) by heating to 75 °C in the presence of RNA refolding buffer, then snap cooling on ice before addition of 10x native RNA loading dye. Gels were run at 100V for 3 hrs in 0.5x TBE and stained with 1 µg/mL ethidium bromide in 0.5x TBE for 30 min prior to visualisation using a UV transilluminator.

3 *In vitro* reconstitution of Zika virus translation initiation

3.1 Introduction

Canonical cap-dependent translation initiation relies on the recruitment of a 43S preinitiation complex comprised of eIF1, eIF1A, eIF3, the ternary complex (eIF2/GTP/Met-tRNA$_i^{Met}$) and the 40S ribosomal subunit onto the mRNA (Jackson *et al*, 2010). This process is facilitated by the cap-binding complex eIF4F, consisting of the cap-binding protein eIF4E, the scaffold protein eIF4G and the helicase protein eIF4A, whose activity is additionally stimulated by eIF4B (Pestova & Kolupaeva, 2002). The 43S preinitiation complex then scans down the mRNA until it reaches the initiation codon to establish correct codon-anticodon base-pairing, the fidelity of which is controlled by eIF1 and eIF1A (Pestova & Kolupaeva, 2002; Pestova *et al*, 1998a). This process is sensitive to RNA secondary structure, which if sufficiently stable can act as a barrier to efficient scanning (Kozak, 1991; Pestova & Kolupaeva, 2002). Indeed, mRNAs possessing highly structured 5′ UTRs additionally require the DeXH-box helicase DHX29 for efficient initiation (Pisareva *et al*, 2008). Following correct start site identification and eIF5-mediated eIF2-GTP hydrolysis, a stable 48S complex is formed. Subsequent 60S subunit joining and initiation factor departure are facilitated by eIF5B, allowing translation to begin in earnest (Pestova *et al*, 2000).

A great deal of the information that is known regarding the contribution of individual eIFs in ribosome scanning and initiation codon selection has come from *in vitro* reconstitution assayed by toeprinting (Pestova & Kolupaeva, 2002; Pestova *et al*, 1998a). In this approach, ribosomal complexes are assembled onto mRNAs using purified translation components; namely, the 40S small ribosomal subunit, initiator Met-tRNA$_i^{Met}$ and eIFs. 48S complex assembly is subsequently analysed by toeprinting, in which extension from a labelled primer by reverse transcriptase (RT) yields truncated cDNA products in the presence of protein complexes stably bound to the RNA. The position of ribosomal complexes on the RNA can be determined by gel electrophoresis using an appropriate sequencing ladder, as 48S complexes yield a toeprint 15-17 nt downstream of the initiation codon upon which they have assembled (Figure 3.1A) (Pisarev *et al*, 2007b). An illustrative example of 48S assembly on an unstructured mRNA is shown in Figure 3.1B, in which a truncated cDNA product corresponding to 48S complex formation at the initiating AUG is only seen upon addition of the translation machinery (compare lanes 1 and 2).

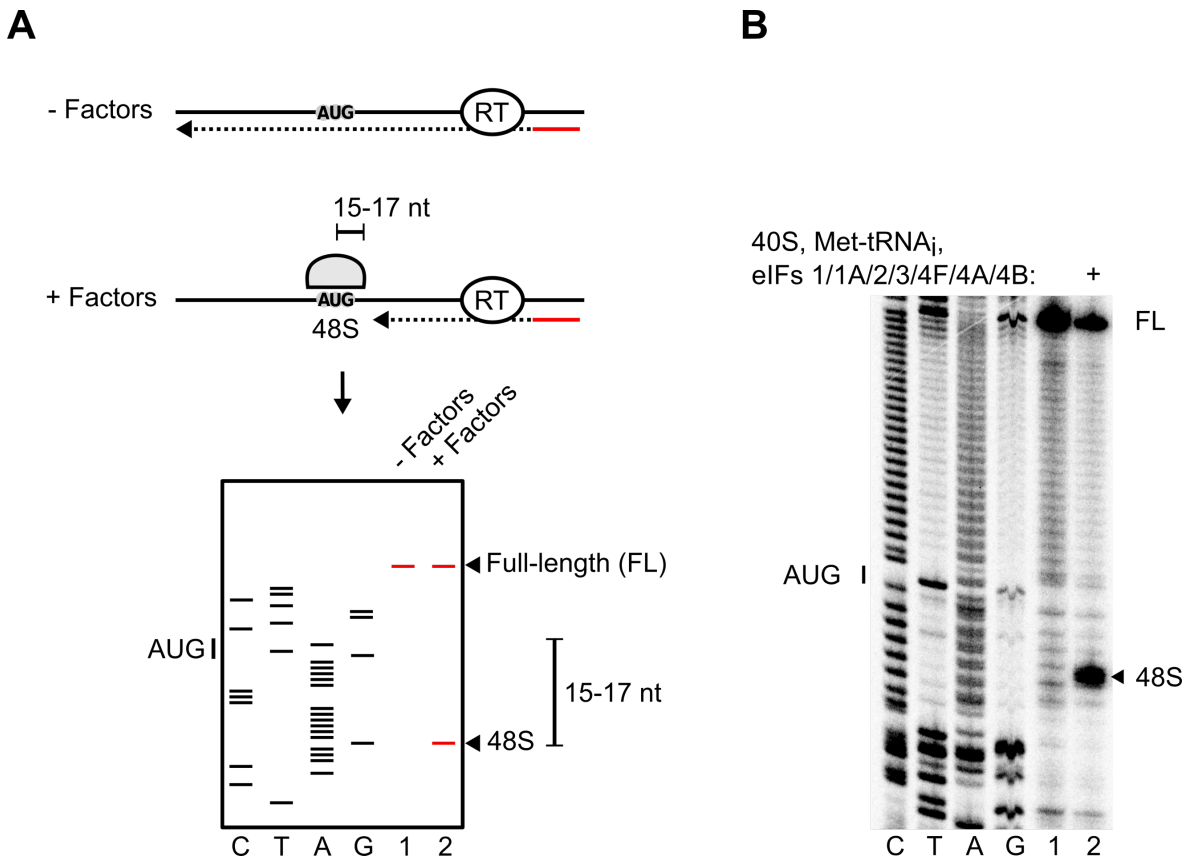

Figure 3.1 The toeprinting approach used to analyse assembled 48S complexes

A) Following 48S complex assembly, a labelled primer is annealed downstream of the region of interest and a reverse transcriptase (RT) reaction is carried out. A ribosomal complex bound to the RNA results in RT arrest 15-17 nt downstream of the ribosomal P site, producing a truncated cDNA product. cDNA products are analysed by denaturing gel electrophoresis and ribosomal complexes are localised using an appropriate sequencing ladder.
B) Toeprinting analysis of 48S assembly on an uncapped model RNA with an unstructured 5′ UTR (G-$(CAA)_{23}$-CACA-AUG). The AUG codon is labelled on the left and the 48S toeprint is marked with an arrowhead on the right. FL, full-length.

The major advantage of this method compared to other more commonly used approaches to study translation is that the minimal set of eIFs required for efficient 48S complex assembly on a given mRNA sequence can be quickly identified. During infection, many viruses bypass the need for the canonical set of eIFs altogether by relying on IRES-mediated translation initiation, in which ribosomes are recruited internally in an end-independent fashion (Jackson *et al*, 2010). *In vitro* reconstitution of translation initiation has been used to study the factor requirement for these noncanonical mechanisms of translation initiation used by different viruses including picornaviruses (Yu *et al*, 2011; Sweeney *et al*, 2014; Pestova *et al*, 1996a) and dicistroviruses (Abaeva *et al*, 2016; Pestova & Hellen, 2003). For example, this approach was used to elucidate the absolute requirement of the EMCV IRES for the central third of eIF4G ($eIF4G_{736-1115}$), containing the eIF3-binding site, and eIF4A (Pestova *et al*, 1996b, 1996a).

Furthermore, this approach allows rapid analysis of the fidelity of initiation codon selection and how this process is influenced by the presence or absence of certain factors (Pestova *et al*, 1998a; Pisareva & Pisarev, 2016b). For instance, the EMCV IRES possesses two AUG codons in close proximity, selection of which is influenced by eIF1 and eIF1A (Pestova *et al*, 1998a). Additionally, the helicase DHX29 has been shown to promote linear scanning and influence codon selection by the scanning 43S preinitiation complex during cap-dependent translation initiation (Abaeva *et al*, 2011; Pisareva & Pisarev, 2016b).

However, this reconstitution approach to study translation initiation does possess several notable drawbacks. As the system is based upon purification of known eIFs, additional regulatory factors within cells that can positively or negatively regulate translation, either through functionally replacing eIFs or modulating their activity, are not present. Furthermore, in the cell the effective concentration of eIFs and other regulatory factors is likely higher than typically used *in vitro* through macromolecular crowding and mechanisms that regulate protein and RNA localisation, which could impact upon translational efficiency. Molecular crowding effects have been shown to enhance the activity of eIF4A by directing the conformational equilibrium towards a closed active conformation, suggesting that eIF4A *in vivo* may be more active than eIF4A *in vitro* (Akabayov *et al*, 2013). Comparatively in *E. coli,* it has been suggested that an increase in molecular crowding within cells induced by osmotic stress limits the diffusion of protein complexes important for translation initiation and thus acts to inhibit translation (Zhang *et al*, 2010; Klumpp *et al*, 2013). These effects provide an additional level of complexity that cannot easily be recapitulated *in vitro*.

ZIKV and other flaviviruses are thought to translate in a cap-dependent manner because of the presence of a virally-encoded cap structure at the 5′ end of the genome (Ray *et al*, 2006; Egloff *et al*, 2002; Issur *et al*, 2009; Bartelma & Padmanabhan, 2002; Wengler & Wengler, 1993). However, it has been shown that DENV and ZIKV induce cap-dependent host cell translational shutoff during infection (Roth *et al*, 2017) and it is presently unclear how viral genomes are translated under these conditions. Furthermore, a recent publication has suggested that the 5′ UTR of both ZIKV and DENV possesses IRES activity (Song *et al*, 2019). Elucidation of eIF requirement during viral infection remains challenging, as siRNA knockdown or pharmacological inhibition of key eIFs is likely to trigger a multitude of cellular responses that could obscure the specific effect on viral translation.

The aim of the work presented in this chapter was to determine *in vitro* the minimal eIF requirement for efficient 48S complex formation on ZIKV RNA to shed light on the mechanism of translation used within a minimalistic system. This required the establishment of a working reconstitution system by purifying and subsequently testing the eIFs required for eukaryotic translation initiation. In addition, the mechanism of scanning performed by the 43S preinitiation complex through the cap-proximal stem-loop within the viral 5′ UTR was investigated by mutation.

3.2 Results

3.2.1 Purification of factors required to reconstitute translation initiation

Cap-dependent translation initiation relies upon the activity and coordination of at least nine eIFs (Jackson *et al*, 2010). The single subunit eIFs that are required for 48S complex assembly can be expressed recombinantly in bacteria (such as eIF1, eIF1A, eIF4A and eIF4B) (Pisarev *et al*, 2007b) and are just as functional as factors natively purified from rabbit reticulocyte lysate (RRL), a rich source of eIFs (Pestova *et al*, 1996a, 1998a). Furthermore, *in vitro* transcribed and aminoacylated Met-tRNA$_i^{Met}$ has been shown to be just as active in translation initiation assays as natively purified Met-tRNA$_i^{Met}$ in scanning-dependent initiation (Pestova & Hellen, 2001). However, multi-subunit eIFs including eIF2, eIF3, eIF4F and the 40S ribosomal subunit must be purified natively from RRL for activity (Pisarev *et al*, 2007b), although a lower yield can also be obtained from HeLa cell lysates (T. Sweeney, personal communication). An overview schematic of this process is shown in Figure 3.2 and the purification of eIF3 will be described in more detail below.

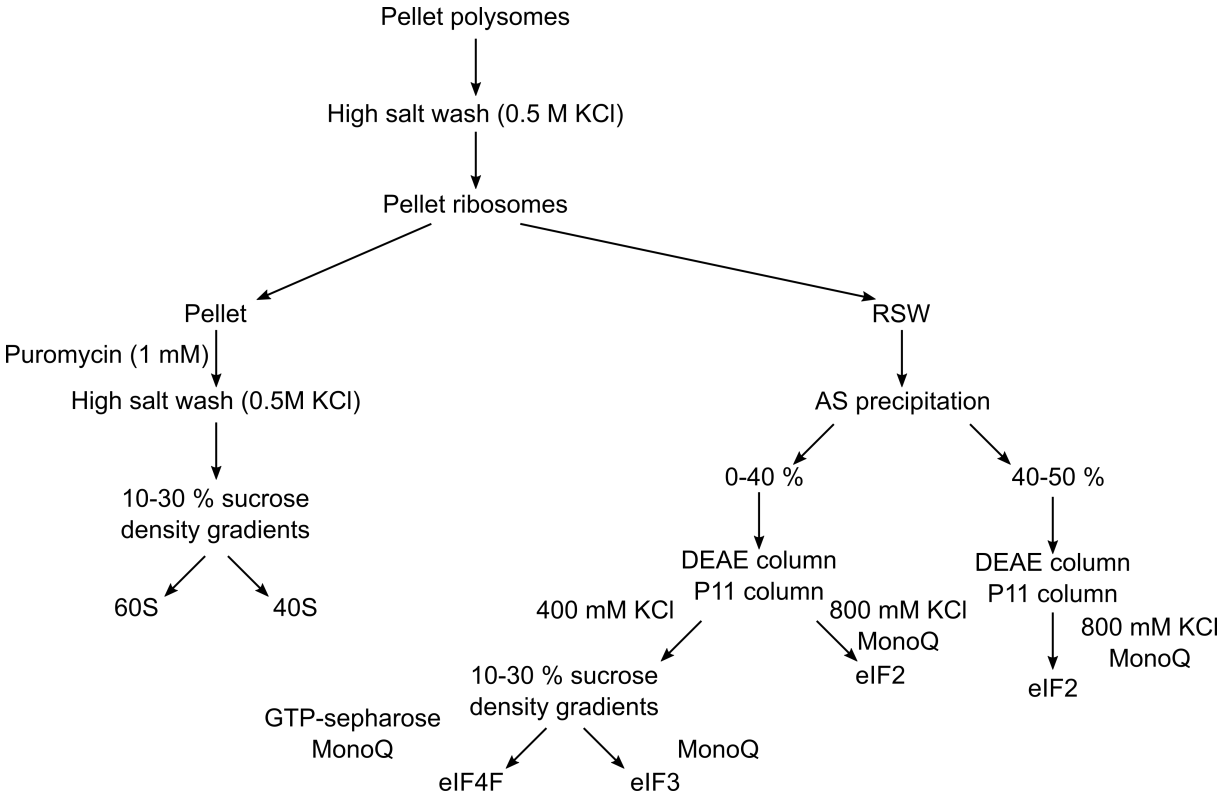

Figure 3.2 Purification of native eIFs from RRL

A schematic illustrating the purification strategy for native eIF2, eIF3 and eIF4F as well as 40S and 60S ribosomal subunits (Pisarev *et al*, 2007b). Briefly, pelleted polysomes are washed with 0.5 M KCl to release eIFs. Following subsequent centrifugation, eIFs are purified from the ribosomal salt wash (RSW) by ammonium sulphate (AS) precipitation and ion-exchange chromatography. The major eIF2 fraction is purified from the 40-50 % AS fraction. In the case of eIF3 and eIF4F, separation is achieved through 10-30 % sucrose density gradients in high salt before eIF4F is further purified by affinity chromatography using GTP-sepharose. Comparatively, small 40S ribosomal subunits are purified from pelleted ribosomes following incubation with puromycin to release nascent peptides and separated from large 60S ribosomal subunits by sucrose density gradient centrifugation.

Following polysome isolation from the RRL and initiation factor release, eIFs of interest were precipitated from the ribosomal salt wash (RSW) through addition of ammonium sulphate (AS). As illustrated by western blot using an eIF3d antibody, eIF3 precipitated in the 0-40 % AS fraction (Figure 3.3A). eIF3 was subsequently purified by ion-exchange chromatography using DEAE and phosphocellulose (P11) resin (Figure 3.3B). As eIF3 co-purifies with eIF4F, the two were separated in high salt using 10-30 % sucrose density gradients and fractions were analysed by SDS-polyacrylamide gel electrophoresis (SDS-PAGE; Figure 3.3C). eIF3 possesses a larger molecular mass than eIF4F therefore penetrated further into the sucrose gradient. eIF3 purification was completed by anion-exchange chromatography on a fast protein liquid chromatography (FPLC) system (Figure 3.3D). eIF3 purified in this way lacks both eIF3j and

eIF3a, the former of which is only loosely associated during the sucrose density gradient and the latter of which is typically degraded in RRL (Pisarev *et al*, 2007b). The loss of either does not influence the activity of eIF3 in 48S initiation complex assembly (Kolupaeva *et al*, 2005; Unbehaun *et al*, 2004a).

To investigate the activity and purity of the eIF3 preparation, 48S complex assembly and toeprinting was performed on the EMCV IRES, assembly on which absolutely requires eIF3 as well as the central portion of eIF4G ($eIF4G_{736-1115,}$ hence referred to as eIF4Gm), a component of eIF4F (Pestova *et al*, 1996a, 1996b). Assembly was performed in the absence of eIF1 to ensure strong complex could be seen at both AUG_{826} and AUG_{834} (Pestova *et al*, 1998a). In the absence of added eIF4F, no complex formation was seen at either initiating AUG in the presence of the newly purified eIF3, illustrating that the eIF3 preparation was not contaminated with eIF4F (Figure 3.4B, lane 2). Addition of recombinantly expressed eIF4Gm led to 48S complex formation, confirming that the purified eIF3 is active (Figure 3.4B, lane 3) (Pestova *et al*, 1996b). As expected, inclusion of a mixture of eIF3/4F promoted 48S complex assembly (Figure 3.4B, lanes 4 and 5).

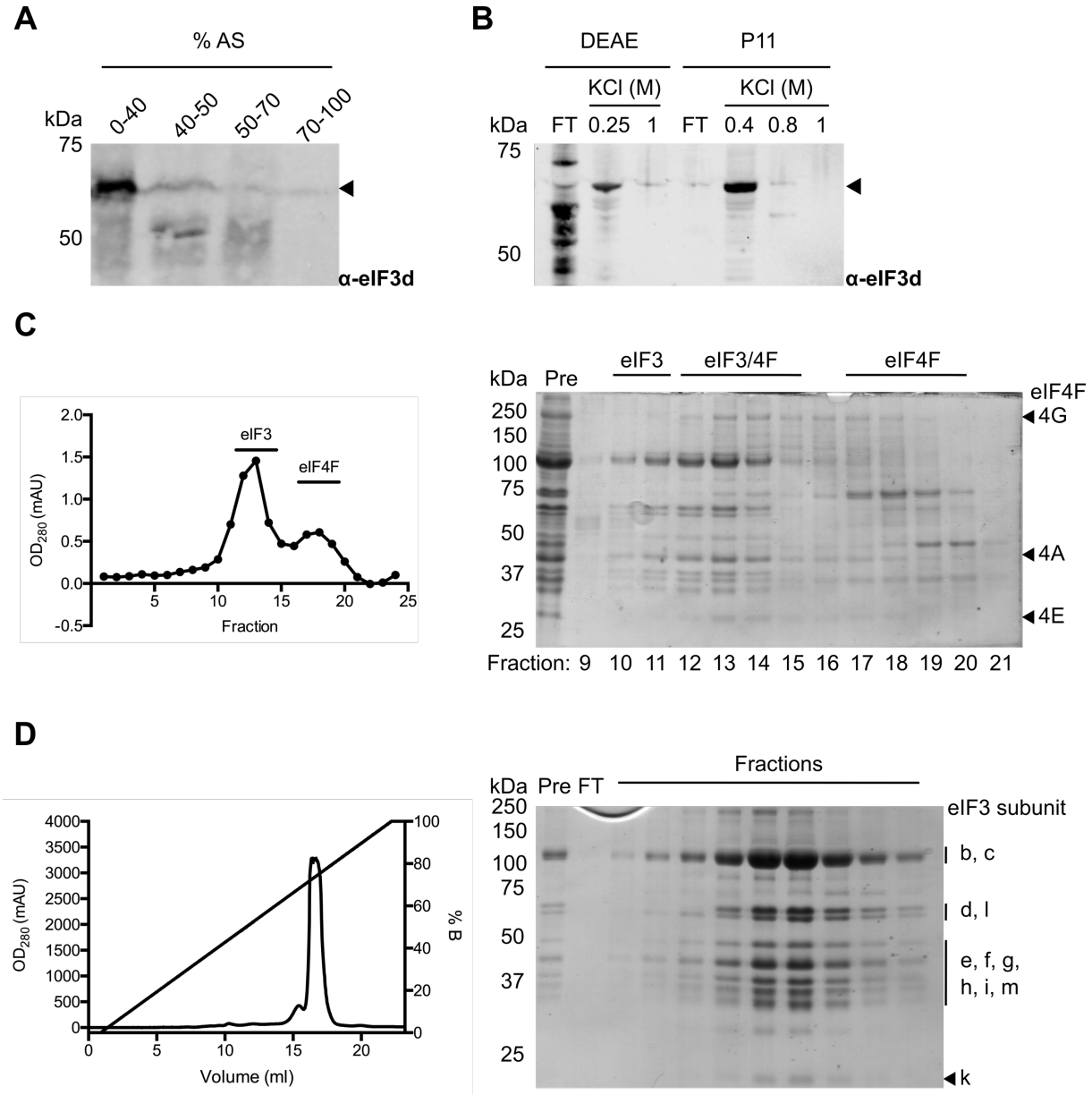

Figure 3.3 Purification of native eIF3 from RRL

A, B) Western blot of fractions following A) ammonium sulphate (AS) precipitation and B) diethylaminoethyl (DEAE) and phosphocellulose (P11) ion-exchange chromatography using an eIF3d antibody. eIF3d is indicated with an arrow.
C) eIF3 and eIF4F were separated by sucrose density centrifugation at high salt (400 mM KCl). Fractions were collected following separation and absorbance at 280 nm measured. Fractions were analysed by Coomassie-stained SDS-PAGE (right). The fraction numbers are labelled below the gel and the protein identities are shown above the gel. Protein components of eIF4F are labelled on the right of the gel. The lane entitled Pre contains a sample of eIF3/eIF4F before the sucrose density gradient separation.
D) eIF3-containing fractions were pooled following the sucrose density gradient separation and applied to a MonoQ column and eluted with a 100 to 500 mM KCl gradient (Buffer B contains 500 mM KCl). eIF3 eluted at 415 mM KCl. Fractions were analysed by Coomassie-stained SDS-PAGE (right). eIF3 subunits are labelled on the right of the gel. The lane entitled Pre contains a sample of eIF3 prior to MonoQ purification. FT, flow through.

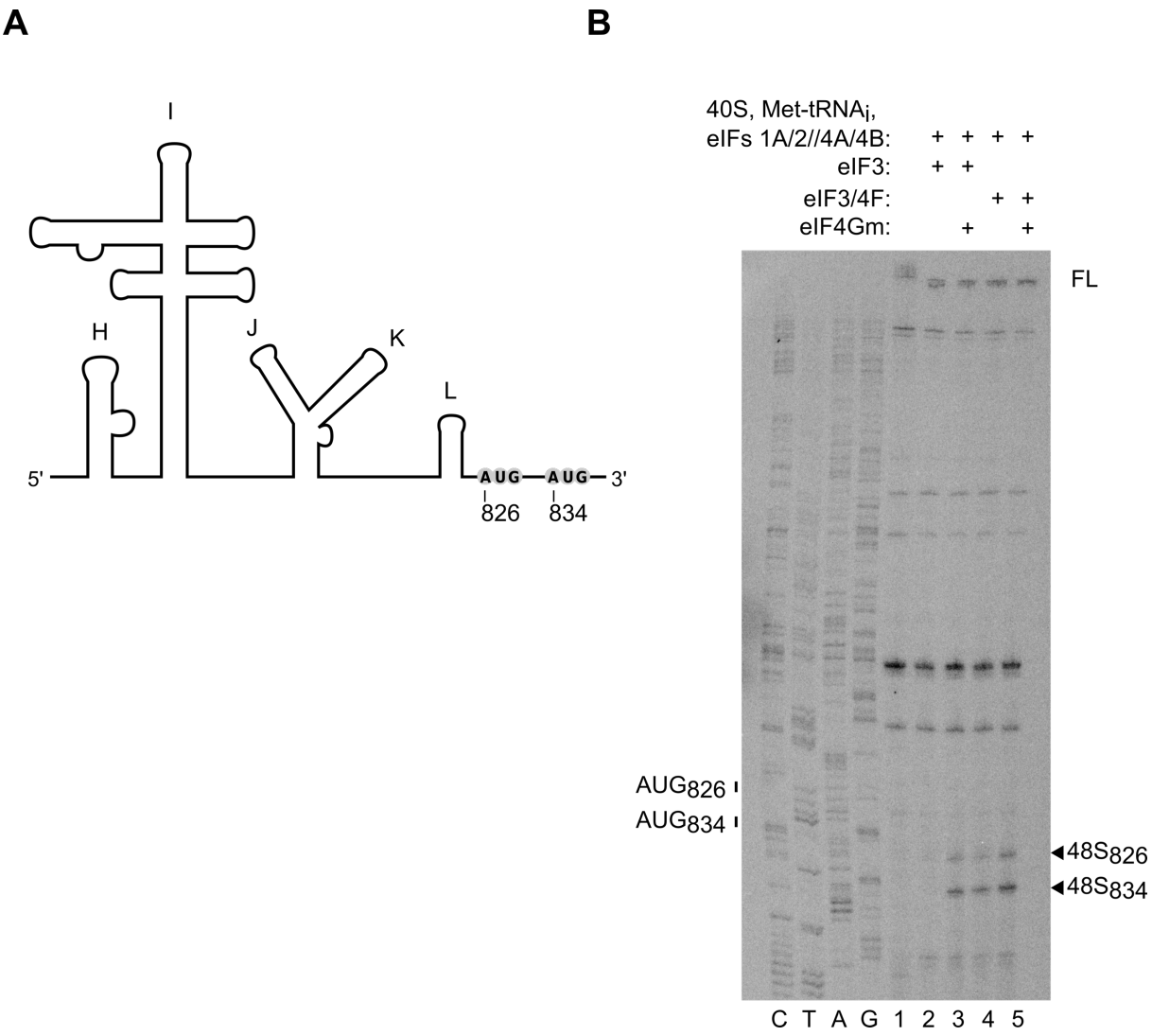

Figure 3.4 48S complex assembly on the EMCV IRES

A) Schematic of the EMCV IRES. Structural domains important for IRES activity (H, I, J, K and L) are indicated (Kolupaeva *et al*, 2003). AUGs at nt 826 and 834 are shown.
B) Toeprinting analysis of 48S assembly on the EMCV IRES (nt 315-1155) in order to test eIF3 purity. The factors used are indicated. eIF4Gm refers to $eIF4G_{736-1115}$. The AUG codons are labelled on the left and 48S toeprints are marked with an arrowhead on the right. $Met\text{-}tRNA_i^{Met}$ natively purified from RRL was used as synthetic $Met\text{-}tRNA_i^{Met}$ forms weaker 48S complexes on the IRES (T Sweeney, personal communication). FL, full-length.

The components of the canonical cap-dependent translation initiation machinery purified for this study are shown in Figure 3.5.

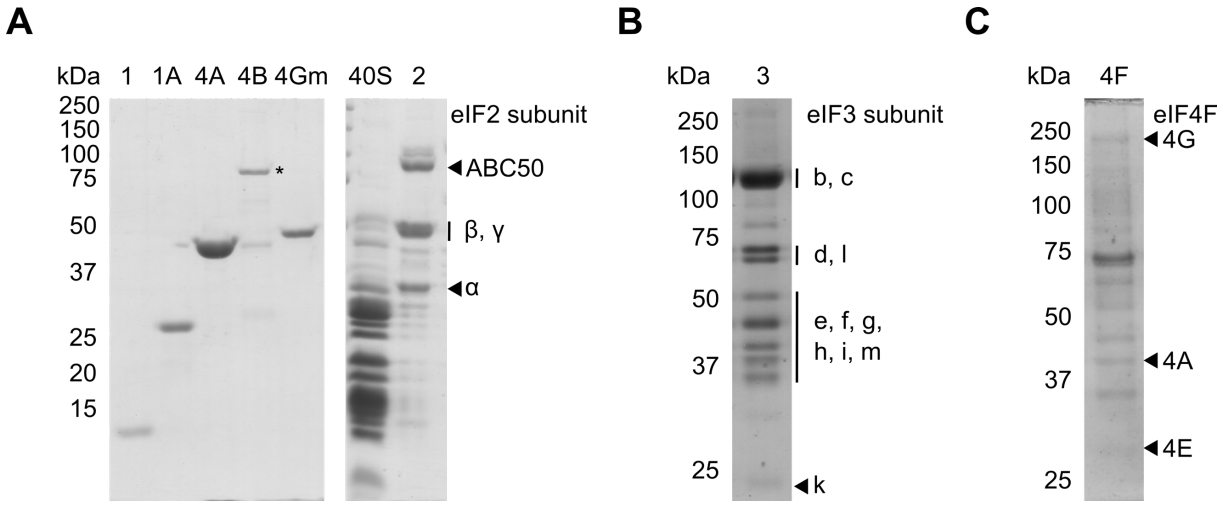

Figure 3.5 The canonical cap-dependent translation initiation machinery purified for this study

A) Canonical translation components purified for the reconstitution of translation initiation *in vitro* were analysed by SDS-PAGE and detected by Coomassie. eIF2 co-purifies from the 40-50 % AS fraction with ABC50 (Tyzack *et al*, 2000). eIF2 subunits are labelled to the right of the gel. 4Gm refers to the eIF4G$_{736\text{-}1115}$, consisting of the central portion of eIF4G. ***** indicates full-length eIF4B; lower bands represent degradation products.
B), C) Lanes containing purified (**B**) eIF3 and (**C**) eIF4F are taken from Figure 3.3D (lane 9) and Figure 3.3C (lane 11) respectively, with protein components labelled to the right of each lane.

3.2.2 Translation initiation on ZIKV occurs in a cap-dependent fashion in the reconstitution system

Following successful establishment of a reconstitution system for translation initiation, the system was then applied to the study of ZIKV translation. A model ZIKV RNA was designed consisting of the first 359 nt of the ZIKV genome including the 5′ UTR and the first 252 nt of the C coding sequence (hence referred to as ZIKV$^{5'utr+}$, the 5′ end of which is shown schematically in Figure 3.6A). This construct contains the 5′ cyclisation elements as well as the cHP stem, previously identified as promoting initiation codon selection in DENV2 by stalling the scanning ribosomal complex (Clyde & Harris, 2006). In addition, full-length ZIKV RNA derived from a reverse genetic system was used (hence referred to as ZIKV^{fl}; described in Chapter 5) (Mutso *et al*, 2017). RNA was transcribed by T7 polymerase and capped *in vitro*.

As ZIKV and other flaviviruses have been previously reported to undergo cap-dependent translation initiation (e.g. Chiu *et al*, 2005; Edgil *et al*, 2006), the effect of the cap structure was examined in the presence of the full complement of canonical eIFs. In the absence of a cap structure, only weak 48S complex formation was detected on ZIKV$^{5'utr+}$ RNA (Figure 3.6B;

lane 2). However, the addition of a 5′ cap greatly enhanced 48S complex assembly at the initiation codon AUG_{108} (Figure 3.6B; compare lanes 4 and 2). Weak 48S complex assembly was observed on the upstream near-cognate codons UUG_{41} and UUG_{86} (highlighted on Figure 3.6A). Similarly, the presence of a cap structure greatly enhanced 48S complex formation at AUG_{108} on $ZIKV^{fl}$ RNA with contains both the viral 5′ and 3′ UTRs (Figure 3.6B; compare lanes 8 and 6). To maintain equal concentrations of $ZIKV^{5'utr+}$ and $ZIKV^{fl}$ RNA in the assembly reaction, a greater mass of $ZIKV^{fl}$ RNA was included. This could explain the weaker 48S assembly seen on $ZIKV^{fl}$ RNA, as some eIFs including eIF3 and eIF4A interact directly with RNA and could be sequestered from active 48S complex formation.

In order to confirm that the *in vitro* transcribed RNA behaved similarly to ZIKV RNA taken directly from infection, toeprinting analysis was performed upon total RNA extracted from ZIKV-infected Vero cells using a ZIKV-specific primer. In an analogous fashion to the $ZIKV^{5'utr+}$ and $ZIKV^{fl}$ RNA, the canonical set of translation factors triggered efficient 48S assembly at AUG_{108} (Figure 3.6B; compare lanes 10, 8 and 4). In DENV2, the AUG present within the 5′ CS element has been shown to be important for viral replication independently of genome circularisation, potentially through production of a truncated C protein (Clyde & Harris, 2006). No efficient complex formation was observed at the equivalent downstream AUG_{158} within the CS element on any ZIKV RNA tested.

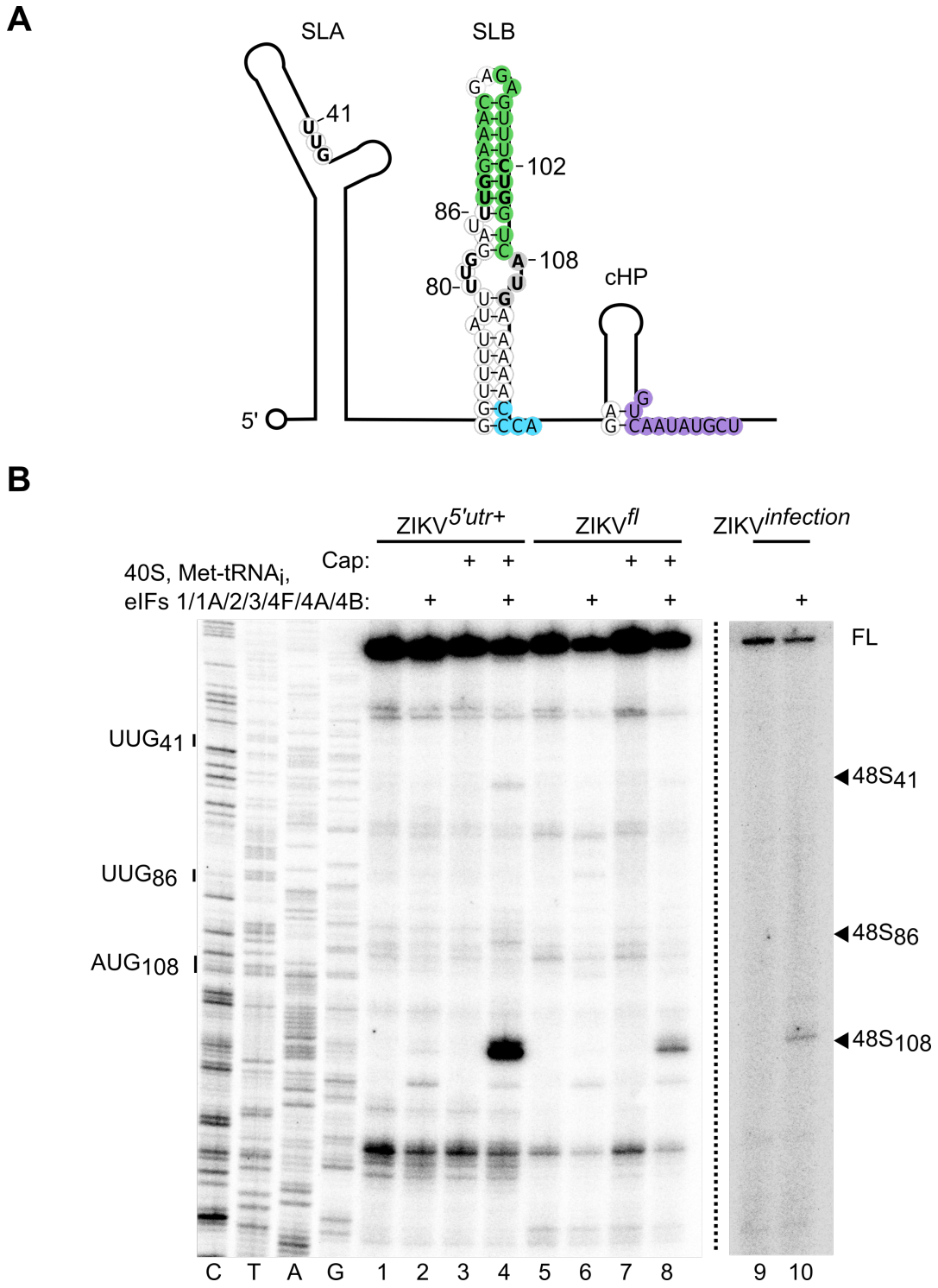

Figure 3.6 Ribosome assembly on ZIKV RNA is enhanced by a 5′ cap structure

A) Schematic of the ZIKV 5′ end from nt 1-160. Near-cognate codons upstream of the initiating AUG at nt position 108 discussed are indicated. Sequences corresponding to the 5′ UAR, DAR and CS sequences involved in genome 5′-3′ hybridisation are highlighted in green, blue and purple, respectively. The 5′ cap structure is represented as a circle. SLA, stem-loop A; SLB, stem-loop B; cHP, C coding region hairpin.
B) Toeprinting analysis of 48S assembly on the RNAs indicated in the presence or absence of a 5′ cap structure (a representative experiment is shown from three independent experiments). Selected codons are labelled on the left and 48S toeprints are marked with an arrowhead on the right. The black line indicates altered contrast to enhance visibility of complex assembly on ZIKV RNA from infected Vero cells (ZIKV^{infection}). FL, full-length.

Next, a factor omission experiment was performed on the ZIKV$^{5'utr+}$ RNA to determine which of the canonical set of eIFs were sufficient for ZIKV translation initiation. In place of the omitted factor, the factor storage buffer was added to ensure that salt concentrations were identical across the different conditions tested. Omission of eIF2 and eIF3 completely abrogated 48S complex assembly at AUG_{108}, whereas omission of eIF4F greatly reduced complex assembly (Figure 3.7 lanes 7, 8 and 9). This concurs with the requirement for a 5′ cap structure for efficient translation initiation in this system (shown in Figure 3.6B). An eIF4F-dependent toeprint at nt 132 was frequently observed (labelled on Figure 3.7).

In comparison to eIF1 whose omission abrogated 48S assembly (Figure 3.7 lane 4), addition of eIF1A was mostly dispensable for ribosome loading onto the ZIKV$^{5'utr+}$ RNA, but omission led to an increase in 48S complex at the upstream near-cognate codon UUG_{41} (Figure 3.7 lane 5). This is consistent with its described role in initiation site selection (Pestova *et al*, 1998a; Pestova & Kolupaeva, 2002).

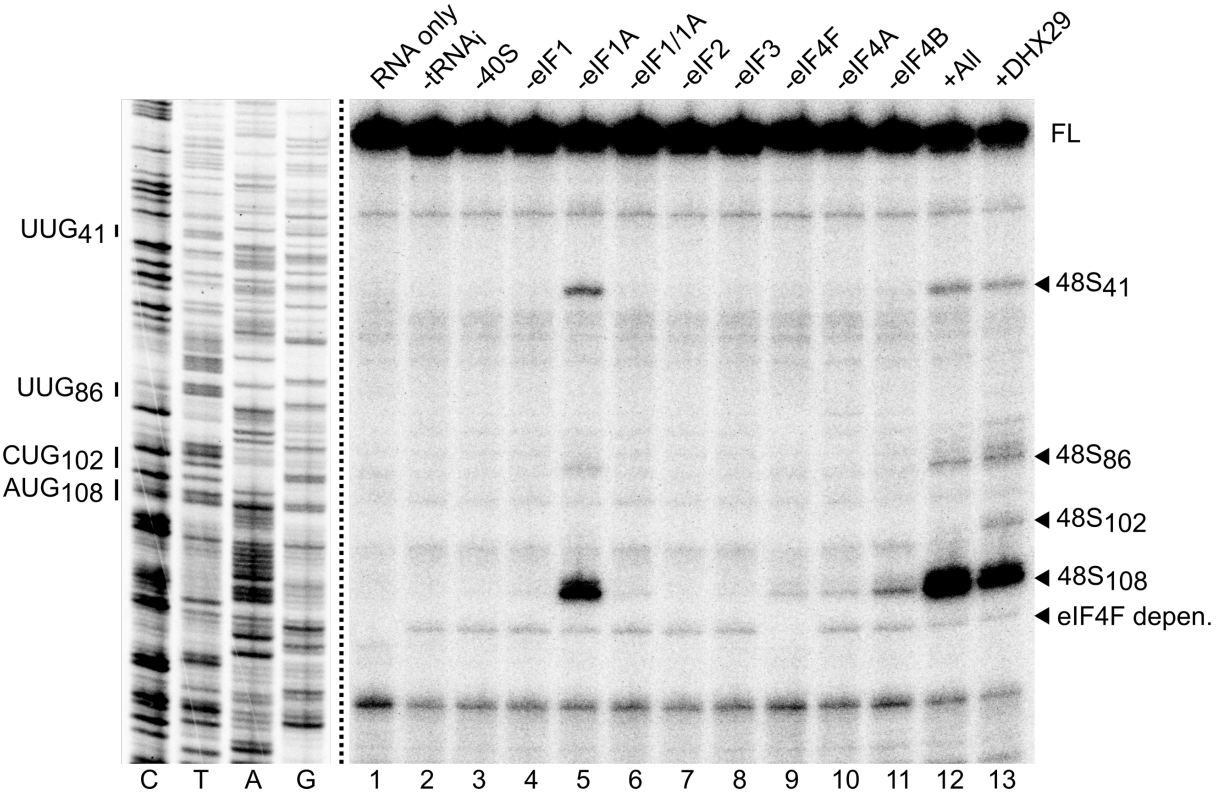

Figure 3.7 Factor omission shows that ZIKV translation requires the canonical set of eIFs

Toeprinting analysis of 48S assembly on capped ZIKV$^{5'utr+}$ as in Figure 3.6 with the omitted factor indicated (a representative experiment is shown from three independent experiments). Selected codons are labelled on the left and 48S toeprints are marked with an arrowhead on the right. The eIF4F-dependent toeprint is additionally labelled on the right. The black line indicates altered contrast to balance the exposure of the sequencing relative to the cDNA. FL, full-length

As flavivirus genomes are highly structured (Gebhard *et al*, 2011; Göertz *et al*, 2018), it was expected that efficient ribosome recruitment will depend on helicases such as eIF4A and DHX29, a DExH-box helicase previously shown to be required for translation initiation on highly structured RNAs (Pisareva *et al*, 2008). Omission of recombinant eIF4A (beyond that present in eIF4F) or its cofactor eIF4B, recently shown to bind flaviviral genomes during infection (Phillips *et al*, 2016), greatly reduced 48S assembly on ZIKV^{5utr+} RNA (Figure 3.7, lanes 10 and 11). Furthermore, the eIF4A inhibitor hippuristanol (Bordeleau *et al*, 2006) inhibited 48S complex assembly in a dose-dependent manner (Figure 3.8; compare lanes 2, 3, 4 and 5). Consistent with this requirement for eIF4A, it has recently been reported that the eIF4A inhibitor silvestrol inhibits ZIKV replication in A549 cells and primary human hepatocytes (Elgner *et al*, 2018). These results were confirmed using the eIF4A inhibitor rocaglamide which inhibited translation of a ZIKV infectious clone containing a nanoluciferase (Nluc) insertion (Mutso *et al*, 2017) following electroporation into Vero cells (Appendix B).

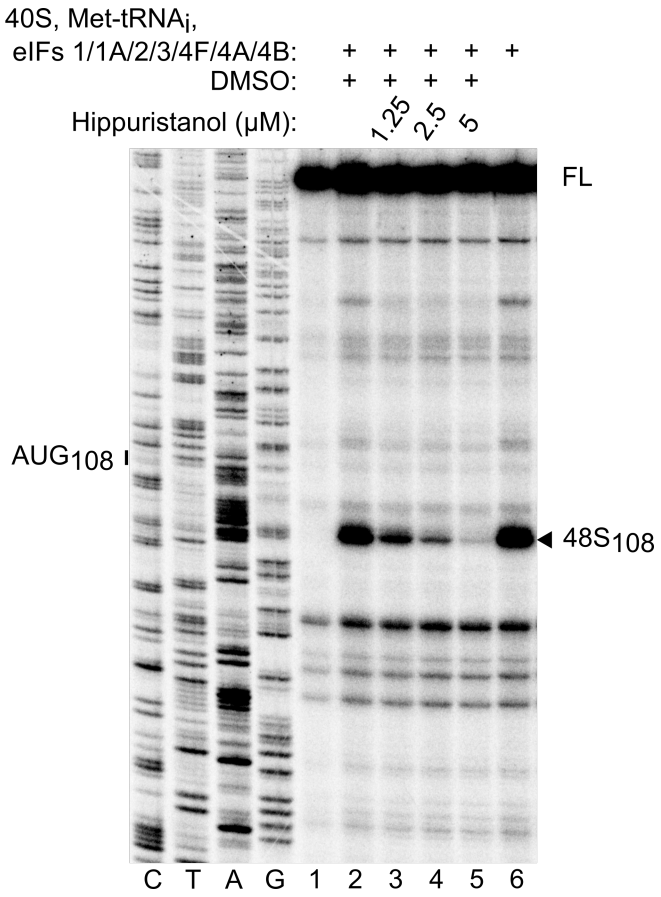

Figure 3.8 The eIF4A inhibitor hippuristanol inhibits 48S complex assembly on ZIKV RNA

Toeprinting analysis of 48S complex formation upon capped ZIKV$^{5'utr+}$ at the indicated concentrations of hippuristanol. Selected codons are labelled on the left and toeprints caused by 48S complex assembly are marked with a closed arrowhead on the right. Lanes with 5 % DMSO are indicated. FL, full-length.

However, 48S complex formation on ZIKV$^{5'utr+}$ RNA occurred in the absence of DHX29 (Figure 3.7, lane 12). Addition of recombinant DHX29 weakly decreased 48S complex assembly at AUG_{108} in favour of assembly at upstream near-cognate codons UUG_{86} and CUG_{102} (Figure 3.7; compare lanes 12 and 13), consistent with a recently described role of DHX29 in influencing initiation codon selection during ribosome scanning (Pisareva & Pisarev, 2016b). In order to confirm recombinant DHX29 activity, 48S assembly and toeprinting analysis was performed on Sindbis virus (SV) 26S mRNA, previously characterised as requiring DHX29, but not eIF4A, activity for 48S complex assembly (Figure 3.9B; compare lanes 2 and 3) (Skabkin *et al*, 2010). Unlike eIF4A, DHX29 activity was not inhibited by the addition of hippuristanol into the assembly reaction (Figure 3.9B; compare lanes 5-8).

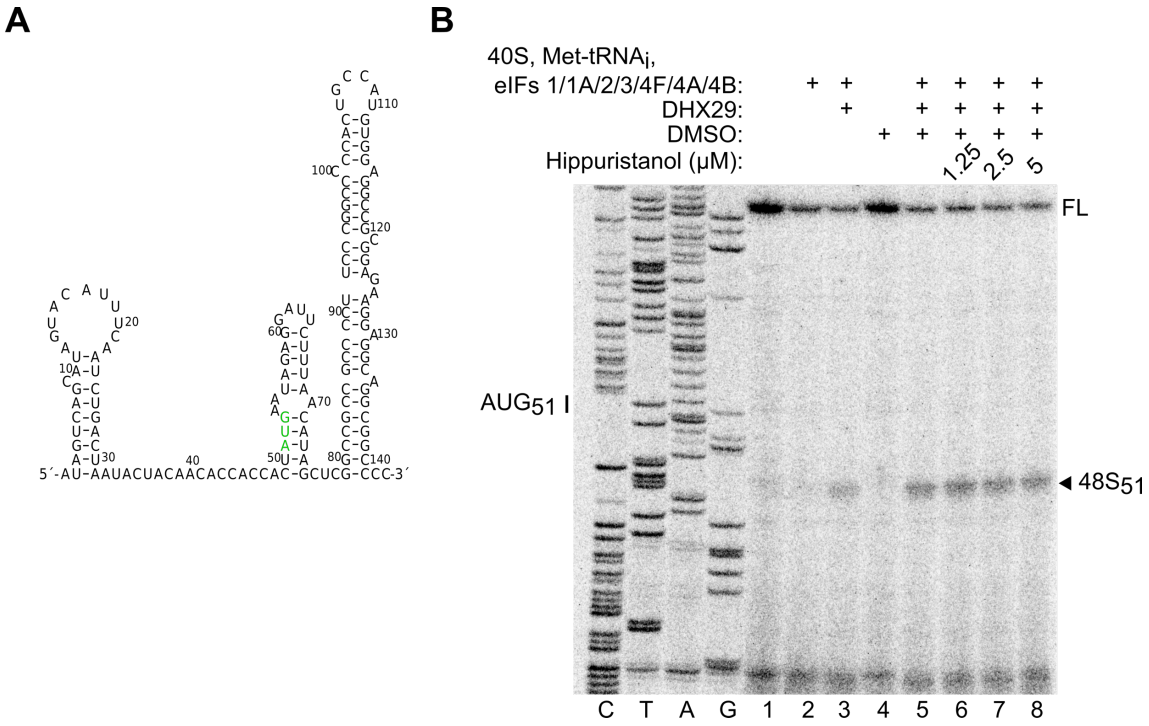

Figure 3.9 48S complex assembly on SV S26 mRNA requires DHX29 whose activity is not inhibited by hippuristanol

A) A schematic of the Sindbis virus (SV) 26S mRNA 5′ end. The initiating AUG codon is highlighted in green.
B) Toeprinting analysis of 48S complex formation upon SV 26S mRNA at the indicated concentrations of hippuristanol. Selected codons are labelled on the left and toeprints caused by 48S complex assembly are marked with a closed arrowhead on the right. Lanes with 5 % DMSO are indicated. FL, full-length.

3.2.3 The 5' UTR of ZIKV is not efficiently scanned

As eIF1A omission reduced, but did not abrogate, 48S complex assembly at AUG_{108} in favour of UUG_{41} (Figure 3.7 lane 5), a mutational approach was carried out to investigate whether initiation codons within SLA were efficiently seen by the scanning ribosome. The near-cognate codon UUG_{41} was changed to AUG_{41} in the context of the $ZIKV^{5'utr+}$ RNA, with an additional G23U mutation to maintain SLA structure. Similarly, an extra AUG was added at the top of SLA by mutating CAG_{31} to AUG_{31}, with additional mutations C28G and G37C to put the new AUG in a more favourable Kozak sequence context (Figure 3.10A) (Kozak, 1989a).

Mutation of UUG_{41} to AUG_{41} enhanced 48S complex assembly at this site, suggesting that a degree of linear scanning within SLA is occurring (Figure 3.10B; compare lanes 4 and 2). However, efficient 48S complex formation at AUG_{108} was not completely abrogated, despite the favourable sequence context of AUG_{41}. Remarkably, addition of AUG_{31} at the top of SLA greatly inhibited 48S assembly upon the $ZIKV^{5'utr+}$ RNA (Figure 3.10B, compare lanes 6 and 2), even in the background of the UUG_{41} to AUG_{41} mutation (Figure 3.10B, compare lanes 8 and 4). Subsequent *in silico* analysis of RNA structure using mfold (Zuker, 2003) suggested that introduction of AUG_{31} in favourable sequence context lead to stabilisation of the upper half of SLA (+AUG_{31} ΔG = -31.50 kcal/mol, wildtype ΔG = -25.70 kcal/mol), providing a possible explanation for this observation (illustrated in Figure 3.10A). This highlights the need to carefully consider RNA secondary structure when making mutations in these viruses.

Instead AGU_{32} at the top of SLA was replaced with AUG_{32}, which was already in a favourable sequence context hence mitigating the need for additional mutations within the stem (Figure 3.10C). Following 48S complex assembly, only very weak assembly was detected at AUG_{32} with the majority still occurring at AUG_{108} (Figure 3.10D; compare lanes 4 and 2). Taken together, these results suggest that SLA is not efficiently scanned by the 43S preinitiation complex in the presence of the canonical set of eIFs.

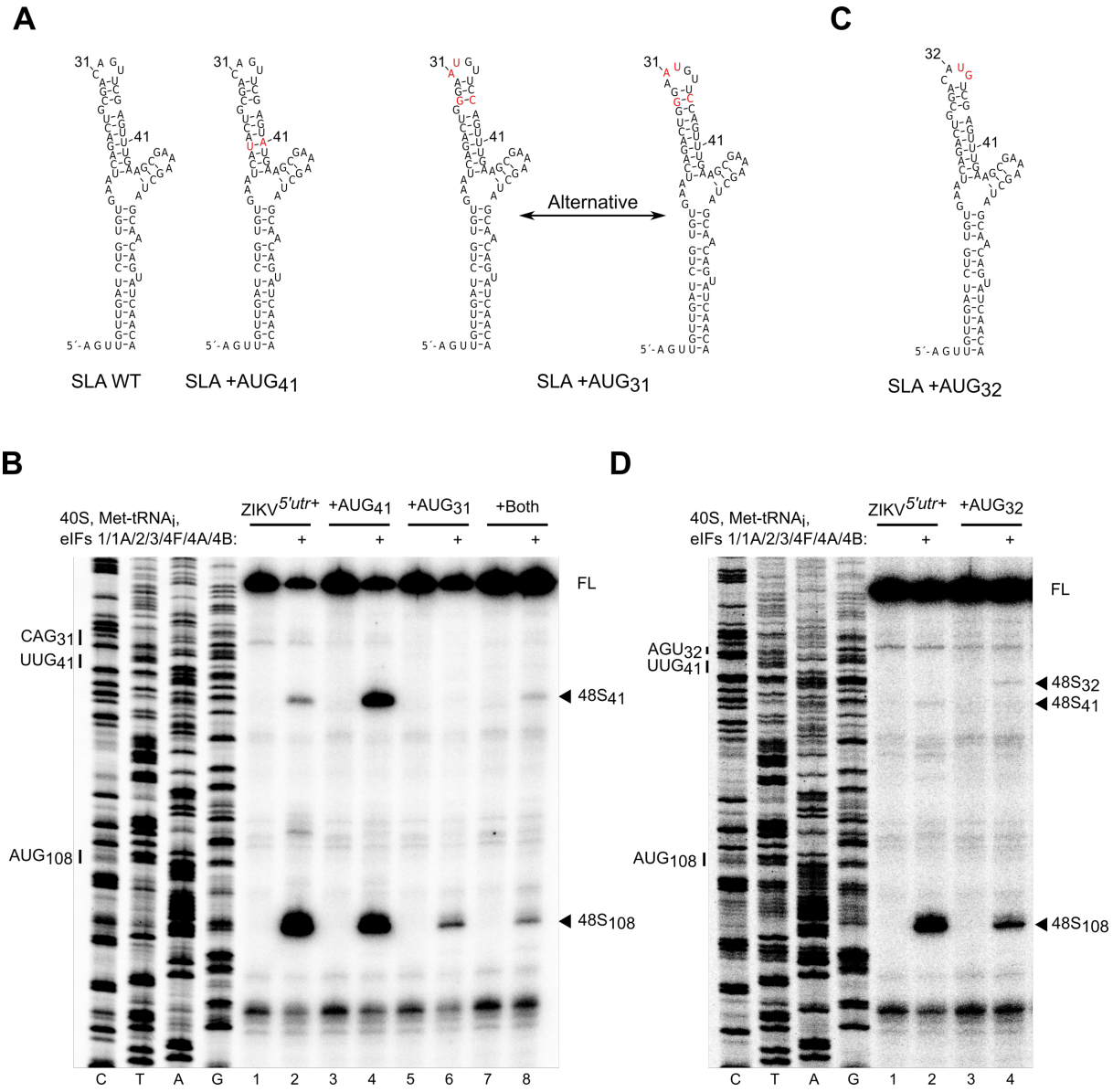

Figure 3.10 SLA is not efficiently scanned by the 43S preinitiation complex

A, C) Stem-loop A (SLA) structures with the different mutations indicated. Mutations are shown in red. Structures were analysed by mfold (Zuker, 2003). Two alternative structures of the SLA +AUG$_{31}$ mutant are shown.
B, C) Toeprinting analysis of 48S complex formation upon capped ZIKV$^{5'utr+}$ RNA with the indicated mutation. Selected codons are labelled on the left and toeprints caused by 48S complex assembly are marked with a closed arrowhead on the right. FL, full-length.

3.3 Discussion

Numerous experimental techniques have been used to study the mechanism of flavivirus translation including *in vitro* translation of reporter mRNAs in translation-competent cell-free extracts, mutational analysis of infectious replicons to identify important *cis*-acting elements, pharmacological intervention or protein knockdown during infection, polysome profiling or, more recently, ribosome profiling of infected cells (Roth *et al*, 2017; Edgil *et al*, 2006; Reid *et al*, 2018; Clyde & Harris, 2006; Clyde *et al*, 2008; Irigoyen *et al*, 2017; Campos *et al*, 2017).

Key advantages of the *in vitro* reconstitution approach are that the eIF requirement for a given RNA can be quickly ascertained and that the fidelity of start codon selection can be analysed, thus providing information about the precise mechanism of translation initiation. This work marks the first time that translation initiation has been reconstituted on a flavivirus.

In the reconstitution system presented here, translation of ZIKV RNA was cap-dependent as addition of a 5′ cap structure greatly enhanced 48S complex formation at the initiating AUG of ZIKV (Figure 3.6), whereas omission of eIF4F abrogated it (Figure 3.7). Consistent with this, it has been previously reported that the antiviral cap-binding protein IFIT1 can attenuate the translation and replication of 2′-O methyltransferase deficient flaviviruses both *in vitro* and *in vivo* (Daffis *et al*, 2010; Fleith *et al*, 2018; Johnson *et al*, 2018). As IFIT1 has been demonstrated to inhibit translation by binding to non-self 5′ cap structures and outcompeting eIF4F binding (Kumar *et al*, 2014), this data is consistent with ZIKV requiring a cap-dependent mechanism for translation initiation during infection.

The inhibitory effect of stable stem-loop structures in close proximity to the 5′ end of mRNAs on translation initiation have been well documented (Babendure *et al*, 2006; Kozak, 1989b). As SLA begins only 4 nt from the 5′ end of the ZIKV genome, it could be envisioned that ribosome recruitment is reliant on unwinding of this cap-proximal structure. Alternatively, a direct loading mechanism might occur to bypass SLA altogether. This has been proposed to occur on the SV 26S mRNA in a DHX29-dependent manner, whose 5′ end also possesses a cap-proximal stem-loop structure (Figure 3.9A) (Skabkin *et al*, 2010). However, evidence presented here suggests that linear scanning from the 5′ end is the dominant mechanism by which ZIKV translation initiation occurs, as omission of eIF1A led to 48S complex formation at the upstream near-cognate codon UUG_{41} (Figure 3.7). In addition, mutations within SLA that increased stability of the stem reduced ribosome loading onto the $ZIKV^{5'utr+}$ RNA (Figure 3.10B).

It is likely however that this mechanism of linear scanning performed by the 43S preinitiation complex is inefficient. Omission of eIF1A or mutation of UUG_{41} to AUG_{41} within SLA did not efficiently abrogate 48S complex formation at AUG_{108} (Figure 3.7 and Figure 3.10), which might be expected if the top half of SLA is inspected efficiently during scanning. Furthermore, an additional AUG in good sequence context introduced at the top of SLA was only weakly selected by the scanning complex (Figure 3.10D). Taken together, these data suggest that the upper half of SLA may not be efficiently scanned during ribosome recruitment when the

canonical set of eIFs are used. While addition of DHX29 did not enhance selection of near-cognate codons within SLA (Figure 3.7), addition into assembly reactions performed on ZIKV$^{5'utr+}$ RNA mutants containing AUG codons introduced within SLA might shift preference from AUG_{108}, as DHX29 has been previously implicated in promoting selection of upstream cognate, but not near-cognate, initiation codons (Pisareva & Pisarev, 2016b). In this instance, DHX29 activity might be required for efficient scanning of the ZIKV 5′ UTR, yet it is clear that efficient selection of AUG_{108} occurs without this activity in the system established here. Further work needs to be performed to investigate the contribution and physiological relevance of DHX29-mediated scanning on ZIKV.

The fact that ZIKV translation initiation is predominately cap- and 5′ end-dependent in this reconstitution system does not rule out the possibility that additional mechanisms occur during infection. It has been shown that under conditions of limited eIF4E availability DENV can switch to a non-IRES cap-independent mode of initiation in a manner requiring both the viral 5′ and 3′ UTRs, suggesting that communication between the two terminal ends is important for this mechanism (Edgil *et al*, 2006). While the impact of long-range RNA-RNA interactions between the 5′ and 3′ ends of flavivirus genomes upon viral translation initiation is the subject of Chapter 5, 48S complex assembly on ZIKV^{fl} RNA exhibited a similar cap-dependency as on ZIKV$^{5'utr+}$ RNA (Figure 3.6), illustrating that the presence of both viral UTRs does not convey cap-independent initiation using the canonical set of eIFs. Alternatively, it has been suggested that the 5′ UTRs of ZIKV and DENV possess IRES activity, although so far this has been poorly characterised (Song *et al*, 2019). Such noncanonical translation initiation mechanisms could facilitate the escape from cap-dependent host cell translation shutoff seen during DENV and ZIKV infection (Roth *et al*, 2017).

These mechanisms are likely to require additional factors beyond the canonical set of eIFs that promote or replace their activity and as a result were not reconstituted here. In support of this, transfection of adenosine-capped full-length DENV RNA only led to productive infection under pharmacologic inhibition of eIF4E, suggesting that a cellular stress response factor might be responsible for this cap-independent mode of translation (Edgil *et al*, 2006). Regardless, the reconstitution system established here provides a powerful investigative tool to study the requirement for such additional factors, which could be identified by supplementing the reconstitution system with fractionated cell lysate until the activity that yields cap-independent ribosome recruitment is isolated. A similar approach was used to identify the novel IRES *trans*-

acting factor $ITAF_{45}$ from RRL, required for the translation of foot-and-mouth disease virus but not Theiler's murine encephalomyelitis virus (Pilipenko *et al*, 2000).

However, several likely candidates for mediating cap- or eIF4E-independent translation initiation have been recently characterised. One such candidate is eIF3d, a cap-binding subunit of eIF3 that has been shown to promote eIF4E-independent translation initiation by binding directly to 5′ cap structures (Lee *et al*, 2016). While no efficient 48S complex formation was seen when eIF4F was omitted from the reconstitution system presented here (Figure 3.7 lane 8), it cannot be concluded that this was as a result of eIF4E omission as eIF4G was also omitted within eIF4F. Another potential mechanism worth investigating involves the mRNA modification N^6-methyladenosine (m^6A). m^6A modifications within the 5′ UTR of Heat shock protein 70 mRNA have been shown to promote cap-independent translation initiation under conditions of cellular stress following heat shock by recruiting eIF3 directly, bypassing the need for a 5′ cap structure (Meyer *et al*, 2015). These modifications have been mapped throughout the ZIKV genome and furthermore DENV was found to possess m^6A modifications within its 3′ UTR (Gokhale *et al*, 2016; Lichinchi *et al*, 2016). While no such modifications within the 5′ UTR of ZIKV have been described, it would be interesting to investigate their effect on ribosome recruitment.

It is notable that an eIF4F-dependent toeprint upon the ZIKV 5′ UTR was often observed at nt position 132 on the $ZIKV^{5'utr+}$ RNA (highlighted on Figure 3.7). This potentially represents a noncanonical interaction of eIF4F with ZIKV RNA and further work must be performed to functionally characterise this interaction. An intriguing possibility is that this interaction might play a role in cap-independent translation initiation under certain conditions or provide selective translation enhancement over host mRNAs. A similar eIF4F-dependent toeprint was previously described at nt 786 upon the EMCV IRES, which the authors proposed was a result of J-K domain stabilisation within the IRES upon binding (Pestova *et al*, 1996a).

Taking all of the evidence into consideration, the reconstitution approach to study translation initiation provides a powerful tool in which to probe the mechanism of small ribosomal subunit recruitment and scanning, as well as the influence of RNA secondary structure on this process. Use of the system to examine translation initiation on ZIKV has revealed that the mechanism is predominately cap- and 5′ end-dependent when the canonical set of eIFs are included. This experimental set-up will be utilised in subsequent chapters to examine the effects of viral polymerase recruitment and genome circularisation on ZIKV translation initiation.

4 Viral polymerase recruitment inhibits cap-dependent ZIKV translation initiation

4.1 Introduction

Flavivirus NS5 is the largest flaviviral protein (103 kDa in ZIKV) and is multifunctional, possessing *de novo* RdRp activity (Guyatt *et al*, 2001; Tan *et al*, 1996; Ackermann & Padmanabhan, 2001) and MTase activity (Egloff *et al*, 2002; Ray *et al*, 2006; Zhou *et al*, 2007). During viral infection, NS5 is efficiently recruited to SLA at the 5′ end of the viral genome in a 1:1 stoichiometry with the RNA (Bujalowski *et al*, 2017) before subsequently translocating to the 3′ end to begin negative-sense RNA synthesis. This process is facilitated by long-range RNA-RNA interactions that effectively circularise the viral genome and bring the two genomic ends into close proximity (Filomatori *et al*, 2006, 2011). It is important to note that as SLA structure is unaffected by genome circularisation, NS5 recruitment can occur to both the linear and circular genome conformations (Filomatori *et al*, 2006, 2011; Liu *et al*, 2016).

It has been demonstrated that the structure of SLA (Figure 4.1) is critical for DENV2 NS5 ($NS5^{DENV2}$) binding, with helical regions within SLA, a top loop (TL) structure and the presence of a side stem-loop (SSL) all contributing (Lodeiro *et al*, 2009; Dong *et al*, 2008b; Li *et al*, 2010; Filomatori *et al*, 2006, 2011). Mutations within the TL were found to impair viral replication during infection, and viruses can be rescued from this defect by spontaneously reverting to the wildtype sequence (Filomatori *et al*, 2006; Lodeiro *et al*, 2009). While deletion of the TL abrogated RdRp activity and impaired NS5 recruitment *in vitro*, nucleotide substitutions within this region have been shown to abolish RdRp activity without impairing recruitment, thus suggesting that NS5 recruitment alone is not sufficient for SLA promoter activity (Filomatori *et al*, 2011). Comparatively, mutations that disrupt the structure of the SSL have been shown to abolish both recruitment and RdRp activity *in vitro* and impair infectivity *in vivo* (Filomatori *et al*, 2011; Lodeiro *et al*, 2009). The base-pairing within helical regions S1 and S2 are essential for DENV2 replication, although mutations within S3 are more tolerated (Filomatori *et al*, 2006; Lodeiro *et al*, 2009). While it was initially demonstrated that deletion of the conserved U-bulge between helical regions S1 and S2 was lethal *in vivo* (Lodeiro *et al*, 2009), a deletion mutant is capable of NS5 binding and promoting RNA synthesis *in vitro* suggesting that this element possesses a different role during infection (Filomatori *et al*, 2011).

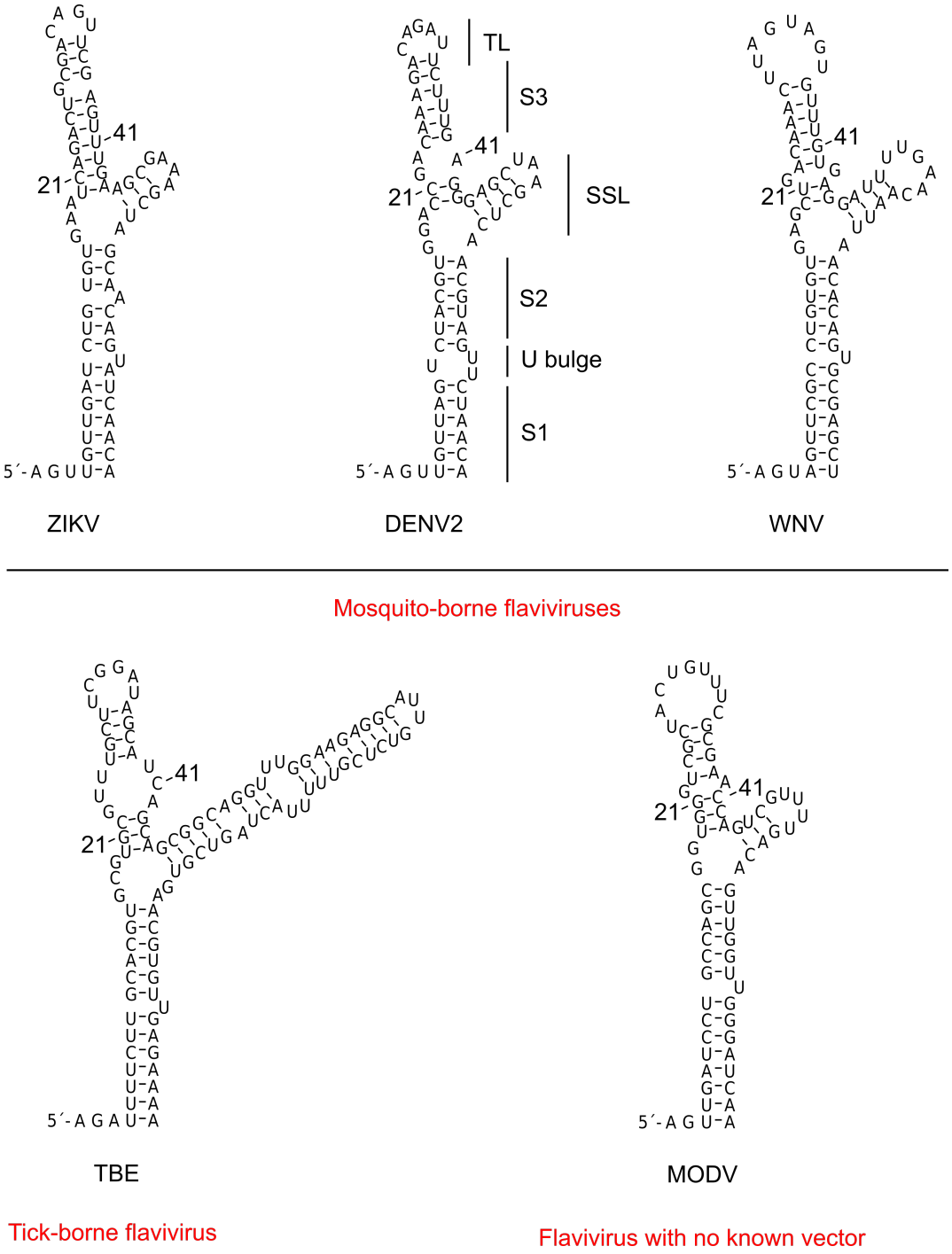

Figure 4.1 SLA structure is conserved within the genus *Flavivirus*

Secondary structure predictions of stem-loop A (SLA) from representative mosquito-borne, tick-borne and no known vector flaviviruses using mFold (Zuker, 2003). Structures within DENV2 SLA discussed in the text are indicated. GenBank accession numbers are in brackets for the following sequences. ZIKV, Zika virus (KX197192.1); DENV2, Dengue serotype 2 (NC_001474); WNV, West Nile virus (L24511.1); TBE, tick-borne encephalitis virus (U27495); MODV, Modoc virus (AJ242984); TL, top loop; SSL, side stem-loop

Similar requirements for SLA structure *in vitro* and *in vivo* have also been described for replication of WNV (Dong *et al*, 2008b; Li *et al*, 2010). As these structural elements are predicted to occur in all members of the *Flavivirus* genus including TBFVs and NKFVs

(Lodeiro *et al*, 2009; Filomatori *et al*, 2006), these viruses likely share a common mechanism of polymerase recruitment. Consistent with this, some compatibility between NS5 polymerases and SLA structures from different flaviviruses have been reported. For example, $NS5^{DENV2}$ is capable of using SLA from DENV1 as a promoter for RNA synthesis (Lodeiro *et al*, 2009) and $NS5^{DENV3}$ binds to SLA from DENV2 (Bujalowski *et al*, 2017). Furthermore, NS5-SLA compatibility has been shown between WNV and DENV2 (Yu *et al*, 2008). However, in a separate study $NS5^{WNV}$ was reported as being incapable of synthesising RNA from a DENV SLA promoter (Li *et al*, 2010), suggesting that some species specific differences could exist. SLA structures from representative flaviviruses are shown in Figure 4.1.

Crystal structures of full-length $NS5^{ZIKV}$ have been recently solved which show strong similarities with NS5 proteins from other flaviviruses (Figure 4.2) (Zhao *et al*, 2017; Upadhyay *et al*, 2017). NS5 consists of a N-terminal MTase domain and a C-terminal RdRp domain separated by a flexible linker thought to regulate the activity of the two domains (Zhao *et al*, 2015; Klema *et al*, 2016). The C-terminal RdRp domain of NS5 is known to adopt a conserved right-hand conformation with subdomains corresponding to the fingers, palm and thumb (Yap *et al*, 2007; Godoy *et al*, 2017). A structural priming element emanates from the thumb subdomain towards the active site to facilitate *de novo* initiation of RNA replication (Selisko *et al*, 2012), which represents an attractive therapeutic target (Lim *et al*, 2016). The catalytic active site (G664-D665-D666 in ZIKV) resides above the palm domain (Yap *et al*, 2007; Godoy *et al*, 2017). The MTase domain is highly conserved between flaviviruses and adopts a classic α/β/α sandwich structure (Zhao *et al*, 2017; Byszewska *et al*, 2014).

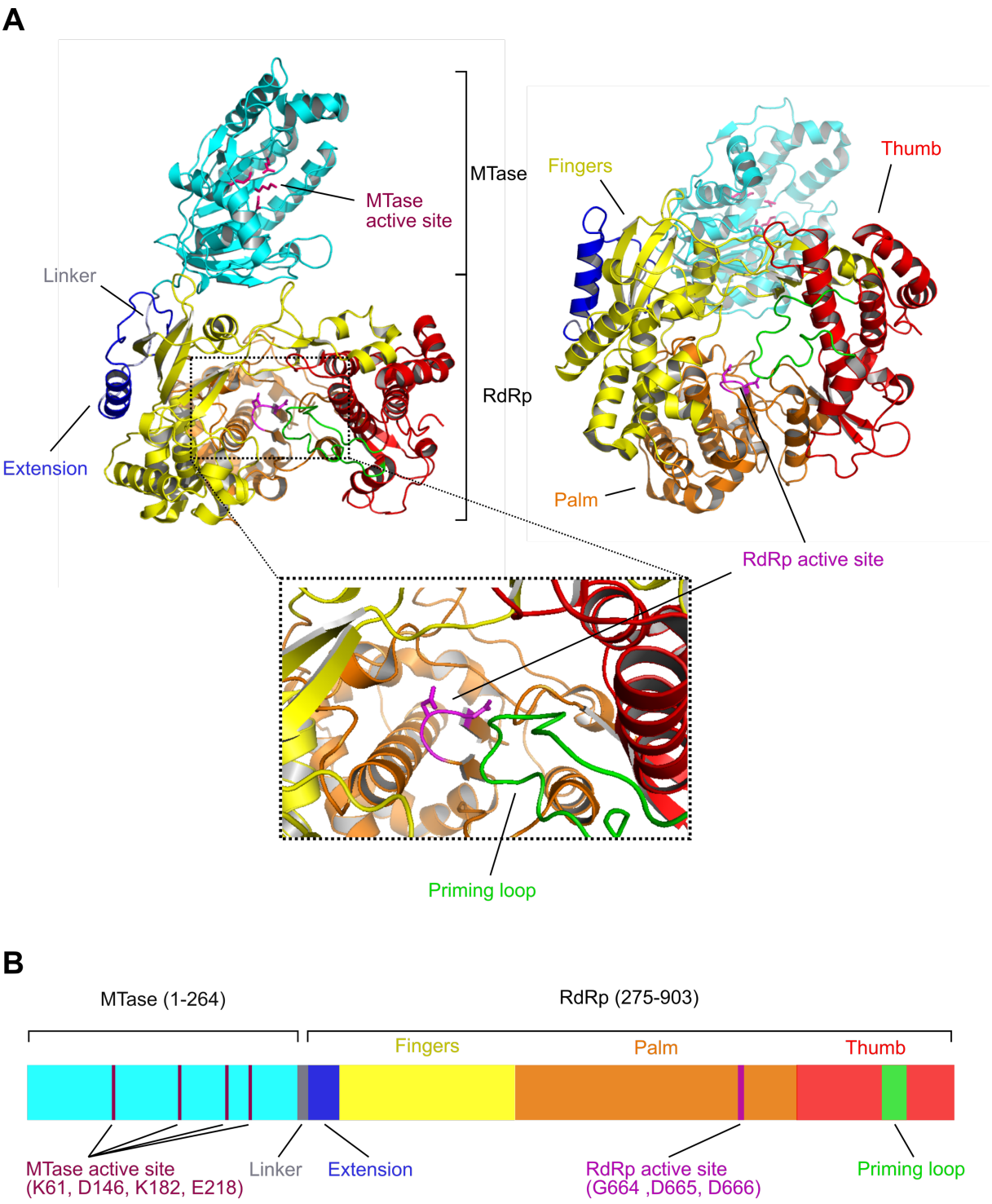

Figure 4.2 Crystal structure of full-length NS5^{ZIKV}

A) Cartoon structure showing the arrangement of the MTase and RdRp domains within NS5^{ZIKV}. A top view is shown on the left with the linker between the two domains and a unique flaviviral extension highlighted. The inset illustrates a close up of the RdRp domain active site with important residues and the priming loop indicated. The right view shows a side view of the RdRp domain illustrating the palm, fingers and thumb subdomains. The structure was downloaded from the Protein Data Bank (accession number 5U0B; Zhao *et al*, 2017) and visualised using Pymol.
B) Schematic representation of ZIKV NS5 domain organisation with features shown in **A)** indicated. MTase, methyltransferase domain; RdRp, RNA-dependent RNA polymerase.

Electrophoretic mobility shift assays (EMSAs) have shown that the RdRp domain of $NS5^{DENV2}$ alone is sufficient to bind to SLA with a high affinity (reported with a K_d of around 10 nM), with the MTase domain alone only weakly binding (Filomatori *et al*, 2006, 2011). The presence of the MTase domain in addition to the RdRp domain in the context of the full-length NS5 protein was not found to enhance binding (Filomatori *et al*, 2011). Indeed, an unbiased yeast three-hybrid approach mapping the interactions of both full-length $NS5^{DENV2}$ and the RdRp domain only with the entire DENV2 genome found that the addition of the MTase domain did not confer additional binding specificity to that of the RdRp alone (Hodge *et al*, 2016). Within the RdRp domain itself the conserved F1 region within the fingers subdomain has been implicated as providing specificity to SLA, as mutation of residues within this region inhibits RNA synthesis from a SLA promoter but not that of a poly(rC) template (Iglesias *et al*, 2011).

Comparatively, it was found by EMSA that the RdRp domain of $NS5^{WNV}$ is not sufficient for SLA recruitment, requiring the MTase domain for specificity (Dong *et al*, 2008b). However, these findings were contradicted in a later study using a different recombinant RdRp construct (Li *et al*, 2010). As it has been reported that His-tagged $NS5^{DENV2}$ possesses lower polymerase activity than untagged protein *in vitro* (Kamkaew & Chimnaronk, 2015), it is clear that differences in protein activity between studies might be as a result of construct design. However, it is important to note that chimeric DENV2 containing either full-length $NS5^{WNV}$ or the RdRp or MTase domains alone was found to be replication-deficient (Dong *et al*, 2010), so it is possible that the precise mechanism of SLA recognition by NS5 differs between flaviviruses.

During viral RNA synthesis, the MTase domain of NS5 binds to and sequentially methylates viral caps at the guanine N-7 position and the ribose 2′-O position (Zhou *et al*, 2007; Ray *et al*, 2006; Dong *et al*, 2010). As such, one could hypothesise that the MTase domain within the context of full-length NS5 protein enhances binding to capped SLA-RNA. However, $NS5^{DENV2}$ was found by EMSA to bind to capped and uncapped DENV RNAs with similar affinities (Iglesias *et al*, 2011). Furthermore, m^7GpppA RNA could not outcompete labelled tri-phosphorylated (pppA) RNA for binding to $NS5^{WNV}$ more efficiently than tri- or non-phosphorylated (A) RNA (Dong *et al*, 2008b). Taken together, these data suggest that efficient NS5 recruitment is independent of a 5′ cap structure and, in the case of $NS5^{DENV2}$ at least, completely independent of the MTase domain. It is important to note however that the presence of the MTase domain within full-length $NS5^{DENV2}$ has been shown to enhance both initiation

and elongation of RNA synthesis, illustrating that interplay between the activities of the two domains does occur (Potisopon *et al*, 2014).

In the previous chapter, it was shown that ZIKV undergoes a cap-dependent mechanism of translation initiation in an *in vitro* reconstitution system. As both $NS5^{ZIKV}$ and the translational machinery localise at the 5′ end, interplay between NS5 recruitment and translation initiation is likely to occur. Therefore, the aim of the work presented in this chapter was to determine whether or not $NS5^{ZIKV}$ recruitment to ZIKV RNA modulates translation initiation.

4.2 Results

4.2.1 NS5 displays selectivity to SLA at the 5' end of the ZIKV genome

Wildtype and RdRp activity-deficient ($G_{664}DD \rightarrow G_{664}AA$; GAA) full-length $NS5^{ZIKV}$ proteins were expressed recombinantly in bacteria and purified by affinity and size-exclusion chromatography (Figure 4.3).

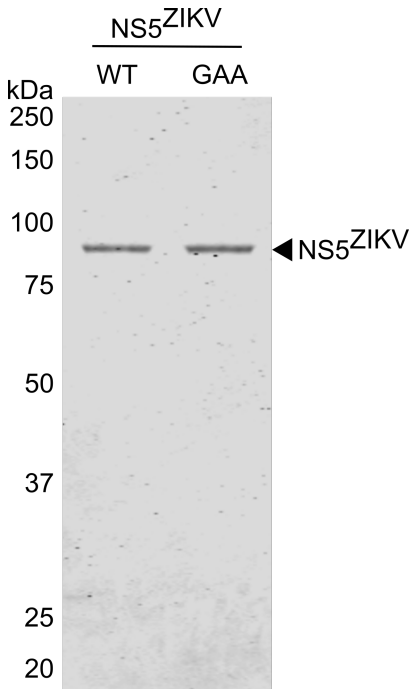

Figure 4.3 Recombinant full-length $NS5^{ZIKV}$

Wildtype (WT) $NS5^{ZIKV}$ and polymerase deficient $G_{664}DD \rightarrow G_{664}AA$ (GAA) $NS5^{ZIKV}$ were expressed recombinantly and following purification visualised on a Coomassie-stained SDS-PAGE gel.

The interaction between $NS5^{ZIKV}$ and ZIKV RNA was analysed by EMSA. In these experiments, an RNA probe corresponding to the ZIKV 5′ end ($ZIKV^{5'utr+}$, previously described in Chapter 3) was incubated with $NS5^{ZIKV}$ in the presence of a binding buffer containing yeast tRNA, which serves as a competitor to inhibit non-specific RNA binding. Protein-bound RNA was subsequently separated from unbound RNA by native PAGE at low temperature to maintain the RNA-protein interaction prior to visualisation. In order to confirm selectivity for SLA, additional constructs derived from $ZIKV^{5'utr+}$ RNA were used. The first contained a destabilised SLA structure ($ZIKV^{5'utr+}$-DS) and the second lacked SLA altogether ($ZIKV^{5'utr+}$-Del) (mutants are shown in Figure 4.4).

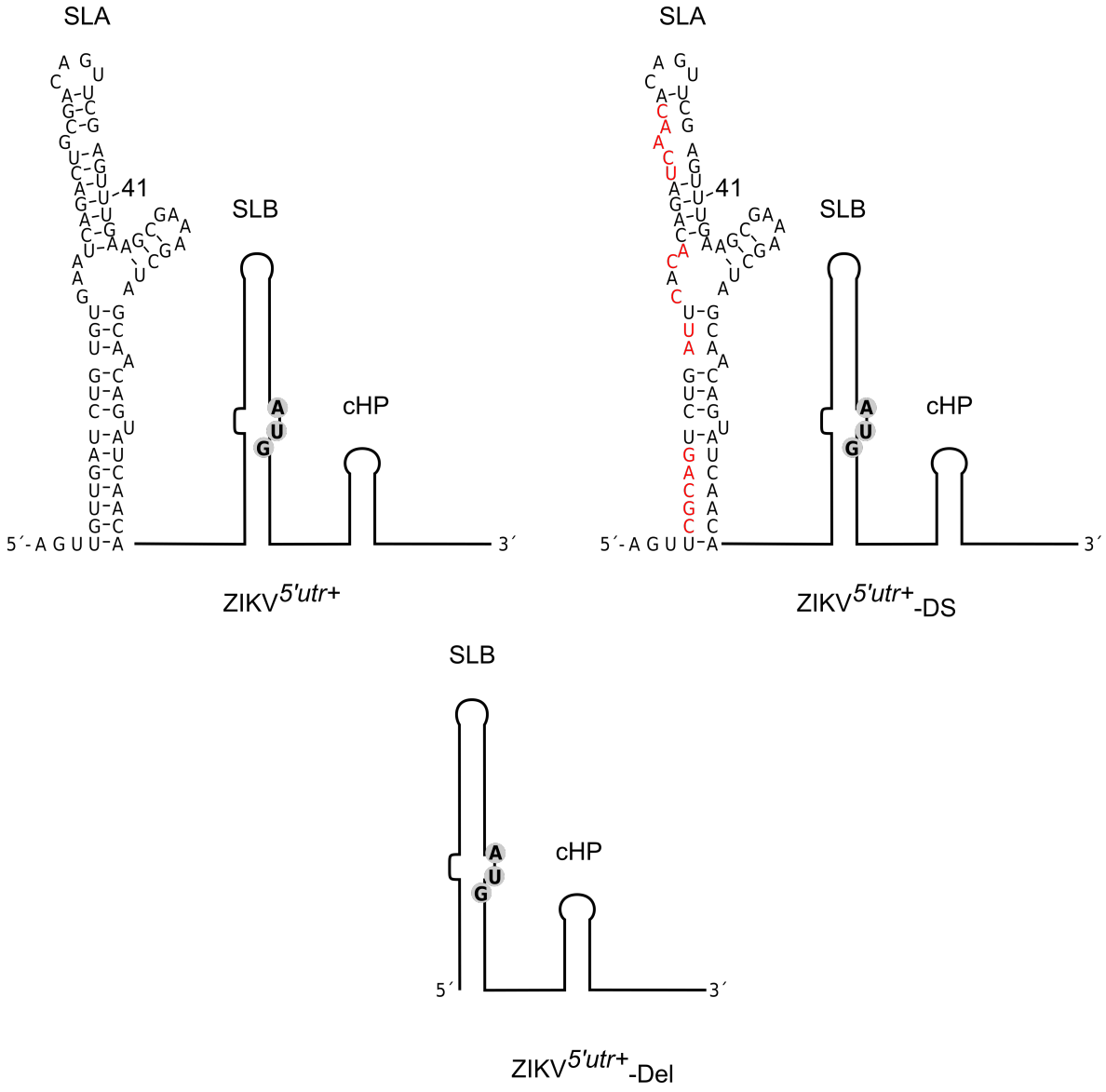

Figure 4.4 The SLA-mutants examined within ZIKV 5′ UTR RNA

Schematics illustrating wildtype $ZIKV^{5'utr+}$, $ZIKV^{5'utr+}$-DS and $ZIKV^{5'utr+}$-Del. Mutations are indicated in red. The initiating AUG within SLB is indicated. SLA, stem-loop A; SLB, stem-loop B; cHP, C coding region hairpin

Capped RNA constructs were incubated with an increasing concentration of $NS5^{ZIKV}$ to determine the relative affinity of $NS5^{ZIKV}$ to each. Addition of $NS5^{ZIKV}$ to wildtype $ZIKV^{5'utr+}$ RNA resulted in a well-defined band corresponding to protein binding, with a 50 % shift occurring when $NS5^{ZIKV}$ concentration was ~128nM (Figure 4.5A lane 7). This is a similar order of magnitude as K_d measurements obtained for $NS5^{DENV2}$ (14 nM by EMSA, Filomatori *et al*, 2011; 52.9 nM by surface plasmon resonance, Kamkaew & Chimnaronk, 2015) and $NS5^{DENV3}$ (100 nM by fluorescence binding assay, Bujalowski *et al*, 2017b) binding to their respective SLA structures. Comparatively, no clear binding was observed to the $ZIKV^{5'utr+}$-DS construct (Figure 4.5B), highlighting the importance of SLA structure in protein recruitment. Surprisingly, binding was detected between $NS5^{ZIKV}$ and the $ZIKV^{5'utr+}$-Del RNA which lacks SLA (Figure 4.5C), albeit at higher $NS5^{ZIKV}$ concentrations than that required to shift wildtype $ZIKV^{5'utr+}$ RNA (50 % shift ~256 nM).

In order to examine whether the interaction between $NS5^{ZIKV}$ and $ZIKV^{5'utr+}$-Del was specific, the effect of increasing the amount of yeast tRNA in the EMSA binding reaction was investigated. Increasing total tRNA amount from 2 µg to 4 µg had no effect on $NS5^{ZIKV}$ binding to either the $ZIKV^{5'utr+}$ or $ZIKV^{5'utr+}$-Del RNA (Figure 6, compare lanes 4 and 3, 8 and 7), thus suggesting that the interaction between $NS5^{ZIKV}$ and $ZIKV^{5'utr+}$-Del RNA is specific.

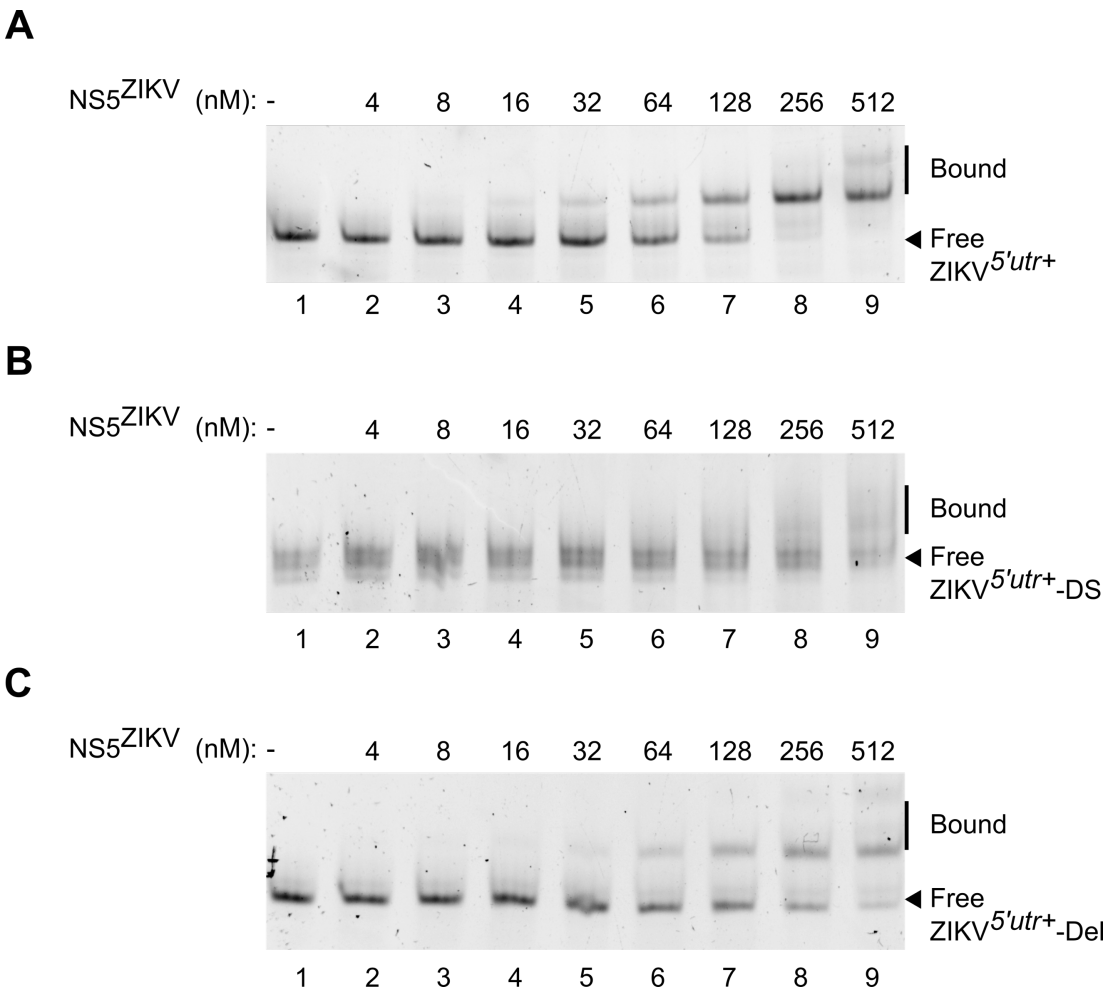

Figure 4.5 Alteration of SLA inhibits NS5^{ZIKV} recruitment to ZIKV RNA

EMSA analysis of capped **A)** ZIKV$^{5'utr+}$, **B)** ZIKV$^{5'utr+}$-DS and **C)** ZIKV$^{5'utr+}$-Del RNA with increasing amounts of NS5^{ZIKV} (a representative experiment is shown from two independent experiments). Gels were poststained with ethidium bromide for detection. Free and bound RNA is indicated.

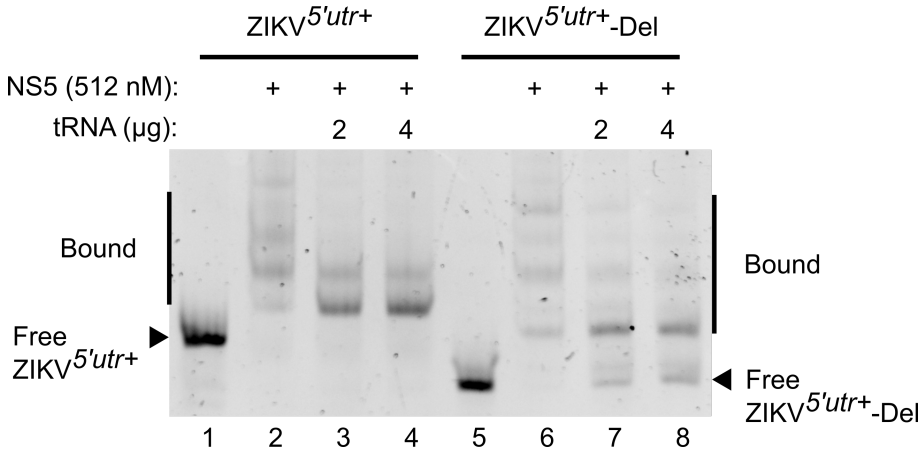

Figure 4.6 The interaction between NS5^{ZIKV} and ZIKV$^{5'utr+}$-Del RNA is specific

EMSA analysis of capped ZIKV$^{5'utr+}$ and ZIKV$^{5'utr+}$-Del RNA binding to NS5^{ZIKV} with the indicated amount of yeast tRNA present in the binding reaction. Gels were poststained with ethidium bromide for detection. Free and bound RNA is indicated.

4.2.2 ZIKV NS5 inhibits translation of a SLA-containing firefly luciferase reporter

In order to ascertain the effect of $NS5^{ZIKV}$ recruitment to SLA on translation, $NS5^{ZIKV}$ was incubated with a capped RNA reporter containing the 5′ and 3′ UTRs of ZIKV separated by Fluc ($ZIKV^{Fluc}$) before addition into a translation-competent Vero cell lysate. Translation was monitored by measuring luminescence from the reporter and subsequently normalised to translation in the absence of $NS5^{ZIKV}$. Inclusion of both wildtype and RdRp activity-deficient ($G_{664}DD \rightarrow G_{664}AA$) mutant $NS5^{ZIKV}$ (GAA; Figure 4.2) significantly inhibited luciferase production from the $ZIKV^{Fluc}$ reporter (around 65 % inhibition; Figure 4.7). Conversely, addition of either protein to a $ZIKV^{Fluc}$ reporter with a destabilised SLA, $ZIKV^{Fluc}$-DS (as in Figure 4.4), failed to inhibit luciferase production (Figure 4.7). In agreement with the EMSA binding experiments, binding of $NS5^{ZIKV}$ to $ZIKV^{Fluc}$ RNA lacking SLA ($ZIKV^{Fluc}$-Del) inhibited luciferase production to a lesser extent than binding to wildtype $ZIKV^{Fluc}$ RNA (Figure 4.7). This data suggests that inhibition of translation by NS5 is independent of RdRp and eIF activity but instead directly related to the ability of NS5 to bind the RNA template.

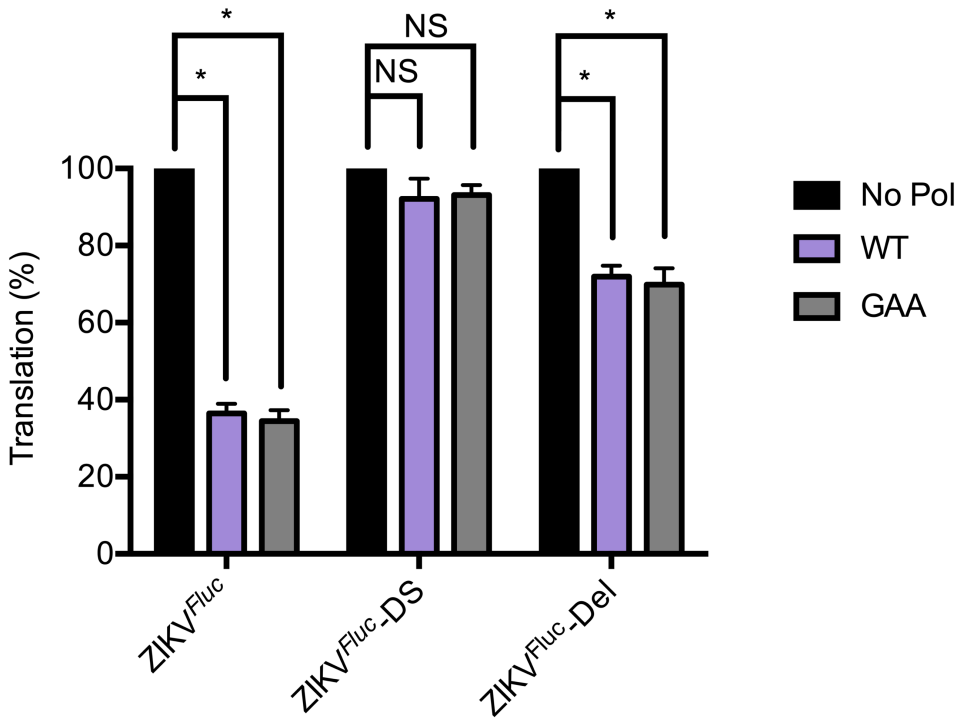

Figure 4.7 $NS5^{ZIKV}$ recruitment inhibits translation of a luciferase reporter

A capped, *in vitro* transcribed firefly luciferase reporter flanked by the ZIKV UTRs containing wildtype ($ZIKV^{Fluc}$), destabilised ($ZIKV^{Fluc}$-DS) or deleted ($ZIKV^{Fluc}$-Del) SLA was incubated with wildtype (WT) or $G_{664}DD \rightarrow G_{664}AA$ (GAA) mutant $NS5^{ZIKV}$ at the highest concentration used in Figure 4.5. Following subsequent addition to a translation-competent Vero cell lysate, luciferase activity was measured. Data are mean+/-SEM of three independent experiments normalised to the absence of $NS5^{ZIKV}$. Statistical significance was assessed by multiple t test analysis. NS, not significant; * represents $p<0.01$.

4.2.3 Recruitment of ZIKV NS5 to SLA inhibits de novo translation initiation

To establish whether inhibition was occurring at the initiation stage of translation, ZIKV$^{5'utr+}$ RNA and the SLA mutants were incubated with increasing amounts of NS5^{ZIKV} before addition into the 48S assembly reaction described in the previous chapter. Addition of NS5^{ZIKV} led to a dose-dependent decrease in 48S complex assembly on ZIKV$^{5'utr+}$ RNA but not ZIKV$^{5'utr+}$-DS RNA (Figure 4.8B, compare lanes 2-5 with 7-10), and to a lesser extent on ZIKV$^{5'utr+}$-Del RNA (Figure 4.8C, compare lanes 2-5 with 7-10).

NS5^{ZIKV} incubation with ZIKV$^{5'utr+}$ RNA in the context of a 48S assembly reaction produced a distinctive RT stop at nt 71 (Figure 4.8B and C, lanes 3-5), present directly at the SLA/SLB boundary within the ZIKV 5′ UTR (indicated on Figure 4.8A). To examine whether this stop occurred in the absence of 48S assembly, ZIKV$^{5'utr+}$ RNA was incubated with NS5^{ZIKV} in the absence of the translational machinery and an RT reaction was carried out. Addition of NS5^{ZIKV} in the absence of other factors was sufficient for the formation of this RT stop (Figure 4.9 lane 3). Additionally, this stop was also present when NS5^{ZIKV} was incubated with full-length ZIKV RNA (ZIKV^{fl}) (Figure 4.9 lane 7), and furthermore pre-incubation with NS5^{ZIKV} inhibited 48S complex formation upon this RNA in a manner similar to that of ZIKV$^{5'utr+}$ RNA (Figure 4.9 compare lanes 8 and 6, 4 and 2).

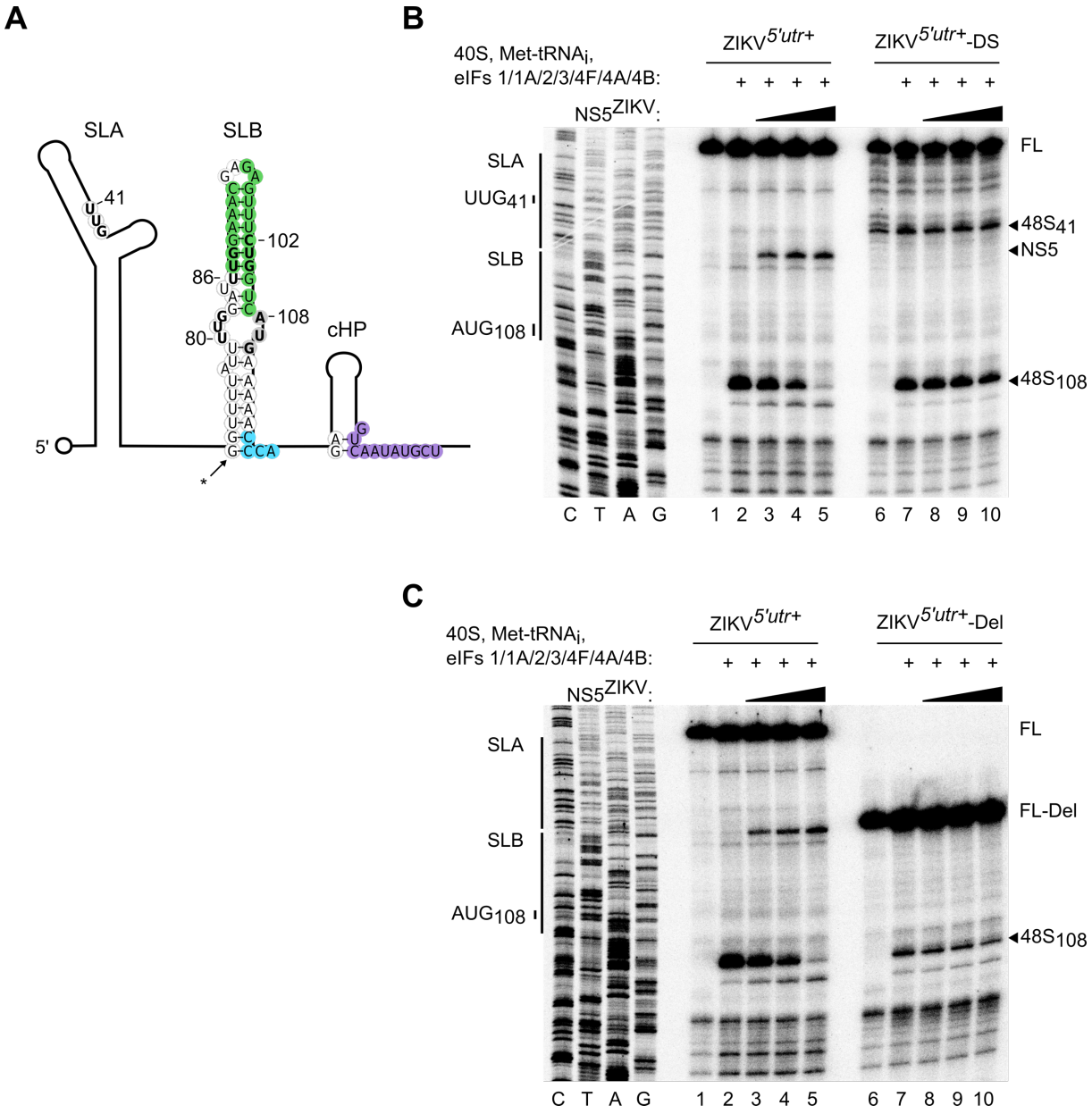

Figure 4.8 NS5^{ZIKV} recruitment inhibits 48S assembly on ZIKV RNA

A) Schematic of wildtype ZIKV$^{5'utr+}$ from nt 1-160. The position of an NS5-dependent RT stop at nt 71 is indicated (*). Sequences corresponding to the 5′ UAR, DAR and CS sequences involved in genome 5′-3′ hybridisation are highlighted in green, blue and purple, respectively. The 5′ cap structure is represented as a circle. SLA, stem-loop A; SLB, stem-loop B; cHP, C coding region hairpin.
B, C) Toeprinting analysis of 48S complex assembly on capped, *in vitro* transcribed ZIKV$^{5'utr+}$ RNA compared to **B**) ZIKV$^{5'utr+}$-DS RNA and **C**) ZIKV$^{5'utr+}$-Del RNA (a representative experiment is shown from two independent experiments). NS5^{ZIKV} was initially pre-incubated with the RNA at the three highest concentrations as in Figure 4.5 before addition of the translation initiation factors. The same assembly reaction on ZIKV$^{5'utr+}$ RNA is used on both gels. Selected codons are labelled on the left and toeprints caused by 48S complex assembly or NS5^{ZIKV} binding are marked with a closed arrowhead on the right. FL, full-length.

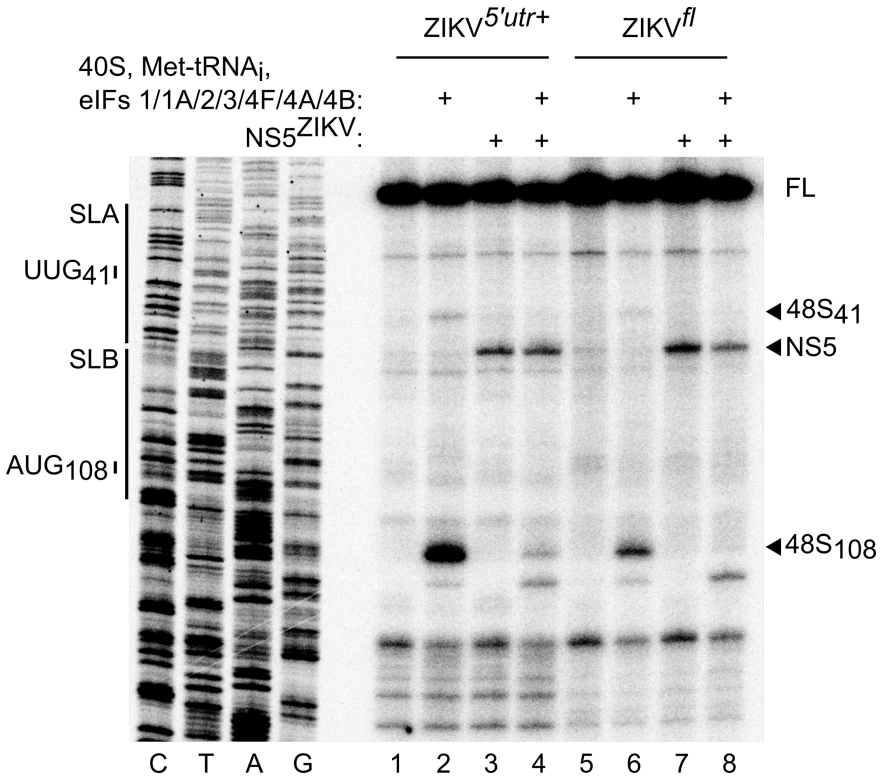

Figure 4.9 NS5^{ZIKV} binding to SLA arrests RT in the absence of translation factors

Toeprinting analysis of 48S complex assembly on capped, *in vitro* transcribed ZIKV$^{5'utr+}$ RNA compared to ZIKV^{fl} RNA. NS5^{ZIKV} was initially pre-incubated with the RNA at the highest concentration used in Figure 4.8 before addition of the translation initiation factors. Selected codons are labelled on the left and toeprints caused by 48S complex assembly or NS5^{ZIKV} binding are marked with a closed arrowhead on the right. FL, full-length.

Finally, in order to investigate whether NS5^{ZIKV} could directly compete with the translational machinery for binding to ZIKV RNA, NS5^{ZIKV} was included in the 48S assembly reaction on ZIKV$^{5'utr+}$ RNA without initial preincubation. Addition of NS5^{ZIKV} inhibited 48S complex assembly strongly at the initiating AUG (Figure 4.10, compare lanes 3 and 2). This indicates that NS5^{ZIKV} recruitment to SLA can directly outcompete ribosome loading and thus potentially inhibit cap-dependent ZIKV translation in the context of infection.

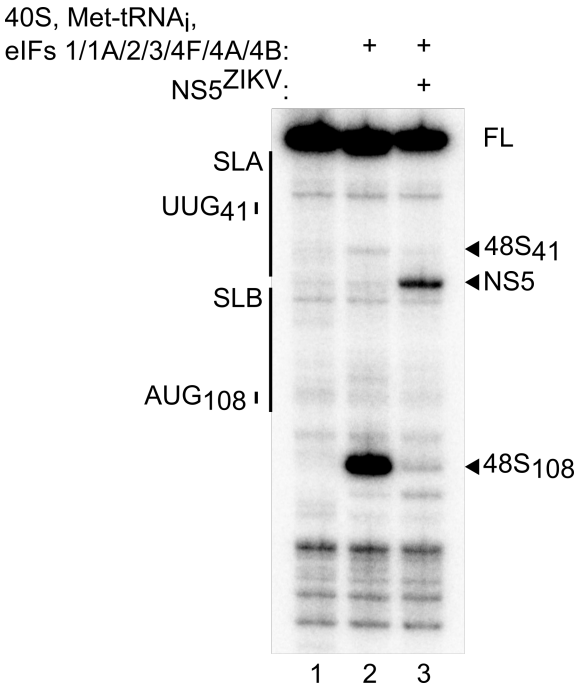

Figure 4.10 NS5^{ZIKV} can outcompete the translational machinery for binding to the ZIKV 5′ end

Toeprinting analysis of 48S complex assembly on capped, *in vitro* transcribed ZIKV$^{5'utr+}$ RNA. NS5^{ZIKV} was added directly into the 48S complex assembly reaction to a final concentration of 256 nM. Selected codons are labelled on the left and toeprints caused by 48S complex assembly or NS5^{ZIKV} binding are marked with a closed arrowhead on the right. FL, full-length.

4.3 Discussion

During infection, a positive-sense RNA virus must carefully regulate the use of its genome for the antagonistic processes of translation and replication. An efficient way in which to modulate the balance between two processes is for the machinery of one process to negatively regulate the other. Indeed, it is known that RNA viruses can modulate translation through polymerase binding. For example, the PV 3CD protein is a precursor of the viral protease (3C^{pro}) and the viral polymerase (3D^{pol}) that binds to a cloverleaf structure within the PV IRES, thus disrupting binding of the key *trans*-acting factor PCBP and negatively regulating translation (Gamarnik & Andino, 1998). Furthermore, binding of bacteriophage Qβ polymerase to the site of ribosome recruitment on Qβ RNA is thought to inhibit ribosome loading thus allowing RNA replication to occur unimpeded (Kolakofsky & Weissmann, 1971). Alternatively, it has been demonstrated that the polymerase of influenza virus (the genome of which is negative-sense) positively regulates viral translation during inhibition of host protein synthesis by compensating for the cap-eIF4E interaction (Yángüez *et al*, 2011; Burgui *et al*, 2007). As such, modulation of translation through the RNA polymerase responsible for replication may be a widespread mechanism to coordinate these two key processes during viral infection.

The results presented in this chapter illustrate that $NS5^{ZIKV}$ recruitment to the 5′ end of the linear ZIKV genome inhibits translation initiation and that recruitment directly outcompetes that of the translation machinery. This therefore provides a mechanism to "prime" genomic RNAs for replication during infection by ensuring that genomes about to undergo replication are cleared of translating ribosomes. Following recruitment, $NS5^{ZIKV}$ translocation to the 3′ end of the ZIKV genome to begin negative-strand RNA synthesis is mediated by genome circularisation (Filomatori *et al*, 2006, 2011). Investigation into the mechanism that ensures ribosome loading is not resumed upon $NS5^{ZIKV}$ departure from the 5′ UTR during RNA replication forms the basis of the Chapter 5.

Additional functions of $NS5^{ZIKV}$ beyond its MTase and RdRp activities have been described, such as its ability to bind STAT-2 and inhibit Type I and Type III interferon signalling (Kumar *et al*, 2016a; Grant *et al*, 2016). However, this represents the first description of this key protein acting as an inhibitor of viral translation. Due to the conserved nature of SLA and NS5 structure between different flaviviruses (Filomatori *et al*, 2006; Lodeiro *et al*, 2009; Zhao *et al*, 2017; Upadhyay *et al*, 2017), it is likely that inhibition of cap-dependent translation upon NS5 recruitment to SLA is common among different flaviviruses.

The mechanism by which translation inhibition is mediated by $NS5^{ZIKV}$ remains unclear, however. One possibility is that the MTase domain of the protein occludes the 5′ cap structure, thus making it inaccessible to eIF4E-binding. As eIF4F was shown in the previous chapter to be essential for 48S complex formation in the reconstitution system, this is a likely mechanism of action which requires further experimental validation. For instance, filter binding assays could be performed to compare the relative affinity of eIF4F binding to the cap structure to that of $NS5^{ZIKV}$. As the RdRp domain of $NS5^{DENV2}$ has been shown to be sufficient for SLA recruitment (Filomatori *et al*, 2006, 2011), it would be prudent to investigate whether this domain alone is capable of mediating translation inhibition on DENV2 RNA or whether the MTase domain is also required. Cap-independent translation has been proposed as occurring in DENV and ZIKV infection under conditions of cellular stress later in infection (Edgil *et al*, 2006; Roth *et al*, 2017), which could provide a potential mechanism to release newly synthesised RNA from translational inhibition mediated by NS5 SLA recruitment to facilitate efficient virion production.

It is important to note that the RNA constructs used in this study all possess a cap0 rather than a cap1 structure, lacking the additional methylation at the first ribose 2′-O position which is catalysed by the MTase of NS5 during infection (Egloff *et al*, 2002). As 2′-O-methylation deficient ZIKV and WNV are functionally indistinct from wildtype viruses in Type I interferon-deficient cells (Daffis *et al*, 2010; Johnson *et al*, 2018), is likely that the major function of 2′-O-methylation lies in immune evasion and gives no functional difference with regards to the NS5-SLA interaction. However, further experimental work is required to confirm that the interaction of $NS5^{ZIKV}$ with SLA is independent of the 5′ cap structure in an analogous fashion to $NS5^{DENV2}$ and $NS5^{WNV}$ (Dong *et al*, 2008b; Iglesias *et al*, 2011).

An alternative possibility to occlusion of the 5′ cap structure is that recruitment of $NS5^{ZIKV}$ to ZIKV RNA stabilises SLA structure, consistent with the RT stop observed between the SLA/SLB interface upon $NS5^{ZIKV}$ binding (Figure 4.9). Such stabilisation could prevent ribosome loading from the 5′ end, which may depend upon SLA unwinding. Evidence for this mechanism comes from the fact that a mutation that stabilised SLA was found to greatly reduce 48S complex assembly on $ZIKV^{5'utr+}$ RNA in Chapter 3. A crystal structure of $NS5^{ZIKV}$ bound to SLA-RNA would help to delineate these two possible mechanisms.

It is currently unclear why specific binding was detected by EMSA between $NS5^{ZIKV}$ and $ZIKV^{5'utr+}$ RNA lacking SLA (although with lower affinity than wildtype RNA), in contrast to similar experiments reported for $NS5^{DENV2}$ and $NS5^{WNV}$ (Filomatori *et al*, 2006; Dong *et al*, 2008b). However, while footprinting analysis of $NS5^{DENV2}$ and $NS5^{WNV}$ bound to SLA has shown that NS5 contacts SLA predominately in the TL structure and the SSL, additional contacts downstream of SLA were reported (Dong *et al*, 2008b; Filomatori *et al*, 2011). $NS5^{WNV}$ was found to contact additional nucleotides, including those present in SLB and the cHP stem, only in the unhybridised linear form of the 5′ UTR but these interactions were found to not be critical for NS5 binding (Dong *et al*, 2008b). This is consistent with the report that $NS5^{DENV4}$ is more selectively recruited to viral RNA present in the linear rather than the circular conformation of the viral genome, suggesting that structures downstream of SLA play a role in modulating NS5 recruitment (Liu *et al*, 2016). Comparatively, it was reported that binding of $NS5^{DENV2}$ to DENV2 RNA led to structural re-arrangement downstream of SLA, increasing the accessibility of those regions to RNase digestion (Filomatori *et al*, 2011). It is clear then that additional contacts downstream of SLA are made upon NS5 recruitment and such contacts may help to explain why $NS5^{ZIKV}$ was recruited to $ZIKV^{5'utr+}$ RNA lacking SLA structure.

However, it also remains to be determined whether the mode of $NS5^{ZIKV}$ binding to SLA is identical to these other well-characterised flaviviruses. Is binding mediated solely by the RdRp domain as described for DENV (Filomatori *et al*, 2006, 2011), or does the MTase domain contribute as suggested for WNV (Dong *et al*, 2008b)? Are the precise requirements for certain SLA structural features for recruitment the same or not?

Taking all of the evidence into consideration then, it is clear that the ZIKV SLA structure acts as a key linchpin for the balance between translation and replication during infection. The work presented here establishes yet another function for $NS5^{ZIKV}$; a translation inhibitor. Follow-up studies are required to ascertain the applicability of the results obtained here to other flaviviruses.

5 Circularisation of ZIKV genomic RNA inhibits *de novo* translation initiation

5.1 Introduction

Circularisation of flavivirus genomic RNA is essential for replication during infection and relies upon the hybridisation of a series of known *cis*-acting elements within the 5′ and 3′ ends of the genome (Villordo & Gamarnik, 2009; Barrows *et al*, 2018). These elements are namely the UAR, the DAR and the CS (highlighted for ZIKV in Figure 5.1, with the complete sequences shown in Appendix A) (Alvarez *et al*, 2005b; Zhang *et al*, 2008a; Friebe & Harris, 2010; Khromykh *et al*, 2001a). While these elements were initially characterised by sequence comparison and mutagenic analysis, more recent studies have illustrated via RNA crosslinking approaches and high-throughput sequencing technology that these structures can be detected *in vivo* during viral infection (Ziv *et al*, 2018; Li *et al*, 2018; Huber *et al*, 2019). Furthermore, these interactions have recently been described as forming within ZIKV and DENV virions (Dethoff *et al*, 2018; Huber *et al*, 2019). The data from these studies shows that the ZIKV genome is highly dynamic during the infectious cycle, adopting numerous different conformations (Ziv *et al*, 2018; Li *et al*, 2018; Huber *et al*, 2019).

Experiments using DENV2 have illustrated that the balance between the linear and the circular conformation of the viral genome is important during infection, suggesting that the two genomic forms have opposing roles (Gebhard *et al*, 2011; Villordo *et al*, 2010). Within the viral 3′ UTR, the sHP structure only exists in the linear conformation as it forms the 3′ half of the UAR interaction in the circular form. Mutations that alter the relative stabilities of these mutually exclusive structures lead to a decrease in viral replication, with subsequent spontaneous revertant mutations arising that restore the equilibrium between the two genomic conformations (Villordo *et al*, 2010). While a large amount of biochemical data has illustrated that circularisation of the flaviviral genome is required for efficient RNA replication by facilitating translocation of the viral polymerase NS5 from the 5′ to 3′ end of the genome (Filomatori *et al*, 2006; Lodeiro *et al*, 2009; Filomatori *et al*, 2011; Iglesias *et al*, 2011), the precise role of the linear form of the genome during infection is unclear.

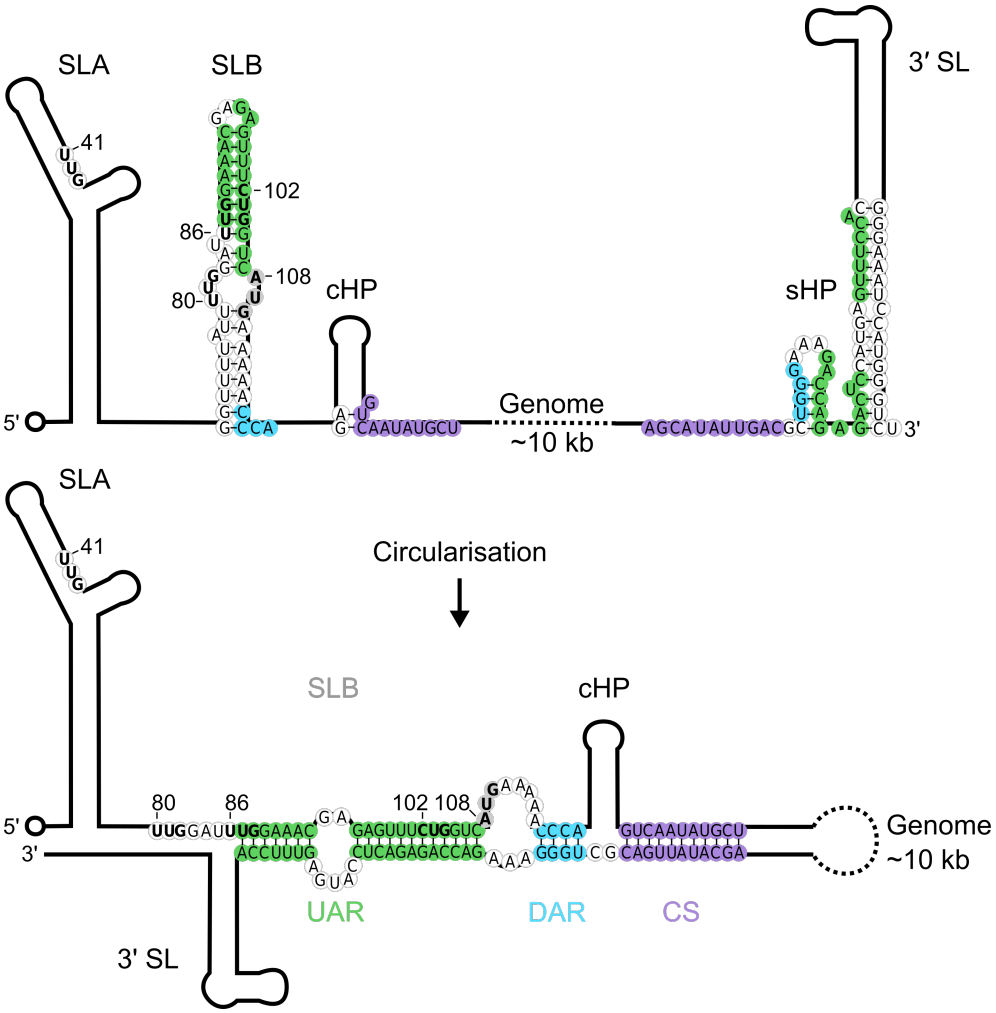

Figure 5.1 The ZIKV genome circularises during infection

A schematic illustrating the linear (top) and the circular (bottom) conformations of the ZIKV genome that occur during infection. Sequences corresponding to the UAR, DAR and CS are highlighted in green, blue and purple, respectively. The initiating AUG at nt 108 and upstream near-cognate codons discussed in the text are highlighted in bold. The 5′ cap structure is represented as a circle. SLA, stem-loop A; SLB, stem-loop B; cHP, C coding region hairpin; sHP, small hairpin; 3' SL, 3' stem-loop.

In the previous chapter, recruitment of $NS5^{ZIKV}$ to SLA was shown to inhibit cap-dependent translation initiation upon the ZIKV 5′ UTR. This was hypothesised to clear the RNA of translating ribosomes, thus allowing subsequent RNA replication to proceed unimpeded. However, departure of NS5 from SLA during replication following genome circularisation would leave the 5′ end of the RNA open to re-engage with the translation machinery, potentially leading to abortive transcription and translation products. It is likely, therefore, that the circular form of the viral genome is not permissive for translation initiation. Consistent with this model, a three-fold decrease in translation was observed from a Fluc reporter flanked by the DENV UTRs following transfection into Vero cells when the first 36 nt of the C coding region containing the 5′ CS element was also included, thus permitting hybridisation of the terminal

elements (Chiu *et al*, 2005). Furthermore, genome circularisation is not essential for translation of DENV replicons following transfection (Alvarez *et al*, 2005a, 2005b, 2008), thus suggesting that translation of the linear genome conformation is the predominant way by which viral genes are expressed.

The aim of the work presented in this chapter was to investigate the effect of 5′ and 3′ ZIKV genome hybridisation on ZIKV translation both within the context of the virus during infection and within the reconstitution system for translation initiation previously described.

5.2 Results

5.2.1 Optimisation of a reverse genetics system for ZIKV

In order to provide a full-length infectious ZIKV genome containing both the 5′ and 3′ UTRs for use in viral infection and *in vitro* assays, a previously described reverse genetic system for ZIKV was adapted (Mutso *et al*, 2017). This plasmid-based system consists of an infectious cDNA (icDNA) clone of a Brazilian isolate of ZIKV (RNA derived from which is referred to as ZIKV^{fl}). Additionally, an icDNA clone containing a stable Nluc insertion fused to an additional copy of the C gene was utilised for *in cellulo* assays (ZIKV^{Nluc}; shown schematically in Figure 5.2A). It has been previously demonstrated that Nluc expression levels remain stably high for up to four passages of the ZIKV^{Nluc} reporter virus (Mutso *et al*, 2017). Similarly tagged reporter constructs have been used to distinguish between translation of input RNA and subsequent replication during DENV infection (Alvarez *et al*, 2005a; Villordo *et al*, 2010; Samsa *et al*, 2009).

Previously reported SP6-driven transcription from the ZIKV icDNA plasmids yielded two RNA products, one corresponding to the full-length ZIKV RNA and another corresponding to a truncated form (Mutso *et al*, 2017). In order to obtain a single RNA species for *in vitro* assays the plasmids were modified, and transcription was instead driven from a T7 promoter to yield a single band corresponding only to full-length RNA (Figure 5.2B). In order to compare the infectivity of ZIKV^{Nluc} RNA transcribed from the two promoters, 10 µg of capped SP6-driven transcript was electroporated into Vero cells alongside different amounts of capped T7-driven RNA and genome copy number was followed by qPCR over a 6-day period. No notable difference in how genome copy number changed over time was observed (Figure 5.2C), illustrating that RNA generated from either promoter can produce a productive ZIKV infection.

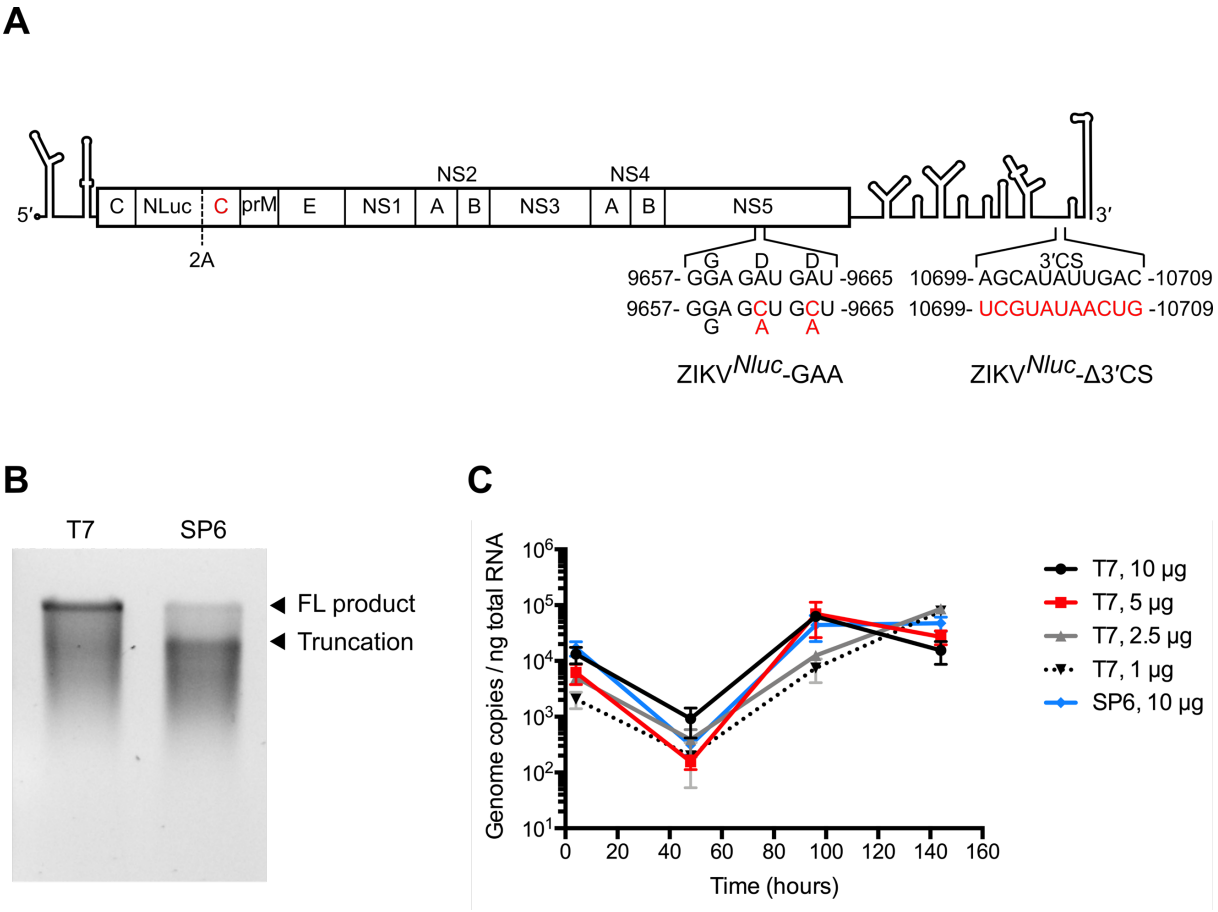

Figure 5.2 T7-driven full-length ZIKV RNA is capable of initiating a productive ZIKV infection

A) A schematic illustrating ZIKV^{Nluc}. The first copy of the C gene is fused to a Nluc reporter and is separated from a second C sequence with altered codons and the rest of the polyprotein by the foot-and-mouth disease virus 2A StopGo (Mutso *et al*, 2017). ZIKV^{Nluc}-GAA and ZIKV^{Nluc}-Δ3′CS polymerase mutations are indicated.
B) ZIKV^{Nluc} RNA transcribed from a T7 or SP6 promoter was denatured using formamide-containing loading dye before analysis by agarose gel electrophoresis. Ethidium bromide was used for detection. The full-length (FL) and truncation products are indicated.
C) Time course of ZIKV genome copies normalised to ng total RNA following electroporation of the indicated amount of capped T7- or SP6-driven ZIKV^{Nluc} RNA into Vero cells. 2.5x10^5 cells were seeded post-electroporation for the T=6 hrs timepoint, whereas 2.5x10^4 cells were seeded for all other time points. Data are mean +/- SEM for three technical repeats within one independent experiment.

To investigate how translation of ZIKV^{Nluc} changes over the course of infection, capped RNA was electroporated into Vero cells and samples were taken to monitor genome copy number and Nluc activity. As a control to help identify Nluc activity produced from initial translation of input RNA versus subsequent replication, ZIKV^{Nluc} RNA containing a mutation within the catalytic site of the NS5 RdRp domain (G_{664}DD → G_{664}AA) was used (ZIKV^{Nluc}-GAA, shown in Figure 5.2A).

Translation of input RNA was found to peak around 3 to 6 hours post-electroporation for both replication-competent and -incompetent ZIKV^{Nluc} (Figure 5.3A). Subsequent reduction in Nluc activity up to 12 hours occurred as a result of degradation of both the input RNA and Nluc initially produced (Figure 5.3A and B), consistent with results obtained from similar experiments (Javorovic *et al*, 2005; Alvarez *et al*, 2005a). However, at 24 and 48 hours post-electroporation the Nluc signal for the wildtype ZIKV^{Nluc} infection rebounds (Figure 5.3A) in a manner that correlates with an increase in genome copy number (Figure 5.3B), while for ZIKV^{Nluc}-GAA both Nluc activity and genome copy number continue to decrease. This indicates that the increase in Nluc signal seen after 24 hours is a result of genome replication and subsequent translation of nascent genomes. ZIKV^{fl} RNA replicated to a similar extent to that of ZIKV^{Nluc} over the time course, indicating the addition of the Nluc reporter has no major effect on viral growth kinetics (Figure 5.3B).

The data presented here illustrates that by using ZIKV^{Nluc} reporter RNA, initial translation can be separated from subsequent replication provided that Nluc activity is measured within the first 12 hours post-electroporation. These viral kinetics are similar to those previously reported for DENV2 and WNV replicons harbouring stable reporters (Alvarez *et al*, 2005a; Lo *et al*, 2003).

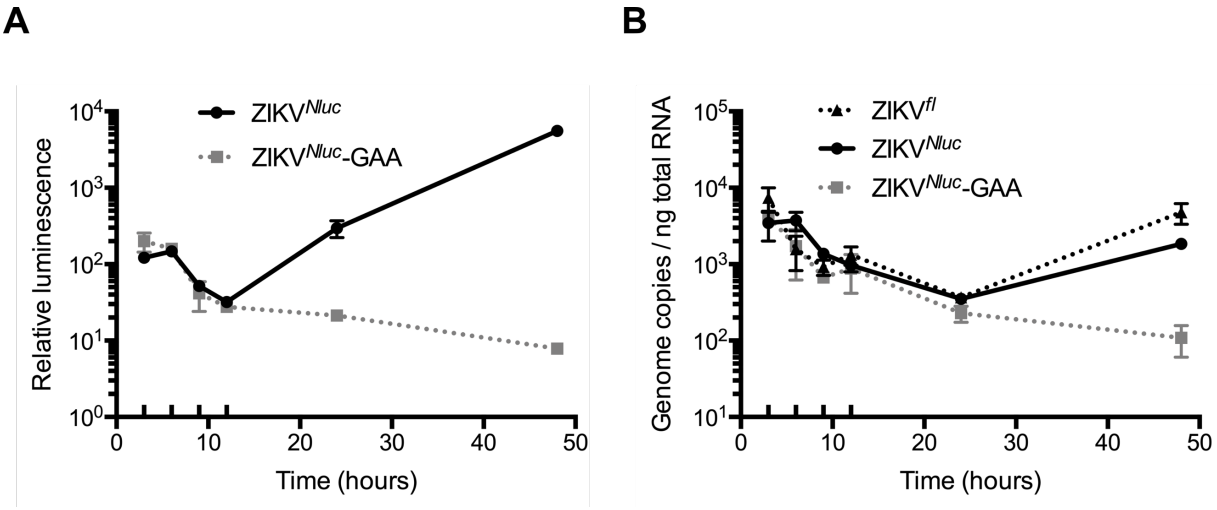

Figure 5.3 ZIKV^{Nluc} can be used to separate initial translation from replication during infection

Time course of **A)** luciferase activity normalised to total protein amount and **B)** ZIKV genome copy number quantified by qPCR following electroporation of capped ZIKV^{fl}, ZIKV^{Nluc} or ZIKV^{Nluc}-GAA into Vero cells. 1x10^5 cells were seeded post-electroporation for each time point. Data are mean +/- SEM for three technical repeats within one independent experiment.

5.2.2 ZIKV replication requires genome circularisation

It has been previously reported for DENV and WNV that genome circularisation via long-range 5′ and 3′ interactions is essential for viral replication but dispensable for translation (Zhang *et al*, 2008a; Lo *et al*, 2003; Alvarez *et al*, 2005a). In order to analyse the effect of ZIKV circularisation on replication and translation, Vero cells were electroporated with capped ZIKV^{Nluc} RNA and a mutant in which the 3′ CS had been replaced with the 5′ CS to abrogate base-pairing between the two elements (ZIKV^{Nluc}-Δ3′CS; sequence is shown Figure 5.2A, represented schematically in Figure 5.4A). Similar mutations made in DENV have been shown to be sufficient to disrupt genome circularisation (Alvarez *et al*, 2005a, 2005b). ZIKV^{Nluc}-GAA was also analysed as a known replication-deficient RNA. Samples throughout the time course were taken to measure both genome translation through Nluc activity and genome copy number by qPCR.

Although the genome copy number of all constructs decreased from 6 hours to 24 hours post-electroporation, only the genome copy number of wildtype ZIKV^{Nluc} recovered after 48 hours, while that of the ZIKV^{Nluc}-Δ3′CS and ZIKV^{Nluc}-GAA continued to decrease (Figure 5.4B). This indicates that the 5′-3′ interaction of the CS element is essential for ZIKV replication, consistent with other flaviviruses (Alvarez *et al*, 2005a; Lo *et al*, 2003; Khromykh *et al*, 2001a). This concurs with Nluc measurements taken over the time course (Figure 5.4C). At 6 hours post-electroporation, when genome copy number was equivalent between the three viruses (Figure 5.4B), measured Nluc activity was similar (Figure 5.4D). As wildtype ZIKV^{Nluc} and ZIKV^{Nluc}-GAA are capable of circularising whereas ZIKV^{Nluc}-Δ3′CS is not, this suggests that circularisation potential does not impact upon translational efficiency of input RNA in this assay. Therefore, circularisation is dispensable for translation at early time points of ZIKV infection in an analogous fashion to DENV (Alvarez *et al*, 2005a, 2005b, 2008). Furthermore, at later timepoints no differences in translation were observed between circularisation-incompetent ZIKV^{Nluc}-Δ3′CS and circularisation-competent ZIKV^{Nluc}-GAA (Figure 5.4C).

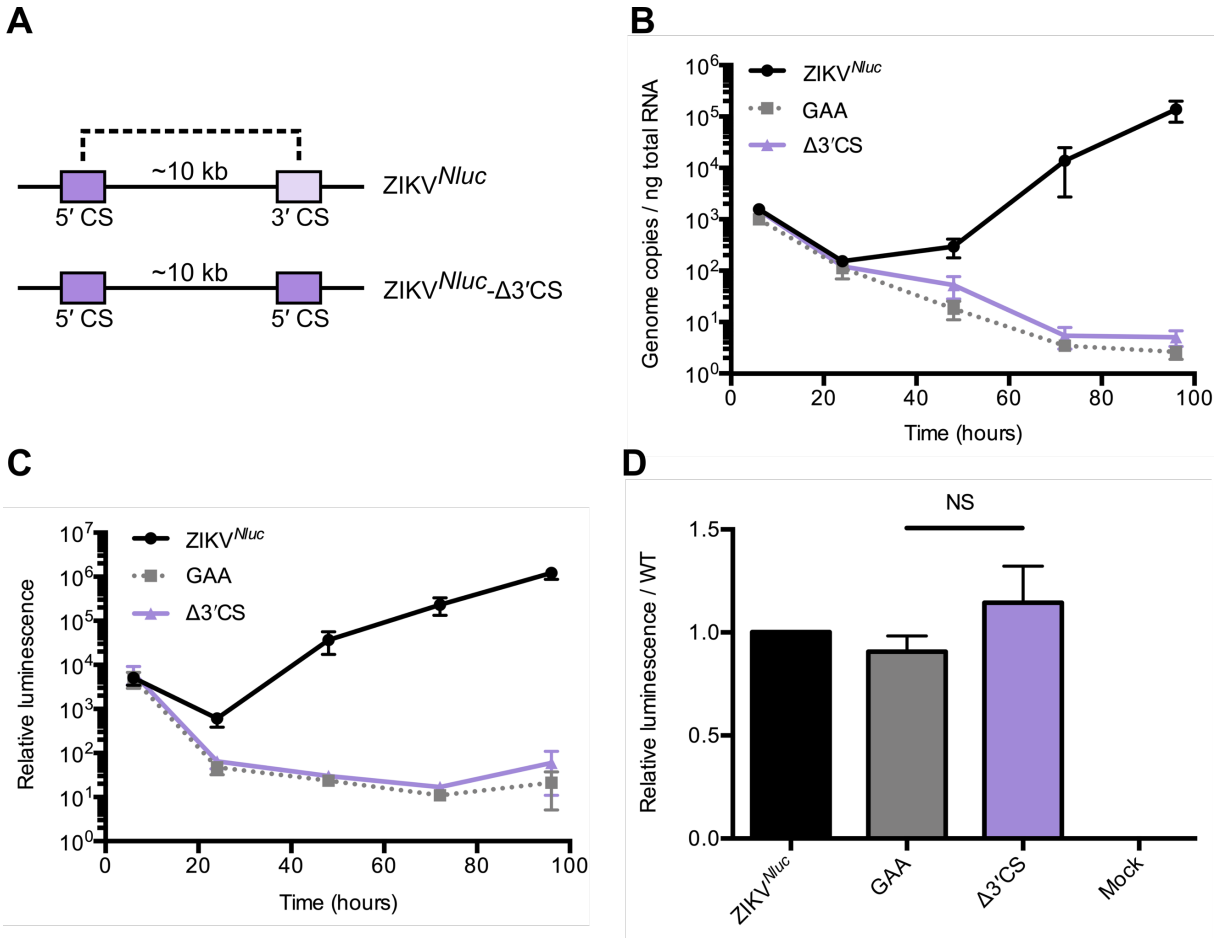

Figure 5.4 Circularisation of the ZIKV genome is required for replication

A) Schematic illustrating the ZIKV^{Nluc}-Δ3′CS mutant. The dark and light purple represent the 5′ CS and 3′ CS, respectively. The black dotted line represents cyclisation potential.
B, C) Time course of **B)** ZIKV genome copy number quantified by qPCR and **C)** luciferase activity normalised to total protein amount after electroporation of capped ZIKV^{Nluc}, ZIKV^{Nluc} -Δ3′CS or ZIKV^{Nluc}-GAA RNA into Vero cells. 2x10^5 cells were seeded post-electroporation for the T=6 hrs timepoint, whereas 5x10^4 cells were seeded for all other time points. Data are mean +/- SEM for three independent experiments.
D) Luciferase activity normalised to total protein amount at 6 hours post-electroporation normalised to the wildtype control (full time course is shown in **C**). Data are mean+/-SEM of three independent experiments. ZIKV^{Nluc}-GAA and ZIKV^{Nluc}-Δ3′CS mutants were compared by Mann-Whitney test (P=0.4). NS, not significant.

While recent studies have shown that circularised RNA can be detected within infected cells using RNA structure mapping approaches (Ziv *et al*, 2018; Huber *et al*, 2019), at late time points post-infection (>20 hours) the majority of ZIKV genomic RNA is linear (Li *et al*, 2018). This ultimately presents a major limitation of cell-based assays to examine the impact of genome circularisation on viral translation, as any changes that occur as a result of switching between linear and circular genome conformations during infection will likely be masked by an excess of the linear form.

5.2.3 Full-length ZIKV RNA adopts a linear conformation in vitro

One way in which to avoid this caveat was to utilise the *in vitro* reconstitution system previously described to examine translation initiation on ZIKV^{fl} RNA. As this RNA possesses both the viral 5′ and 3′ UTRs, it might be expected that this RNA would circularise *in vitro* as it has been shown that the generic properties of large RNA molecules often result in the two ends being in close proximity to each other (Liu *et al*, 2016; Yoffe *et al*, 2011; Leija-Martínez *et al*, 2014). In order to confirm this, selective 2′-hydroxyl acylation analysed by primer extension (SHAPE) RNA structure analysis was performed (Wilkinson *et al*, 2006). This technique relies on the fact that flexible RNA nucleotides preferentially sample conformations that enhance the reactivity of their 2′-hydroxyl groups to the electrophile N-methylisatoic anhydride (NMIA). Flexible nucleotides can be subsequently mapped by primer extension inhibition using a suitable sequencing ladder as modified sites yield RT stops.

The SHAPE reactivity of wildtype ZIKV^{fl} RNA was compared to that of ZIKV^{fl}-Δ3′CS RNA, which as previously described lacks base-pairing potential between the 5′ and 3′ CS elements. SHAPE reactivity across the 5′ CS element of the two RNAs was found to be practically identical, suggesting that within both RNA constructs *in vitro* the 5′ CS is unhybridised (Figure 5.5A; a representative SHAPE gel is shown in Appendix C). This is consistent with the fact that DENV genomic RNA released from capsids by proteinase K treatment and phenol-chloroform extraction was found to adopt a linear structure (Dethoff *et al*, 2018). Taken together, this data suggests that in the absence of other factors *in vitro* ZIKV^{fl} RNA preferentially adopts a linear conformation. In agreement with this, when analysed within the reconstitution system for translation initiation (the 5′ end of the linear ZIKV genome is shown schematically in Figure 5.5B), 48S complex assembly occurred to a similar efficiency at the initiation codon AUG$_{108}$ on both ZIKV^{fl} and ZIKV^{fl}-Δ3′CS RNA (Figure 5.5C; compare lanes 4 and 2).

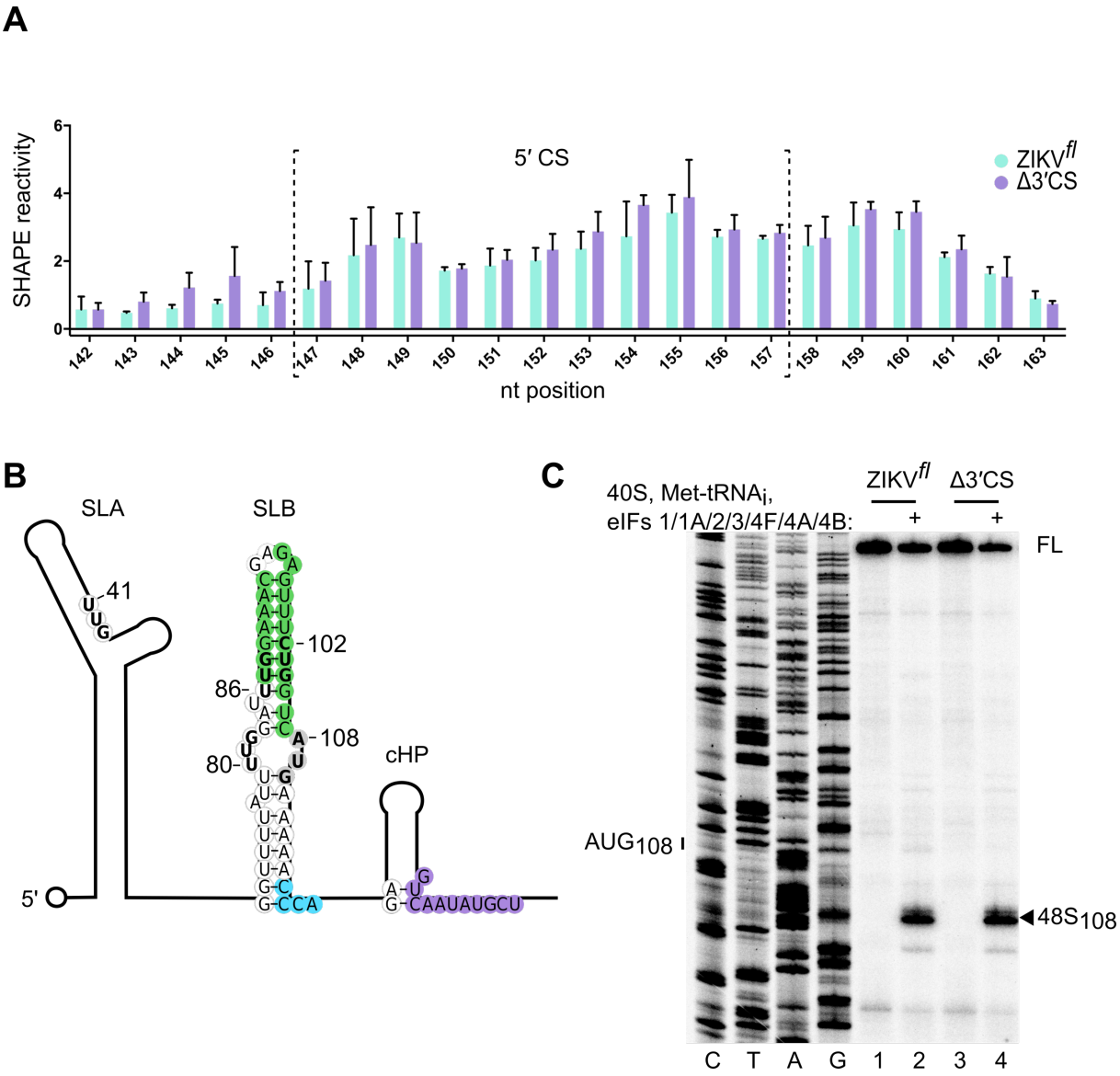

Figure 5.5 ZIKV RNA adopts a linear conformation *in vitro*

A) SHAPE reactivity around the 5′ CS of ZIKV^{fl} (green) and ZIKV^{fl}-Δ3′CS (purple). Nucleotides within the 5′ CS are enclosed by the dotted brackets. Data are normalised SHAPE reactivities from three experiments, mean+/- SD at each base.
B) Schematic of linear ZIKV from nt 1-160. Sequences corresponding to the 5′ UAR, DAR and CS sequences involved in genome 5′-3′ hybridisation are highlighted in green, blue and purple, respectively. The initiating AUG at nt 108 and upstream near-cognate codons discussed in the text are highlighted in bold. The 5′ cap structure is represented as a circle. SLA, stem-loop A; SLB, stem-loop B; cHP, C coding region hairpin.
C) Toeprinting analysis of 48S complex assembly on capped ZIKV^{fl} and ZIKV^{fl}-Δ3′CS RNA (a representative experiment is shown from two independent experiments). Selected codons are labelled on the left and toeprints caused by 48S complex assembly are marked with an arrowhead on the right. FL, full-length.

5.2.4 Genome circularisation inhibits de novo ZIKV translation initiation

It was hypothesised that by reducing the distance between the ZIKV 5′ and 3′ UTRs, the circularised conformation of the viral genome might be preferentially adopted *in vitro* over the linear form. Similar minigenomes have been used previously to approximate the circularised conformation of DENV in *in vitro* assays to examine NS5 recruitment and RdRp activity (Hodge *et al*, 2016; Liu *et al*, 2016; Filomatori *et al*, 2006, 2011; Sztuba-Solinska *et al*, 2013; You & Padmanabhan, 1999; Potisopon *et al*, 2014).

To this end, the ~10 kb genome separating the two viral UTRs of ZIKV was replaced by a 60 nt linker to generate ZIKV^{mini}. Additional constructs were produced that contained mutations within the 5′ and 3′ cyclisation elements (shown schematically in Figure 5.6A). In an analogous manner to the ZIKV^{fl}-Δ3′CS mutant, the 3′ CS was replaced with the 5′ CS, disrupting base-pairing, to generate ZIKV^{mini}-Δ3′CS. Similarly, the ZIKV^{mini}-Δ5′CS construct was generated by replacing the 5′ CS with the 3′ CS. Comparatively, within the ZIKV^{mini}-CS/Swap construct the 5′ and 3′ CS elements were swapped, thus retaining base-pairing potential between the 5′ and 3′ ends. Corresponding mutations were also made within the UAR sequence to generate ZIKV^{mini}-Δ3′UAR, ZIKV^{mini}-Δ5′UAR and ZIKV^{mini}-UAR/Swap minigenomes, respectively.

The conformation of these minigenome constructs was initially examined by native PAGE. Circularised constructs are expected to migrate faster through a gel matrix due to their more compact structure than those in a linear conformation. Indeed, consistently slower migration was observed for the ZIKV^{mini}-Δ3′CS and ZIKV^{mini}-Δ5′CS mutants in comparison to wildtype ZIKV^{mini} RNA (Figure 5.6B; compare lanes 3 and 2 with 1). This suggests that disruption of the 5′-3′ CS interaction is sufficient to force these RNAs to adopt a more linear conformation. Comparatively, the ZIKV^{mini}-CS/Swap RNA migrated in a manner similar to that of the wildtype minigenome (Figure 5.6B; compare lanes 4 and 1), indicating that by swapping the CS elements hybridisation between the two RNA ends was retained. Similar results were observed upon mutation of the UAR element (Figure 5.6B; compare lanes 7, 6 and 5 to 1). It is important to note that the wildtype ZIKV^{mini} RNA was observed as a single band upon native PAGE analysis, suggesting that intramolecular rather than intermolecular interactions between the cyclisation elements dominate.

To confirm these results, the minigenome RNAs were subjected to SHAPE analysis. The SHAPE reactivity of nucleotides present within the 5′ CS element of the wildtype ZIKV^{mini} was significantly reduced compared to ZIKV^{mini}-Δ3′CS RNA (Figure 5.6C), as well as ZIKV^{fl} RNA

(Figure 5.5A). These results suggest that the 5′ CS element is base-paired within the wildtype ZIKV minigenome. Similar SHAPE reactivity around this region was also observed within the ZIKV^{mini}-CS/Swap RNA where base-pairing potential between the 5′ and 3′ CS elements was retained. Taken together with the native PAGE analysis described above, this data illustrates that wildtype ZIKV^{mini} RNA adopts a circular conformation *in vitro* whereas ZIKV^{mini}-Δ3′CS RNA adopts a linear conformation. Consistent with this, the SHAPE reactivity of nucleotides within the 5′ region beyond the CS element of ZIKV^{mini} RNA correlates well with the circular genome conformation (Figure 5.6D, left), whereas the SHAPE reactivity of the ZIKV^{mini}-Δ3′CS maps better to the linear conformation (Figure 5.6D, right). A representative SHAPE gel is shown in Appendix C and the complete SHAPE dataset across the 5′ region is shown in Appendix D.

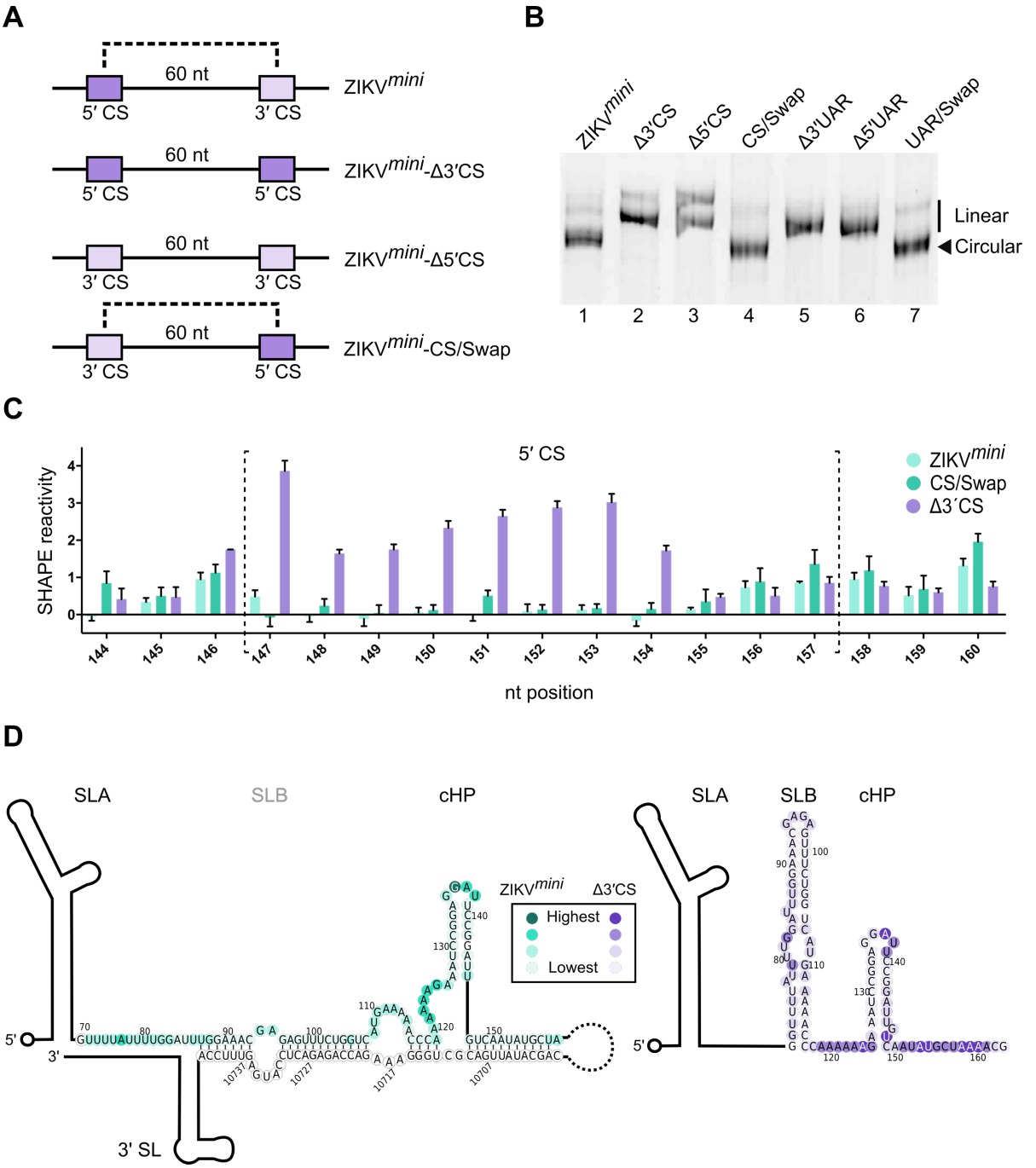

Figure 5.6 The ZIKV minigenome RNA adopts a circular conformation *in vitro*

A) Schematic illustration of the ZIKV^{mini} mutants examined. The dark and light purple represent the 5′ CS and 3′ CS, respectively. The black dotted line represents cyclisation potential.
B) Native PAGE analysis of ZIKV^{mini} containing mutations in either the CS or UAR elements (a representative experiment is shown from two independent experiments). Gels were poststained with ethidium bromide for detection. Migration corresponding to RNA in a circular or linear conformation is indicated.
C) SHAPE reactivity within the 5′ CS of the wildtype and mutant ZIKV^{mini} RNA. Wildtype SHAPE reactivity in light green is compared to CS/Swap (dark green) and Δ3′ CS (purple). Data are mean+/-SD of normalised SHAPE reactivities at each base from three experiments.
D) Heat map of SHAPE reactivities from a representative experiment overlaid onto circular genome (ZIKV^{mini}; left/green) and linear genome (ZIKV^{mini}-Δ3′CS; right/purple). The colour intensity represents increasing SHAPE reactivity as indicated in the box. SLA, stem-loop A; SLB, stem-loop B; cHP, C coding region hairpin; 3' SL, 3' stem-loop.

These RNA constructs were next assayed for their ability to assemble 48S complexes within the reconstitution system for translation initiation (schematics illustrating the linear and circular genome conformations are shown in Figure 5.7A and B). In comparison to 48S complex formation on ZIKV^{fl} RNA (Figure 5.5C), only weak complex was observed at AUG_{108} upon wildtype ZIKV^{mini} RNA (Figure 5.7C, lane 2). By mutating either the 5′ or 3′ CS element thus preventing the base-pairing required for genome circularisation, efficient 48S complex formation could be restored on the ZIKV^{mini}-Δ3′CS and ZIKV^{mini}-Δ5′CS RNA (Figure 5.7C, lanes 4 and 6). When the CS elements were swapped within the ZIKV^{mini}-CS/Swap RNA thus restoring the circularised conformation, efficient 48S complex formation was abrogated thus showing that this defect occurs directly as a result of genome circularisation (Figure 5.7C, lane 8). Mutations within the UAR elements behaved in a similar manner, with mutations that prevent genome circularisation rescuing the efficiency of 48S complex assembly (Figure 5.7D; compare lanes 2 to 4 and 6) and subsequent restoration of circularisation in the UAR/Swap mutant again abrogating it (Figure 5.7D, compare lanes 2 and 8). Even in the absence of the translational machinery, additional RT stops that aligned with the UAR and CS cyclisation elements occurred upon the circularised ZIKV^{mini} RNA constructs (Figure 5.7C and D, indicated by open arrowheads).

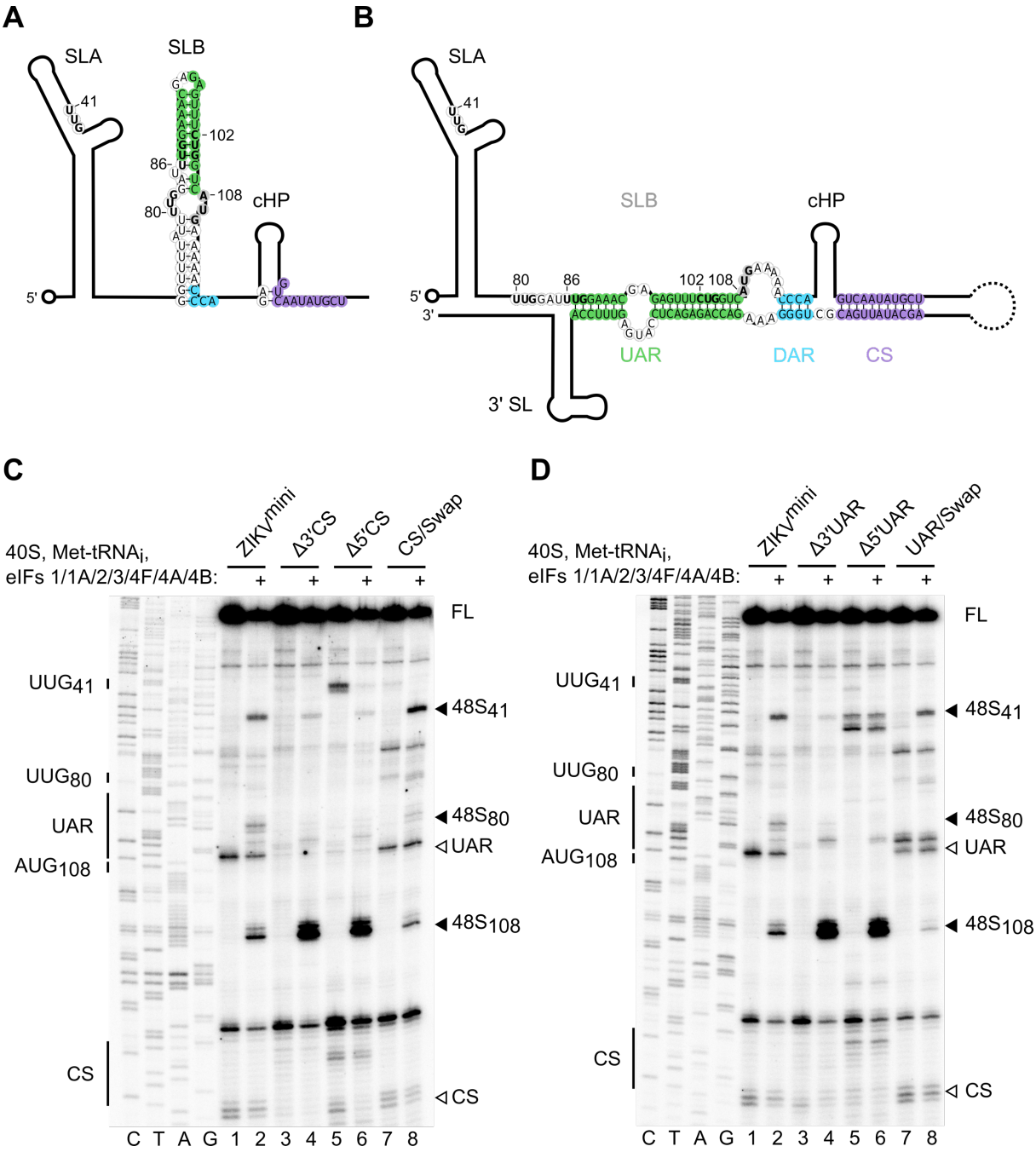

Figure 5.7 ZIKV minigenome circularisation inhibits 48S complex assembly

A, B) Schematics illustrating the **A**) linear and the **B**) circular conformations of the ZIKV genome. Sequences corresponding to the UAR, DAR and CS are highlighted in green, blue and purple, respectively. The initiating AUG at nt 108 and upstream near-cognate codons discussed in the text are highlighted in bold. The 5′ cap structure is represented as a circle. SLA, stem-loop A; SLB, stem-loop B; cHP, C coding region hairpin; 3' SL, 3' stem-loop.
C, D) Toeprinting analysis of 48S complex assembly on wildtype capped ZIKV^{mini} RNA and **C**) CS mutants or **D**) UAR mutants (a representative experiment is shown from two independent experiments). The same assembly reaction on ZIKV^{mini} is used on both gels. Selected codons are labelled on the left and toeprints caused by 48S complex assembly are marked with a closed arrowhead on the right. Open arrowheads mark RT stops on RNAs with 5′-3′ hybridisation potential. FL, full-length.

In order to ensure that differences within these minigenome constructs other than circularisation state were not responsible for these observations, a 32 nt antisense oligonucleotide (ASO) complimentary to the 3′ UAR, DAR and CS elements was designed (shown schematically in Figure 5.8A). This oligonucleotide, but not a scrambled sequence of the same length (SCR), when heated and snap-cooled with wildtype ZIKV^{mini} RNA was found to shift its migration pattern to that of the ZIKV^{mini}-Δ3′CS by native PAGE analysis (Figure 5.8B). The linear minigenome-ASO hybrid is retarded to a greater extent due to the additional mass of the annealed oligo. Furthermore, binding of the ASO to the ZIKV^{mini} RNA enhanced the SHAPE reactivity of nucleotides within the 5′ CS element (Figure 5.8C; a representative SHAPE gel is shown in Appendix C and the complete dataset across the 5′ region is shown in Appendix D). These data are consistent with the ASO disrupting the base-pairing required for circularisation within the ZIKV minigenome, thus shifting its conformation towards the linear form.

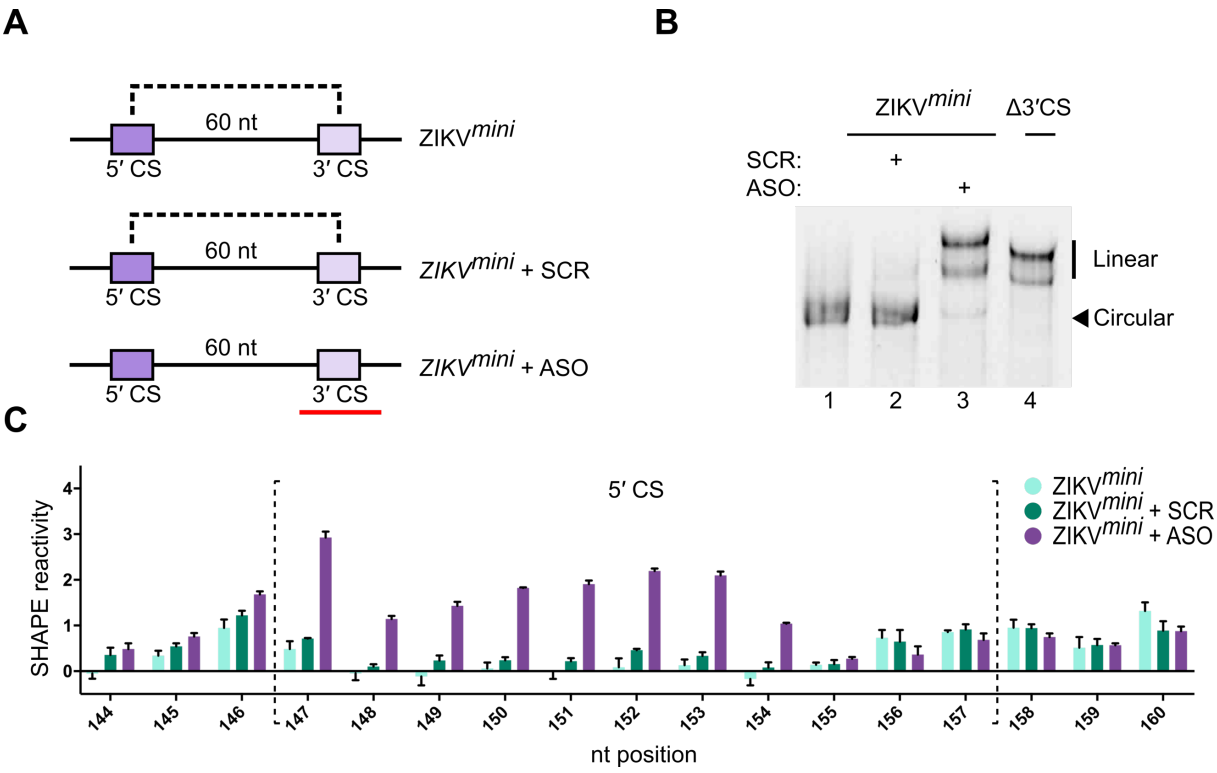

Figure 5.8 Circularisation can be disrupted by a small antisense oligonucleotide

A) Schematic illustration of the effect of a scrambled (SCR) or anti-sense oligo (ASO) targeted towards the 3′ cyclisation elements. The black dotted line represents cyclisation potential and the red bar represents the ASO.
B) Native PAGE analysis of wildtype ZIKV^{mini} after heating and snap-cooling in the presence or absence of ASO or SCR (a representative experiment is shown from two independent experiments).
C) SHAPE reactivity within the 5′ CS of the wildtype ZIKV^{mini} RNA. Wildtype SHAPE reactivity in light green is compared to wildtype annealed to SCR (dark green) or ASO (purple). Data are normalised SHAPE reactivities from three experiments, mean+/-SD at each base. The same wildtype dataset as in Figure 5.6C is illustrated.

Addition of ASO, but not SCR, into the 48S complex assembly reaction was found to rescue 48S complex formation at AUG_{108} on wildtype $ZIKV^{mini}$ RNA (Figure 5.9, compare lanes 5 and 6). This occurred in a manner analogous to mutation of the 3′ CS element (Figure 5.9, lane 8). Taken together with the mutational analysis, this data illustrates that circularisation of the ZIKV minigenome inhibits *de novo* translation initiation.

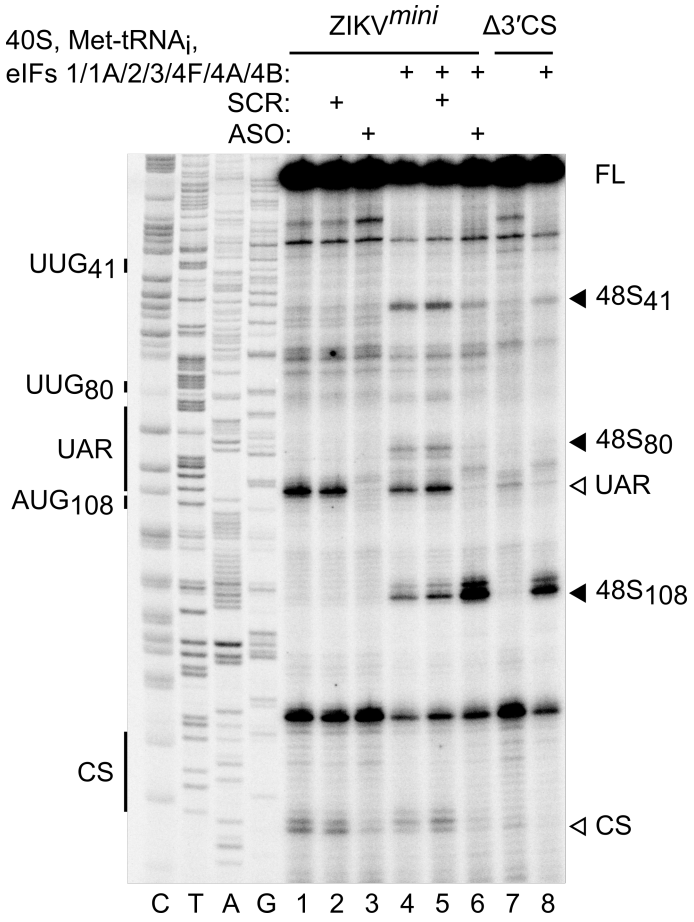

Figure 5.9 Inhibition of ZIKV minigenome circularisation by use of a small antisense oligonucleotide rescues 48S complex assembly

Toeprinting analysis of 48S complex assembly on wildtype capped $ZIKV^{mini}$ (a representative experiment is shown from two independent experiments). Scrambled (SCR) or anti-sense (ASO) RNA oligos were annealed to minigenomes prior to the assembly reaction as indicated. Selected codons are labelled on the left and toeprints caused by 48S complex assembly are marked with a closed arrowhead on the right. Open arrowheads mark RT stops on RNAs with 5′-3′ hybridisation potential. FL, full-length.

5.2.5 Genome circularisation impairs scanning

While genome circularisation of the wildtype ZIKV^{mini} RNA inhibited 48S complex formation at AUG_{108}, increased 48S complex assembly was observed at the two upstream near-cognate codons UUG_{41} and UUG_{80} relative to the linear confirmation (Figure 5.7C and D; compare lanes 2 and 8 with 4 and 6). This was despite inclusion of an excess of eIF1A, whose omission from this reconstitution system was previously shown to promote increased complex assembly on UUG_{41} on linear ZIKV RNA (Chapter 3). This suggests that the scanning 43S preinitiation complex cannot efficiently penetrate the structure found in the circular form of the ZIKV genome around the initiating AUG, thus assembling instead at upstream near-cognate codons. Consistent with this model, the additional RT stops at the hybridised cyclisation elements observed for the wildtype ZIKV^{mini}, ZIKV^{mini}-CS/Swap and ZIKV^{mini}-UAR/Swap minigenomes (indicated on Figure 5.7C and D with open arrowheads) were maintained within the 48S assembly reaction even in the presence of the helicase eIF4A (e.g. Figure 5.7C, compare lanes 1 and 2).

As the helicase DHX29 has been described as facilitating efficient 48S complex assembly on RNAs possessing highly structured 5′ UTRs (Pisareva *et al*, 2008), the effect of DHX29 inclusion within the 48S assembly reaction on capped ZIKV^{mini} RNA was investigated. DHX29 addition led to a decrease in 48S complex assembly at AUG_{108} on both the circular ZIKV^{mini} and linear ZIKV^{mini}-Δ3′CS RNA (Figure 5.10; compare lanes 5 and 10 with 2 and 7). This is consistent with previous observations that DHX29 is not required for efficient 48S complex formation at AUG_{108} on the ZIKV 5′ end (Chapter 3). Therefore, addition of DHX29 could not overcome the circularisation-induced scanning defect. Furthermore, while inclusion of additional eIF3/4F led to an increase in 48S complex formation on ZIKV^{mini} RNA (Figure 5.10; compare lanes 2 and 4), an increase of similar magnitude was also observed on ZIKV^{mini}-Δ3′CS RNA (Figure 5.10; compare lanes 7 and 9), indicating that 48S complex formation at AUG_{108} under these assembly conditions was still inhibited by genome circularisation (Figure 5.10; compare lanes 9 and 4). These data suggest that the scanning defect induced by circularisation cannot be overridden by the canonical translation machinery.

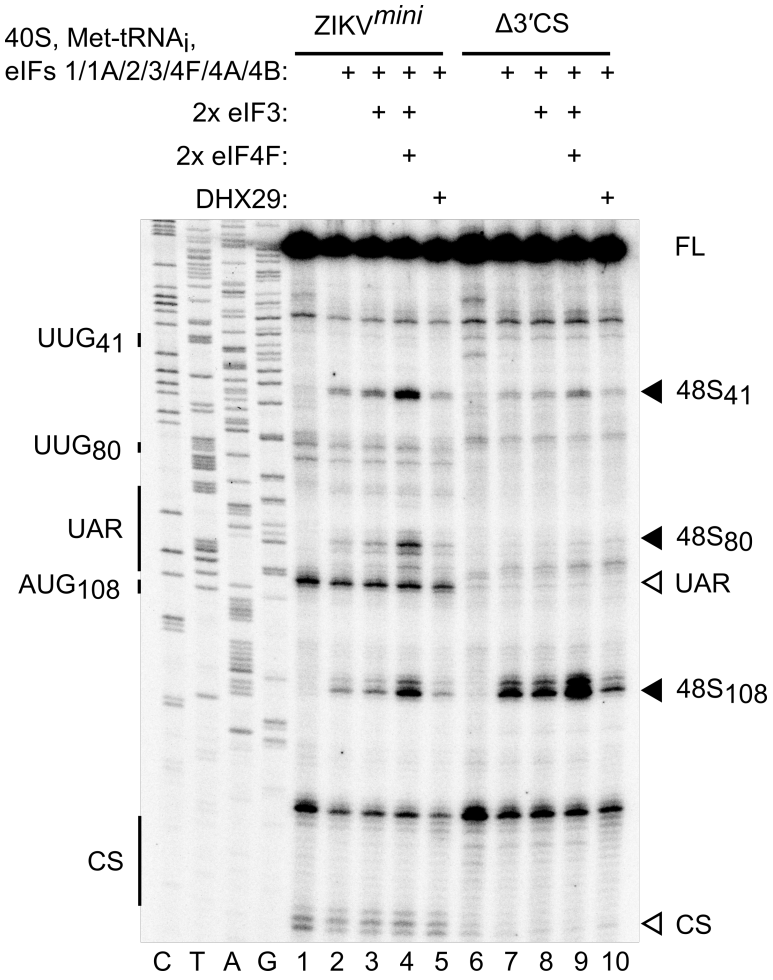

Figure 5.10 Addition of more eIF4F or DHX29 cannot overcome the circularisation-induced scanning defect

Toeprinting analysis of 48S complex assembly on capped ZIKV^{mini} or ZIKV^{mini}-Δ3′CS using the conditions illustrated (a representative experiment is shown from two independent experiments). Selected codons are labelled on the left and toeprints caused by 48S complex assembly are marked with a closed arrowhead on the right. Open arrowheads mark RT stops on RNAs with 5′-3′ hybridisation potential. FL, full-length.

In order to investigate the effect of mutating UUG_{41} and UUG_{80} on codon selection within the ZIKV^{mini} construct, mutational analysis was carried out (the mutations made are shown in Figure 5.11A). UUG_{41} was changed to UUU_{41}, with a corresponding C21A mutation to maintain SLA structure, while UUG_{80} was changed to UCC_{80}. The introduced mutations abrogated 48S complex formation at UUG_{41} and UUG_{80} respectively (Figure 5.11B; compare lanes 2, 4 and 6), while simultaneous mutation of both sites did not restore efficient 48S complex formation at AUG_{108} (Figure 5.11B, lane 8). Instead, increased 48S complex formation occurred at UUG_{86} at the 5′ end of the UAR element in the absence of UUG_{41} and UUG_{80} (Figure 5.11B, lane 8). The data presented here suggests that 48S complex formation at UUG_{41} or UUG_{80} is not required for the inhibition of complex formation seen at AUG_{108} within the circularised state and instead that the RNA structure alone is capable of mediating this effect.

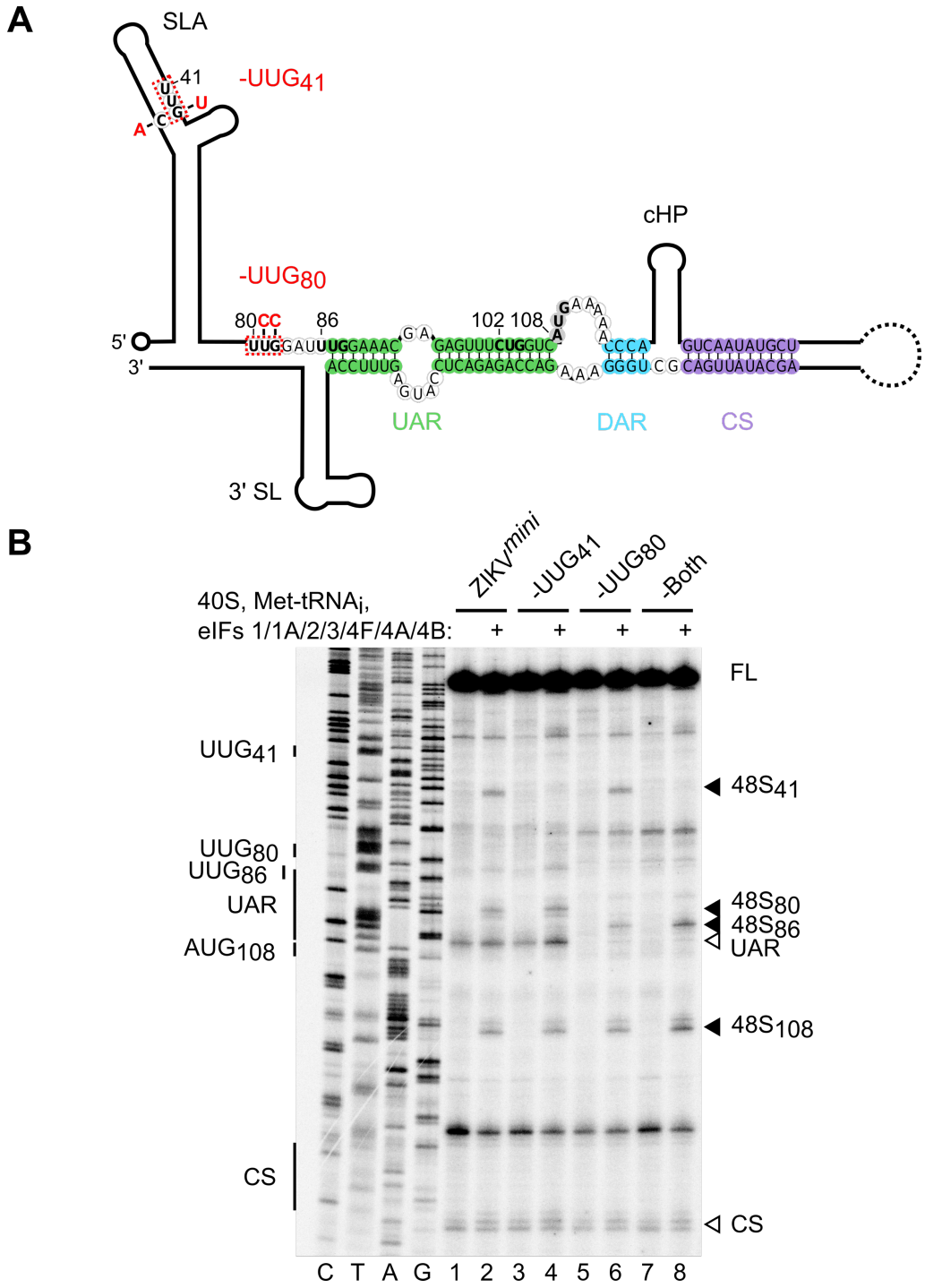

Figure 5.11 Mutation of UUG$_{40}$ and UUG$_{81}$ does not restore efficient 48S complex assembly at AUG$_{108}$ in the circularised form

A) Schematic of the ZIKV minigenome with mutations shown in red. These mutations were predicted by mfold to not change RNA secondary structure (Zuker, 2003). Sequences corresponding to the UAR, DAR and CS are highlighted in green, blue and purple, respectively. The 5′ cap structure is represented as a circle. SLA, stem-loop A; SLB, stem-loop B; cHP, C coding region hairpin; 3' SL, 3' stem-loop.
B) Toeprinting analysis of 48S complex assembly on wildtype capped ZIKV^{mini} RNA and upstream near-cognate codon mutants. Selected codons are labelled on the left and toeprints caused by 48S complex assembly are marked with a closed arrowhead on the right. Open arrowheads mark RT stops on RNAs with 5′-3′ hybridisation potential. Fl, full-length.

5.2.6 Genome circularisation inhibits translation initiation in other flaviviruses

As genome circularisation is a common feature of flavivirus replication, it was hypothesised that circularisation would also inhibit *de novo* translation initiation in other flaviviruses. To this end, minigenome constructs were designed containing the UTRs of DENV1 and DENV4 in the same manner previously described for ZIKV^{mini} (shown schematically in Figure 5.12A and C; the complete sequence of the 5′ terminal ends in the two genomic forms are illustrated in Appendix A). The 5′ and 3′ UTRs of DENV1 and DENV4 are the most divergent among the DENV serotypes. Of these two constructs, DENV4 is most similar to ZIKV^{mini} as the initiating AUG is present in good Kozak sequence context (Kozak, 1989a). Comparatively, the initiation codon of DENV1 is in poorer sequence context similar to DENV2, which has previously been reported as requiring the downstream cHP stem for efficient codon selection (Clyde & Harris, 2006).

The effect of circularisation on 48S complex assembly was examined as before by mutating the 3′ CS element or by inclusion of a short ASO complimentary to the 3′ cyclisation elements. Circularisation of DENV4 and DENV1 minigenomes was found to inhibit 48S complex assembly at the initiating AUG (AUG_{102} for DENV4 and AUG_{95} for DENV1), which could be rescued when circularisation was disrupted by mutation or oligo annealing (Figure 5.12B and D; compare lane 4 to 6 and 8). Similar to ZIKV, an increase in 48S assembly on the upstream near-cognate codon UUG_{48} was observed for both DENV4 and DENV1 minigenomes in the circular form, consistent with a scanning defect driving translation inhibition. Taken together, this data suggests that inhibition of cap-dependent translation initiation by genome circularisation might be a conserved mechanism of translational control during flavivirus infection.

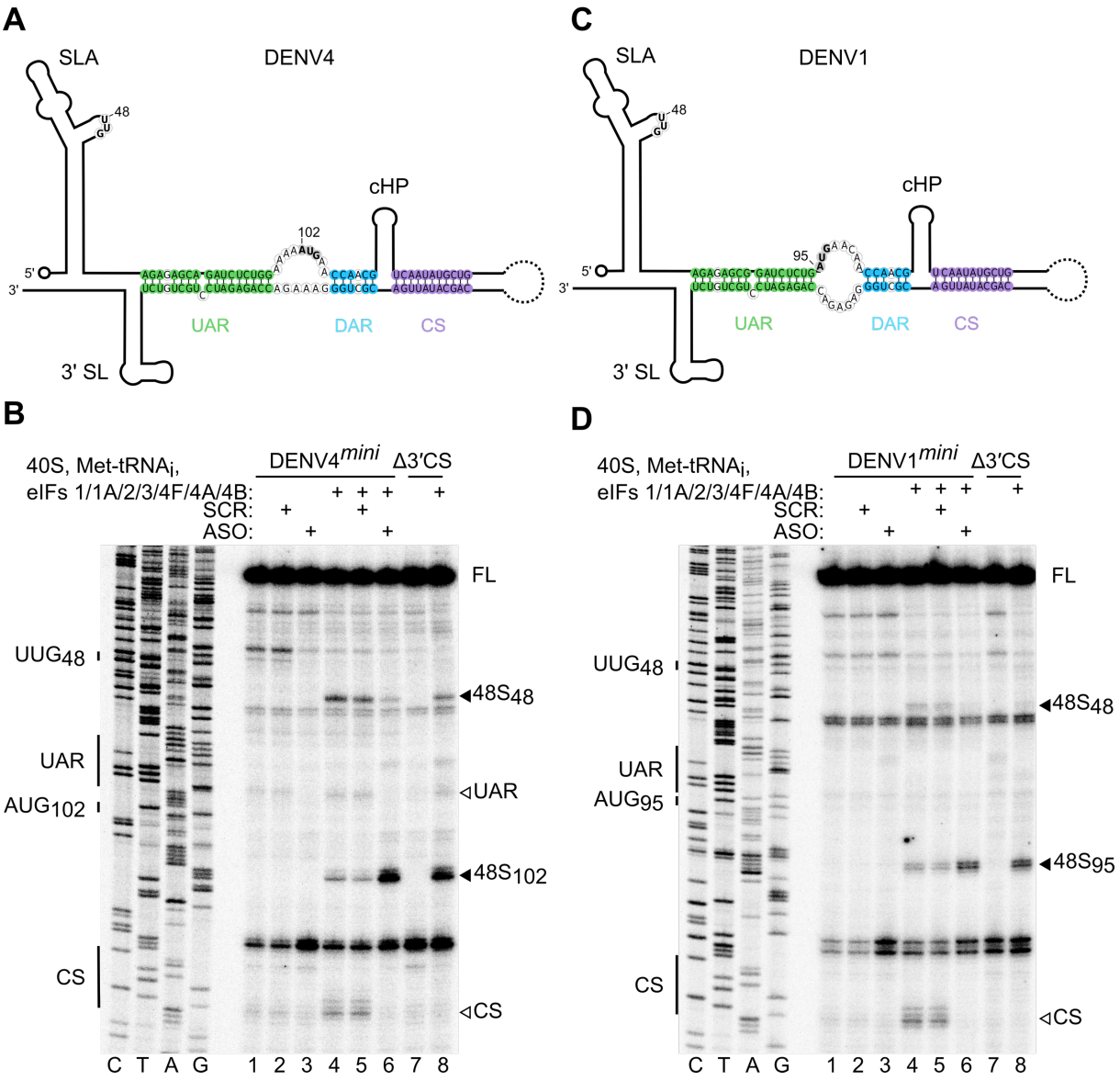

Figure 5.12 Circularisation inhibits translation initiation on DENV1 and DENV4

A, **C**) Schematics of the **A**) DENV4 and **C**) DENV1 genomes in the circular conformation. Nucleotides of the UAR, DAR and CS are shown in green, blue and purple, respectively. The initiating AUG and upstream near-cognate codons discussed in the text are in bold. The 5′ cap structure is represented as a circle. SLA, stem-loop A; SLB, stem-loop B; cHP, C coding region hairpin; 3' SL, 3' stem-loop.
B, **D**) Toeprinting analysis of 48S complex assembly on capped **B**) wildtype and Δ3′ CS DENV4 minigenome RNA or **D**) wildtype and Δ3′ CS DENV1 minigenome RNA (a representative experiment is shown from two independent experiments). Selected codons are labelled on the left and toeprints caused by 48S complex assembly are marked with a closed arrowhead on the right. Open arrowheads mark RT stops on RNAs with 5′-3′ hybridisation potential. Scrambled (SCR) or anti-sense (ASO) RNA oligos were annealed to minigenomes prior to the assembly reaction as indicated. FL, full-length.

5.3 Discussion

RNA circularisation is believed to be a common mechanism by which the genomes of positive-sense RNA viruses are replicated during infection (Herold & Andino, 2001). These interactions can be proteinaceous in nature, mediated by bridging of the two genome ends by protein binding, or depend on long-range RNA-RNA interactions. As an example of the former, PV genome replication during infection relies on circularisation mediated by the interaction between PCBP2 at the 5′ end and PABP bound to the 3′ poly(A) tail (Perera *et al*, 2007; Herold & Andino, 2001). Similarly, replication of HCV is thought to depend on PCBP2-mediated genome circularisation (Wang *et al*, 2011), although bioinformatic analysis suggests that a long-range RNA-RNA interaction may also be involved (Fricke *et al*, 2015; Romero-López & Berzal-Herranz, 2009). A possible reason for this widespread requirement for template circularisation in replication is to ensure that only full-length viral genomes possessing both ends are replicated.

However, interactions between the 5′ and 3′ UTRs of RNA have also been linked to translation enhancement (Jackson *et al*, 2010). The 5′ cap structure and poly(A) tail act synergistically to promote efficient translation of cellular mRNAs in a manner dependent on the interaction between eIF4G and PABP (Tarun & Sachs, 1996; Kahvejian *et al*, 2001; Imataka *et al*, 1998). This forms the basis of the "closed loop" model of translation, whereby the translating mRNA is hypothesised to circularise in a protein-dependent manner (Wells *et al*, 1998; Jackson *et al*, 2010). Indeed, even some mammalian viruses reliant on IRES sequences for translation initiation, such as picornaviruses, possess poly(A) tails, the presence of which can enhance translation efficiency through PABP binding (Michel *et al*, 2001). Moreover, members of the plant virus families *Luteoviridae* and *Tombusviridae,* lacking both 5′ caps and poly(A) tails, circularise through long-range RNA-RNA interactions during infection which is thought to promote translation by delivering eIF4F from its binding site within the 3′ UTR to the 5′ end (Fabian & White, 2004; Guo *et al*, 2001; Treder *et al*, 2008; Gazo *et al*, 2004).

It is clear then that RNA circularisation can have a variety of different effects depending on context. Here, it is shown that genome circularisation mediated by long-range RNA-RNA interactions inhibits *de novo* cap-dependent translation initiation at the initiating AUG of ZIKV and DENV. As these same interactions have previously been shown to promote RNA replication (Villordo & Gamarnik, 2009), this provides a mechanism to ensure that ribosomes are not loaded onto actively replicating genomes thus ensuring that viral replication occurs

unimpeded. Furthermore, this defines a major role for the linear form of the viral genome in translation during infection.

Initial attempts to examine the effect of genome hybridisation on translation in the context of the full-length ZIKV genome failed, as both ZIKV^{fl} and ZIKV^{fl}-Δ3′CS RNAs were found to adopt the linear conformation *in vitro.* This is surprising, as previous studies have illustrated that 5′-3′ complexes can form *in trans* between separate RNA probes corresponding to the 5′ and 3′ ends of DENV (Alvarez *et al*, 2005b; Liu *et al*, 2016; Filomatori *et al*, 2011). This suggests that local RNA secondary structures within the ZIKV genome may be responsible for keeping the two ends apart *in vitro* and thus prevent their interaction. Consistent with this notion, it has been reported that the genome of DENV is highly structured *in vitro* in the absence of viral proteins (Dethoff *et al*, 2018). This might explain the requirement for proteins such as virally encoded NS3 and the cellular AUF1 p45 isoform in mediating genome circularisation *in vivo* during infection (Gebhard *et al*, 2012; Friedrich *et al*, 2018, 2014), and for other long-range RNA-RNA interactions beyond the UAR, DAR and CS elements that enhance genome replication (Liu *et al*, 2013; de Borba *et al*, 2015). Indeed, the mere fact that the wildtype ZIKV minigenome RNA adopted a circularised conformation suggests that the circularised state is more thermodynamically favoured when the structure of the rest of the ZIKV genome is not considered. Importantly, the structure of ZIKV^{mini} RNA matches that recently described as occurring in full-length viral RNA during infection by three independent groups (Ziv *et al*, 2018; Huber *et al*, 2019; Li *et al*, 2018).

The inhibitory effect of genome circularisation on translation initiation could only be revealed using minigenome RNAs within the reconstitution system. This approach overcame the various challenges associated with the use of ZIKV^{Nluc} RNA inside cells during virus infection, namely that of correlating circularisation state with translation, as initial translation following electroporation was independent of genome circularisation. However, a limitation of the study presented here is that while the inhibitory effect was observed within this minimalistic system, further experiments illustrating that circularisation-induced translation inhibition occurs inside cells would validate these findings. One of the major reasons why this was not pursued is due to concerns that increasing the size of the linker between the two UTRs in the ZIKV minigenome by incorporation of a reporter might reduce the proportion of circularised RNA, thus diluting out the inhibitory effect seen on translation. However, small reporters such as a split-GFP tag could be used to get around this problem (Cabantous *et al*, 2005).

However, conflicting reports regarding the role of the 3′ UTR of DENV in translation enhancement and RNA stability complicates the use of such reporter constructs in cells. For instance, it has been reported that the 3′ UTR of DENV enhances translation of an Fluc reporter independently of the 5′ UTR following transfection into BHK cells, in a manner partially dependent upon the 3′ SL structure (Holden & Harris, 2004). Furthermore, it was observed using an Fluc reporter flanked by the DENV genome ends that mutation of the 3′ CS site to decrease complementarity with the 5′ element actually led to a 85 % reduction of Fluc production in Vero cells, whereas mutation of the 5′ element alone led to a 10 % enhancement (Chiu *et al*, 2005). Whether this is due to the 3′ mutation interfering with the ability of the 3′ UTR to convey translation enhancement or whether RNA stability is sufficiently decreased upon mutation to have an impact is unclear. Comparatively, it was observed for DENV replicons in BHK and C6/36 mosquito cells that removal of the entire 3′ UTR did not significantly affect viral translation but instead abrogated replication (Alvarez *et al*, 2005a). The use of the *in vitro* system presented here avoids the issue of RNA stability in cells and allows examination solely of the effect of genome circularisation on *de novo* translation initiation.

The mechanism by which *de novo* translation initiation inhibition occurs as a result of circularisation is likely through inhibition of scanning rather than inhibition of eIF recruitment, as an increase in 48S complex assembly was seen on upstream near-cognate codons in the circular form. Mutation of these codons from the 5′ end was found to enhance picking of an additional near-cognate codon in close proximity to the circularised UAR element. This suggests that the circularised form of the ZIKV genome represents a structure that cannot be resolved efficiently by the scanning 43S preinitiation complex, even in the presence of DHX29. DHX29 has been shown to promote translation on a model RNA containing a stable stem in the 5′ UTR with a predicted free energy of -27.6 kCal/mol (Pisareva *et al*, 2008), similar to that of the 5′-3′ UAR interaction in the circularised form calculated by mfold (ΔG=-26.7 kCal/mol; Zuker, 2003). As such, it is not immediately apparent why DHX29 could not resolve this structure. However, notable similarities exist between these observations and the mechanism by which sfRNAs are generated during infection by stalling of the 5′-3′ exonuclease Xrn1 at complex tertiary structures within the viral 3′ UTR (Chapman *et al*, 2014; Akiyama *et al*, 2016). As such, structural analysis of the ZIKV minigenome, either by x-ray crystallography or cryo-EM, might yield valuable information regarding any such tertiary interactions capable of stalling ribosome scanning within the circularised form.

The physiological relevance of upstream near-cognate codon selection in the circularised state is unclear. This may just represent a side effect of arresting the scanning ribosome, or alternatively circularisation could be a deliberate mechanism to promote their selection in order to facilitate uORF expression. In this scenario, RNA structural changes mediated by circularisation would act in a manner similar to the cHP stem in DENV2, which promotes selection of the poor context initiating AUG (Clyde & Harris, 2006). In the ZIKV PE243 strain, translation from UUG_{80} would produce a short-conserved polypeptide out-of-frame with the main ORF. Indeed, a recent preprint has illustrated by ribosome profiling that significant ribosome occupancy occurs at UUG_{80} during ZIKV infection of both Vero cells and insect C6/36 cells (Irigoyen *et al*, 2017), supporting the *in vitro* findings presented here. However, further work needs to be performed to establish if the peptide produced from this uORF is functionally significant or whether selection of UUG_{80} during infection acts only to modulate translation of the main ORF, in a manner akin to canonical uORF function (Somers *et al*, 2013).

It is interesting to speculate about additional control mechanisms that might regulate the balance between the linear and circular genome conformations during infection in light of the results presented here. It was recently reported that the human microRNA miR-21 interacts with the 5′ CS element of ZIKV in a pro-viral fashion (Ziv *et al*, 2018). This interaction might prevent the hybridisation of the CS element and facilitate translation early in infection. Additionally, the neurodevelopmental protein Musashi-1 has been described as binding to the 3′ end of ZIKV genomes during infection of neuronal U251 cells and promoting genome replication, potentially through enhancement of translation (Chavali *et al*, 2017). Whether this occurs through modulation of cyclisation is unclear and further work is required to investigate this possibility.

Although characterisation of the precise structure of the DENV minigenome constructs by SHAPE is required to confirm this, it is likely that RNA-mediated circularisation represents a widespread mechanism among flaviviruses to both facilitate genome replication and inhibit ribosome loading. However, while these viruses lack a poly(A) tail, it has been demonstrated that PABP binding directly within the 3′ UTR of DENV enhances translation (Polacek *et al*, 2009b). This, combined with the fact these viruses possess a 5′ cap structure, suggests that an additional mode of genome circularisation may occur during infection that mirrors the “closed loop” reported for cellular mRNAs. Furthermore, while the cap-independent mechanism of translation proposed for DENV during conditions of cellular stress has been shown to require the two UTRs (Edgil *et al*, 2006), it is unlikely that hybridisation between the cyclisation elements is necessary and instead a RNA-protein bridge has been speculated as playing a role

(Edgil & Harris, 2006). This illustrates the variety of ways in which the ends of the viral genome can communicate during infection, regulating the use of the RNA template.

Taking all of the evidence into consideration then, the RNA genomes of ZIKV and other flaviviruses are highly dynamic structures. The work presented here illustrates that the long-range RNA-RNA interactions that mediate genome circularisation are critical for both promotion of genome replication and inhibition of viral protein synthesis, thus ensuring correct temporal regulation of the RNA template. Furthermore, this defines opposing roles for the linear and circular genome conformations during infection.

6 Summary and Future Directions

During infection, the genomes of positive-sense RNA viruses have three major functions. They have to act as templates for both viral translation and viral replication, two key processes that are antagonistic in nature as each requires the use of the RNA template in opposite directions. The third major function is that the RNA genomes have to be successfully encapsidated following replication to propagate the virus. As a result, numerous transitions occur during infection to ensure that these events are temporally coordinated, the first of which is the translation-replication switch. In the case of ZIKV and other flaviviruses, many of the key *cis*- and *trans*-acting factors determining these transitions are poorly characterised.

Based on the experimental data presented in this thesis, a model for the ZIKV translation-replication switch emerges (Figure 6.1). Upon infection, the ZIKV RNA genome is released into the cytosol in a linear conformation and engages with the translational machinery. This is consistent with the fact that the circularised genome conformation is not required for translation of input viral RNA following electroporation (illustrated in Chapter 5) and with reports using RNA structure mapping approaches which show that ZIKV genomes typically possess a more open structure inside cells (Huber *et al*, 2019; Li *et al*, 2018). The ZIKV genome is subsequently localised to the ER membrane following C protein transmembrane domain recognition by the SRP during polyprotein synthesis (Garcia-Blanco *et al*, 2016). Resulting translation is highly ER-localised, as shown by ribosome profiling coupled with cell fractionation (Reid *et al*, 2018), and viral replication complexes are established.

Over time, viral protein expression leads to NS5 accumulation at the ER membrane which subsequently binds to the cap-proximal SLA structure of the ZIKV genome and inhibits further translation initiation (Chapter 4). While NS5 can bind to both linear and circular genome conformations, it has been shown using $NS5^{DENV4}$ by EMSA that NS5 recruitment to SLA occurs more efficiently when the genome is in the linear conformation (Liu *et al*, 2016). While this difference was small, a similar enhancement was observed for $NS5^{ZIKV}$ binding to the linear form of the ZIKV minigenome described here (Appendix E). Furthermore it has been shown for DENV2 that the 3′ SL structure in the linear form of the genome represses polymerase activity, because the terminal 3′ nucleotides are sequestered within RNA secondary structure (Filomatori *et al*, 2011). This data is consistent with the idea that NS5 is recruited to and held at the 5′ end of the linear genome at a defined point in infection. This outcompetes the translation machinery for binding, thus preventing additional ribosomes from loading onto the

RNA genome template. Thus, a key component of the translation-replication switch involves the oscillation of local NS5 concentration.

As ribosomes are believed to be a major helicase activity in the cell (Takyar *et al*, 2005), it is likely that ZIKV genome circularisation can only occur once the template has been cleared of translating ribosomes as circularisation is reliant upon the formation of long-range RNA-RNA interactions (Alvarez *et al*, 2005b; Filomatori *et al*, 2006). The precise mechanism that mediates circularisation is unclear, but as NS5 is likely membrane-associated within the ER through its interaction with the NS3-NS2B complex (Yu *et al*, 2013), the two dimensional nature of the membrane may help to facilitate this conformational change. Viral proteins such as NS3 (Gebhard *et al*, 2012) and NS5 (Pong *et al*, 2011), as well as cellular proteins such as the AUF1 p45 isoform (Friedrich *et al*, 2014, 2018), enhance this process through their respective RNA annealing and chaperone activities. Upon genome circularisation, the repression exerted by the 3′ SL on polymerase activity is relieved upon the release of the 3′ terminal nucleotides through formation of the 5′-3′ UAR interaction, which also brings the two genomic ends into close proximity, thus allowing RNA synthesis to begin in earnest (Filomatori *et al*, 2011). Sequences within the 3′ SL that interact with NS5 are likely involved in correct positioning of SLA to facilitate polymerase translocation to the 3′ end (Hodge *et al*, 2016).

In order to maintain an obstruction-free template for RNA synthesis at this point, it is imperative that additional ribosomes are not loaded onto the ZIKV genome following disengagement of NS5 with the 5′ end. A mechanism by which this may occur is through the circularisation-induced scanning defect seen upon circularised ZIKV minigenome RNAs (Chapter 5). This may also direct the ribosome to translate uORFs, the physiological relevance of which remains to be determined. Alternatively, another NS5 protein may re-engage with the free 5′ end thus preventing ribosome recruitment.

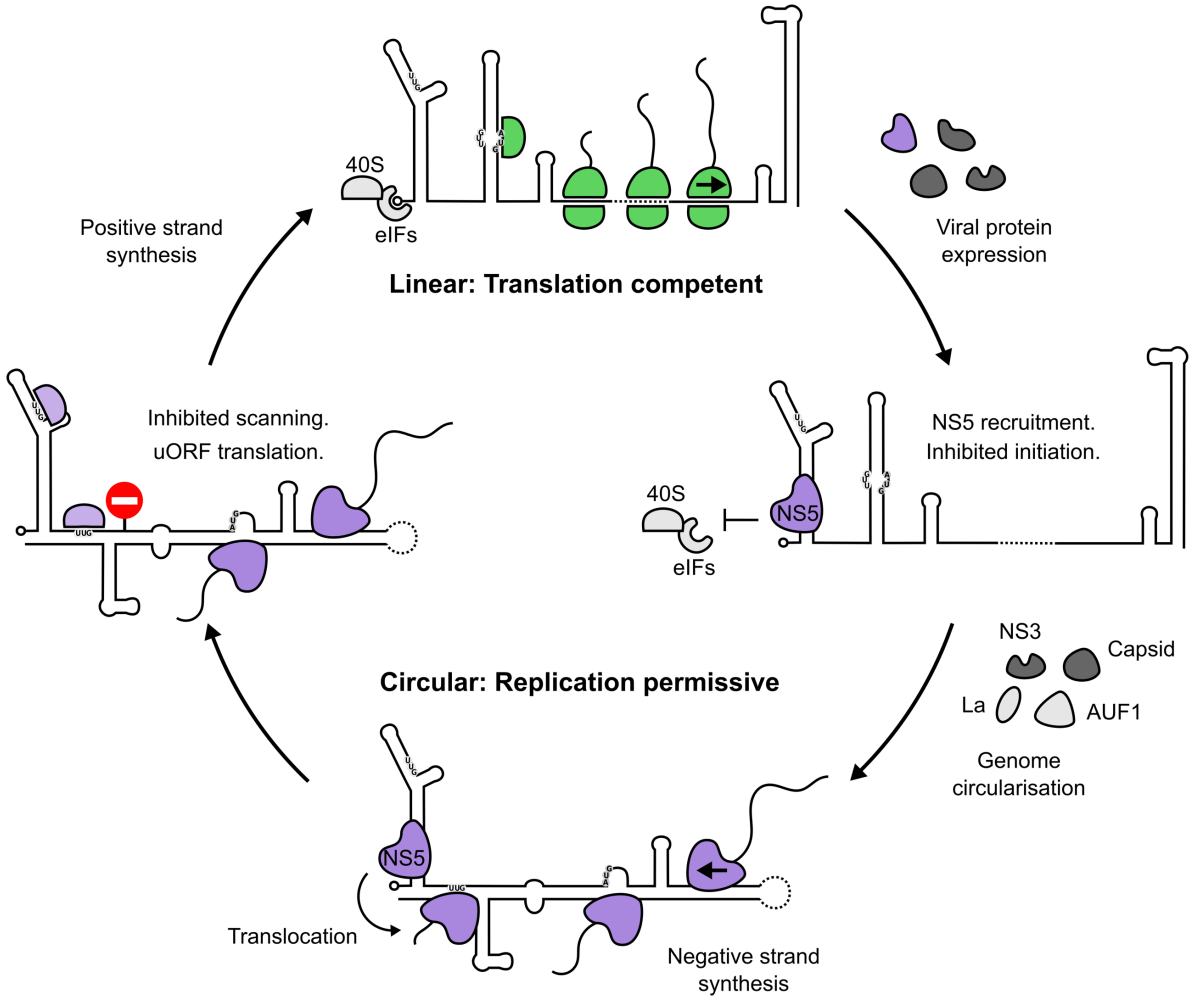

Figure 6.1 Model for the ZIKV translation-replication switch

Linear genomic RNA recruits eIFs and 40S ribosomal subunits in a cap-dependent manner. Secondary structure in the 5′ UTR is effectively resolved by the scanning ribosome to allow efficient translation from the authentic initiation codon, leading to the accumulation of viral proteins. NS5 is subsequently recruited to SLA and antagonises translation initiation, priming the RNA for replication. Following genome circularisation promoted by viral and host factors (Gebhard *et al*, 2012; Ivanyi-Nagy & Darlix, 2012; Friedrich *et al*, 2014, 2018; Vashist *et al*, 2009), NS5 translocates to the 3′ end of the genome to begin negative-strand synthesis. The circularised conformation of the viral genome acts as a barrier to prevent further ribosome loading by impeding scanning ribosomes, indicated by the red stop sign, thus keeping the replicating template free of ribosomes.

It is important to note however that this model simplifies the effect of replication on the conformation of the ZIKV genome. As flavivirus negative-sense RNA is synthesised in a semi-conservative fashion (Wengler *et al*, 1978), a dsRNA intermediate between the positive and negative-strand RNA is formed, theoretically preventing the 3′ cyclisation elements of the positive-strand from interacting with the 5′ end of the same strand during replication. Abrogation of this interaction would release the 5′ end of the genome from circularisation-induced inhibition for further engagement by the translational machinery. However, as

subsequent synthesis of positive-strand RNA from the dsRNA intermediate likely requires the promoter function of SLA (Garcia-Blanco *et al*, 2016), it is conceivable that terminal RNA secondary structures are retained during replication. This could be achieved through unwinding of the dsRNA intermediate by NS3 or other cellular factors that interact with the UTRs, thus permitting the RNA-RNA interactions between the 5′ and 3′ ends of the positive-strand RNA genome to be maintained during replication. A major challenge moving forward lies in the elucidation of RNA structures within these replicative intermediates.

Alternatively, genome circularisation might act only to prevent ribosome loading onto the main ORF during the transition phase between polymerase initiation and elongation described for DENV NS5-mediated replication. Using a short 10 nt DENV RNA corresponding to the 3′ end of the antigenome, it was demonstrated *in vitro* that short dinucleotides (pppAG) are generated before productive elongation begins in a manner dependent upon the NS5 priming loop (Selisko *et al*, 2012; Potisopon *et al*, 2014). This provides a mechanistic basis for the nucleotide conservation at the terminal ends of flaviviral genomes (Selisko *et al*, 2012). The transition phase was shown to be rate-limiting *in vitro* and has been speculated to arise because of conformational changes required within the NS5 RdRp domain to begin elongation (Potisopon *et al*, 2014). Genome circularisation during infection could ensure that the template is kept clear of translating ribosomes while these required conformational changes occur. Then, subsequent rapid polymerase elongation could disrupt the cyclisation elements through formation of a dsRNA intermediate and complete negative-strand synthesis before ribosome loading at the 5′ end can occur. Additional kinetic data regarding the timescale upon which these events take place within the viral replication complex is necessary to properly evaluate these models.

After ZIKV genome replication is completed, the amount of positive-strand genomic template should exceed the relative amount of NS5 protein thus permitting additional rounds of translation initiation. As such, in this model template usage in either translation or replication is driven by oscillations in the relative concentrations of NS5 and viral RNA genome against a background of fairly constant eIF concentration (Figure 6.2). Direct regulation of translation initiation by polymerase recruitment represents an efficient mechanism to temporally regulate genome template usage that may be widespread among positive-sense RNA viruses. While this model has been previously speculated (Garcia-Blanco *et al*, 2016; Friedrich *et al*, 2018), the data presented in this thesis provides the first evidence to support it.

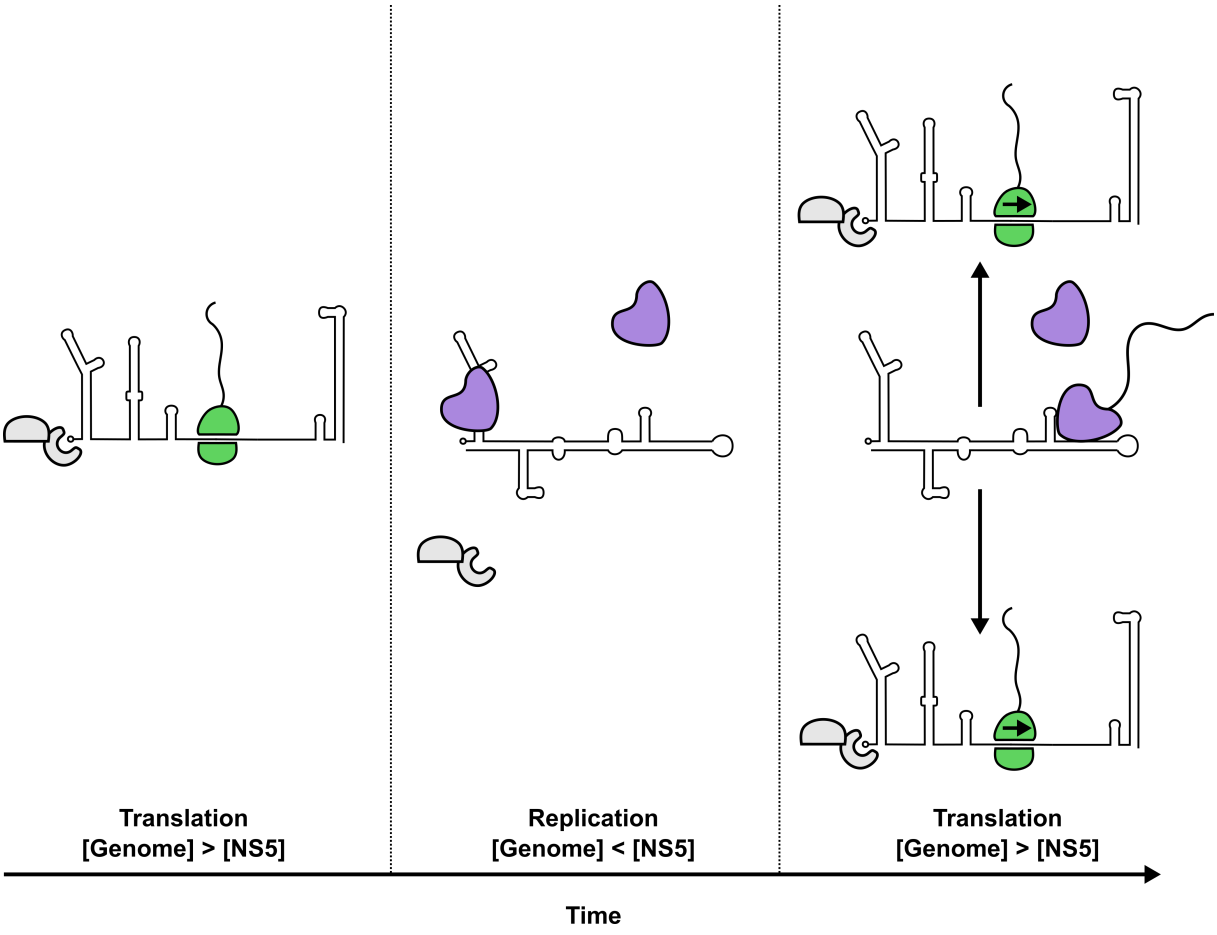

Figure 6.2 ZIKV translation-replication is controlled by oscillations in the relative concentration of NS5 and viral genome

Early in infection, ZIKV genomes are translated and viral proteins accumulate. NS5 accumulation results in recruitment to the viral genome and inhibition of translation initiation. Following successful genome replication, the number of genomes exceeds the relative amount of NS5 thus permitting translation of nascently synthesised genomes. Oscillations in the relative concentrations of NS5 and viral genome could theoretically permit numerous rounds of translation and replication. eIFs and 40S in the process of mRNA recruitment are shown in grey, elongating ribosomes are in green and NS5 is in purple. Arrows illustrate the synthesis of nascent genomes from replicating genomes.

It is clear that the reconstitution system for translation initiation used here provides an effective platform to examine the impact of individual eIFs, RNA secondary structure and protein recruitment on 48S complex assembly in a manner that deconvolutes some of the complex interplay that occurs in cells. However, a series of important questions remain. The mechanism and eIFs required for eIF4E-independent translation of the flavivirus genome during infection remain poorly characterised, although the reconstitution system represents a powerful tool that can be used in the elucidation of this mechanism. Furthermore, additional experiments are required to investigate the precise mechanism of cap-dependent translation inhibition mediated by NS5 recruitment to SLA, whether this be through stabilisation of SLA

structure or occlusion of the eIF4E-cap interaction, as well as the applicability to other flaviviruses. Whether cap- or eIF4E-independent modes of translation facilitate escape from this mode of inhibition also remains to be determined.

Recent in-cell structure mapping studies have identified additional long-range RNA-RNA interactions beyond the well-characterised CS, UAR and DAR elements that occur during ZIKV infection. One such interaction results in an alternative conformation of the 5′ UTR in which SLA and SLB are not formed and instead this region base-pairs with the downstream E coding sequence (Ziv *et al*, 2018; Li *et al*, 2018). Other long-range RNA-RNA interactions have been identified within the coding sequence of ZIKV and DENV that could represent conformational intermediates or stabilising interactions for one genome conformation over another (Huber *et al*, 2019; Li *et al*, 2018). It remains to be determined whether many of these additional long-range RNA-RNA interactions are functionally relevant during infection. Attempting to reconstitute circularisation of the full-length flaviviral genome *in vitro*, while technically challenging, could provide a useful system to examine in more detail the effect of protein binding in mediating conformational changes and the influence of long-range RNA-RNA interactions in stabilising various genome conformations. This could be achieved through recombinant expression and purification of RNA-binding proteins implicated in this process.

While attempts have been made here to characterise the template switch from translation to replication, it is still unclear how template switching from translation/replication to packaging occurs during flavivirus infection. One possibility is that accumulation of the viral C protein could circularise the viral genome to facilitate this switch, driven through its RNA annealing activity (Ivanyi-Nagy & Darlix, 2012). In this regard, C protein-mediated genome circularisation could act in a similar fashion to coat protein binding in bacteriophage genomes, shutting down translation prior to encapsidation (Bernardi & Spahr, 1972). Further work needs to be performed to investigate the lifecycle stage at which the RNA annealing activity of the C protein is required, but it is clear that alterations in viral genome conformation provide an effective method to regulate genome template usage.

Like other positive-sense RNA viruses, the genomes of flaviviruses are highly dynamic structures. This structural plasticity is instrumental in allowing these viruses containing a single RNA species expressing a single polyprotein to infect both mammalian and insect hosts. Detailed mechanistic understanding of how genome template usage is regulated by viral and

cellular proteins as well as RNA structure is essential for the development of novel antivirals against this important class of pathogen.

7 References

Abaeva IS, Marintchev A, Pisareva VP, Hellen CUT & Pestova T V (2011) Bypassing of stems versus linear base-by-base inspection of mammalian mRNAs during ribosomal scanning. *EMBO J.* **30:** 115–29

Abaeva IS, Pestova T V. & Hellen CUT (2016) Attachment of ribosomal complexes and retrograde scanning during initiation on the Halastavi árva virus IRES. *Nucleic Acids Res.* **44:** 2362–2377

Acker MG, Shin B-S, Dever TE & Lorsch JR (2006) Interaction between Eukaryotic Initiation Factors 1A and 5B Is Required for Efficient Ribosomal Subunit Joining. *J. Biol. Chem.* **281:** 8469–8475

Acker MG, Shin BS, Nanda JS, Saini AK, Dever TE & Lorsch JR (2009) Kinetic Analysis of Late Steps of Eukaryotic Translation Initiation. *J. Mol. Biol.* **385:** 491–506

Ackermann M & Padmanabhan R (2001) De Novo Synthesis of RNA by the Dengue Virus RNA-dependent RNA Polymerase Exhibits Temperature Dependence at the Initiation but Not Elongation Phase. *J. Biol. Chem.* **276:** 39926–39937

Acosta EG, Castilla V & Damonte EB (2008) Functional entry of dengue virus into Aedes albopictus mosquito cells is dependent on clathrin-mediated endocytosis. *J. Gen. Virol.* **89:** 474–484

Adams Waldorf KM, Stencel-Baerenwald JE, Kapur RP, Studholme C, Boldenow E, Vornhagen J, Baldessari A, Dighe MK, Thiel J, Merillat S, Armistead B, Tisoncik-Go J, Green RR, Davis MA, Dewey EC, Fairgrieve MR, Gatenby JC, Richards T, Garden GA, Diamond MS, Juul SE, Grant RF, Kuller L, Shaw DWW, Ogle J, Gough GM, Lee W, English C, Hevner RF, Dobyns WB, Gale M & Rajagopal L (2016) Fetal brain lesions after subcutaneous inoculation of Zika virus in a pregnant nonhuman primate. *Nat. Med.* **22:** 1256–1259

Ahlquist P, Noueiry AO, Lee W-M, Kushner DB & Dye BT (2003) Host Factors in Positive-Strand RNA Virus Genome Replication. *J. Virol.* **77:** 8181–8186

Akabayov SR, Akabayov B, Richardson CC & Wagner G (2013) Molecular crowding enhanced ATPase activity of the RNA helicase eIF4A correlates with compaction of its quaternary structure and association with eIF4G. *J. Am. Chem. Soc.* **135:** 10040–10047

Akiyama BM, Laurence HM, Massey AR, Costantino DA, Xie X, Yang Y, Shi P, Nix JC, Beckham JD & Kieft JS (2016) Zika virus produces noncoding RNAs using a multi-pseudoknot structure that confounds a cellular exonuclease. *Science* **354:** 1148–1152

Algire MA, Maag D & Lorsch JR (2005) Pi Release from eIF2, Not GTP Hydrolysis, Is the Step Controlled by Start-Site Selection during Eukaryotic Translation Initiation. *Mol. Cell*

20: 251–262

Alvarez DE, Filomatori C V. & Gamarnik A V. (2008) Functional analysis of dengue virus cyclization sequences located at the 5′ and 3′UTRs. *Virology* **375:** 223–235

Alvarez DE, De Lella Ezcurra AL, Fucito S & Gamarnik A V. (2005a) Role of RNA structures present at the 3′UTR of dengue virus on translation, RNA synthesis, and viral replication. *Virology* **339:** 200–212

Alvarez DE, Lodeiro MF, Ludueña SJ, Pietrasanta LI & Gamarnik A V (2005b) Long-range RNA-RNA interactions circularize the dengue virus genome. *J. Virol.* **79:** 6631–6643

Andersen CBF, Ballut L, Johansen JS, Chamieh H, Nielsen KH, Oliveira CLP, Pedersen JS, Séraphin B, Hir H Le & Andersen GR (2006) Structure of the exon junction core complex with a trapped DEAD-Box ATPase bound to RNA. *Science* **313:** 1968–1972

de Araújo TVB, Rodrigues LC, de Alencar Ximenes RA, de Barros Miranda-Filho D, Montarroyos UR, de Melo APL, Valongueiro S, de Albuquerque M de FPM, Souza WV, Braga C, Filho SPB, Cordeiro MT, Vazquez E, Di Cavalcanti Souza Cruz D, Henriques CMP, Bezerra LCA, da Silva Castanha PM, Dhalia R, Marques-Júnior ETA & Martelli CMT (2016) Association between Zika virus infection and microcephaly in Brazil, January to May, 2016: preliminary report of a case-control study. *Lancet Infect. Dis.* **16:** 1356–1363

de Araújo TVB, Ximenes RA de A, Miranda-Filho D de B, Souza WV, Montarroyos UR, de Melo APL, Valongueiro S, de Albuquerque M de FPM, Braga C, Filho SPB, Cordeiro MT, Vazquez E, Cruz D di CS, Henriques CMP, Bezerra LCA, Castanha PM da S, Dhalia R, Marques-Júnior ETA, Martelli CMT, Rodrigues LC, Dhalia C, Santos M, Cortes F, Kleber de Oliveira W, Evelim Coelho G, Cortez-Escalante JJ, Campelo de Albuquerque de Melo CF, Ramon-Pardo P, Aldighieri S, Mendez-Rico J, Espinal M, Torres L, Nassri Hazin A, Van der Linden A, Coentro M, Santiago Dimech G, Siqueira de Assuncao R, Ismael de Carvalho P & Felix Oliveira V (2018) Association between microcephaly, Zika virus infection, and other risk factors in Brazil: final report of a case-control study. *Lancet Infect. Dis.* **18:** 328–336

Babendure JR, Babendure JL, Ding JH & Tsien RY (2006) Control of mammalian translation by mRNA structure near caps. *Rna* **12:** 851–861

Back SH, Kim YK, Kim WJ, Cho S, Oh HR, Kim J-E & Jang SK (2002) Translation of Polioviral mRNA Is Inhibited by Cleavage of Polypyrimidine Tract-Binding Proteins Executed by Polioviral 3Cpro. *J. Virol.* **76:** 2529–2542

Barrows NJ, Campos RK, Liao K-C, Prasanth KR, Soto-Acosta R, Yeh S-C, Schott-Lerner G, Pompon J, Sessions OM, Bradrick SS & Garcia-Blanco MA (2018) Biochemistry and

Molecular Biology of Flaviviruses. *Chem. Rev.* **118:** 4448–4482

Barrows NJ, Campos RK, Powell ST, Prasanth KR, Schott-Lerner G, Soto-Acosta R, Galarza-Muñoz G, McGrath EL, Urrabaz-Garza R, Gao J, Wu P, Menon R, Saade G, Fernandez-Salas I, Rossi SL, Vasilakis N, Routh A, Bradrick SS & Garcia-Blanco MA (2016) A Screen of FDA-Approved Drugs for Inhibitors of Zika Virus Infection. *Cell Host Microbe* **20:** 259–270

Bartelma G & Padmanabhan R (2002) Expression, purification, and characterization of the RNA 5′-triphosphatase activity of dengue virus type 2 nonstructural protein 3. *Virology* **299:** 122–132

Barton DJ, Morasco BJ & Flanegan JB (1999) Translating ribosomes inhibit poliovirus negative-strand RNA synthesis. *J. Virol.* **73:** 10104–10112

Basu M & Brinton MA (2011) West Nile virus (WNV) genome RNAs with up to three adjacent mutations that disrupt long distance 5′-3′ cyclization sequence basepairs are viable. *Virology* **412:** 220–232

Bazzini AA, Lee MT & Giraldez AJ (2012) Ribosome profiling shows that miR-430 reduces translation before causing mRNA decay in Zebrafish. *Science* **336:** 233–237

Ben-Shem A, Jenner L, Yusupova G & Yusupov M (2010) Crystal structure of the eukaryotic ribosome. *Science* **330:** 1203–1209

Ben-Shem A, De Loubresse NG, Melnikov S, Jenner L, Yusupova G & Yusupov M (2011) The structure of the eukaryotic ribosome at 3.0 Å resolution. *Science* **334:** 1524–1529

Benelli G & Mehlhorn H (2016) Declining malaria, rising of dengue and Zika virus: insights for mosquito vector control. *Parasitol. Res.* **115:** 1747–1754

Bera AK, Kuhn RJ & Smith JL (2007) Functional Characterization of cis and trans Activity of the Flavivirus NS2B-NS3 Protease. *J. Biol. Chem.* **282:** 12883–12892

Bernardi A & Spahr PF (1972) Nucleotide sequence at the binding site for coat protein on RNA of bacteriophage R17. *Proc. Natl. Acad. Sci. U. S. A.* **69:** 3033–7

Berthelot K, Muldoon M, Rajkowitsch L, Hughes J & McCarthy JEG (2004) Dynamics and processivity of 40S ribosome scanning on mRNA in yeast. *Mol. Microbiol.* **51:** 987–1001

Bidet K, Dadlani D & Garcia-Blanco MA (2014) G3BP1, G3BP2 and CAPRIN1 are required for translation of interferon stimulated mRNAs and are targeted by a dengue virus non-coding RNA. *PLoS Pathog.* **10:** e1004242

Bienz K, Egger D & Pasamontes L (1987) Association of Polioviral Proteins of the Viral Replication complex and virus-induces membran synthesis as visualized by electron microscopic immunohistochemistry and autoradiography. *Proteins* **226:** 220–226

Blitvich BJ & Firth AE (2017) A review of flaviviruses that have no known arthropod vector.

Viruses **9:** 154

Bollati M, Alvarez K, Assenberg R, Baronti C, Canard B, Cook S, Coutard B, Decroly E, de Lamballerie X, Gould EA, Grard G, Grimes JM, Hilgenfeld R, Jansson AM, Malet H, Mancini EJ, Mastrangelo E, Mattevi A, Milani M, Moureau G, Neyts J, Owens RJ, Ren J, Selisko B, Speroni S, Steuber H, Stuart DI, Unge T & Bolognesi M (2010) Structure and functionality in flavivirus NS-proteins: Perspectives for drug design. *Antiviral Res.* **87:** 125–148

de Borba L, Villordo SM, Iglesias NG, Filomatori C V., Gebhard LG & Gamarnik A V. (2015) Overlapping Local and Long-Range RNA-RNA Interactions Modulate Dengue Virus Genome Cyclization and Replication. *J. Virol.* **89:** 3430–3437

de Borba L, Villordo SM, Marsico FL, Carballeda JM, Filomatori C V, Gebhard LG, Pallarés HM, Lequime S, Lambrechts L, Sánchez Vargas I, Blair CD & Gamarnik A V (2019) RNA Structure Duplication in the Dengue Virus 3′ UTR: Redundancy or Host Specificity? *MBio* **10:** e02506-18

Bordeleau M-E, Mori A, Oberer M, Lindqvist L, Chard LS, Higa T, Belsham GJ, Wagner G, Tanaka J & Pelletier J (2006) Functional characterization of IRESes by an inhibitor of the RNA helicase eIF4A. *Nat. Chem. Biol.* **2:** 213–220

Bredenbeek PJ, Kooi EA, Lindenbach B, Huijkman N, Rice CM & Spaan WJM (2003) A stable full-length yellow fever virus cDNA clone and the role of conserved RNA elements in flavivirus replication. *J. Gen. Virol.* **84:** 1261–1268

de Breyne S, Yu Y, Unbehaun A, Pestova T V. & Hellen CUT (2009) Direct functional interaction of initiation factor eIF4G with type 1 internal ribosomal entry sites. *Proc. Natl. Acad. Sci.* **106:** 9197–9202

Brinton MA & Dispoto JH (1988) Sequence and secondary structure analysis of the 5′-terminal region of flavivirus genome RNA. *Virology* **162:** 290–299

Brinton MA, Fernandez A V. & Dispoto JH (1986) The 3′-nucleotides of flavivirus genomic RNA form a conserved secondary structure. *Virology* **153:** 113–121

Bujalowski PJ, Bujalowski W & Choi KH (2017) Interactions between the Dengue Virus Polymerase NS5 and Stem-Loop A. *J. Virol.* **91:** e00047-17

Burgui I, Yanguez E, Sonenberg N & Nieto A (2007) Influenza Virus mRNA Translation Revisited: Is the eIF4E Cap-Binding Factor Required for Viral mRNA Translation? *J. Virol.* **81:** 12427–12438

Byk LA, Iglesias NG, De Maio FA, Gebhard LG, Rossi M & Gamarnik A V (2016) Dengue Virus Genome Uncoating Requires Ubiquitination. *MBio* **7:** e00804-16

Byszewska M, Smietański M, Purta E & Bujnicki JM (2014) RNA methyltransferases involved

in 5′ cap biosynthesis. *RNA Biol.* **11:** 1597–1607

Cabantous S, Terwilliger TC & Waldo GS (2005) Protein tagging and detection with engineered self-assembling fragments of green fluorescent protein. *Nat. Biotechnol.* **23:** 102–107

Caliguiri LA & Tamm I (1969) Membranous structures associated with translation and transcription of poliovirus RNA. *Science* **166:** 885–886

Calvet G, Aguiar RS, Melo ASO, Sampaio SA, de Filippis I, Fabri A, Araujo ESM, de Sequeira PC, de Mendonça MCL, de Oliveira L, Tschoeke DA, Schrago CG, Thompson FL, Brasil P, dos Santos FB, Nogueira RMR, Tanuri A & de Filippis AMB (2016) Detection and sequencing of Zika virus from amniotic fluid of fetuses with microcephaly in Brazil: a case study. *Lancet Infect. Dis.* **16:** 653–660

Campos RK, Wong B, Xie X, Lu Y-F, Shi P-Y, Pompon J, Garcia-Blanco MA & Bradrick SS (2017) RPLP1 and RPLP2 Are Essential Flavivirus Host Factors That Promote Early Viral Protein Accumulation. *J. Virol.* **91:** e01706-16

Cao-Lormeau VM, Blake A, Mons S, Lastère S, Roche C, Vanhomwegen J, Dub T, Baudouin L, Teissier A, Larre P, Vial AL, Decam C, Choumet V, Halstead SK, Willison HJ, Musset L, Manuguerra JC, Despres P, Fournier E, Mallet HP, Musso D, Fontanet A, Neil J & Ghawché F (2016) Guillain-Barré Syndrome outbreak associated with Zika virus infection in French Polynesia: A case-control study. *Lancet* **387:** 1531–1539

Cervantes-Salazar M, Angel-Ambrocio AH, Soto-Acosta R, Bautista-Carbajal P, Hurtado-Monzon AM, Alcaraz-Estrada SL, Ludert JE & Del Angel RM (2015) Dengue virus NS1 protein interacts with the ribosomal protein RPL18: This interaction is required for viral translation and replication in Huh-7 cells. *Virology* **484:** 113–126

Chambers TJ, Weir RC, Grakoui A, McCourt DW, Bazan JF, Fletterick RJ & Rice CM (1990) Evidence that the N-terminal domain of nonstructural protein NS3 from yellow fever virus is a serine protease responsible for site-specific cleavages in the viral polyprotein. *Proc. Natl. Acad. Sci. U. S. A.* **87:** 8898–902

Chang JH, Jiao X, Chiba K, Oh C, Martin CE, Kiledjian M & Tong L (2012) Dxo1 is a new type of eukaryotic enzyme with both decapping and 5′-3′ exoribonuclease activity. *Nat. Struct. Mol. Biol.* **19:** 1011–1019

Chapman EG, Moon SL, Wilusz J & Kieft JS (2014) RNA structures that resist degradation by Xrn1 produce a pathogenic Dengue virus RNA. *Elife* **3:** e01892

Chase AJ, Daijogo S & Semler BL (2014) Inhibition of Poliovirus-Induced Cleavage of Cellular Protein PCBP2 Reduces the Levels of Viral RNA Replication. *J. Virol.* **88:** 3192–3201

Chavali PL, Stojic L, Meredith LW, Joseph N, Nahorski MS, Sanford TJ, Sweeney TR, Krishna BA, Hosmillo M, Firth AE, Bayliss R, Marcelis CL, Lindsay S, Goodfellow I, Woods CG & Gergely F (2017) Neurodevelopmental protein Musashi-1 interacts with the Zika genome and promotes viral replication. *Science* **357:** 83–88

Cheung Y-N, Maag D, Mitchell SF, Fekete CA, Algire MA, Takacs JE, Shirokikh N, Pestova T, Lorsch JR & Hinnebusch AG (2007) Dissociation of eIF1 from the 40S ribosomal subunit is a key step in start codon selection in vivo. *Genes Dev.* **21:** 1217–1230

Chiu W, Kinney RM & Dreher TW (2005) Control of Translation by the 5′- and 3′-Terminal Regions of the Dengue Virus Genome. *J. Virol.* **79:** 8303–8315

Chu JJH & Ng ML (2004) Infectious Entry of West Nile Virus Occurs through a Clathrin-Mediated Endocytic Pathway. *J. Virol.* **78:** 10543–10555

Chuang RY, Weaver PL, Liu Z & Chang TH (1997) Requirements of the DEAD-box protein Ded1p for messenger RNA translation. *Science* **275:** 1468–1471

Clyde K, Barrera J & Harris E (2008) The capsid-coding region hairpin element (cHP) is a critical determinant of dengue virus and West Nile virus RNA synthesis. *Virology* **379:** 314–323

Clyde K & Harris E (2006) RNA secondary structure in the coding region of dengue virus type 2 directs translation start codon selection and is required for viral replication. *J. Virol.* **80:** 2170–2182

Cook S & Holmes EC (2006) A multigene analysis of the phylogenetic relationships among the flaviviruses (Family: Flaviviridae) and the evolution of vector transmission. *Arch. Virol.* **151:** 309–325

Cook S, Moureau G, Kitchen A, Gould EA, de Lamballerie X, Holmes EC & Harbach RE (2012) Molecular evolution of the insect-specific flaviviruses. *J. Gen. Virol.* **93:** 223–234

Cortese M, Goellner S, Acosta EG, Neufeldt CJ, Oleksiuk O, Lampe M, Haselmann U, Funaya C, Schieber N, Ronchi P, Schorb M, Pruunsild P, Schwab Y, Chatel-Chaix L, Ruggieri A & Bartenschlager R (2017) Ultrastructural Characterization of Zika Virus Replication Factories. *Cell Rep.* **18:** 2113–2123

Corver J, Lenches E, Smith K, Robison RA, Sando T, Strauss EG & Strauss JH (2003) Fine mapping of a cis-acting sequence element in yellow fever virus RNA that is required for RNA replication and cyclization. *J. Virol.* **77:** 2265–70

Cruz-Oliveira C, Freire JM, Conceição TM, Higa LM, Castanho MARB & Da Poian AT (2015) Receptors and routes of dengue virus entry into the host cells. *FEMS Microbiol. Rev.* **39:** 155–170

Cugola FR, Fernandes IR, Russo FB, Freitas BC, Dias JLM, Guimarães KP, Benazzato C,

Almeida N, Pignatari GC, Romero S, Polonio CM, Cunha I, Freitas CL, Brandaõ WN, Rossato C, Andrade DG, Faria DDP, Garcez AT, Buchpigel CA, Braconi CT, Mendes E, Sall AA, Zanotto PMDA, Peron JPS, Muotri AR & Beltrao-Braga PCBB (2016) The Brazilian Zika virus strain causes birth defects in experimental models. *Nature* **534:** 267–271

Daffis S, Szretter KJ, Schriewer J, Li J, Youn S, Errett J, Lin TY, Schneller S, Zust R, Dong H, Thiel V, Sen GC, Fensterl V, Klimstra WB, Pierson TC, Buller RM, Gale Jr M, Shi PY & Diamond MS (2010) 2′-O methylation of the viral mRNA cap evades host restriction by IFIT family members. *Nature* **468:** 452–456

Deas TS, Bennett CJ, Jones SA, Tilgner M, Ren P, Behr MJ, Stein DA, Iversen PL, Kramer LD, Bernard KA & Shi PY (2007) In vitro resistance selection and in vivo efficacy of morpholino oligomers against west nile virus. *Antimicrob. Agents Chemother.* **51:** 2470–2482

Deas TS, Binduga-Gajewska I, Tilgner M, Ren P, Stein DA, Moulton HM, Iversen PL, Kauffman EB, Kramer LD & Shi P-Y (2005) Inhibition of Flavivirus Infections by Antisense Oligomers Specifically Suppressing Viral Translation and RNA Replication. *J. Virol.* **79:** 4599–4609

Dethoff EA, Boerneke MA, Gokhale NS, Muhire BM, Martin DP, Sacco MT, McFadden MJ, Weinstein JB, Messer WB, Horner SM & Weeks KM (2018) Pervasive tertiary structure in the dengue virus RNA genome. *Proc. Natl. Acad. Sci.* **115:** 11513–11518

Dhote V, Sweeney TR, Kim N, Hellen CUT & Pestova T V. (2012) Roles of individual domains in the function of DHX29, an essential factor required for translation of structured mammalian mRNAs. *Proc. Natl. Acad. Sci.* **109:** E3150–E3159

Djuranovic S, Nahvi A & Green R (2012) miRNA-mediated gene silencing by translational repression followed by mRNA deadenylation and decay. *Science* **336:** 237–240

Dmitriev SE, Terenin IM, Andreev DE, Ivanov PA, Dunaevsky JE, Merrick WC & Shatsky IN (2010) GTP-independent tRNA delivery to the ribosomal P-site by a novel eukaryotic translation factor. *J. Biol. Chem.* **285:** 26779–26787

Dong H, Chang DC, Xie X, Toh YX, Chung KY, Zou G, Lescar J, Lim SP & Shi PY (2010) Biochemical and genetic characterization of dengue virus methyltransferase. *Virology* **405:** 568–578

Dong H, Ray D, Ren S, Zhang B, Puig-Basagoiti F, Takagi Y, Ho CK, Li H & Shi P-Y (2007) Distinct RNA Elements Confer Specificity to Flavivirus RNA Cap Methylation Events. *J. Virol.* **81:** 4412–4421

Dong H, Ren S, Zhang B, Zhou Y, Puig-Basagoiti F, Li H & Shi P-Y (2008a) West Nile Virus

Methyltransferase Catalyzes Two Methylations of the Viral RNA Cap through a Substrate-Repositioning Mechanism. *J. Virol.* **82:** 4295–4307

Dong H, Zhang B & Shi PY (2008b) Terminal structures of West Nile virus genomic RNA and their interactions with viral NS5 protein. *Virology* **381:** 123–135

Dowd KA, Demaso CR, Pelc RS, Diamond MS, Ledgerwood JE, Pierson TC, Dowd KA, Demaso CR, Pelc RS, Speer SD, Smith ARY, Goo L, Platt DJ, Mascola JR, Graham BS, Mulligan MJ, Diamond MS, Ledgerwood JE & Pierson TC (2016) Broadly Neutralizing Activity of Zika Virus-Immune Sera Identifies a Single Viral Serotype Report Broadly Neutralizing Activity of Zika Virus-Immune Sera Identifies a Single Viral Serotype. *CellReports* **16:** 1485–1491

Driggers RW, Ho C-Y, Korhonen EM, Kuivanen S, Jääskeläinen AJ, Smura T, Rosenberg A, Hill DA, DeBiasi RL, Vezina G, Timofeev J, Rodriguez FJ, Levanov L, Razak J, Iyengar P, Hennenfent A, Kennedy R, Lanciotti R, du Plessis A & Vapalahti O (2016) Zika Virus Infection with Prolonged Maternal Viremia and Fetal Brain Abnormalities. *N. Engl. J. Med.* **374:** 2142–2151

Edgil D & Harris E (2006) End-to-end communication in the modulation of translation by mammalian RNA viruses. *Virus Res.* **119:** 43–51

Edgil D, Polacek C & Harris E (2006) Dengue Virus Utilizes a Novel Strategy for Translation Initiation When Cap-Dependent Translation Is Inhibited. *J. Virol.* **80:** 2976–2986

Egloff MP, Benarroch D, Selisko B, Romette JL & Canard B (2002) An RNA cap (nucleoside-2 ’-O-)-methyltransferase in the flavivirus RNA polymerase NS5: crystal structure and functional characterization. *EMBO J.* **21:** 2757–2768

Elgner F, Sabino C, Basic M, Ploen D, Grünweller A & Hildt E (2018) Inhibition of Zika Virus Replication by Silvestrol. *Viruses* **10:** 149

Erbel P, Schiering N, D’Arcy A, Renatus M, Kroemer M, Lim SP, Yin Z, Keller TH, Vasudevan SG & Hommel U (2006) Structural basis for the activation of flaviviral NS3 proteases from dengue and West Nile virus. *Nat. Struct. Mol. Biol.* **13:** 372–373

Evstafieva AG, Ugarova TY, Chernov BK & Shatsky IN (1991) A complex RNA sequence detemines the internal initiation of encephalomyocarditis virus RNA translation. *Nucleic Acids Res.* **19:** 665–671

Fabian MR & White KA (2004) 5′-3′ RNA-RNA Interaction Facilitates Cap- and Poly(A) Tail-independent Translation of Tomato Bushy Stunt Virus mRNA. *J. Biol. Chem.* **279:** 28862–28872

Falgout B, Pethel M, Zhang YM & Lai CJ (1991) Both nonstructural proteins NS2B and NS3 are required for the proteolytic processing of dengue virus nonstructural proteins. *J. Virol.*

65: 2467–75

Fernández-Sanlés A, Ríos-Marco P, Romero-López C & Berzal-Herranz A (2017) Functional information stored in the conserved structural RNA domains of flavivirus genomes. *Front. Microbiol.* **8:** 546

Filomatori C V., Carballeda JM, Villordo SM, Aguirre S, Pallarés HM, Maestre AM, Sánchez-Vargas I, Blair CD, Fabri C, Morales MA, Fernandez-Sesma A & Gamarnik A V. (2017) Dengue virus genomic variation associated with mosquito adaptation defines the pattern of viral non-coding RNAs and fitness in human cells. *PLoS Pathog.* **13:** e1006265

Filomatori C V., Iglesias NG, Villordo SM, Alvarez DE & Gamarnik A V. (2011) RNA sequences and structures required for the recruitment and activity of the dengue virus polymerase. *J. Biol. Chem.* **286:** 6929–6939

Filomatori C V., Lodeiro MF, Alvarez DE, Samsa MM, Pietrasanta L & Gamarnik A V. (2006) A 5' RNA element promotes dengue virus RNA synthesis on a circular genome. *Genes Dev.* **20:** 2238–2249

Fleith RC, Mears H V, Leong XY, Sanford TJ, Emmott E, Graham SC, Mansur DS & Sweeney TR (2018) IFIT3 and IFIT2/3 promote IFIT1-mediated translation inhibition by enhancing binding to non-self RNA. *Nucleic Acids Res.* **46:** 5269–5285

Forgac M (2007) Vacuolar ATPases: Rotary proton pumps in physiology and pathophysiology. *Nat. Rev. Mol. Cell Biol.* **8:** 917–929

Fricke M, Dünnes N, Zayas M, Bartenschlager R, Niepmann M & Marz M (2015) Conserved RNA secondary structures and long-range interactions in hepatitis C viruses. *Rna* **21:** 1219–1232

Friebe P & Harris E (2010) Interplay of RNA elements in the dengue virus 5' and 3' ends required for viral RNA replication. *J. Virol.* **84:** 6103–6118

Friebe P, Shi P-Y & Harris E (2011) The 5' and 3' Downstream AUG Region Elements Are Required for Mosquito-Borne Flavivirus RNA Replication. *J. Virol.* **85:** 1900–1905

Friedrich S, Engelmann S, Schmidt T, Szczepankiewicz G, Bergs S, Liebert UG, Kümmerer BM, Golbik RP & Behrens S-E (2018) The Host Factor AUF1 p45 Supports Flavivirus Propagation by Triggering the RNA Switch Required for Viral Genome Cyclization. *J. Virol.* **92:** e01647-17

Friedrich S, Schmidt T, Geissler R, Lilie H, Chabierski S, Ulbert S, Liebert UG, Golbik RP & Behrens S-E (2014) AUF1 p45 Promotes West Nile Virus Replication by an RNA Chaperone Activity That Supports Cyclization of the Viral Genome. *J. Virol.* **88:** 11586–11599

Funk A, Truong K, Nagasaki T, Torres S, Floden N, Balmori Melian E, Edmonds J, Dong H,

Shi P-Y & Khromykh AA (2010) RNA Structures Required for Production of Subgenomic Flavivirus RNA. *J. Virol.* **84:** 11407–11417

Furic L, Rong L, Larsson O, Koumakpayi IH, Yoshida K, Brueschke A, Petroulakis E, Robichaud N, Pollak M, Gaboury LA, Pandolfi PP, Saad F & Sonenberg N (2010) eIF4E phosphorylation promotes tumorigenesis and is associated with prostate cancer progression. *Proc. Natl. Acad. Sci.* **107:** 14134–14139

Galicia-Vázquez G, Cencic R, Robert F, Agenor AQ & Pelletier J (2012) A cellular response linking eIF4AI activity to eIF4AII transcription. *Rna* **18:** 1373–1384

Galicia-Vázquez G, Di Marco S, Lian XJ, Ma JF, Gallouzi IE & Pelletier J (2014) Regulation of eukaryotic initiation factor 4AII by MyoD during murine myogenic cell differentiation. *PLoS One* **9:** e87237

Gamarnik A V. & Andino R (1998) Switch from translation to RNA replication in a positive-stranded RNA virus. *Genes Dev.* **12:** 2293–2304

Garcia-Blanco MA, Vasudevan SG, Bradrick SS & Nicchitta C (2016) Flavivirus RNA transactions from viral entry to genome replication. *Antiviral Res.* **134:** 244–249

García-García C, Frieda KL, Feoktistova K, Fraser CS & Block SM (2015) Factor-dependent processivity in human eIF4A DEAD-box helicase. *Science* **348:** 1486–1488

García-Montalvo BM, Medina F & Del Angel RM (2004) La protein binds to NS5 and NS3 and to the 5′ and 3′ ends of Dengue 4 virus RNA. *Virus Res.* **102:** 141–150

Gazo BM, Murphy P, Gatchel JR & Browning KS (2004) A Novel Interaction of Cap-binding Protein Complexes Eukaryotic Initiation Factor (eIF) 4F and eIF(iso)4F with A Region in the 3′-Untranslated Region of Satellite Tobacco Necrosis Virus. *J. Biol. Chem.* **279:** 13584–13592

Gebauer F & Hentze MW (2004) Molecular mechanisms of translational control. *Nat. Rev. Mol. Cell Biol.* **5:** 827–835

Gebhard LG, Filomatori C V. & Gamarnik A V. (2011) Functional RNA elements in the dengue virus genome. *Viruses* **3:** 1739–1756

Gebhard LG, Kaufman SB & Gamarnik A V. (2012) Novel ATP-independent RNA annealing activity of the dengue virus NS3 helicase. *PLoS One* **7:** e36244

des Georges A, Dhote V, Kuhn L, Hellen CUT, Pestova T V, Frank J & Hashem Y (2015) Structure of mammalian eIF3 in the context of the 43S preinitiation complex. *Nature* **525:** 491–495

Godoy AS, Lima GMA, Oliveira KIZ, Torres NU, Maluf F V., Guido RVC & Oliva G (2017) Crystal structure of Zika virus NS5 RNA-dependent RNA polymerase. *Nat. Commun.* **8:** 14764

Göertz GP, Abbo SR, Fros JJ & Pijlman GP (2018) Functional RNA during Zika virus infection. *Virus Res.* **254:** 41–53

Gokhale NS, McIntyre ABR, McFadden MJ, Roder AE, Kennedy EM, Gandara JA, Hopcraft SE, Quicke KM, Vazquez C, Willer J, Ilkayeva OR, Law BA, Holley CL, Garcia-Blanco MA, Evans MJ, Suthar MS, Bradrick SS, Mason CE & Horner SM (2016) N6-Methyladenosine in Flaviviridae Viral RNA Genomes Regulates Infection. *Cell Host Microbe* **20:** 654–665

Gradi A, Svitkin Y V, Imataka H & Sonenberg N (1998) Proteolysis of human eukaryotic translation initiation factor eIF4GII, but not eIF4GI, coincides with the shutoff of host protein synthesis after poliovirus infection. *Proc. Natl. Acad. Sci. U. S. A.* **95:** 11089–11094

Grant A, Ponia SS, Tripathi S, Balasubramaniam V, Miorin L, Sourisseau M, Schwarz MC, Sánchez-Seco MP, Evans MJ, Best SM & García-Sastre A (2016) Zika Virus Targets Human STAT2 to Inhibit Type i Interferon Signaling. *Cell Host Microbe* **19:** 882–890

Gray NK & Hentze MW (1994) Iron regulatory protein prevents binding of the 43S translation pre-initiation complex to ferritin and eALAS mRNAs. *EMBO J.* **13:** 3882–91

Gross JD, Moerke NJ, von der Haar T, Lugovskoy AA, Sachs AB, Mccarthy JEG & Wagner G (2003) Ribosome Loading onto the mRNA Cap Is Driven by Conformational Coupling between eIF4G and eIF4E University of California at Berkeley. *Cell* **115:** 739–750

Guo L, Allen EM & Miller WA (2001) Base-Pairing between Untranslated Regions Facilitates Translation of Uncapped , Nonpolyadenylated Viral RNA. *Mol. Cell* **7:** 1103–1109

Guyatt KJ, Westaway EG & Khromykh AA (2001) Expression and purification of enzymatically active recombinant RNA-dependent RNA polymerase (NS5) of the flavivirus Kunjin. *J. Virol. Methods* **92:** 37–44

Guzman MG, Alvarez M & Halstead SB (2013) Secondary infection as a risk factor for dengue hemorrhagic fever/dengue shock syndrome: An historical perspective and role of antibody-dependent enhancement of infection. *Arch. Virol.* **158:** 1445–1459

Von Der Haar T, Gross JD, Wagner G & McCarthy JEG (2004) The mRNA cap-binding protein eIF4E in post-transcriptional gene expression. *Nat. Struct. Mol. Biol.* **11:** 503–511

Haddow AD, Schuh AJ, Yasuda CY, Kasper MR, Heang V, Huy R, Guzman H, Tesh RB & Weaver SC (2012) Genetic characterization of zika virus strains: Geographic expansion of the asian lineage. *PLoS Negl. Trop. Dis.* **6:** e1477

Hahn CS, Hahn YS, Rice CM, Lee E, Dalgarno L, Strauss EG & Strauss JH (1987) Conserved elements in the 3′ untranslated region of flavivirus RNAs and potential cyclization sequences. *J. Mol. Biol.* **198:** 33–41

Halstead SB & O'Rourke EJ (1977) Antibody-enhanced dengue virus infection in primate leukocytes. *Nature* **265:** 739–741

Hamel R, Dejarnac O, Wichit S, Ekchariyawat P, Neyret A, Luplertlop N, Perera-Lecoin M, Surasombatpattana P, Talignani L, Thomas F, Cao-Lormeau V-M, Choumet V, Briant L, Desprès P, Amara A, Yssel H & Missé D (2015) Biology of Zika Virus Infection in Human Skin Cells. *J. Virol.* **89:** 8880–8896

Hashem Y, Des Georges A, Dhote V, Langlois R, Liao HY, Grassucci RA, Hellen CUT, Pestova T V. & Frank J (2013a) Structure of the mammalian ribosomal 43S preinitiation complex bound to the scanning factor DHX29. *Cell* **153:** 1108–1119

Hashem Y, des Georges A, Dhote V, Langlois R, Liao HY, Grassucci RA, Pestova T V, Hellen CUT & Frank J (2013b) Hepatitis-C-virus-like internal ribosome entry sites displace eIF3 to gain access to the 40S subunit. *Nature* **503:** 539–543

Hellen CUT (2009) IRES-induced conformational changes in the ribosome and the mechanism of translation initiation by internal ribosomal entry. *Biochim. Biophys. Acta - Gene Regul. Mech.* **1789:** 558–570

Herdy B, Jaramillo M, Svitkin Y V, Rosenfeld AB, Kobayashi M, Walsh D, Alain T, Sean P, Robichaud N, Topisirovic I, Furic L, Dowling RJO, Sylvestre A, Rong L, Colina R, Costa-Mattioli M, Fritz JH, Olivier M, Brown E, Mohr I & Sonenberg N (2012) Translational control of the activation of transcription factor NF-κB and production of type I interferon by phosphorylation of the translation factor eIF4E. *Nat. Immunol.* **13:** 543–550

Herold J & Andino R (2001) Poliovirus RNA replication requires genome circularization through a protein-protein bridge. *Mol. Cell* **7:** 581–591

Hinnebusch AG & Lorsch JR (2012) The mechanism of eukaryotic translation initiation: New insights and challenges. *Cold Spring Harb. Perspect. Biol.* **4:** a011544

Hodge K, Tunghirun C, Kamkaew M, Limjindaporn T, Yenchitsomanus PT & Chimnaronk S (2016) Identification of a conserved RNA-dependent RNA polymerase (RdRp)-RNA interface required for flaviviral replication. *J. Biol. Chem.* **291:** 17437–17449

Hoenen A, Liu W, Kochs G, Khromykh AA & Mackenzie JM (2007) West Nile virus-induced cytoplasmic membrane structures provide partial protection against the interferon-induced antiviral MxA protein. *J. Gen. Virol.* **88:** 3013–3017

Holden KL & Harris E (2004) Enhancement of dengue virus translation: Role of the 3' untranslated region and the terminal 3' stem-loop domain. *Virology* **329:** 119–133

Holden KL, Stein DA, Pierson TC, Ahmed AA, Clyde K, Iversen PL & Harris E (2006) Inhibition of dengue virus translation and RNA synthesis by a morpholino oligomer targeted to the top of the terminal 3′ stem-loop structure. *Virology* **344:** 439–452

Huang YJS, Higgs S, Horne KME & Vanlandingham DL (2014) Flavivirus-Mosquito interactions. *Viruses* **6:** 4703–4730

Huber RG, Lim XN, Ng WC, Sim AYL, Poh HX, Shen Y, Lim SY, Sundstrom KB, Sun X, Aw JG, Too HK, Boey PH, Wilm A, Chawla T, Choy MM, Jiang L, de Sessions PF, Loh XJ, Alonso S, Hibberd M, Nagarajan N, Ooi EE, Bond PJ, Sessions OM & Wan Y (2019) Structure mapping of dengue and Zika viruses reveals functional long-range interactions. *Nat. Commun.* **10:** 1408

Iglesias NG, Filomatori C V. & Gamarnik A V. (2011) The F1 Motif of Dengue Virus Polymerase NS5 Is Involved in Promoter-Dependent RNA Synthesis. *J. Virol.* **85:** 5745–5756

Imataka H, Gradi A & Sonenberg N (1998) A newly identified N-terminal amino acid sequence of human eIF4G binds poly(A)-binding protein and functions in poly(A)-dependent translation. *EMBO J.* **17:** 7480–7489

Imperato PJ (2016) The Convergence of a Virus , Mosquitoes , and Human Travel in Globalizing the Zika Epidemic. *J. Community Health* **41:** 674–679

Irigoyen N, Dinan AM, Meredith LW, Goodfellow I, Brierley I & Firth AE (2017) The translational landscape of Zika virus during infection of mammalian and insect cells. *bioRxiv***:** 112904

Irurzun A, Perez L & Carrasco L (1992) Involvement of membrane traffic in the replication of poliovirus genomes: Effects of brefeldin A. *Virology* **191:** 166–175

Issur M, Geiss BJ, Bougie I, Picard-Jean F, Despins S, Mayette J, Hobdey SE & Bisaillon M (2009) The flavivirus NS5 protein is a true RNA guanylyltransferase that catalyzes a two-step reaction to form the RNA cap structure. *Rna* **15:** 2340–2350

Ivanyi-Nagy R & Darlix JL (2012) Core protein-mediated 5'-3' annealing of the West Nile virus genomic RNA in vitro. *Virus Res.* **169:** 448–457

Jackson RJ (1991) The ATP requirement for initiation of eukaryotic translation varies according to the mRNA species. *Eur. J. Biochem.* **200:** 285–294

Jackson RJ, Hellen CUT & Pestova T V (2010) The mechanism of eukaryotic translation initiation and principles of its regulation. *Nat. Rev. Mol. Cell Biol.* **11:** 113–127

Jang SK, Kräusslich HG, Nicklin MJ, Duke GM, Palmenberg AC & Wimmer E (1988) A segment of the 5' nontranslated region of encephalomyocarditis virus RNA directs internal entry of ribosomes during in vitro translation. *J. Virol.* **62:** 2636–2643

Javorovic M, Pohla H, Frankenberger B, Wölfel T & Schendel DJ (2005) RNA Transfer by Electroporation into Mature Dendritic Cells Leading to Reactivation of Effector-Memory Cytotoxic T Lymphocytes: A Quantitative Analysis. *Mol. Ther.* **12:** 734–743

Jennings MD & Pavitt GD (2010) eIF5 has GDI activity necessary for translational control by eIF2 phosphorylation. *Nature* **465:** 378–381

Jiao X, Chang JH, Kilic T, Tong L & Kiledjian M (2013) A Mammalian Pre-mRNA 5' End Capping Quality Control Mechanism and an Unexpected Link of Capping to Pre-mRNA Processing. *Mol. Cell* **50:** 104–115

Johnson B, VanBlargan LA, Xu W, White JP, Shan C, Shi PY, Zhang R, Adhikari J, Gross ML, Leung DW, Diamond MS & Amarasinghe GK (2018) Human IFIT3 Modulates IFIT1 RNA Binding Specificity and Protein Stability. *Immunity* **48:** 487–499

Junjhon J, Pennington JG, Edwards TJ, Perera R, Lanman J & Kuhn RJ (2014) Ultrastructural Characterization and Three-Dimensional Architecture of Replication Sites in Dengue Virus-Infected Mosquito Cells. *J. Virol.* **88:** 4687–4697

Kahvejian A, Roy G & Sonenberg N (2001) The mRNA closed-loop model: The function of PABP and PABP-interacting proteins in mRNA translation. *Cold Spring Harb. Symp. Quant. Biol.* **66:** 293–300

Kamkaew M & Chimnaronk S (2015) Characterization of soluble RNA-dependent RNA polymerase from dengue virus serotype 2: The polyhistidine tag compromises the polymerase activity. *Protein Expr. Purif.* **112:** 43–49

Kang S, Shields AR, Jupatanakul N & Dimopoulos G (2014) Suppressing Dengue-2 Infection by Chemical Inhibition of Aedes aegypti Host Factors. *PLoS Negl. Trop. Dis.* **8:** e3084

Kapp LD & Lorsch JR (2004) GTP-dependent Recognition of the Methionine Moiety on Initiator tRNA by Translation Factor eIF2. *J. Mol. Biol.* **335:** 923–936

Khatter H, Myasnikov AG, Natchiar SK & Klaholz BP (2015) Structure of the human 80S ribosome. *Nature* **520:** 640–645

Khromykh A a, Meka H, Guyatt KJ & Westaway EG (2001a) Essential Role of Cyclization Sequences in Flavivirus RNA Replication. *J. Virol.* **75:** 6719–6728

Khromykh AA, Varnavski AN, Sedlak PL & Westaway EG (2001b) Coupling between Replication and Packaging of Flavivirus RNA: Evidence Derived from the Use of DNA-Based Full-Length cDNA Clones of Kunjin Virus. *J. Virol.* **75:** 4633–4640

Kieft JS, Rabe JL & Chapman EG (2015) New hypotheses derived from the structure of a flaviviral Xrn1-resistant RNA: Conservation, folding, and host adaptation. *RNA Biol.* **12:** 1117–1169

Kinney RM, Huang CY, Rose BC, Kroeker AD, Dreher TW, Iversen PL & Stein DA (2005) Inhibition of Dengue Virus Serotypes 1 to 4 in Vero Cell Cultures with Morpholino Oligomers. *J. Virol.* **79:** 5116–5128

Klema VJ, Ye M, Hindupur A, Teramoto T, Gottipati K, Padmanabhan R & Choi KH (2016)

Dengue Virus Nonstructural Protein 5 (NS5) Assembles into a Dimer with a Unique Methyltransferase and Polymerase Interface. *PLoS Pathog.* **12:** e1005451

Klumpp S, Scott M, Pedersen S & Hwa T (2013) Molecular crowding limits translation and cell growth. *Proc. Natl. Acad. Sci.* **110:** 16754–16759

Kolakofsky D & Weissmann C (1971) Possible Mechanism for Transition of Viral RNA from Polysome to Replication Complex. *Nat. New Biol.* **231:** 42–46

Kolupaeva VG, Lomakin IB, Pestova T V. & Hellen CUT (2003) Eukaryotic Initiation Factors 4G and 4A Mediate Conformational Changes Downstream of the Initiation Codon of the Encephalomyocarditis Virus Internal Ribosomal Entry Site. *Mol. Cell. Biol.* **23:** 687–698

Kolupaeva VG, Unbehaun A, Lomakin IB, Hellen CUT & Pestova T V. (2005) Binding of eukaryotic initiation factor 3 to ribosomal 40S subunits and its role in ribosomal dissociation and anti-association. *Rna* **11:** 470–486

Kondrashov N, Pusic A, Stumpf CR, Shimizu K, Hsieh AC, Xue S, Ishijima J, Shiroishi T & Barna M (2011) Ribosome-Mediated Specificity in Hox mRNA Translation and Vertebrate Tissue Patterning. *Cell* **145:** 383–397

Kostyuchenko VA, Lim EXY, Zhang S, Fibriansah G, Ng TS, Ooi JSG, Shi J & Lok SM (2016) Structure of the thermally stable Zika virus. *Nature* **533:** 425–428

Kozak M (1989a) The scanning model for translation:an update. *J. Cell Biol.* **108:** 229–241

Kozak M (1989b) Circumstances and mechanisms of inhibition of translation by secondary structure in eucaryotic mRNAs. *Mol. Cell. Biol.* **9:** 5134–42

Kozak M (1990) Downstream secondary structure facilitates recognition of initiator codons by eukaryotic ribosomes. *Proc. Natl. Acad. Sci.* **87:** 8301–8305

Kozak M (1991) Structural features in eukaryotic mRNAs that modulate the initiation of translation. *J. Biol. Chem.* **266:** 19867–19870

Kuhn RJ, Zhang W, Rossmann MG, Pletnev S V., Corver J, Lenches E, Jones CT, Mukhopadhyay S, Chipman PR, Strauss EG, Baker TS & Strauss JH (2002) Structure of dengue virus: Implications for flavivirus organization, maturation, and fusion. *Cell* **108:** 717–725

Kumar A, Airo AM, Hou S, Hobman TC, Limonta D, Mancinelli V, Power C & Branton W (2016a) Zika virus inhibits type-I interferon production and downstream signaling. *EMBO Rep.* **17:** 1766–1775

Kumar P, Hellen CUT & Pestova T V (2016b) Toward the mechanism of eIF4F-mediated ribosomal attachment to mammalian capped mRNAs. *Genes Dev* **30:** 1573–1588

Kumar P, Sweeney TR, Skabkin MA, Skabkina O V., Hellen CUT & Pestova T V. (2014) Inhibition of translation by IFIT family members is determined by their ability to interact

selectively with the 5'-terminal regions of cap0-, cap1- and 5'ppp- mRNAs. *Nucleic Acids Res.* **42:** 3228–3245

Kuno G (2007) Host range specificity of flaviviruses: correlation with in vitro replication. *J. Med. Entomol.* **44:** 93–101

Kuno G, Chang GJ, Tsuchiya KR, Karabatsos N & Cropp CB (1998) Phylogeny of the genus Flavivirus. *J. Virol.* **72:** 73–83

Kwan T & Thompson SR (2019) Noncanonical Translation Initiation in Eukaryotes. *Cold Spring Harb. Perspect. Biol.***:** a032672

Laemmli UK (1970) Cleavage of Structural Proteins during the Assembly of the Head of Bacteriophage T4. *Nature* **227:** 680–685

Lee ASY, Kranzusch PJ & Cate JHD (2015) EIF3 targets cell-proliferation messenger RNAs for translational activation or repression. *Nature* **522:** 111–114

Lee ASY, Kranzusch PJ, Doudna JA & Cate JHD (2016) EIF3d is an mRNA cap-binding protein that is required for specialized translation initiation. *Nature* **536:** 96–99

Leija-Martínez N, Casas-Flores S, Cadena-Nava RD, Roca JA, Mendez-Cabañas JA, Gomez E & Ruiz-Garcia J (2014) The separation between the 5'-3' ends in long RNA molecules is short and nearly constant. *Nucleic Acids Res.* **42:** 13963–13968

Li C, Zhu X, Ji X, Quanquin N, Deng YQ, Tian M, Aliyari R, Zuo X, Yuan L, Afridi SK, Li XF, Jung JU, Nielsen-Saines K, Qin FXF, Qin CF, Xu Z & Cheng G (2017) Chloroquine, a FDA-approved Drug, Prevents Zika Virus Infection and its Associated Congenital Microcephaly in Mice. *EBioMedicine* **24:** 189–194

Li P, Wei Y, Mei M, Tang L, Sun L, Huang W, Zhou J, Zou C, Zhang S, Qin CF, Jiang T, Dai J, Tan X & Zhang QC (2018) Integrative Analysis of Zika Virus Genome RNA Structure Reveals Critical Determinants of Viral Infectivity. *Cell Host Microbe* **24:** 875–886

Li W & Brinton MA (2001) The 3′ stem loop of the West Nile virus genomic RNA can suppress translation of chimeric mRNAs. *Virology* **287:** 49–61

Li XF, Jiang T, Yu XD, Deng YQ, Zhao H, Zhu QY, Qin E De & Qin CF (2010) RNA elements within the 5′ untranslated region of the West Nile virus genome are critical for RNA synthesis and virus replication. *J. Gen. Virol.* **91:** 1218–1223

Liang G, Gao X & Gould EA (2015) Factors responsible for the emergence of arboviruses; strategies, challenges and limitations for their control. *Emerg. Microbes Infect.* **4:** e18

Lichinchi G, Zhao BS, Wu Y, Lu Z, Qin Y, He C & Rana TM (2016) Dynamics of Human and Viral RNA Methylation during Zika Virus Infection. *Cell Host Microbe* **20:** 666–673

Lim SP, Noble CG, Seh CC, Soh TS, El Sahili A, Chan GKY, Lescar J, Arora R, Benson T, Nilar S, Manjunatha U, Wan KF, Dong H, Xie X, Shi PY & Yokokawa F (2016) Potent

Allosteric Dengue Virus NS5 Polymerase Inhibitors: Mechanism of Action and Resistance Profiling. *PLoS Pathog.* **12:** e1005737

Lin K-C, Chang H-L & Chang R-Y (2004) Accumulation of a 3'-Terminal Genome Fragment in Japanese Encephalitis Virus-Infected Mammalian and Mosquito Cells. *J. Virol.* **78:** 5133–5138

Lindenbach BD & Rice CM (1999) Genetic interaction of flavivirus nonstructural proteins NS1 and NS4A as a determinant of replicase function. *J. Virol.* **73:** 4611–4621

Liu N (2015) Insecticide Resistance in Mosquitoes: Impact, Mechanisms, and Research Directions. *Annu. Rev. Entomol.* **60:** 537–559

Liu Z-Y, Li X-F, Jiang T, Deng Y-Q, Ye Q, Zhao H, Yu J-Y & Qin C-F (2016) Viral RNA switch mediates the dynamic control of flavivirus replicase recruitment by genome cyclization. *Elife* **5:** e17636

Liu Z-Y, Li X-F, Jiang T, Deng Y-Q, Zhao H, Wang H-J, Ye Q, Zhu S-Y, Qiu Y, Zhou X, Qin E-D & Qin C-F (2013) Novel cis-Acting Element within the Capsid-Coding Region Enhances Flavivirus Viral-RNA Replication by Regulating Genome Cyclization. *J. Virol.* **87:** 6804–6818

Llácer JL, Hussain T, Saini AK, Nanda JS, Kaur S, Gordiyenko Y, Kumar R, Hinnebusch AG, Lorsch JR & Ramakrishnan V (2018) Translational initiation factor eIF5 replaces eIF1 on the 40S ribosomal subunit to promote start-codon recognition. *Elife* **7:** e39273

Lo MK, Tilgner M, Bernard KA & Shi P (2003) Functional Analysis of Mosquito-Borne Flavivirus Conserved Sequence Elements within 3 J Untranslated Region of West Nile Virus by Use of a Reporting Replicon That Differentiates between Viral Translation and RNA Replication. *J. Virol.* **77:** 10004–10014

Locker N, Easton LE & Lukavsky PJ (2007) HCV and CSFV IRES domain II mediate eIF2 release during 80S ribosome assembly. *EMBO J.* **26:** 795–805

Lodeiro MF, Filomatori C V. & Gamarnik A V. (2009) Structural and Functional Studies of the Promoter Element for Dengue Virus RNA Replication. *J. Virol.* **83:** 993–1008

Lomakin IB, Hellen CUT & Pestova T V (2000) Physical association of eukaryotic initiation factor 4G (eIF4G) with eIF4A strongly enhances binding of eIF4G to the internal ribosomal entry site of encephalomyocarditis virus and is required for internal initiation of translation. *Mol. Cell. Biol.* **20:** 6019–6029

Lomakin IB, Kolupaeva VG, Marintchev A, Wagner G & Pestova T V (2003) Position of eukaryotic initiation factor eIF1 on the 40S ribosomal subunit determined by directed hydroxyl radical probing. *Genes Dev.* **17:** 2786–2797

Lomakin IB, Shirokikh NE, Yusupov MM, Hellen CUT & Pestova T V. (2006) The fidelity of

translation initiation: Reciprocal activities of elF1, IF3 and YciH. *EMBO J.* **25:** 196–210

Lomakin IB, Stolboushkina EA, Vaidya AT, Zhao C, Garber MB, Dmitriev SE & Steitz TA (2017) Crystal Structure of the Human Ribosome in Complex with DENR-MCT-1. *Cell Rep.* **20:** 521–528

Lozano G & Martínez-Salas E (2015) Structural insights into viral IRES-dependent translation mechanisms. *Curr. Opin. Virol.* **12:** 113–120

Ma XM & Blenis J (2009) Molecular mechanisms of mTOR-mediated translational control. *Nat. Rev. Mol. Cell Biol.* **10:** 307–318

Maag D, Algire MA & Lorsch JR (2006) Communication between eukaryotic translation initiation factors 5 and 1A within the ribosomal pre-initiation complex plays a role in start site selection. *J. Mol. Biol.* **356:** 724–737

Maag D, Fekete CA, Gryczynski Z & Lorsch JR (2005) A conformational change in the eukaryotic translation preinitiation complex and release of eIF1 signal recognition of the start codon. *Mol. Cell* **17:** 265–275

MacKenzie JM, Khromykh AA, Jones MK & Westaway EG (1998) Subcellular localization and some biochemical properties of the flavivirus Kunjin nonstructural proteins NS2A and NS4A. *Virology* **245:** 203–215

Manzano M, Reichert ED, Polo S, Falgout B, Kasprzak W, Shapiro BA & Padmanabhan R (2011) Identification of Cis-Acting Elements in the 3′-Untranslated Region of the Dengue Virus Type 2 RNA That Modulate Translation and Replication. *J. Biol. Chem.* **286:** 22521–22534

Marceau CD, Puschnik AS, Majzoub K, Ooi YS, Brewer SM, Fuchs G, Swaminathan K, Mata MA, Elias JE, Sarnow P & Carette JE (2016) Genetic dissection of Flaviviridae host factors through genome-scale CRISPR screens. *Nature* **535:** 159–163

Marintchev A, Edmonds KA, Marintcheva B, Hendrickson E, Oberer M, Suzuki C, Herdy B, Sonenberg N & Wagner G (2009) Topology and Regulation of the Human eIF4A/4G/4H Helicase Complex in Translation Initiation. *Cell* **136:** 447–460

Marintchev A, Kolupaeva VG, Pestova T V. & Wagner G (2003) Mapping the binding interface between human eukaryotic initiation factors 1A and 5B: A new interaction between old partners. *Proc. Natl. Acad. Sci.* **100:** 1535–1540

Masaki T, Arend KC, Li Y, Yamane D, McGivern DR, Kato T, Wakita T, Moorman NJ & Lemon SM (2015) MiR-122 stimulates hepatitis C virus RNA synthesis by altering the balance of viral RNAs engaged in replication versus translation. *Cell Host Microbe* **17:** 217–228

Matsuda D & Dreher TW (2006) Close spacing of AUG initiation codons confers dicistronic

character on a eukaryotic mRNA. *Rna* **12:** 1338–1349

McCracken MK, Gromowski GD, Friberg HL, Lin X, Abbink P, De La Barrera R, Eckles KH, Garver LS, Boyd M, Jetton D, Barouch DH, Wise MC, Lewis BS, Currier JR, Modjarrad K, Milazzo M, Liu M, Mullins AB, Putnak JR, Michael NL, Jarman RG & Thomas SJ (2017) Impact of prior flavivirus immunity on Zika virus infection in rhesus macaques. *PLoS Pathog.* **13:** e1006487

McInerney GM, Kedersha NL, Kaufman RJ, Anderson P & Liljeström P (2005) Importance of eIF2alpha phosphorylation and stress granule assembly in alphavirus translation regulation. *Mol. Biol. Cell* **16:** 3753–3763

Meijer HA, Kong YW, Lu WT, Wilczynska A, Spriggs R V., Robinson SW, Godfrey JD, Willis AE & Bushell M (2013) Translational repression and eIF4A2 activity are critical for microRNA-mediated gene regulation. *Science* **340:** 82–85

Men R, Bray M, Clark D, Chanock RM & Lai CJ (1996) Dengue type 4 virus mutants containing deletions in the 3' noncoding region of the RNA genome: analysis of growth restriction in cell culture and altered viremia pattern and immunogenicity in rhesus monkeys. *J. Virol.* **70:** 3930–3937

Meyer KD, Patil DP, Zhou J, Zinoviev A, Skabkin MA, Elemento O, Pestova T V., Qian SB & Jaffrey SR (2015) 5′ UTR m6A Promotes Cap-Independent Translation. *Cell* **163:** 999–1010

Meyers JA, Sanchez D, Elwell LP & Falkow S (1976) Simple Agarose Gel Electrophoretic Method for the Identification and Characterization of Plasmid Deoxyribonucleic Acid. *J. Bacteriol.* **127:** 1529–1537

Michel YM, Borman AM, Paulous S & Kean KM (2001) Eukaryotic Initiation Factor 4G-Poly(A) Binding Protein Interaction Is Required for Poly(A) Tail-Mediated Stimulation of Picornavirus Internal Ribosome Entry Segment-Driven Translation but Not for X-Mediated Stimulation of Hepatitis C Virus Translation. *Mol. Cell. Biol.* **21:** 4097–4109

Miller JL, DeWet BJM, Martinez-Pomares L, Radcliffe CM, Dwek RA, Rudd PM & Gordon S (2008) The mannose receptor mediates dengue virus infection of macrophages. *PLoS Pathog.* **4:** e17

Miller S, Kastner S, Krijnse-Locker J, Bühler S & Bartenschlager R (2007) The non-structural protein 4A of dengue virus is an integral membrane protein inducing membrane alterations in a 2K-regulated manner. *J. Biol. Chem.* **282:** 8873–8882

Miller S, Sparacio S & Bartenschlager R (2006) Subcellular localization and membrane topology of the dengue virus type 2 non-structural protein 4B. *J. Biol. Chem.* **281:** 8854–8863

Miner JJ, Cao B, Govero J, Smith AM, Fernandez E, Cabrera OH, Garber C, Noll M, Klein RS, Noguchi KK, Mysorekar IU & Diamond MS (2016) Zika Virus Infection during Pregnancy in Mice Causes Placental Damage and Fetal Demise. *Cell* **165:** 1081–1091

Miras M, Miller WA, Truniger V & Aranda MA (2017) Non-canonical translation in Plant RNA viruses. *Front. Plant Sci.* **8:** 494

Mlakar J, Korva M, Tul N, Popović M, Poljšak-Prijatelj M, Mraz J, Kolenc M, Resman Rus K, Vesnaver Vipotnik T, Fabjan Vodušek V, Vizjak A, Pižem J, Petrovec M & Avšič Županc T (2016) Zika Virus Associated with Microcephaly. *N. Engl. J. Med.* **374:** 951–958

Modis Y, Ogata S, Clements D & Harrison SC (2004) Structure of the dengue virus envelope protein after membrane fusion. *Nature* **427:** 313–319

Mosso C, Galván-Mendoza IJ, Ludert JE & del Angel RM (2008) Endocytic pathway followed by dengue virus to infect the mosquito cell line C6/36 HT. *Virology* **378:** 193–199

Muckenthaler M, Gray NK & Hentze MW (1998) IRP-1 Binding to Ferritin mRNA Prevents the Recruitment of the Small Ribosomal Subunit by the Cap-Binding Complex eIF4F. *Mol. Cell* **2:** 383–388

Mukhopadhyay S, Kim BS, Chipman PR, Rossmann MG & Kuhn RJ (2003) Structure of West Nile virus. *Science* **302:** 248

Mukhopadhyay S, Kuhn RJ & Rossmann MG (2005) A structural perspective of the Flavivirus life cycle. *Nat. Rev. Microbiol.* **3:** 13–22

Murphy BR & Whitehead SS (2011) Immune Response to Dengue Virus and Prospects for a Vaccine. *Annu. Rev. Immunol.* **29:** 587–619

Mutso M, Saul S, Rausalu K, Susova O, Žusinaite E, Mahalingam S & Merits A (2017) Reverse genetic system, genetically stable reporter viruses and packaged subgenomic replicon based on a Brazilian zika virus isolate. *J. Gen. Virol.* **98:** 2712–2724

De Nova-Ocampo M, Villegas-Sepúlveda N & Del Angel RM (2002) Translation elongation factor-1α, La, and PTB interact with the 3′ untranslated region of dengue 4 virus RNA. *Virology* **295:** 337–347

Novak JE & Kirkegaard K (1994) Coupling between genomic translation and replication in an RNA virus. *Genes and Devel.* **8:** 1726–1737

Nowak T, Färber PM, Wengler G & Wengler G (1989) Analyses of the terminal sequences of west nile virus structural proteins and of the in vitro translation of these proteins allow the proposal of a complete scheme of the proteolytic cleavages involved in their synthesis. *Virology* **169:** 365–376

Nowakowski TJ, Pollen AA, Di Lullo E, Sandoval-Espinosa C, Bershteyn M & Kriegstein AR (2016) Expression analysis highlights AXL as a candidate zika virus entry receptor in

neural stem cells. *Cell Stem Cell* **18:** 591–596

Oberer M, Marintchev A & Wagner G (2005) Structural basis for the enhancement of eIF4A helicase activity by eIF4G. *Genes Dev.* **19:** 2212–2223

Olsen DS, Savner EM, Mathew A, Zhang F, Krishnamoorthy T, Phan L & Hinnebusch AG (2003) Domains of eIF1A that mediate binding to eIF2, eIF3 and eIF5B and promote ternary complex recruitment in vivo. *EMBO J.* **22:** 193–204

Pantoja P, Pérez-Guzmán EX, Rodríguez I V., White LJ, González O, Serrano C, Giavedoni L, Hodara V, Cruz L, Arana T, Martínez MI, Hassert MA, Brien JD, Pinto AK, De Silva A & Sariol CA (2017) Zika virus pathogenesis in rhesus macaques is unaffected by pre-existing immunity to dengue virus. *Nat. Commun.* **8:** 15674

Parsyan A, Shahbazian D, Martineau Y, Petroulakis E, Alain T, Larsson O, Mathonnet G, Tettweiler G, Hellen CUT, Pestova T V., Svitkin Y V. & Sonenberg N (2009) The helicase protein DHX29 promotes translation initiation, cell proliferation, and tumorigenesis. *Proc. Natl. Acad. Sci.* **106:** 22217–22222

Passmore LA, Schmeing TM, Maag D, Applefield DJ, Acker MG, Algire MAA, Lorsch JR & Ramakrishnan V (2007) The Eukaryotic Translation Initiation Factors eIF1 and eIF1A Induce an Open Conformation of the 40S Ribosome. *Mol. Cell* **26:** 41–50

Patkar CG & Kuhn RJ (2008) Yellow Fever Virus NS3 Plays an Essential Role in Virus Assembly Independent of Its Known Enzymatic Functions. *J. Virol.* **82:** 3342–3352

Paulin FEM, Campbell LE, O 'brien K, Loughlin J & Proud CG (2001) Eukaryotic translation initiation factor 5 (eIF5) acts as a classical GTPase-activator protein. *Curr. Biol.* **11:** 55–59

Peer E, Moshitch-Moshkovitz S, Rechavi G & Dominissini D (2018) The Epitranscriptome in Translation Regulation. *Cold Spring Harb. Perspect. Biol.***:** a032623

Pelletier J & Sonenberg N (1988) Internal initiation of translation of eukaryotic mRNA directed by a sequence derived from poliovirus RNA. *Nature* **334:** 320–325

Perera R, Daijogo S, Walter BL, Nguyen JHC & Semler BL (2007) Cellular Protein Modification by Poliovirus: the Two Faces of Poly(rC)-Binding Protein. *J. Virol.* **81:** 8919–8932

Pestova T V., Borukhov SI & Hellen CUT (1998a) Eukaryotic ribosomes require initiation factors 1 and 1A to locate initiation codons. *Nature* **394:** 854–859

Pestova T V., De Breyne S, Pisarev A V., Abaeva IS & Hellen CUT (2008) eIF2-dependent and eIF2-independent modes of initiation on the CSFV IRES: A common role of domain II. *EMBO J.* **27:** 1060–1072

Pestova T V. & Hellen CUT (2003) Translation elongation after assembly of ribosomes on the

Cricket paralysis virus internal ribosomal entry site without initiation factors or initiator tRNA. *Genes Dev.* **17:** 181–186

Pestova T V. & Kolupaeva VG (2002) The roles of individual eukaryotic translation initiation factors in ribosomal scanning and initiation codon selection. *Genes Dev.* **16:** 2906–2922

Pestova T V & Hellen CUT (2001) Preparation and activity of synthetic unmodified mammalian tRNAi(Met) in initiation of translation in vitro. *RNA* **7:** 1496–1505

Pestova T V, Hellen CUT & Shatsky IN (1996a) Canonical eukaryotic initiation factors determine initiation of translation by internal ribosomal entry. *Mol. Cell. Biol.* **16:** 6859–6869

Pestova T V, Lomakin IB, Lee JH, Choi SK, Dever TE & Hellen CUT (2000) The joining of ribosomal subunits in eukaryotes requires eIF5B. *Nature* **403:** 332–335

Pestova T V, Shatsky IN, Fletcher SP, Jackson RJ & Hellen CUT (1998b) A prokaryotic-like mode of cytoplasmic eukaryotic ribosome binding to the initiation codon during internal translation initation of hepatitis C and classical swine fever virus RNAs. *Genes Dev.* **12:** 67–83

Pestova T V, Shatsky IN & Hellen CUT (1996b) Functional dissection of eukaryotic initiation factor 4F: the 4A subunit and the central domain of the 4G subunit are sufficient to mediate internal entry of 43S preinitiation complexes. *Mol. Cell. Biol.* **16:** 6870–6878

Petersen LR, Jamieson DJ, Powers AM & Honein MA (2016) Zika Virus. *N. Engl. J. Med.* **374:** 1552–1563

Phillips SL, Soderblom EJ, Bradrick SS & Garcia-Blanco MA (2016) Identification of Proteins Bound to Dengue Viral RNA In Vivo Reveals New Host Proteins Important for Virus Replication. *MBio* **7:** e01865-15

Pijlman GP, Funk A, Kondratieva N, Leung J, Torres S, van der Aa L, Liu WJ, Palmenberg AC, Shi P-Y, Hall RA & Khromykh AA (2008) A Highly Structured, Nuclease-Resistant, Noncoding RNA Produced by Flaviviruses Is Required for Pathogenicity. *Cell Host Microbe* **4:** 579–591

Pilipenko EV, Pestova TV, Kolupaeva VG, Khitrina EV, Poperechnaya AN, Agol VI & Hellen CUT (2000) A cell cycle-dependent protein serves as a template-specific translation initiation factor. *Genes Dev.* **14:** 2028–2045

Pisarev A V., Hellen CUT & Pestova T V. (2007a) Recycling of Eukaryotic Posttermination Ribosomal Complexes. *Cell* **131:** 286–299

Pisarev A V., Skabkin MA, Pisareva VP, Skabkina O V., Rakotondrafara AM, Hentze MW, Hellen CUT & Pestova T V. (2010) The Role of ABCE1 in Eukaryotic Posttermination Ribosomal Recycling. *Mol. Cell* **37:** 196–210

Pisarev A V., Unbehaun A, Hellen CUT & Pestova T V. (2007b) Assembly and Analysis of Eukaryotic Translation Initiation Complexes. *Methods Enzymol.* **430:** 147–177

Pisarev A V, Kolupaeva VG, Pisareva VP, Merrick WC, Hellen CUT & Pestova T V (2006) Specific functional interactions of nucleotides at key -3 and +4 positions flanking the initiation codon with components of the mammalian 48S translation initiation complex. *Genes Dev.* **20:** 624–636

Pisareva VP & Pisarev A V. (2016a) DHX29 and eIF3 cooperate in ribosomal scanning on structured mRNAs during translation initiation. *Rna* **22:** 1859–1870

Pisareva VP & Pisarev A V. (2016b) DHX29 reduces leaky scanning through an upstream AUG codon regardless of its nucleotide context. *Nucleic Acids Res.* **44:** 4252–4265

Pisareva VP, Pisarev A V., Komar AA, Hellen CUT & Pestova T V. (2008) Translation Initiation on Mammalian mRNAs with Structured 5'UTRs Requires DExH-Box Protein DHX29. *Cell* **135:** 1237–1250

Pokidysheva E, Zhang Y, Battisti AJ, Bator-Kelly CM, Chipman PR, Xiao C, Gregorio GG, Hendrickson WA, Kuhn RJ & Rossmann MG (2006) Cryo-EM Reconstruction of Dengue Virus in Complex with the Carbohydrate Recognition Domain of DC-SIGN. *Cell* **124:** 485–493

Polacek C, Foley JE & Harris E (2009a) Conformational Changes in the Solution Structure of the Dengue Virus 5' End in the Presence and Absence of the 3' Untranslated Region. *J. Virol.* **83:** 1161–1166

Polacek C, Friebe P & Harris E (2009b) Poly(A)-binding protein binds to the non-polyadenylated 3' untranslated region of dengue virus and modulates translation efficiency. *J. Gen. Virol.* **90:** 687–692

Pong WL, Huang ZS, Teoh PG, Wang CC & Wu HN (2011) RNA binding property and RNA chaperone activity of dengue virus core protein and other viral RNA-interacting proteins. *FEBS Lett.* **585:** 2575–2581

Pooggin MM, Hohn T & Futterer J (1998) Forced Evolution Reveals the Importance of Short Open Reading Frame A and Secondary Structure in the Cauliflower Mosaic Virus 35S RNA Leader. *J. Virol.* **72:** 4157–4169

Potisopon S, Priet S, Collet A, Decroly E, Canard B & Selisko B (2014) The methyltransferase domain of dengue virus protein NS5 ensures efficient RNA synthesis initiation and elongation by the polymerase domain. *Nucleic Acids Res.* **42:** 11642–11656

Pöyry TAA, Kaminski A & Jackson RJ (2004) What determines whether mammalian ribosomes resume scanning after translation of a short upstream open reading frame? *Genes Dev.* **18:** 62–75

Proud CG (2005) eIF2 and the control of cell physiology. *Semin. Cell Dev. Biol.* **16:** 3–12

Qian X, Nguyen HN, Song MM, Hadiono C, Ogden SC, Hammack C, Yao B, Hamersky GR, Jacob F, Zhong C, Yoon KJ, Jeang W, Lin L, Li Y, Thakor J, Berg DA, Zhang C, Kang E, Chickering M, Nauen D, Ho CY, Wen Z, Christian KM, Shi PY, Maher BJ, Wu H, Jin P, Tang H, Song H & Ming GL (2016) Brain-Region-Specific Organoids Using Mini-bioreactors for Modeling ZIKV Exposure. *Cell* **165:** 1238–1254

Quade N, Boehringer D, Leibundgut M, Van Den Heuvel J & Ban N (2015) Cryo-EM structure of Hepatitis C virus IRES bound to the human ribosome at 3.9-Å resolution. *Nat. Commun.* **6:** 7646

Querol-Audi J, Sun C, Vogan JM, Smith MD, Gu Y, Cate JHD & Nogales E (2013) Architecture of human translation initiation factor 3. *Structure* **21:** 920–928

Rabl J, Leibundgut M, Ataide SF, Haag A & Ban N (2011) Crystal Structure of the Eukaryotic 40S Initiation Factor 1. *Science* **730:** 730–737

Rakotondrafara AM & Hentze MW (2011) An efficient factor-depleted mammalian in vitro translation system. *Nat. Protoc.* **6:** 563–571

Ramakrishnan V (2002) Ribosome structure and the mechanism of translation. *Cell* **108:** 557–572

Rauscher S, Flamm C, Mandl CW, Heinz FX & Stadler PF (1997) Secondary structure of the 3'-noncoding region of flavivirus genomes: comparative analysis of base pairing probabilities. *RNA* **3:** 779–791

Ray D, Shah A, Tilgner M, Guo Y, Zhao Y, Dong H, Deas TS, Zhou Y, Li H & Shi P-Y (2006) West Nile Virus 5'-Cap Structure Is Formed by Sequential Guanine N-7 and Ribose 2'-O Methylations by Nonstructural Protein 5. *J. Virol.* **80:** 8362–8370

Reid DW, Campos RK, Child JR, Zheng T, Chan KWK, Bradrick SS, Vasudevan SG, Garcia-Blanco MA & Nicchitta C V. (2018) Dengue Virus Selectively Annexes Endoplasmic Reticulum-Associated Translation Machinery as a Strategy for Co-opting Host Cell Protein Synthesis. *J. Virol.* **92:** e01766-17

Resnik DB (2014) Ethical issues in field trials of genetically modified disease-resistant mosquitoes. *Dev. World Bioeth.* **14:** 37–46

Retallack H, Di Lullo E, Arias C, Knopp KA, Laurie MT, Sandoval-Espinosa C, Mancia Leon WR, Krencik R, Ullian EM, Spatazza J, Pollen AA, Mandel-Brehm C, Nowakowski TJ, Kriegstein AR & DeRisi JL (2016) Zika virus cell tropism in the developing human brain and inhibition by azithromycin. *Proc. Natl. Acad. Sci.* **113:** 14408–14413

Reynolds JE, Kaminski A, Carroll AR, Clarke BE, Rowlands DJ & Jackson RJ (1996) Internal initiation of translation of hepatitis C virus RNA: the ribosome entry site is at the authentic

initiation codon. *RNA* **2:** 867–878

Rice CM, Lenches EM, Eddy SR, Shin SJ, Sheets RL & Strauss JH (1985) Nucleotide Sequence of Yellow Fever Virus: Implications for Flavivirus Gene Expression and Evolution. **229:** 726–733

Rogers GW, Richter NJ, Lima WF & Merrick WC (2001) Modulation of the Helicase Activity of eIF4A by eIF4B, eIF4H, and eIF4F. *J. Biol. Chem.* **276:** 30914–30922

Romero-López C & Berzal-Herranz A (2009) A long-range RNA-RNA interaction between the 5′ and 3′ ends of the HCV genome. *Rna* **15:** 1740–1752

Roosendaal J, Westaway EG, Khromykh A & Mackenzie JM (2006) Regulated Cleavages at the West Nile Virus NS4A-2K-NS4B Junctions Play a Major Role in Rearranging Cytoplasmic Membranes and Golgi Trafficking of the NS4A Protein. *J. Virol.* **80:** 4623–4632

Roth H, Magg V, Uch F, Mutz P, Klein P, Haneke K, Lohmann V, Bartenschlager R, Fackler OT, Locker N, Stoecklin G & Ruggieri A (2017) Flavivirus Infection Uncouples Translation Suppression from Cellular Stress Responses. *MBio* **8:** e02150-16

Ryabova LA & Hohn T (2000) Ribosome shunting in the cauliflower mosaic virus 35S RNA leader is a special case of reinitiation of translation functioning in plant and animal systems. *Genes Dev.* **14:** 817–829

Saeedi BJ & Geiss BJ (2013) Regulation of flavivirus RNA synthesis and capping. *Wiley Interdiscip. Rev. RNA* **4:** 723–735

Samsa MM, Mondotte JA, Iglesias NG, Assunção-Miranda I, Barbosa-Lima G, Da Poian AT, Bozza PT & Gamarnik A V. (2009) Dengue virus capsid protein usurps lipid droplets for viral particle formation. *PLoS Pathog.* **5:** e1000632

Sasaki J & Nakashima N (2002) Methionine-independent initiation of translation in the capsid protein of an insect RNA virus. *Proc. Natl. Acad. Sci.* **97:** 1512–1515

Savidis G, McDougall WM, Meraner P, Perreira JM, Portmann JM, Trincucci G, John SP, Aker AM, Renzette N, Robbins DR, Guo Z, Green S, Kowalik TF & Brass AL (2016) Identification of Zika Virus and Dengue Virus Dependency Factors using Functional Genomics. *Cell Rep.* **16:** 232–246

van der Schaar HM, Rust MJ, Chen, Van Der Ende-Metselaar H, Wilschut J, Zhuang X & Smit JM (2008) Dissecting the cell entry pathway of dengue virus by single-particle tracking in living cells. *PLoS Pathog.* **4:** e1000244

Schmeing TM & Ramakrishnan V (2009) What recent ribosome structures have revealed about the mechanism of translation. *Nature* **461:** 1234–1242

Schnettler E, Leung JY, Sterken MG, Metz SW, Geertsema C, Goldbach RW, Vlak JM, Kohl

A, Khromykh A a. & Pijlman GP (2013) Non-coding flavivirus RNA displays RNAi suppressor activity in insect and mammalian cells. *J. Virol.* **86:** 13486–13500

Schuessler A, Funk A, Lazear HM, Cooper DA, Torres S, Daffis S, Jha BK, Kumagai Y, Takeuchi O, Hertzog P, Silverman R, Akira S, Barton DJ, Diamond MS & Khromykh AA (2012) West Nile Virus Noncoding Subgenomic RNA Contributes to Viral Evasion of the Type I Interferon-Mediated Antiviral Response. *J. Virol.* **86:** 5708–5718

Schüler M, Connell SR, Lescoute A, Giesebrecht J, Dabrowski M, Schroeer B, Mielke T, Penczek PA, Westhof E & Spahn CMT (2006) Structure of the ribosome-bound cricket paralysis virus IRES RNA. *Nat. Struct. &Amp; Mol. Biol.* **13:** 1092–1096

Schutz P, Bumann M, Oberholzer AE, Bieniossek C, Trachsel H, Altmann M & Baumann U (2008) Crystal structure of the yeast eIF4A-eIF4G complex: An RNA-helicase controlled by protein-protein interactions. *Proc. Natl. Acad. Sci.* **105:** 9564–9569

Selisko B, Potisopon S, Agred R, Priet S, Varlet I, Thillier Y, Sallamand C, Debart F, Vasseur JJ & Canard B (2012) Molecular Basis for Nucleotide Conservation at the Ends of the Dengue Virus Genome. *PLoS Pathog.* **8:** e1002912

Sharma S Das, Kraft JJ, Miller WA & Goss DJ (2015) Recruitment of the 40S ribosomal subunit to the 3'-untranslated region (UTR) of a viral mRNA, via the eIF4 complex, facilitates cap-independent translation. *J. Biol. Chem.* **290:** 11268–11281

Shin B-S, Maag D, Roll-Mecak A, Arefin MS, Burley SK, Lorsch JR & Dever TE (2002) Uncoupling of Initiation Factor eIF5B/IF2 GTPase and Translational Activities by Mutations that Lower Ribosome Affinity. *Cell* **111:** 1015–1025

Shiryaev SA, Mesci P, Pinto A, Fernandes I, Sheets N, Shresta S, Farhy C, Huang C-T, Strongin AY, Muotri AR & Terskikh A V (2017) Repurposing of the anti-malaria drug chloroquine for Zika Virus treatment and prophylaxis. *Sci. Rep.* **7:** 15771

Sirohi D, Chen Z, Sun L, Klose T, Pierson TC, Rossmann MG & Kuhn RJ (2016) The 3.8 Å resolution cryo-EM structure of Zika virus. *Science* **352:** 467–470

Skabkin M a, Skabkina O V, Dhote V, Komar AA, Hellen CUT & Pestova T V (2010) Activities of Ligatin and MCT-1 / DENR in eukaryotic translation initiation and ribosomal recycling. *Genes Dev.* **24:** 1787–1801

Slepenkov S V., Korneeva NL & Rhoads RE (2008) Kinetic mechanism for assembly of the m 7GpppG·eIF4E·eIF4G complex. *J. Biol. Chem.* **283:** 25227–25237

Somers J, Pöyry T & Willis AE (2013) A perspective on mammalian upstream open reading frame function. *Int. J. Biochem. Cell Biol.* **45:** 1690–1700

Sonenberg N & Hinnebusch AG (2009) Regulation of translation initiation in eukaryotes: mechanisms and biological targets. *Cell* **136:** 731–745

Song Y, Mugavero J, Stauft CB & Wimmer E (2019) Dengue and Zika Virus 5′ Untranslated Regions Harbor Internal Ribosomal Entry Site Functions. *MBio* **10:** e00459-19

Spahn CMT, Jan E, Mulder A, Grassucci RA, Sarnow P & Frank J (2004) Cryo-EM Visualization of a Viral Internal Ribosome Entry Site Bound to Human Ribosomes: The IRES Functions as an RNA-Based Translation Factor. *Cell* **118:** 465–475

Spahn CMT, Kieft JS, Grassucci RA, Penczek PA, Zhou K, Doudna JA & Frank J (2001) Hepatitis C virus IRES RNA-induced changes in the conformation of the 40S ribosomal subunit. *Science* **291:** 1959–1962

Spirin AS (2009) How does a scanning ribosomal particle move along the 5′-untranslated region of eukaryotic mRNA? Brownian ratchet model. *Biochemistry* **48:** 10688–10692

Stadler K, Allison SL, Schalich J & Heinz FX (1997) Proteolytic activation of tick-borne encephalitis virus by furin. *J. Virol.* **71:** 8475–8481

Stebbins-Boaz B, Cao Q, de Moor CH, Mendez R & Richter JD (1999) Maskin Is a CPEB-Associated Factor that Transiently Interacts with eIF-4E. *Mol. Cell* **4:** 1017–1027

Stern-Ginossar N, Thompson SR, Mathews MB & Mohr I (2018) Translational Control in Virus-Infected Cells. *Cold Spring Harb. Perspect. Biol.* **11:** a033001

Sun Y, Atas E, Lindqvist L, Sonenberg N, Pelletier J & Meller A (2012) The eukaryotic initiation factor eIF4H facilitates loop-binding, repetitive RNA unwinding by the eIF4A DEAD-box helicase. *Nucleic Acids Res.* **40:** 6199–6207

Suthar MS, Aguirre S & Fernandez-Sesma A (2013) Innate Immune Sensing of Flaviviruses. *PLoS Pathog.* **9:** e1003541

Suzuki R, Fayzulin R, Frolov I & Mason PW (2008) Identification of Mutated Cyclization Sequences That Permit Efficient Replication of West Nile Virus Genomes: Use in Safer Propagation of a Novel Vaccine Candidate. *J. Virol.* **82:** 6942–6951

Svitkin Y V., Pause A, Haghighat A, Pyronnet S, Witherall G, Belsham GJ & Sonenberg N (2001) The requirement for eukaryotic initiation factor 4A (eIF4A) in translation is in direct proportion to the degree of mRNA 5′ secondary structure. *Rna* **7:** 382–394

Sweeney TR, Abaeva IS, Pestova T V & Hellen CUT (2014) The mechanism of translation initiation on Type 1 picornavirus IRESs. *EMBO J.* **33:** 76–92

Sztuba-Solinska J, Teramoto T, Rausch JW, Shapiro BA, Padmanabhan R & Le Grice SFJ (2013) Structural complexity of Dengue virus untranslated regions: Cis-acting RNA motifs and pseudoknot interactions modulating functionality of the viral genome. *Nucleic Acids Res.* **41:** 5075–5089

Takyar S, Hickerson RP & Noller HF (2005) mRNA helicase activity of the ribosome. *Cell* **120:** 49–58

Tan B-H, Fu J, Sugrue RJ, Yap E-H, Chan Y-C & Tan YH (1996) Recombinant Dengue Type 1 Virus NS5 Protein Expressed in Escherichia coli Exhibits RNA-Dependent RNA Polymerase Activity. *Virology* **216:** 317–325

Tang H, Hammack C, Ogden SC, Wen Z, Qian X, Li Y, Yao B, Shin J, Zhang F, Lee EM, Christian KM, Didier RA, Jin P, Song H & Ming GL (2016) Zika virus infects human cortical neural progenitors and attenuates their growth. *Cell Stem Cell* **18:** 587–590

Tarun SZ & Sachs AB (1996) Association of the yeast poly(A) tail binding protein with translation initiation factor eIF-4G. *EMBO J.* **15:** 7168–7177

Terzian ACB, Schanoski AS, De Oliveira Mota MT, Da Silva RA, Estofolete CF, Colombo TE, Rahal P, Hanley KA, Vasilakis N, Kalil J & Nogueira ML (2017) Viral load and cytokine response profile does not support antibody-dependent enhancement in Dengue-Primed Zika Virus-infected patients. *Clin. Infect. Dis.* **65:** 1260–1265

Thurner C, Witwer C, Hofacker IL & Stadler PF (2004) Conserved RNA secondary structures in Flaviviridae genomes. *J. Gen. Virol.* **85:** 1113–1124

Tilgner M, Deas TS & Shi PY (2005) The flavivirus-conserved penta-nucleotide in the 3′ stem-loop of the West Nile virus genome requires a specific sequence and structure for RNA synthesis, but not for viral translation. *Virology* **331:** 375–386

Treder K, Kneller ELP, Allen EM, Wang Z, Browning KS & Miller WA (2008) The 3' cap-independent translation element of Barley yellow dwarf virus binds eIF4F via the eIF4G subunit to initiate translation. *RNA* **14:** 134–147

Tuplin A, Struthers M, Cook J, Bentley K & Evans DJ (2015) Inhibition of HCV translation by disrupting the structure and interactions of the viral CRE and 3' X-tail. *Nucleic Acids Res.* **43:** 2914–2926

Tuplin A, Struthers M, Simmonds P & Evans DJ (2012) A twist in the tail: SHAPE mapping of long-range interactions and structural rearrangements of RNA elements involved in HCV replication. *Nucleic Acids Res.* **40:** 6908–6921

Tyzack JK, Wang X, Belsham GJ & Proud CG (2000) ABC50 interacts with eukaryotic initiation factor 2 and associates with the ribosome in an ATP-dependent manner. *J. Biol. Chem.* **275:** 34131–34139

Ueda T, Watanabe-Fukunaga R, Fukuyama H, Nagata S & Fukunaga R (2004) Mnk2 and Mnk1 Are Essential for Constitutive and Inducible Phosphorylation of Eukaryotic Initiation Factor 4E but Not for Cell Growth or Development. *Mol. Cell. Biol.* **24:** 6539–6549

Unbehaun A, Borukhov SI, Hellen CUT & Pestova T V (2004a) The 40S subunit in 48S complexes formed at the initiation codon of mRNA is bound to eukaryotic initiation factor (eIF) 3, eIF1, eIF1A, and an eIF2/GTP/Met-tRNA. *Genes Dev.* **18:** 3078–3093

Unbehaun A, Borukhov SI, Hellen CUT & Pestova T V (2004b) Release of initiation factors from 48S complexes during ribosomal subunit joining and the link between establishment of codon-anticodon base-pairing and hydrolysis of eIF2-bound GTP. *Genes Dev.* **18:** 3078–3093

Upadhyay AK, Cyr M, Longenecker K, Tripathi R, Sun C & Kempf DJ (2017) Crystal structure of full-length Zika virus NS5 protein reveals a conformation similar to Japanese encephalitis virus NS5. *Acta Crystallogr. Sect. Struct. Biol. Commun.* **73:** 116–122

Vashist S, Anantpadma M, Sharma H & Vrati S (2009) La protein binds the predicted loop structures in the 3' non-coding region of Japanese encephalitis virus genome: role in virus replication. *J. Gen. Virol.* **90:** 1343–1352

Vashist S, Bhullar D & Vrati S (2011) La Protein Can Simultaneously Bind to Both 3′- and 5′-Noncoding Regions of Japanese Encephalitis Virus Genome. *DNA Cell Biol.* **30:** 339–346

Vattem KM & Wek RC (2004) Reinitiation involving upstream ORFs regulates ATF4 mRNA translation in mammalian cells. *Proc. Natl. Acad. Sci.* **101:** 11269–11274

Ventoso I, Sanz MA, Molina S, Berlanga JJ, Carrasco L & Esteban M (2006) Translational resistance of late alphavirus mRNA to eIF2α phosphorylation: A strategy to overcome the antiviral effect of protein kinase PKR. *Genes Dev.* **20:** 87–100

Villordo SM, Alvarez DE & Gamarnik A V. (2010) A balance between circular and linear forms of the dengue virus genome is crucial for viral replication. *RNA* **16:** 2325–2335

Villordo SM, Filomatori C V., Sánchez-Vargas I, Blair CD & Gamarnik A V. (2015) Dengue Virus RNA Structure Specialization Facilitates Host Adaptation. *PLoS Pathog.* **11:** e1004604

Villordo SM & Gamarnik A V. (2009) Genome cyclization as strategy for flavivirus RNA replication. *Virus Res.* **139:** 230–239

Villordo SM & Gamarnik A V. (2013) Differential RNA Sequence Requirement for Dengue Virus Replication in Mosquito and Mammalian Cells. *J. Virol.* **87:** 9365–9372

Walsh D & Mohr I (2011) Viral subversion of the host protein synthesis machinery. *Nat. Rev. Microbiol.* **9:** 860–875

Wang E, Weaver SC, Shope RE, Tesh RB, Watts DM & Barrett ADT (1996) Genetic Variation in Yellow Fever Virus: Duplication in the 3′ Noncoding Region of Strains from Africa. *Virology* **225:** 274–281

Wang L, Jeng K-S & Lai MMC (2011) Poly(C)-Binding Protein 2 Interacts with Sequences Required for Viral Replication in the Hepatitis C Virus (HCV) 5' Untranslated Region and Directs HCV RNA Replication through Circularizing the Viral Genome. *J. Virol.* **85:** 7954–7964

Ward AM, Bidet K, Yinglin A, Ler SG, Hogue K, Blackstock W, Gunaratne J & Garcia-Blanco MA (2011) Quantitative mass spectrometry of DENV-2 RNA-interacting proteins reveals that the DEAD-box RNA helicase DDX6 binds the DB1 and DB2 3' UTR structures. *RNA Biol.* **8:** 1173–1186

Waskiewicz AJ, Flynn A, Proud CG & Cooper JA (1997) Mitogen-activated protein kinases activate the serine/threonine kinases Mnk1 and Mnk2. *EMBO J.* **16:** 1909–1920

Weisser M, Schäfer T, Leibundgut M, Böhringer D, Aylett CHS & Ban N (2017) Structural and Functional Insights into Human Re-initiation Complexes. *Mol. Cell* **67:** 447–456

Wek RC (2018) Role of eIF2α kinases in translational control and adaptation to cellular stress. *Cold Spring Harb. Perspect. Biol.* **10:** a032870

Wells SE, Hillner PE, Vale RD & Sachs AB (1998) Circularization of mRNA by Eukaryotic Translation Initiation Factors. *Mol. Cell* **2:** 135–140

Welsch S, Miller S, Romero-Brey I, Merz A, Bleck CKE, Walther P, Fuller SD, Antony C, Krijnse-Locker J & Bartenschlager R (2009) Composition and Three-Dimensional Architecture of the Dengue Virus Replication and Assembly Sites. *Cell Host Microbe* **5:** 365–375

Wengler G & Wengler G (1981) Terminal sequences of the genome and replicative-form RNA of the flavivirus west nile virus: absence of poly(A) and possible role in RNA replication. *Virology* **113:** 544–555

Wengler G & Wengler G (1993) The NS 3 Nonstructural Protein of Flaviviruses Contains an RNA Triphosphatase Activity. *Virology* **197:** 265–273

Wengler G, Wengler G & Gross HJ (1978) Studies on virus-specific nucleic acids synthesized in vertebrate and mosquito cells infected with flaviviruses. *Virology* **89:** 423–437

Wilkinson KA, Merino EJ & Weeks KM (2006) Selective 2'-hydroxyl acylation analyzed by primer extension (SHAPE): quantitative RNA structure analysis at single nucleotide resolution. *Nat. Protoc.* **1:** 1610–1616

Xi Q, Cuesta R & Schneider RJ (2005) Regulation of Translation by Ribosome Shunting through Phosphotyrosine-Dependent Coupling of Adenovirus Protein 100k to Viral mRNAs. *J. Virol.* **79:** 5676–5683

Xie X, Zou J, Puttikhunt C, Yuan Z & Shi P-Y (2014) Two Distinct Sets of NS2A Molecules Are Responsible for Dengue Virus RNA Synthesis and Virion Assembly. *J. Virol.* **89:** 1298–1313

Xu M, Lee EM, Wen Z, Cheng Y, Huang WK, Qian X, Tcw J, Kouznetsova J, Ogden SC, Hammack C, Jacob F, Nguyen HN, Itkin M, Hanna C, Shinn P, Allen C, Michael SG, Simeonov A, Huang W, Christian KM, Goate A, Brennand KJ, Huang R, Xia M, Ming

GL, Zheng W, Song H & Tang H (2016) Identification of small-molecule inhibitors of Zika virus infection and induced neural cell death via a drug repurposing screen. *Nat. Med.* **22:** 1101–1107

Xue S, Tian S, Fujii K, Kladwang W, Das R & Barna M (2015) RNA regulons in Hox 59 UTRs confer ribosome specificity to gene regulation. *Nature* **517:** 33–38

Yamamoto H, Collier M, Loerke J, Ismer J, Schmidt A, Hilal T, Sprink T, Yamamoto K, Mielke T, Bu rger J, Shaikh TR, Dabrowski M, Hildebrand PW, Scheerer P & Spahn CM (2015) Molecular architecture of the ribosome-bound Hepatitis C Virus internal ribosomal entry site RNA. *EMBO J.* **34:** 3042–3058

Yanagiya A, Svitkin Y V., Shibata S, Mikami S, Imataka H & Sonenberg N (2009) Requirement of RNA Binding of Mammalian Eukaryotic Translation Initiation Factor 4GI (eIF4GI) for Efficient Interaction of eIF4E with the mRNA Cap. *Mol. Cell. Biol.* **29:** 1661–1669

Yángüez E, Rodriguez P, Goodfellow I & Nieto A (2011) Influenza virus polymerase confers independence of the cellular cap-binding factor eIF4E for viral mRNA translation. *Virology* **422:** 297–307

Yap TL, Xu T, Chen Y-L, Malet H, Egloff M-P, Canard B, Vasudevan SG & Lescar J (2007) Crystal Structure of the Dengue Virus RNA-Dependent RNA Polymerase Catalytic Domain at 1.85-Angstrom Resolution. *J. Virol.* **81:** 4753–4765

Yoffe AM, Prinsen P, Gelbart WM & Ben-Shaul A (2011) The ends of a large RNA molecule are necessarily close. *Nucleic Acids Res.* **39:** 292–299

You S, Falgout B, Markoff L & Padmanabhan R (2001) In Vitro RNA Synthesis from Exogenous Dengue Viral RNA Templates Requires Long Range Interactions between 5′- and 3′-Terminal Regions that Influence RNA Structure. *J. Biol. Chem.* **276:** 15581–15591

You S & Padmanabhan R (1999) A Novel in Vitro Replication System for Dengue Virus. *J. Biol. Chem.* **274:** 33714–33722

Yu L, Nomaguchi M, Padmanabhan R & Markoff L (2008) Specific requirements for elements of the 5′ and 3′ terminal regions in flavivirus RNA synthesis and viral replication. *Virology* **374:** 170–185

Yu L, Takeda K & Markoff L (2013) Protein-protein interactions among West Nile non-structural proteins and transmembrane complex formation in mammalian cells. *Virology* **446:** 365–377

Yu Y, Marintchev A, Kolupaeva VG, Unbehaun A, Veryasova T, Lai SC, Hong P, Wagner G, Hellen CUT & Pestova T V. (2009) Position of eukaryotic translation initiation factor eIF1A on the 40S ribosomal subunit mapped by directed hydroxyl radical probing. *Nucleic*

Acids Res. **37:** 5167–5182

Yu Y, Sweeney TR, Kafasla P, Jackson RJ, Pestova T V & Hellen CUT (2011) The mechanism of translation initiation on Aichivirus RNA mediated by a novel type of picornavirus IRES. *EMBO J.* **30:** 4423–4436

Yueh A & Schneider RJ (1996) Selective translation initiation by ribosome jumping in adenovirus-infected and heat-shocked cells. *Genes Dev.* **10:** 1557–1567

Yueh A & Schneider RJ (2000) Translation by ribosome shunting on adenovirus and hsp70 mRNAs facilitated by complementarity to 18S rRNA. *Genes Dev.* **14:** 414–421

Zeng L, Falgout B & Markoff L (1998) Identification of specific nucleotide sequences within the conserved 3'-SL in the dengue type 2 virus genome required for replication. *J. Virol.* **72:** 7510–7522

Zhang B, Dong H, Stein DA, Iversen PL & Shi PY (2008a) West Nile virus genome cyclization and RNA replication require two pairs of long-distance RNA interactions. *Virology* **373:** 1–13

Zhang B, Dong H, Stein DA & Shi PY (2008b) Co-selection of West Nile virus nucleotides that confer resistance to an antisense oligomer while maintaining long-distance RNA/RNA base pairings. *Virology* **382:** 98–106

Zhang B, Dong H, Zhou Y & Shi P-Y (2008c) Genetic Interactions among the West Nile Virus Methyltransferase, the RNA-Dependent RNA Polymerase, and the 5' Stem-Loop of Genomic RNA. *J. Virol.* **82:** 7047–7058

Zhang G, Fedyunin I, Miekley O, Valleriani A, Moura A & Ignatova Z (2010) Global and local depletion of ternary complex limits translational elongation. *Nucleic Acids Res.* **38:** 4778–4787

Zhang R, Miner JJ, Gorman MJ, Rausch K, Ramage H, White JP, Zuiani A, Zhang P, Fernandez E, Zhang Q, Dowd KA, Pierson TC, Cherry S & Diamond MS (2016) A CRISPR screen defines a signal peptide processing pathway required by flaviviruses. *Nature* **535:** 164–168

Zhang X, Ge P, Yu X, Brannan JM, Bi G, Zhang Q, Schein S & Hong Zhou Z (2013) Cryo-EM structure of the mature dengue virus at 3.5-Å resolution. *Nat. Struct. Mol. Biol.* **20:** 105–110

Zhang Y, Corver J, Chipman PR, Zhang W, Pletnev S V, Sedlak D, Baker TS, Strauss JH, Kuhn RJ & Rossmann MG (2003) Structures of immature flavivirus particles. *EMBO J.* **22:** 2604–2613

Zhao B, Yi G, Du F, Chuang YC, Vaughan RC, Sankaran B, Kao CC & Li P (2017) Structure and function of the Zika virus full-length NS5 protein. *Nat. Commun.* **8:** 14762

Zhao Y, Soh TS, Zheng J, Chan KWK, Phoo WW, Lee CC, Tay MYF, Swaminathan K, Cornvik TC, Lim SP, Shi P-Y, Lescar J, Vasudevan SG & Luo D (2015) A Crystal Structure of the Dengue Virus NS5 Protein Reveals a Novel Inter-domain Interface Essential for Protein Flexibility and Virus Replication. *PLOS Pathog.* **11:** e1004682

Zhou J, Wan J, Gao X, Zhang X, Jaffrey SR & Qian S-B (2015) Dynamic m(6)A mRNA methylation directs translational control of heat shock response. *Nature* **526:** 591–594

Zhou Y, Ray D, Zhao Y, Dong H, Ren S, Li Z, Guo Y, Bernard KA, Shi P-Y & Li H (2007) Structure and Function of Flavivirus NS5 Methyltransferase. *J. Virol.* **81:** 3891–3903

Ziv O, Gabryelska MM, Lun ATL, Gebert LFR, Sheu-Gruttadauria J, Meredith LW, Liu ZY, Kwok CK, Qin CF, MacRae IJ, Goodfellow I, Marioni JC, Kudla G & Miska EA (2018) COMRADES determines in vivo RNA structures and interactions. *Nat. Methods* **15:** 785–788

Zuker M (2003) Mfold web server for nucleic acid folding and hybridization prediction. *Nucleic Acids Res.* **31:** 3406–3415

8 Appendices

Appendix A Flaviviral terminal genome structures including full sequence

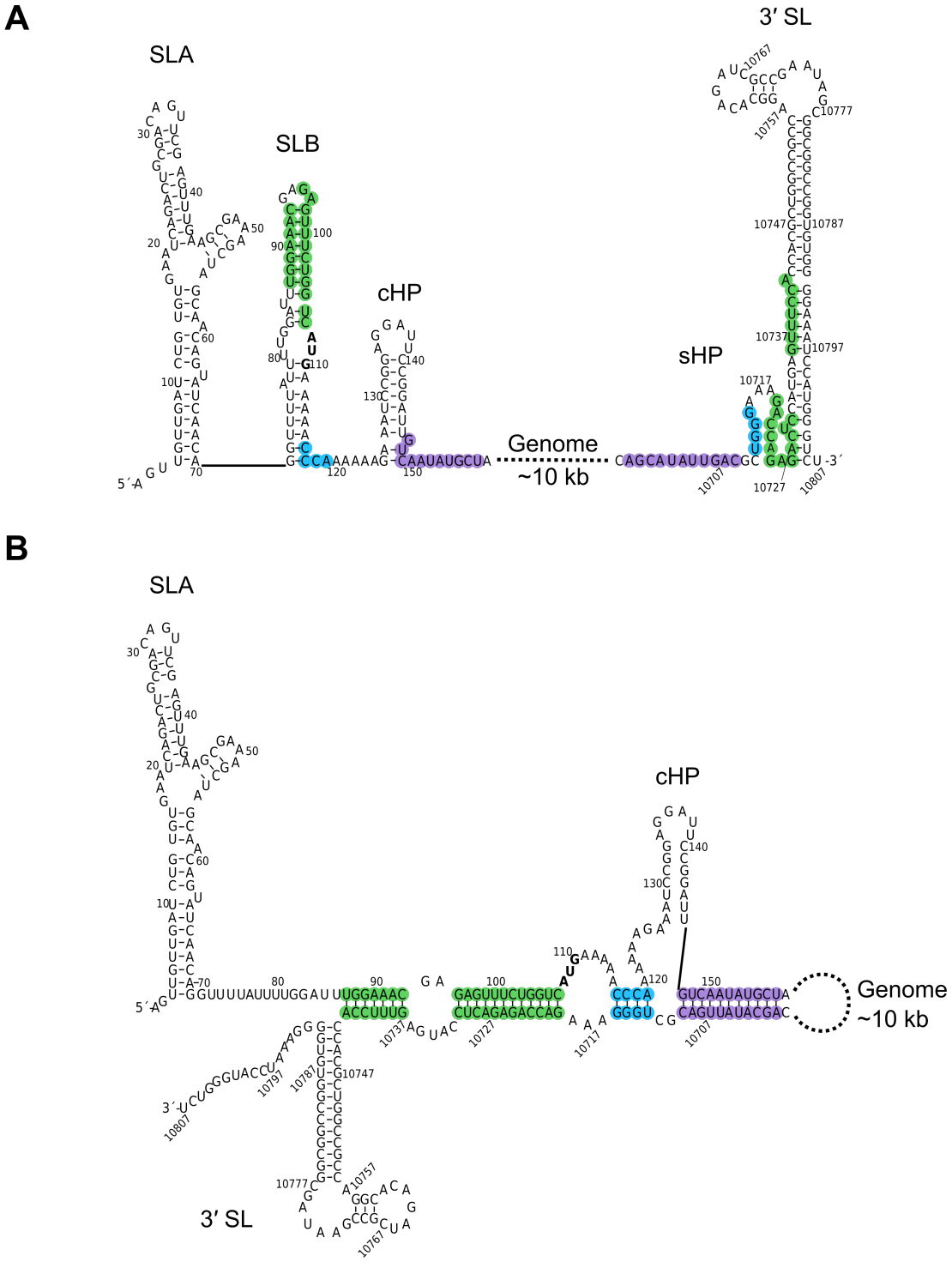

Structure of the ZIKV PE243 terminal ends including the full sequence in the linear and circular conformations

Schematics of the terminal ends of the ZIKV genome including the full sequence in the **A**) linear conformation and **B**) the circular conformation. Sequences corresponding to the UAR, DAR and CS are highlighted in green, blue and purple, respectively. The initiating AUG at nt 108 is highlighted in bold. SLA, stem-loop A; SLB, stem-loop B; cHP, C coding region hairpin; sHP, small hairpin; 3' SL, 3' stem-loop.

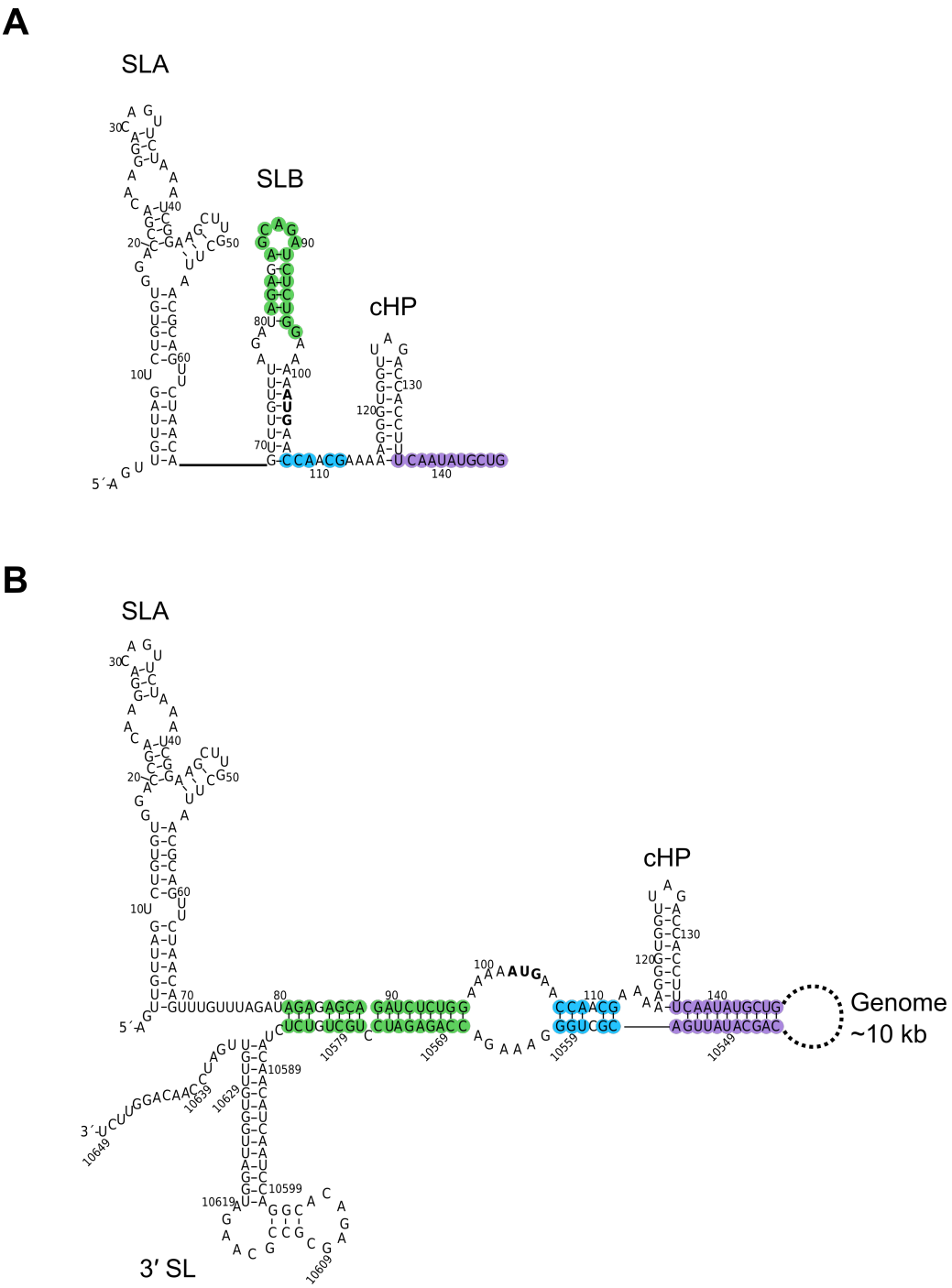

Structure of the DENV4 5′ terminal end including the full sequence in the linear and circular conformations

Schematics of the terminal ends of the DENV4 genome including the full 5′ sequence in the **A**) linear conformation and **B**) the circular conformation. Sequences corresponding to the UAR, DAR and CS are highlighted in green, blue and purple, respectively. The initiating AUG at nt 102 is highlighted in bold. SLA, stem-loop A; SLB, stem-loop B; cHP, C coding region hairpin; 3' SL, 3' stem-loop.

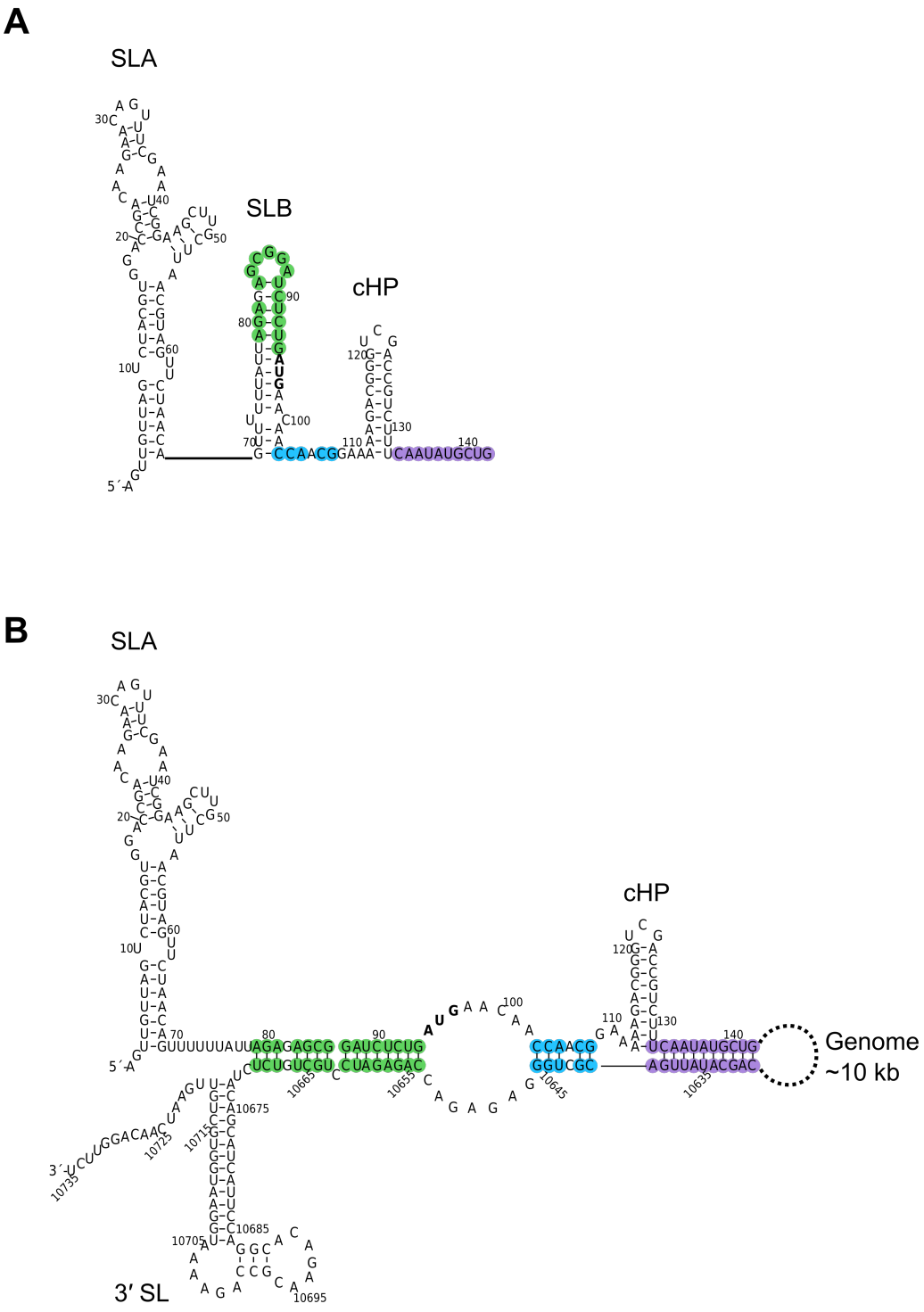

Structure of the DENV1 5′ terminal end including the full sequence in the linear and circular conformations

Schematics of the terminal ends of the DENV1 genome including the full 5′ sequence in the **A**) linear conformation and **B**) the circular conformation. Sequences corresponding to the UAR, DAR and CS are highlighted in green, blue and purple, respectively. The initiating AUG at nt 95 is highlighted in bold. SLA, stem-loop A; SLB, stem-loop B; cHP, C coding region hairpin; 3' SL, 3' stem-loop.

Appendix B eIF4A inhibition reduces translation of ZIKV^{Nluc} post-electroporation

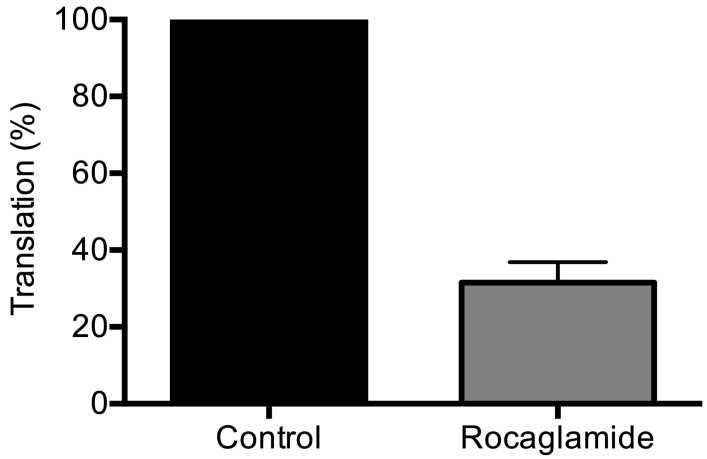

Luciferase activity at 6 hrs post electroporation of capped T7-driven ZIKV^{Nluc} RNA (5 μg) in the presence of 30 nM rocaglamide A relative to the absence of drug. Vero cells were pre-treated with rocaglamide A for 3 hours before electroporation. Rocaglamide was maintained over the time course. Data are mean+/-SEM of three independent experiments. Experiment was performed by Dr Ted Fajardo.

Appendix C Representative primer extension inhibition gels for SHAPE analysis

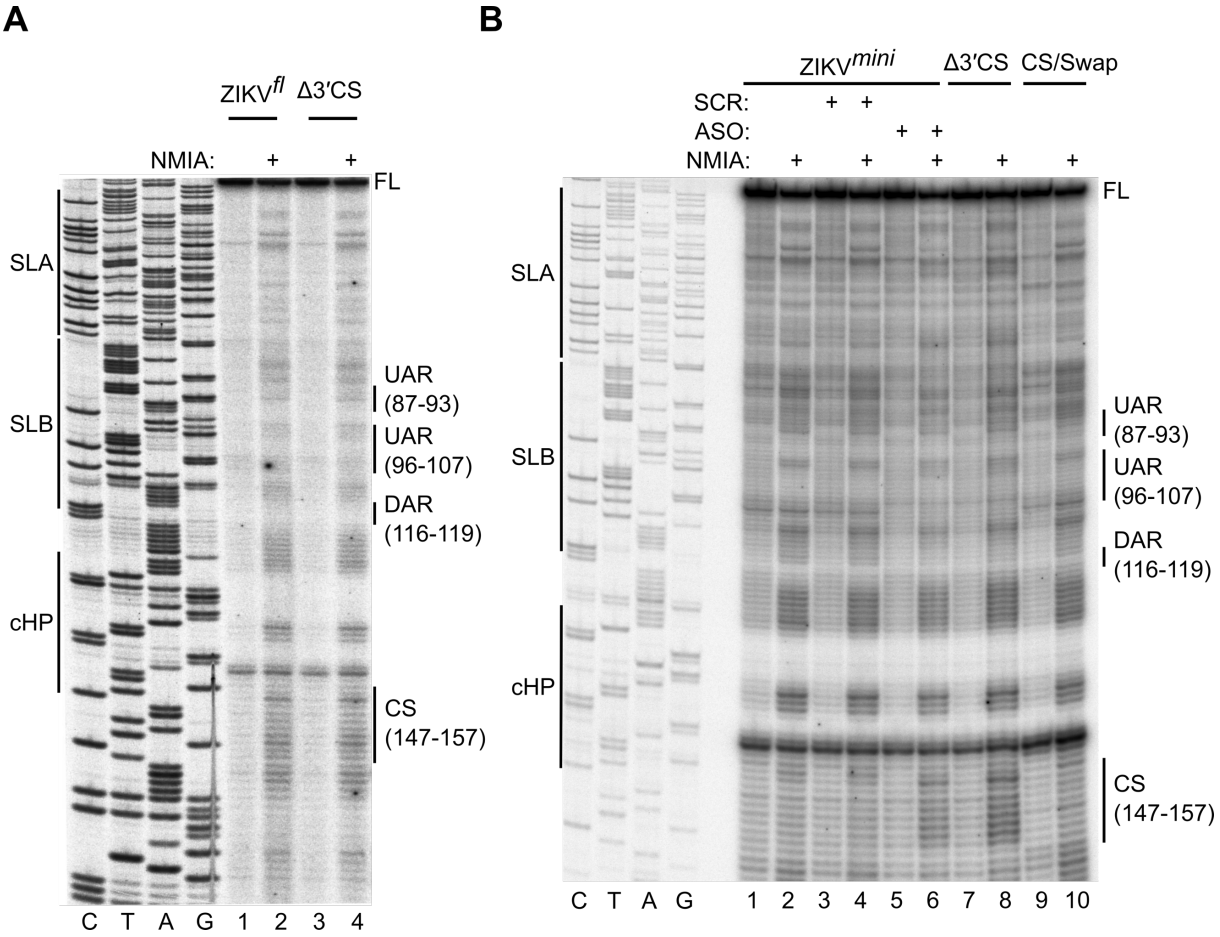

Representative SHAPE gels showing **A**) SHAPE analysis of ZIKV^{fl} and ZIKV^{fl}-Δ3′CS or **B**) ZIKV^{mini} (in presence or absence of ASO or SCR), ZIKV^{mini}-Δ3′CS and ZIKV^{mini}-CS/Swap. Indicated are the regions corresponding to the UAR, the DAR and the CS.

Appendix D Complete SHAPE reactivity across the 5′ terminal region of ZIKV

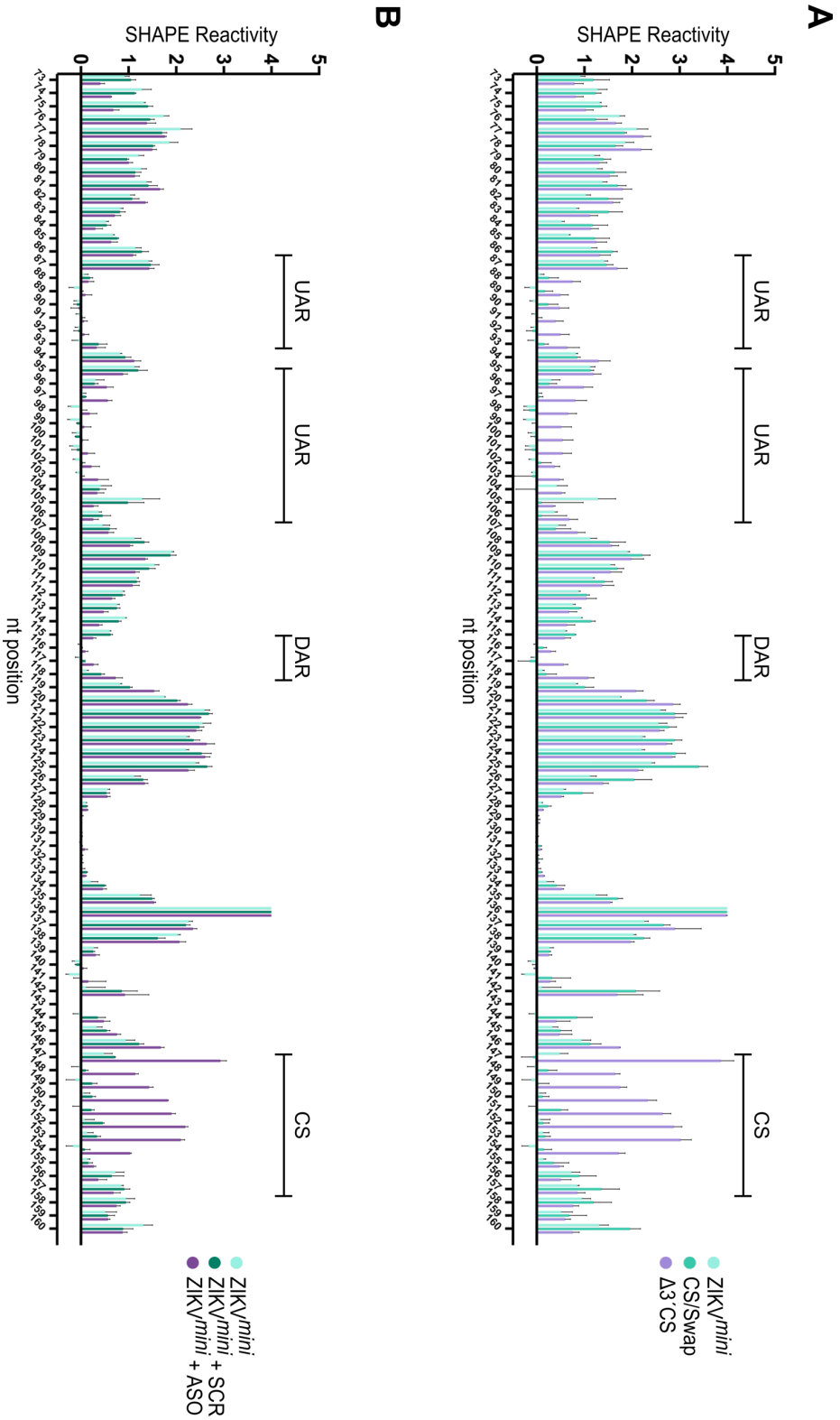

SHAPE reactivity of nucleotides within ZIKV^{mini} compared to **A**) ZIKV^{mini}-CS/Switch and ZIKV^{mini}-Δ3′CS or **B**) ZIKV^{mini} + SCR and ZIKV^{mini} + ASO. Error bars show the mean +/- SD across three independent experiments.

Appendix E NS5^{ZIKV} binds linear genome with higher affinity than circularised genome

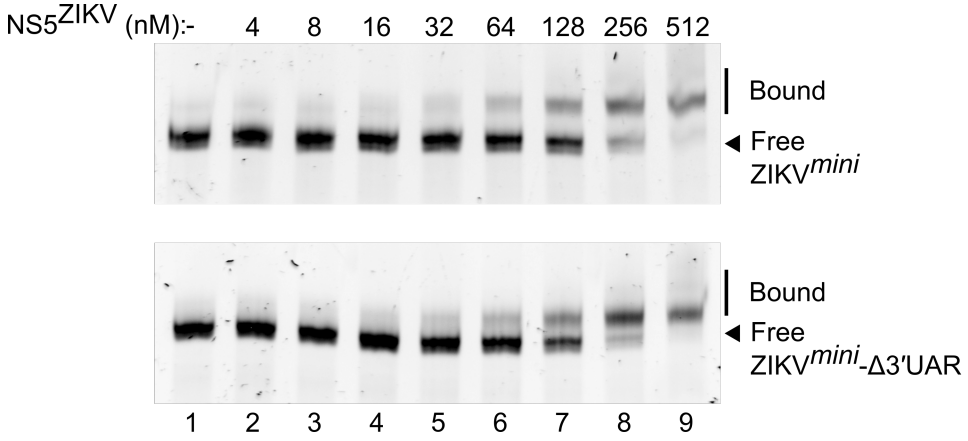

Native PAGE analysis of ZIKV^{mini} and ZIKV^{mini}-Δ3′UAR RNA in the presence of increasing concentrations of NS5^{ZIKV}. Gels were poststained with ethidium bromide for detection. Free and bound RNA is indicated.